TAMPEREEN TEKNILLINEN YLIOPISTO
TAMPERE UNIVERSITY OF TECHNOLOGY

Jason Kramb

The Role of Inorganics in Biomass Gasification: Catalytic Effects on Char Reactions and Toxic Emissions

Julkaisu 1450 • Publication 1450

Tampere 2017

Tampereen teknillinen yliopisto. Julkaisu 1450
Tampere University of Technology. Publication 1450

Jason Kramb

The Role of Inorganics in Biomass Gasification: Catalytic Effects on Char Reactions and Toxic Emissions

Thesis for the degree of Doctor of Philosophy to be presented with due permission for public examination and criticism in Konetalo Building, Auditorium K1702, at Tampere University of Technology, on the 13th of January 2017, at 12 noon.

Tampereen teknillinen yliopisto - Tampere University of Technology
Tampere 2017

ISBN 978-952-15-3883-4 (printed)
ISBN 978-952-15-3897-1 (PDF)
ISSN 1459-2045

Abstract

This thesis studied the role of inorganic elements in biomass gasification, focusing on catalytic effects in char gasification and removal of toxic metals from the product gas. A combination of experimental, including gasification using thermogravimetric analysis and fluidized beds, and modeling techniques were used.

Spruce and birch woods were leached of the naturally occurring ash forming elements and loaded with varying amounts of calcium or potassium. These woods were then gasified in either an isothermal thermogravimetric analysis device or a bubbling fluidized bed reactor. In the case of the spruce wood gasified using the thermogravimetric analysis device, char conversion models were evaluated against the measured data and an empirical model was developed which uses the concentration of calcium and potassium in wood to predict the conversion rate behavior of the char when gasified in CO_2. The results from the fluidized bed gasification tests of birch wood showed that calcium was the primary active catalyst in the wood and the increased reactivity resulting from calcium doping was clear even in the much larger scale of a fluidized bed compared to the thermogravimetric analysis. The potassium doped samples did not exhibit increased reactivity in the fluidized bed due a nonreactive layer of secondary char being deposited on the char surface.

The behavior of arsenic in the product gas of chromated-copper arsenate wood was modeled using equilibrium calculations and measured experimentally in a bubbling fluidized bed. The equilibrium model accurately predicted that the product gas could be cleaned by cooling the gas below 260°C and filtering to remove condensed arsenic.

While there are methods for modeling the effects of inorganics in catalyzing char gasification, further research into interconnected issues of surface area, pore sizes, pyrolysis conditions and inorganic concentrations is needed. Similarly, while equilibrium modeling has been shown to predict the behavior of arsenic during gasification in some cases, there are many gaps in understanding which arsenic compounds are most relevant.

Preface

This study was carried out at the Department of Chemistry of the University of Jyväskylä (2012-2014) and the Department of Chemistry and Bioengineering at Tampere University of Technology (2015-2016). Funding for this work from the Academy of Finland through the GASIFREAC project and the Doctoral Program in Energy Efficiency and Systems (EES) is gratefully acknowledged. The financial support of Department of Chemistry and Bioengineering at Tampere University of Technology is also appreciated.

I would like to express my appreciation to my supervisor, Prof. Jukka Konttinen, for giving me the opportunity to pursue this work. I owe special thanks to my colleague Tharaka Doddapaneni for his assistance at various points throughout the process. I would also like to thank Dr. Nikolai DeMartini, Prof. Alberto Gómez Barea, Dr. Antero Moilanen, Associate Prof. Kentaro Umeki and Magnus Perander for their valuable guidance in the experimental, modeling and analysis work. In addition I am grateful to the entire staff of the Department of Chemistry at the University of Jyväskylä and the Department of Chemistry and Bioengineering at Tampere University of Technology for helping with so many practical matters. The Laboratory of Inorganic Chemistry at Åbo Akademi and the Bioenergy Group at the University of Seville were also essential to the completion of the experimental measurements. Mari Honkanen's assistance with performing the SEM images and Henrik Romar's assistance with the BET surface area measurements were also extremely helpful.

Finally I would like to thank my family and my wife Tähti Pohjanmies for their support throughout the past years.

Jyväskylä, November 16, 2016
Jason Kramb

Contents

Abstract **i**

Preface **iii**

Acronyms **vii**

Nomenclature **ix**

List of Publications **xi**

1 Introduction **1**

2 Background **5**
2.1 Char gasification reactions 5
2.2 Role of surface area in gasification rate 9
2.3 Role of arsenic in char gasification 12

3 Modeling methods **15**
3.1 Char conversion modeling 15
3.2 Char conversion models involving catalysts 16
3.3 Hybrid random pore model 17
3.4 Arsenic equilibrium modeling 18

4 Experimental methods **21**
4.1 Sample preparation 21
4.2 TGA measurements 22
4.3 Fluidized bed measurements 22
4.4 Char analysis 26
4.5 Isolating char gasification in TGA measurements with simultaneous devolatilization and char gasification 27

5 Results and discussion **33**
5.1 Char reactivity measurements 33
5.2 Arsenic removal from gasification product gas 59

6 Conclusion **67**

Bibliography **69**

Publications **83**

Acronyms

BET	Branauer, Emmett and Teller
BJH	Barret-Joyner-Halenda
BW	Birch wood
CCA	Chromated copper arsenate
EDS	Energy-dispersive X-ray spectroscopy
FB	Fluidized bed
GM	Grain model
HRPM	Hybrid random pore model
ICP-OES	Inductively coupled plasma optical emission spectrometry
MRPM	Modified random pore model
PS	Pine sawdust
RPM	Random pore model
SEM	Scanning electron microscope
SSA	Specific surface area
SW	Spruce wood
TGA	Thermogravimetric analysis
TSA	Total surface area
UCM	Uniform conversion model

Nomenclature

a	Fitting parameter of the modified random pore model	-
A	Arrhenius prefactor	s^{-1}
b	Fitting parameter	-
c	Fitting parameter of the modified random pore model	-
E_a	Activation energy	kJ mol^{-1}
F	Structural term of conversion rate equation	-
g	Fitting parameter	-
k	kinetic coefficient	s^{-1}
K_r	Kinetic term of conversion rate equation	s^{-1}
L	Pore length	m
p	Partial pressure	Pa
r	instantaneous reactivity	s^{-1}
S	Specific surface area	m^2 g^{-1}, m^2 m^{-3}
t	Time	s
T	Temperature	K
w	Mass concentration in original biomass	g kg^{-1}
X	Conversion	-
y	Mass fraction	g g^{-1}
ϵ	Porosity	-
ξ	Catalytic decay term in parallel reaction model	-
ρ	Density	kg m^{-3}
ψ	Random pore model structural term	-

Subscripts

0	Initial
b	Bulk
ccg	Catalytic char gasification
ch	Char
dev	Devolatilizaiton
g	Mass basis
ncg	Non-catalytic char gasification
v	Volume basis
vol	Volatile

List of Publications

I Jason Kramb, Jukka Konttinen, Alberto Gómez-Barea, Antero Moilanen, Kentaro Umeki, "Modeling biomass char gasification kinetics for improving prediction of carbon conversion in a fluidized bed gasifier," *Fuel*, vol 132, pp. 107-115 2016.

II Jason Kramb, Nikolai DeMartini, Magnus Perander, Antero Moilanen, Jukka Konttinen, "Modeling of the catalytic effects of potassium and calcium on spruce wood gasification in CO2," *Fuel Processing Technology*, vol 148, pp- 50-59 2016

III Jason Kramb, Jukka Konttinen, Rainer Backman, Kari Salo, Michael Roberts, "Elimintaion of arsenic-containing emissions from gasification of chromated copper arsenate wood", *Fuel*, vol. 181, pp. 319-324 2016

IV Jason Kramb, Alberto Gómez-Barea, Nikolai DeMartini, Henrik Romar, Tharaka Doddapaneni, Jukka Konttinen, "The effects of calcium and potassium on CO2 gasification of birch wood in a fluidized bed", *Submitted to Fuel in October 2016*

Author's Contributions

I The author processed and analyzed the experimental data, wrote the reactor modeling program, and wrote the manuscript.

II The author did the data analysis, model fitting, and wrote the manuscript; in addition, the author was involved in planning the experimental measurements.

III The author did the analysis of the modeling and experimental results and wrote the manuscript.

IV The author planned the measurements, conducted the fluidized bed experiments, did the analysis of the results and wrote the manuscript.

1 Introduction

Gasification is a thermochemical conversion process in which solid fuels are converted into usable gas, often called syngas. The conversion process is accomplished by heating the solid fuel in a reactor with limited oxygen supply. A fraction of the fuel is combusted, providing energy needed by the endothermic gasification reactions which convert the remaining fuel into the product gas. Gasification as a process involves a number of steps which begin to occur once the fuel is injected into the reactor. The steps are generally considered to be: fuel drying, devolatilization, and char gasification.

A simplistic schematic of the process is shown in Figure 1.1 which depicts the steps occurring in a linear fashion; in reality this is not the case and steps are all interconnected and overlapping. Devolatilization involves the release of volatiles and the formation of solid char. Volatiles consist of a number of different compounds including tars, light hydrocarbons, and volatile gases (CO_2, CO, CH_4, H_2). Char consists primarily of solid carbon and ash, though there are typically small amounts of hydrogen and oxygen as well. Char gasification is usually the slowest of the steps shown in Figure 1.1 and so can be considered the rate limiting step of the gasification process. Char can contain as much as 25% of the energy content of the original fuel for biomass [9] and so obtaining good char conversion is essential to achieving high overall efficiency.

Gasification of solid fuels is of increasing interest for its ability to produce a gaseous product from a solid fuel which can be used in many applications in which the original feedstock cannot, such as production of chemicals or transport fuels. In addition, gasification can be used as an efficient method for heat and power production. Biomass gasification has been observed to be well suited for production of automotive fuels [138] and co-generation of heat, power and fuels is particularly attractive [5]. In addition to the flexibility of gasification for different end uses, higher potential energy efficiency and environmental benefits are also often cited as advantages over direct combustion [46, 104]. Gasification has also been shown to be potentially more suitable for CO_2 capture than direction

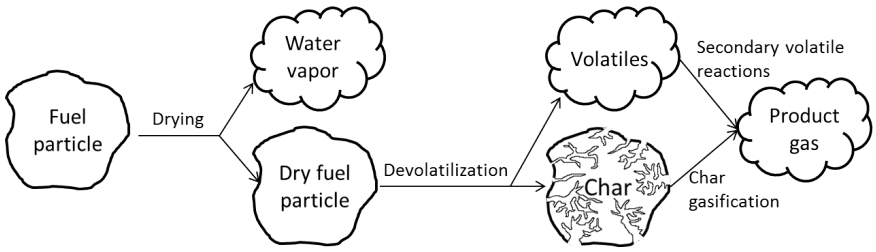

Figure 1.1: A simplified schematic of the overall fuel gasification process showing the steps of: drying, devolatilization and char gasification.

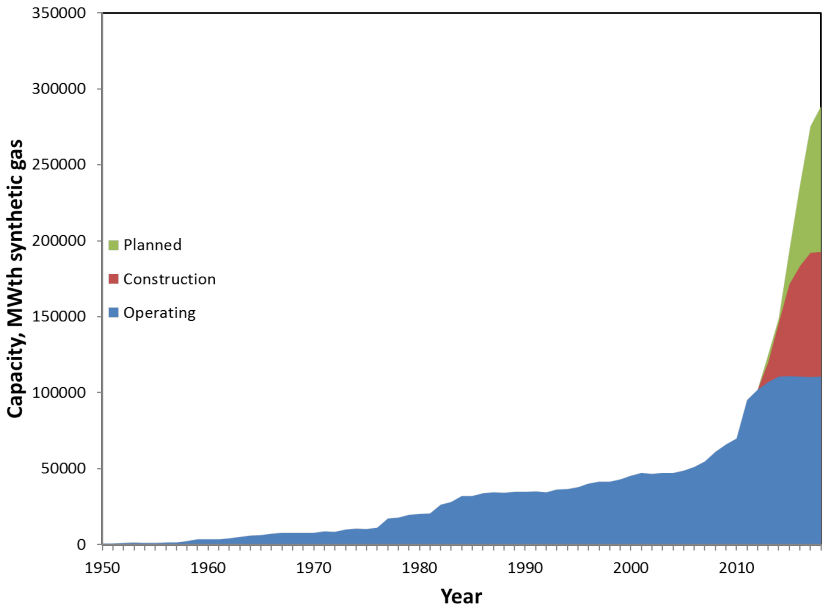

Figure 1.2: The worldwide gasification capacity separated in three categories: operating capacity, under construction capacity and planned capacity. Data was taken from the Gasification & Syngas Technologies Council [1].

combustion in some situations [122].

The increasing interest in gasification is shown by the increasing installed gasification capacity worldwide, which can be seen in Figure 1.2 where the historical development of the worldwide gasification capacity and estimated growth through 2017 is shown. It is estimated that between 2010 and 2017 the gasification capacity will nearly double. However, the vast majority of the current and planned gasification capacity uses coal as the fuel [1] and biomass gasification still lags far behind.

In a general review of biomass gasification research and technologies by Kirkels and Verbong [61], it was shown that while overall gasification research peaked in the early 1980s (as indicated by scientific publications and patent filings), scientific research into biomass gasification has been steadily increasing since the late 1990s. This is a result of the increasing value placed on biomass as a renewable and, for many countries, domestic energy source. In addition, biomass can offer significant environmental benefits over fossil fuels, such as reduced greenhouse gas emissions, when projects are implemented and managed responsibly.

Forest based biomass is generally considered carbon neutral by both EU [11] and US [18] regulations at the present time. This classification is highly controversial as multiple studies have shown that the carbon balance for forest based biomass is not straightforward and must consider issues such as the properties of the forest from which the biomass is obtained [17, 134]. Because the origin of the biomass must be considered, the carbon balance for bioenergy should be determined on a case by case basis. While greenhouse gas reductions for forest biomass compared with fossil fuels can be dramatic, potentially up to 90% [17], most reductions are only seen over the long term and there is often little

benefit in emission reductions in the short or medium term [134]. In cases where forests with high carbon stocks are cleared and used for energy production there can be negative impacts when compared with fossil fuel use. Despite these complications, there remains a strong case for using biomass from sustainably managed sources for reducing greenhouse gas emissions. Governments have included bioenergy in plans to reach greenhouse gas emissions reduction targets [87] and it is commonly predicted that bioenergy will see growth throughout the world [3, 19].

Research into improving overall gasification efficiency and reducing potential harmful emissions is important to find ways to reduce the costs of gasification and allow for a wider variety of fuels to be used. These advancements are necessary for biomass gasification to play an important role in future sustainable energy production. Inorganic elements which are found in biomass and biomass derived fuels play a major role in determining the char behavior and toxic emissions. Accurate models for predicting the behavior of inorganics in biomass fuels are essential for overcoming some of the challenges facing widespread use of biomass gasification and for the cost-effective design of large-scale gasifiers. Improving the usefulness of these models includes, for example, appropriate model selection and accurate parameter fitting.

In this work the effect of two common, naturally occurring elements, calcium and potassium, on wood gasification is studied. These two ash-forming elements were chosen for this work because they, along with silicon, typically occur in the highest concentrations in most biomasses. This was studied by leaching the naturally occurring ash-forming elements from wood samples and then adding back varying amounts of potassium or calcium. These woods were then gasified in either a thermogravimetric analysis device or a bubbling fluidized bed. From these measurements the char conversion rate was calculated and the effects of the ash-forming elements on the char conversion determined. Char conversion models were fit to the experimental data. In addition, the behavior of arsenic in the product gas of wood gasification is investigated using equilibrium modeling and experimentally in a bubbling fluidized bed reactor. Specifically, the work aims to answer the following questions: does adding measured amounts of potassium and calcium to wood result in predictable changes in char reactivity during gasification; and can arsenic emissions from gasification of highly contaminated wood be accurately predicted by equilibrium modeling.

An overview on important background topics is given in Chapter 2, with a focus on char gasification reaction schemes and the role of surface area in char gasification. Chapter 3 presents the modeling techniques used for describing char conversion, the effects of inorganics on char gasification reaction rates, and equilibrium modeling of arsenic behavior. The experimental equipment and methods used in this work are described in Chapter 4. Chapter 5 presents the results of the char reactivity and arsenic behavior research performed in this thesis, including a thorough discussion in the context of earlier research. Finally, Chapter 6 summarizes the main findings and their implications.

2 Background

Numerous literature reviews have been published on many of the topics which are discussed in the present work. For example, Lahijani et al. have reviewed literature on the Boudouard reaction [77], focusing on the char characteristics which affect gasification reactivity and the kinetics of CO_2 gasification. Steam gasification has been reviewed by de Lasa et al. [22] who covered a broader selection of topics, including the design and operation of steam gasifiers as well as the thermodynamics and kinetics of steam gasification. Nzihou et al. have reviewed catalysts for biomass gasification [101] and Di Blasi has reviewed the literature on char gasification and combustion [23]. Shifting to reactor models, Puig-Arnavat et al. [106] have reviewed biomass gasification models and Gómez-Barea and Leckner [38] focused on models for biomass gasification in fluidized beds. In this chapter the literature which is most relevant to the present work is reviewed, focusing on topics which complement the existing literature reviews.

2.1 Char gasification reactions

Char gasification is a heterogeneous conversion process during which solid char reacts with the surrounding gas. Typically in char gasification the gasifying gas is H_2O or CO_2. The main global heterogeneous reactions which occur during carbon gasification are given in Reactions R1-R5,

$$\mathrm{C(s)} + \mathrm{CO_2(g)} \rightleftharpoons 2\,\mathrm{CO(g)} \qquad \Delta H_{R1} = 170\,\mathrm{kJ/mol} \tag{R1}$$

$$\mathrm{C(s)} + \mathrm{H_2O(g)} \rightleftharpoons \mathrm{H_2(g)} + \mathrm{CO(g)} \qquad \Delta H_{R2} = 136\,\mathrm{kJ/mol} \tag{R2}$$

$$\mathrm{C(s)} + 2\,\mathrm{H_2(g)} \rightleftharpoons \mathrm{CH_4(g)} \qquad \Delta H_{R3} = -91.0\,\mathrm{kJ/mol} \tag{R3}$$

$$\mathrm{C(s)} + 0.5\,\mathrm{O_2(g)} \longrightarrow \mathrm{CO(g)} \qquad \Delta H_{R4} = -111\,\mathrm{kJ/mol} \tag{R4}$$

$$\mathrm{C(s)} + \mathrm{O_2(g)} \longrightarrow \mathrm{CO_2(g)} \qquad \Delta H_{R5} = -395\,\mathrm{kJ/mol}, \tag{R5}$$

where the reaction enthalpies are given for 850°C. Reactions R1 and R2 are the primary gasification reactions, showing the Boudouard reaction and water-gas reaction, respectively. Reaction R3 shows the formation of methane through hydrogen gasification. Reactions R4 and R5 show partial and full combustion, respectively. The reaction enthalpies are taken from Prins et al. [105] and Gómez-Barea and Leckner [38]. The values will vary slightly depending on the source and the conditions for which they are reported. Reactions R1 and R2 are endothermic, in contrast with Reactions R3-R5. Additionally, the gasification reactions will occur much slower than the combustion reactions at a given temperature. The current work deals primarily with gasification reactions R1 and R2.

2.1.1 Non-catalytic carbon gasification reaction schemes

The global reactions R1 and R2 have been studied extensively for a variety of fuels and simplified reaction mechanisms have been proposed for uncatalyzed char gasification, or catalyzed char gasification where the behavior of the catalyst is not explicitly accounted for. For example, Mayers [84] proposed the following steps for the Boudouard reaction:

$$\mathrm{CO_2} + \mathrm{C}_f \rightleftarrows \mathrm{CO} + \mathrm{C(O)} \tag{R6}$$
$$\mathrm{C(O)} \longrightarrow \mathrm{CO}. \tag{R7}$$

Free carbon sites where the gasification reaction can take place are represented by C_f and C(O) is an adsorbed oxygen on the char surface which is occupying the reaction site. Reactions R6 and R7 have been used in numerous works to describe the uncatalyzed gasification of carbon or char by $\mathrm{CO_2}$ [7, 29, 62, 74, 81, 132]. When using this reaction mechanism it is commonly thought that the desorption of CO from the char surface by R7 is relatively slow compared to the other steps [129].

Walker et al. [129] proposed a more general reaction scheme:

$$\mathrm{C}_f + \mathrm{CO_2} \rightleftarrows \mathrm{C(CO_2)} \tag{R8}$$
$$\mathrm{C}_f + \mathrm{C(CO_2)} \rightleftarrows \mathrm{C(O)} + \mathrm{C(CO)}_A \tag{R9}$$
$$\mathrm{C}_f + \mathrm{C(O)} \rightleftarrows \mathrm{C(CO)}_B \tag{R10}$$
$$\mathrm{C(CO)}_A \rightleftarrows \mathrm{CO}_{(g)} + \mathrm{C}_f \tag{R11}$$
$$\mathrm{C(CO)}_B \rightleftarrows \mathrm{CO}_{(g)} + \mathrm{C}_f \tag{R12}$$
$$\mathrm{CO}_{(g)} + \mathrm{C}_f \rightleftarrows \mathrm{C(CO)}_C. \tag{R13}$$

Here $\mathrm{C(CO_2)}$ is a chemisorbed $\mathrm{CO_2}$ molecule on the char surface and C(CO) is an chemisorbed carbon monoxide molecule. The subscripts A, B and C indicated different carbon sites for the chemisorption. Walker et al. simplified these steps using the assumptions that $\mathrm{C(CO_2)}$ and $\mathrm{C(CO)}_A$ decompose quickly (i.e. the forward rates of R9 and R11 are relatively large) and R10 is relatively slow compared to R12, which results in

$$\mathrm{C}_f + \mathrm{CO_2} \rightleftarrows \mathrm{C(O)} + \mathrm{CO}_{(g)} \tag{R14}$$
$$\mathrm{C(O)} \rightleftarrows \mathrm{CO}_{(g)} \tag{R15}$$
$$\mathrm{CO}_{(g)} + \mathrm{C}_f \rightleftarrows \mathrm{C(CO)}. \tag{R16}$$

This can be further simplified if the backwards rate of R15 is negligible and R16 does not contribute significantly, which gives Reactions R6 and R7.

A reaction mechanism such as R6 and R7 or R8-R13 is also used implicitly when a kinetic expression which derives from this form of mechanism is used. Perhaps the most common kinetic expression for char gasification in $\mathrm{CO_2}$ is given by Equation 2.1 [35],

$$r_{\mathrm{CO_2}} = \frac{k_1 p_{\mathrm{CO_2}}}{1 + k_2 p_{\mathrm{CO}} + k_3 p_{\mathrm{CO_2}}}, \tag{2.1}$$

where $p_{\mathrm{CO_2}}$ is the partial pressure of $\mathrm{CO_2}$ and p_{CO} is the partial pressure of CO. The derivation of this rate expression from the reaction steps R6 and R7 can be found, for example, in Walker et al. [129].

A similar oxygen-exchange mechanism has been proposed for steam gasification [40],

$$H_2O + C_f \rightleftarrows H_2 + C(O) \quad \text{(R17)}$$

$$C(O) \longrightarrow CO, \quad \text{(R18)}$$

which will lead to a kinetic expression similar to Equation 2.1,

$$r_{H_2O} = \frac{k_1 p_{H_2O}}{1 + k_2 p_{H_2} + k_3 p_{H_2O}}, \quad (2.2)$$

where p_{H_2O} and p_{CO} are the partial pressures of H_2O and H_2 respectively. A brief discussion of some of the variations of the steam gasification mechanisms is given in Di Blasi [23].

Equations 2.1 and 2.2 are commonly referred to as Langmuir-Hinshelwood kinetic expressions. Due to the reversibility of, for example, Equations R6 and R17, CO and H_2 will have an inhibiting effect on the gasification reactions. This inhibiting effect is accounted for in the $k_2 p_{CO}$ and $k_2 p_{H_2}$ terms of Equations 2.1 and 2.2.

According to CO_2 gasification shown in R6 and R7 and H_2O gasification in R17 and R18, both CO_2 and H_2O gasification involve a carbon-oxygen surface complex which desorps as a CO molecule. Karlström et al. [58] have shown that this desorption occurs in the same way for both CO_2 and H_2O gasification, and so the surface complex formed by each can be interchanged, meaning that R7 and R18 are effectively the same. This allows for a relatively simple reaction mechanism to be developed which includes both CO_2 and H_2O gasification. Tilghman and Mitchell [121] demonstrate one example of this, by presenting an eighteen step reaction mechanism which covers both carbon gasification by CO_2 and H_2O as well as oxidation by O_2.

2.1.2 Char gasification reaction schemes including catalysts

While considering uncatalyzed carbon gasification allows for simplifications which aid in the understanding of the underlying physical processes, it does not reflect the reality of biomass char gasification. It has been proposed that both the location of the carbon atom in the char structure and interactions with inorganics in the char will determine whether, and to what extent, a carbon site is 'active' [16, 88, 129, 131]. Biomass fuels typically contain 5-20% ash-forming elements by weight, with calcium, silicon, and potassium being the most common [127]. Significant amounts of these ash-forming elements will be retained in the char which means that for real chars, which are not pure carbon, the observed gasification behavior will deviate from the uncatalyzed carbon. In biomass chars which contain impurities it becomes important to understand what determines the number of active carbon sites and whether all active carbon sites behave in the same way. It is often thought that catalytic effects due to ash-forming elements play the primary role in determining the reactivity of different biomass chars [23]; however, there are some studies which report the surface area is, in fact, the major contributor rather than catalytic effects [26, 45]. Still others conclude that neither the inorganic content or surface areas are the primary determinants of char reactivity, but rather crystalline structure of the carbon has the largest role [49]. There is no general consensus on the exact role catalysts play in the gasification reactions, however reaction mechanisms which explicitly show the role of catalysts in carbon gasification have been proposed by a number of researchers.

Moulijn et al. reviewed the early proposed mechanisms for potassium catalyzation of CO_2 gasification [94]. In that work it was concluded that the following reaction mechanism

was the most likely:

$$\mathrm{CO_2} + \mathrm{K}_x\mathrm{O}_y \rightleftarrows \mathrm{CO} + \mathrm{K}_x\mathrm{O}_{y+1} \tag{R19}$$
$$\mathrm{K}_x\mathrm{O}_{y+1} + \mathrm{C} \rightleftarrows \mathrm{K}_x\mathrm{O}_y + \mathrm{C(O)} \tag{R20}$$
$$\mathrm{C(O)} \rightleftarrows \mathrm{CO} \tag{R21}$$

In this mechanism the exact form of $\mathrm{K}_x\mathrm{O}_y$ is not known. It was proposed by Moulijn et al. that the same basic mechanism would apply for $\mathrm{H_2O}$ and $\mathrm{O_2}$ reactions with carbon as well. Moulijn et al. also summarizes the evidence that when potassium is added to char as potassium carbonate, the $\mathrm{K_2CO_3}$ on the char surface will decompose below the melting temperature of bulk $\mathrm{K_2CO_3}$. This decomposition will release $\mathrm{CO_2}$ and result in the formation of a potassium oxide on the char surface, of which the exact composition is not known.

Chen and Yang [16] gave a more recent summary of the catalytic mechanisms of alkali and alkaline earth metals for carbon gasification. The authors proposed a new reaction mechanism for uncatalyzed and catalyzed gasification which was developed from molecular orbital calculations and their review of experimental results. A slightly modified version of the mechanism can be expressed as:

$$\mathrm{CO_2} + \mathrm{M}_x\mathrm{O}_y \rightleftarrows \mathrm{CO} + \mathrm{M}_x\mathrm{O}_{y+1} \tag{R22}$$
$$\mathrm{M}_x\mathrm{O}_{y+1} + \mathrm{C}_f \rightleftarrows \mathrm{C}_f(\mathrm{M}_x\mathrm{O}_{y+1}) \tag{R23}$$
$$\mathrm{M}_x\mathrm{O}_{y+1} + \mathrm{C}_f(\mathrm{M}_x\mathrm{O}_{y+1}) + \mathrm{C} \rightleftarrows \mathrm{C}(\mathrm{M}_x\mathrm{O}_{y+1})\mathrm{C}_f(\mathrm{M}_x\mathrm{O}_{y+1}) \tag{R24}$$
$$\mathrm{C}(\mathrm{M}_x\mathrm{O}_{y+1})\mathrm{C}_f(\mathrm{M}_x\mathrm{O}_{y+1}) \longrightarrow \mathrm{CO} + \mathrm{CC}_f(\mathrm{M}_x\mathrm{O}_{y+1}) + \mathrm{M}_x\mathrm{O}_y \tag{R25}$$
$$\mathrm{CC}_f(\mathrm{M}_x\mathrm{O}_{y+1}) \longrightarrow \mathrm{CO} + \mathrm{C}_f + \mathrm{M}_x\mathrm{O}_y + \mathrm{C} \tag{R26}$$

where $\mathrm{C}_f(\mathrm{M}_x\mathrm{O}_{y+1})$ and $\mathrm{C}(\mathrm{M}_x\mathrm{O}_{y+1})\mathrm{C}_f(\mathrm{M}_x\mathrm{O}_{y+1})$ are different oxygen complexes, $\mathrm{M}_x\mathrm{O}_y$ and $\mathrm{M}_x\mathrm{O}_{y+1}$ are the catalyst clusters, and C_f is an edge carbon. This mechanism would apply for uncatalyzed gasification if the catalyst cluster is removed and the oxygen surface complexes will become $\mathrm{C}_f(\mathrm{O})$ and $\mathrm{C(O)C}_f\mathrm{(O)}$ respectively.

Two recent works have proposed additional mechanisms, each supported by experimental observations. Kopyscinski et al. [67] proposed the following steps for potassium carbonate catalysizing coal char gasification in $\mathrm{CO_2}$:

$$2\,\mathrm{KOC} \longrightarrow 2\,{\sim}\,\mathrm{K} + 2\,\mathrm{CO} \tag{R27}$$
$$2\,{\sim}\,\mathrm{K} + 2\,\mathrm{C}_f \longrightarrow 2\,\mathrm{KC} \tag{R28}$$
$$2\,\mathrm{KC} + \mathrm{CO_2} \longrightarrow \mathrm{KC} + \mathrm{KOC} + \mathrm{CO} \tag{R29}$$
$$\mathrm{KC} + \mathrm{KOC} + \mathrm{CO_2} \longrightarrow 2\,\mathrm{KOC} + \mathrm{CO}. \tag{R30}$$

In this scheme ${\sim}\,\mathrm{K}$ represents a reduced potassium surface complex whose precise chemical composition and structure are unknown. The potassium cluster transfers to a new carbon site in reaction R28 and is oxidized, releasing CO, in R29 and R30.

Zhang et al. [137] reported that electron transfer occurs between aromatic carbon to the catalyst and that a K-Char intermediary is formed. The following reaction steps were proposed for catalytic steam gasification:

$$\mathrm{K_2CO_3} + 2\,\mathrm{Char} \rightleftarrows 2\,\mathrm{K{-}Char} + \mathrm{CO_2} \tag{R31}$$
$$\mathrm{K{-}Char} + \mathrm{H_2O} \longrightarrow \mathrm{K{-}Char{-}O} + \mathrm{H_2} \tag{R32}$$
$$\mathrm{K{-}Char{-}O} \longrightarrow \mathrm{K{-}Char} + \mathrm{CO}. \tag{R33}$$

Many studies have reported that the apparent activation energy of char gasification reactions is not dependent on the catalyst loading of the char [54, 85], however others have reported the opposite [128]. In other cases the results are somewhat mixed, for example Hanaoka and Okumura [43] reported that chars made from demineralized wood had lower activation energy than chars containing metal catalysts, but the amount of catalyst in the char did not always correlate to the measured activation energy.

Among the studies which reported that inorganic catalysts affect the activation energy, both positive and negative correlations have been observed. For example, an increase in activation energy when catalysts are present was reported by Kopyscinski et al. [66]. Lahijani et al. [76] and Floess et al. [32] reported the opposite effect, that adding metal catalysts decreased the activation energy when compared to demineralized chars. Koening et al. [63] also reported that potassium lowered the activation energy of CO_2 gasification, in particular for the desorption of CO step (i.e. reaction R15). Marquez-Montesinos et al. reported that washed chars had lower activation energies than unwashed chars [83] for chars made from grapefruit skins, though the difference was not large. It has been theorized that the effect of catalyst loading on activation energy my be due to a temperature dependence on the number of active sites, rather than a change in the activation energy of the actual reaction steps [57].

After 60 years of research there is no clear consensus on the exact role of catalysts during carbon gasification. There are a variety of proposed mechanisms, each supported by some experimental evidence, however none seem to satisfy all the outstanding questions (e.g. do inorganics change the reaction mechanism or only increase the number of active reaction sites, does the activation energy of the gasification reaction change as a function of catalyst concentration, what is the active catalyst species on the char surface, etc.).

2.2 Role of surface area in gasification rate

Char gasification is a heterogeneous reaction between the solid char and gas phase, and it is generally thought to occur on the surface of the char. The common modeling approach for char gasification is to assume that for a given temperature, pressure and gas composition the reaction rate is constant, and that the gasification rate will vary with the changing surface area which is available for the reactions to take place. There have been, generally, two ways of quantifying the surface area over which the heterogeneous gasification reactions take place: the total physical surface or the active surface. These two measures of surface area lead to two different formulations of the reaction rate: the surface reaction rate, which is the reaction rate per unit surface area; and the intrinsic reaction rate, which is the reaction rate per active site.

2.2.1 Total surface area vs active surface area

The total surface area (TSA) of a char particle includes the outer char surface and the internal pore surfaces. The specific surface area (SSA) is typically reported instead of TSA, which is the TSA per unit mass of char. The measured value of SSA will depend on the measurement technique used and the pore size range which is covered by the measurement. Surface area measurements using Branauer, Emmett and Teller (BET) theory and N_2 gas is a common way of reporting SSA for chars [76, 109, 133], but there is some disagreement about whether that is the most relevant way to measure the property [31]. Sing [114] has also reviewed the use of N_2 adsorption for characterizing porous materials in the general case. Some studies include surface area measured with CO_2 adsorption either in place of

or in addition to N_2 surface area [37, 73, 118] because measuring with CO_2 will include pores smaller than 1.5 nm, which is typically the smallest pore diameter included in N_2 surface area measurements. In some cases surface area measurements are reported but details, such as the adsoprtion gas, are left out [95, 113], making interpretation of the results difficult.

Regardless of the adsorbate gas being used, the basic process for measuring total surface by physical adsorption is typically the same. First, any existing physically adsorbed molecules on the sample surface must be removed, such as by outgassing. The amount of adsorbate gas (e.g. N_2) which is adsorbed on the surface of the sample is measured at various conditions. The adsorbate gas is held to the surface by a weak Van der Waals attraction between the gas molecules and the sample surface. The relationship between the amount of adsorbed gas and the pressure can then be used to calculate the surface area, for example by using the BET theory.

The concept of active surface area (ASA) has been applied to carbon gasification since at least the early 1960s [78]. It has been clear since then that ASA is in many cases more useful than TSA in understanding the behavior of carbon during gasification. Because the exact form of the carbon-oxygen surface complex on the char surface is not known, it is difficult to obtain a true area value for the active surface area. Rather than measuring the active surface area, typically the amount of a chemisorbed gas is reported and the chemisorbed gas is assumed to be directly proportional to the the number of active sites. However, some studies have tried to report the active surface area of chars by making assumptions about the behavior of the chemisorbed gas on the char surface, such as Molina et al. where the chemisorbed CO_2 is assumed to occupied an area of 0.17 nm^2 [92].

Measuring the ASA of chars is a less established process than TSA and so there is less standardization of the measurement technique. In some ways the measurement is similar to that of the TSA, in that the amount of adsorbed gas on the sample surface is measured. In the case of ASA the gas is chemically adsorbed to the solid surface, however. Typically the measurement is done at elevated temperatures, in contrast to the cryogenic temperatures of TSA measurements. One method for ASA measurement involves measuring the mass change of a sample when the atmosphere is switched from a gas which is inert to a gas which will chemically adsorb to the solid surface [140]. The amount of adsorbed gas is determined from the mass change of the sample. This is related to the ASA by the stoichiometry and and size of the formed surface complex, which often must be guessed, as mentioned above.

It is often assumed that TSA is proportional to ASA throughout the char conversion process, but this has been shown to not be generally true [75]. Even for uncatalyzed carbon or char gasification, Kudo et al. [73] reported that BET surface as measured by CO_2 and N_2 did not correlate to non-catalytic gasification rates in steam of leached biomass chars. This is the same result as reported by Kajita et al. [55] for similar leached biomass chars. However it has been shown that TSA can still be used to predict char reactivity during gasification of coal char in CO_2 and O_2 [31]. Huo et al. [49] reported that BET surface had no correlation to the reactivity of five biomass chars and petroleum coke in CO_2 gasification. However, total surface of chars, as measured by BET, is still commonly reported as it is a well understood measurement.

2.2.2 Evolution of surface area during conversion

As gasification reactions occur and solid char is converted to gaseous products the structure of the char matrix evolves. There exist many theories which describe the potential behavior of the char. Typically, it is thought that the pores of the char enlarge as reactions occur on the pore walls and carbon is gasified. Eventually pores enlarge to the point where they overlap and coalesce.

This behaviour of pore growth and coalescence can be described by the random pore model developed by Bhatia and Perlmutter [10], which can be written as

$$S_v = S_{v0}(1 - X_{ch})\sqrt{1 - \psi ln(1 - X_{ch})}, \tag{2.3}$$

where S_v (m^2/m^3) is the SSA at char conversion X_{ch}, S_{v0} (m^2/m^3) is the initial SSA (i.e. at $X_{ch} = 0$) and ψ is a structural constant which can be calculated from

$$\psi = \frac{4\pi L_{v0}(1 - \epsilon_0)}{S_{v0}^2}, \tag{2.4}$$

where L_{v0} and ϵ are the pore length and and porosity, respectively. As can be seen from Equation 2.4, the structural constant can be calculated from measurements of the physical properties of char; however, it is common that ψ is treated as a fitting parameter if fitting the RPM to conversion rate measurements. Surface area measurements are typically made on a mass basis rather than a volumetric basis, and so it can be useful to rewrite Equation 2.3 in such terms,

$$S_g = S_{g0}\sqrt{1 - \psi ln(1 - X_{ch})}, \tag{2.5}$$

where S_g is the SSA on a mass basis (m^2/g) and S_{g0} is the initial SSA on a mass basis (m^2/g). S_v and S_g are related by $S_v = S_g\rho_b = S_g(1 - X_{ch})\rho_{b0}$ where ρ_b is the bulk density of the char and ρ_{b0} is the initial bulk density [31]. S_{v0} and S_{g0} are related by $S_{v0} = S_{g0}\rho_{b0}$. The RPM has been shown to fit well to the measured TSA of a wide range of chars during gasification and combustion [31, 110, 116, 121]. However, as mentioned in Section 2.2.1 there is some debate over the connection of TSA and char reactivity.

In addition to the random pore model there have been a variety of more complicated structural models proposed to describe the evolution of the internal surface of char during conversion. These models typically explicitly account for pores of varying sizes which will behave differently as a result of diffusion effects [6, 30, 115].

There have been many reported measurements of the evolution of coal char structure during conversion, for example the measurements of Feng and Bhatia [31], and there is also some data available on biomass char surface areas during conversion. Figure 2.1 shows a compilation of BET surface area measurements for biomass chars as a function of char conversion taken from literature sources. With the exception of the two leached cedar chars the surface area evolution shows significant similarity between the chars. The RPM was fit to the measured surface area values, excluding the leached chars, which gave a value for ψ of 7.4. The RPM fitting matches most of the measured SSA values well, however the measured values show a trend of leveling off after approximately 60% char conversion which does not happen in the RPM. The sharp increase in SSA predicted by the RPM at the end of char conversion cannot be validated from this data set due to the lack of SSA measurements at char conversion greater than 90%. Both leached chars included in Figure 2.1 show initial surface areas which are similar to the non leached chars.

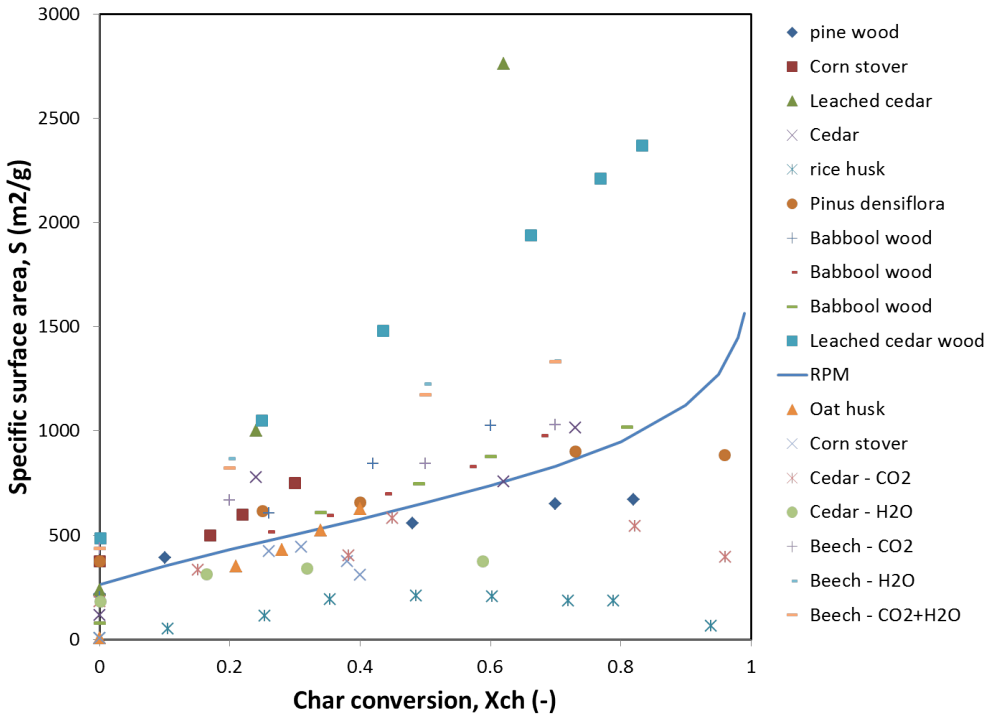

Figure 2.1: Measured BET surface areas for various biomass chars as a function of conversion taken from literature sources [34, 42, 73, 82, 110, 116, 120, 121].

However already at 20% char conversion the leached chars show significantly higher SSA values. The difference between the SSA of the leached chars and the non leached chars grows as conversion progresses. The larger SSA of leached chars is generally explained by inorganics blocking some pores of the char, and these inorganics are removed in the leaching process [83].

2.3 Role of arsenic in char gasification

While calcium, potassium, silicon and magnesium are generally the most common inorganic elements found in forest based biomass [50], other elements can be present in smaller amounts and these may have important implications on the operation of a gasifier. The fate of trace fuel elements, including arsenic, in combustion systems has been studied extensively. Gasification conditions have been studied to a lesser extent. Arsenic, and many other trace elements, can have severe health and environmental consequences and much of the research involving these elements has focused on reducing emissions of volatile metals in exit gases or preventing leeching of metals from the ashes where the metals have concentrated. While most metals will remain in the ash and therefor leave the reactor through the bottom ash (or potentially cyclone ash), arsenic has been identified as one which can potentially escape as vapor [100].

Chromated copper arsenate wood (CCA) is a chemically treated wood used for a variety of demanding applications. The wood contains elevated levels of arsenic, chromium

and copper which can pose disposal problems. Helsen and Van den Bulck [44] reviewed disposal technologies for CCA wood and found that gasification of CCA wood can be an attractive option but gas cleaning is a key obstacle. Cleaning of the product gas by cooling below the condensation temperature of the contaminants (i.e. As, Cd, Cr, Cu, Co, Hg, Mn, Ni, Pb, Sb, V and Zn) has been shown to be possible for waste fuels [65], but it is essential to know what the condensation temperature will be. This can be difficult as the form of various contaminants in the product gas is not always known. Thermodynamic equilibrium modeling has been used to gain insight into the behavior of metals during combustion and gasification [33, 65, 80].

The catalytic effect of arsenic on char gasification has been studied minimally due to the relatively small amounts of arsenic naturally present in most biomass fuels. When arsenic is present in high levels, it is the prevention of its release into the environment that becomes the primary concern. Hill et al. [47] conducted coal gasification measurements without catalysts and with arsenic as a catalyst. The results indicated that arsenic did increase coal gasification reactivity but the effect was relatively minor.

It is clear that whatever benefits may occur in the form of increased char reactivity due to arsenic in these fuels are far outweighed by the potential health impacts of arsenic emissions. If contaminated wood is to be used as fuel in gasification systems a thorough understanding of the behavior of toxic elements is necessary. Cost effective gas cleaning options are necessary for these fuels to be used on a large scale.

3 Modeling methods

Char gasification was modeled using char conversion rate models taken from literature. The conversion rate models were evaluated for their ability to describe the behavior of wood chars during gasification as measured using thermogravimetric analysis. An overview of the modeling methods and conversion rate models used is presented below. In addition, a description of the equilibrium model used to predict arsenic behavior is given.

3.1 Char conversion modeling

A complete model for the conversion of a char particle during gasification or combustion involves modeling many interrelated processes, such as the energy balance of the particle, the evolution of the physical structure, and the reaction kinetics on the particle surface. There are many such models in existence with varying levels of complexity. Simplifications can be used for different aspects of the model based on an understanding of the conditions which will be modeled. It is common to simplify the modeling of reactions in porous solids by creating three regimes where in which the rate determining step is different. In Regime I the reaction kinetics are generally slower than the diffusion of the gas to the reaction sites, and so the observed reaction rate is determined by the reaction kinetics. For Regime III the reaction kinetics are much faster than the gas diffusion and so the diffusion rate to the external surface becomes the limiting step. Regime II exits in between these extremes and the observed reaction rate is determined by pore diffusion.

In some combustion systems it is common that the combustion occurs in Regime III, where diffusion at the boundary layer is controlling the reaction rate [38]. If Regime III conditions can be assumed then there is no benefit to include a detailed model of the reactions on the internal pore surfaces. For gasification processes, where the heterogeneous gas-char reactions are slower than the combustion reactions, Regime II conditions are common. If the char particle sizes are small enough inside the gasifier, it may be possible that Regime I conditions exist as well [123]. In these cases it becomes more important to have an accurate model for the surface reaction kinetics.

The conversion of a char particle can be defined as

$$X_{ch} = \frac{m_{ch,0} - m_{ch}}{m_{ch,0}}, \tag{3.1}$$

where $m_{ch,0}$ is the initial mass of the carbon in the char and m_{ch} is the mass of carbon in the char at time t. During the conversion process the instantaneous reactivity of the char can be expressed as

$$r = -\frac{1}{m_{ch}}\frac{dm_{ch}}{dt} = \frac{1}{(1 - X_{ch})}\frac{dX_{ch}}{dt}. \tag{3.2}$$

While there are many approaches to modeling the conversion of char during gasification, it is relatively common to use an equation in the form of Equation 3.3 to express the rate of char conversion as a function of temperature, gas composition, and char conversion,

$$\frac{dX_{ch}}{dt} = f(T, p_i, X_{ch}), \tag{3.3}$$

where T is the temperature of the char particle, and p_i are the partial pressures of the relevant gases. It is common to separate the conversion dependence from the temperature and pressure dependence and write the conversion rate as a product of two independent functions,

$$\frac{dX_{ch}}{dt} = k(T, p_i)F(X). \tag{3.4}$$

The conversion dependent term in Equation 3.4, $F(X_{ch})$, can be replaced with a function which describes the surface structure of the char, such as the RPM given in Equation 2.3. The kinetic term in Equation 3.4 can be replaced with a kinetic model for describing the surface reaction rates. In many cases an nth order reaction is assumed and the kinetic term is expressed as

$$k(T, p_i) = Ae^{-E_a/RT}{p_i}^n. \tag{3.5}$$

In other cases a Langmuir-Hinshelwood expression, such as Equation 2.1 can be used.

Reviews of different forms of $k(T, p_i)$ and $F(X_{ch})$ have been performed elsewhere and so will not be repeated here. For example, many examples of $k(T, p)$ for biomass char gasification and combustion can be found in the review by Di Blasi [23], as well as some examples of $F(X_{ch})$. Some common examples of $F(X_{ch})$, written as $f(X_{ch})(1 - X_{ch})$, can be found in Gómez-Berea and Leckner [38]. Molina and Mondragón [91] also review some common models for char conversion in slightly more detail.

3.2 Char conversion models involving catalysts

While there has been significant work on understanding the role of catalysts during char gasification, the effects of catalysts are rarely accounted for in an explicit manner in char conversion models, as can be seen by the fact that Equation 3.3 has no dependence on inorganic content of the char. Typically the catalytic effects of the ash elements in char are accounted for implicitly, in that if a biomass has significant amounts of catalytic ash elements and in turn has a high reactivity, this will be seen in the pre-exponential factor of the Arrhenius equation. This can be observed in the wide range of pre-exponential terms which can be found in the review by Di Blasi [23].

There has been some attempt to account for the effects of inorganic ash elements by correlating the kinetic term k to the inorganic content of the biomass. This will allow the overall reactivity of the char to be determined by the ash composition, but the shape of the conversion rate curve as determined by F(X) from Equation 3.4 will remain unaffected. Dupont et al. [27] used the grain model (i.e. $F(X) = (1 - X_{ch})^{2/3}$) and developed a correlation relating the pre-exponential factor in the Arrhenius equation of k for steam gasification to the potassium and silicon concentrations of 19 woody biomasses. The resulting model is given by,

$$\frac{dX_{ch}}{dt} = 8.77 \cdot 10^4 exp(\frac{-167000}{RT})(0.1812\frac{y_K}{y_{Si}} + 0.5877)p_{H_2O}^{0.6}(1 - X_{ch})^{2/3} \tag{3.6}$$

where y_K and y_{Si} are the potassium and silicon contents of the biomass (kg/kg), respectively. This method of correlating the pre-exponential factor to the ash composition could be theoretically justified by the idea that the inorganics only increase the number of active reaction sites on the char and do not fundamentally change the reaction mechanism. There has been at least one attempt to correlate the activation energy of char gasification to the ash composition, but this was done only for coal chars [36]. The issue of whether the activation energy is affected is debated, as discussed in Section 2.1.2.

In some cases both the kinetic term, k and the conversion dependent term, F(X), will vary based on the inorganic content of the char [48, 117, 139]. For example, Lahijani et al. [76] used the RPM, among other models, to fit conversion rate data from Na loaded char and found that the structural term ψ changed with catalyst loading, as did k. Zhang et al. [139] modified the RPM to include two additional empirical parameters which change the shape of the conversion rate curve to allow for a conversion rate maximum much later in the conversion process than can be achieved with the RPM. This modified random pore model (MRPM) is given by Equation 3.7,

$$\frac{dX_{ch}}{dt} = k(1 - X_{ch})\sqrt{1 - \psi \log(1 - X_{ch})}(1 + (cX_{ch})^a), \tag{3.7}$$

where c and a are the new fitting parameters. This model was shown to fit well to conversion rate curves from 14 different biomass chars. The best fit parameters for those chars also showed a trend that c and a were dependent on the potassium concentration of the char. The parameter ψ had no clear dependence on the ash composition of the chars, however.

3.3 Hybrid random pore model

The random pore model was originally developed to describe the behavior of coal and the assumptions made in the model generally become less applicable in gasification involving high concentrations of catalysts, such as with many types of biomass. It has been observed that during gasification of some biomass chars that there may be first a stage in which the gasification reactions are dominated by the presence of the catalysts [126]. During this stage the catalytic effect is decreasing due to loss of the catalysts from the char surface which was theorized to occur as a result of agglomeration, sintering or vaporization of the catalysts.

Based on this, a hybrid random pore model (HRPM) was developed [70] which combines the catalytic gasification with deactivation of the catalyst stage from Equation 3.9 with the random pore model, resulting in

$$\frac{dX_{ch}}{dt} = k(\alpha \exp(-\xi X_{ch}^2) + (1 - X)\sqrt{1 - \psi \log(1 - X)}). \tag{3.14}$$

In order to separate the temperature and conversion dependent terms it was assumed that $k_{ccg,1}$ from Equation 9 is linearly dependent on kinetic term of the random pore model (i.e. $k_{ccg,1} = \alpha k$). This model describes a gasification process in which the conversion rate is dominated by the behavior of the catalysts at first and later becomes dependent on the growth and coalescence of the pores. A similar model can be developed based on the modified random pore model, resulting in a hybrid modified random pore model (HMRPM)

$$\frac{dX_{ch}}{dt} = k(\alpha \exp(-\xi X_{ch}^2) + (1 - X)\sqrt{1 - \psi \log(1 - X)}(1 + (cX_{ch})^a)). \tag{3.15}$$

Table 3.1: Char conversion equations taken from literature which have been developed to account for the effects of inorganic ash elements on the char conversion rate during gasification or applied to catalyst loaded char samples. The models given by Equations 3.7, 3.9, 3.10, and 3.11 were evaluated for their ability to fit conversion rate data of wood char in the present work. Acronyms have been included for models with a commonly used name. Acronyms: RPM - Random pore model, MRPM - Modified random pore model, GM - Grain model, PRM - Parallel reaction model, ICM - Integrated core model.

Model	$f(T,p_i,X_{ch}) = k(T,p_i)F(X_{ch})$	Eq.	Ref.
RPM	$k(1-X_{ch})\sqrt{1-\psi log(1-X_{ch})}$	(3.8)	[10]
MRPM	$k(1-X_{ch})\sqrt{1-\psi log(1-X_{ch})}(1+(cX_{ch})^a)$	(3.7)	[139]
GM	$8.77\cdot 10^4 \exp(\frac{-167000}{RT})(0.1812\frac{y_K}{y_{Si}}+0.5877)p_{H_2O}^{0.6}(1-X_{ch})^{2/3}$	(3.6)	[27]
PRM	$k_{ccg,1}\exp(-\xi X_{ch}^2)+k_{ncg}(1-X_{ch})+k_{ccg,2}$	(3.9)	[126]
	$k(1-X_{ch})\sqrt{1-\psi log(1-X_{ch})}[1+(g+1)(bt)^g]$	(3.10)	[117]
	$A_{cat}\exp(-\xi t)+Eq.\ 3.10$	(3.11)	[117]
ICM	$k(1-X_{ch})^n$	(3.12)	[48]
	$k_0\exp(-\frac{E_a+\frac{\alpha}{AIk}}{RT})f_1(1-X)$	(3.13)	[36]

3.4 Arsenic equilibrium modeling

Equilibrium modeling was used in order to predict the behavior of arsenic in the product gas of wood containing high concentrations of arsenic. The thermodynamic equilibrium calculations were performed using ChemSheet [68] which minimizes the Gibbs energy of the system using ChemApp [103]. The thermodynamic data used in this work was compiled from several databases by selecting species and compounds relevant to the gasification conditions. In total 199 gas phase compounds and 505 solid or liquid phase compounds were included in the equilibrium calculations. This approach is similar to that used by Konttinen et al. [64, 65] for modeling the behavior of trace elements in gasification systems. A complete list of the arsenic containing compounds included in the modeling work is shown in Table 3.2.

Six cases were modeled using the equilibrium calculation approach described above. Each case considered a different combination of compounds and test conditions. Cases A1, A2 and A3 use the conditions inside the gasifier, which are described in Section 4.3.2. Cases B1, B2 and B3 use the conditions after the gas cleaning where the product gas is cooled from the gasification temperature from 850°C to 260°C. The inputs for B1, B2 and B3 are the outputs from A1, A2, and A3 respectively. The compounds included in the equilibrium calculations were increased stepwise, with cases A1 and B1 having the

Table 3.2: The complete list of arsenic containing compounds considered in the equilibrium model.

Gas	Liquid	Solid
As	As	As_2O_3 arsenolite
As_2	As_2O_3	As_2O_3 claudetite
As_2S_3	As_2S_2	As_2O_5
As_3	As_2S_3	As_2S_2 realgar
As_4		As_2S_3 orpiment
As_4O_{10}		As rhombohedral
As_4O_6		$Ca_3(AsO_4)_2$
As_4O_7		$Cd_3(AsO_4)_2$
As_4O_8		$Co_3(AsO_4)_2$
As_4O_9		$Cu_3(AsO_4)_2$
As_4S_4		$Ni_3(AsO_4)_2$
$AsCL_3$		$Zn_3(AsO_4)_2$
AsH		
AsH_2		
AsH_3		
AsO		
AsO_2		
AsS		

most restricted set of compounds while A3 and B3 included all compounds. For cases A1 and B1 the gas feeds, main components of the fuel feed and trace elements in the fuel were considered, but the main ash components were excluded. Specifically, the elements considered in these cases were: Ar, As, C, Cd, Cl, Co, Cr, Cu, H, Hg, Mn, Mo, Ni, O, Pb, S, Sb, Sb, Ti, V, and Zn. For A2 and B2, all the elements in A1 and B1 were included as well the main ash elements (Ca, Fe, K, Mg, Na, P) but Si was excluded. For cases A3 and B3 all fuel elements were included as well as the bed material.

This stepwise introduction of elements to the equilibrium calculation is based on earlier studies of high temperature behavior of inorganic elements in gasification and combustion systems [69, 108]. It has been shown that equilibrium calculations for some elements will predict the formation of compounds which are not found in real systems due to limited residence times inside the reactor and slow reaction kinetics.

4 Experimental methods

This chapter presents the experimental methods used in the thesis. Wood samples were gasified in a TGA device and bubbling fluidized bed reactor in order to measure char reactivity. Arsenic containing wood was gasified in a different fluidized bed reactor to study the behavior of arsenic in the product gas. Various methods for analyzing properties of chars were also used to understand the char reactivity. Finally an empirical technique for separating the effects of devolatilization and char gasification during TGA measurements is presented.

4.1 Sample preparation

Four general types of wood were used in this work: pine sawdust (PS), spruce wood (SW), birch wood (BW), and chromated copper arsenate (CCA) wood. Proximate and ultimate analysis for these wood samples are given in Table 4.1. The PS, SW and BW contained little to no bark and the PS in particular had very low levels of ash forming elements as can be seen in Table 4.2. The CCA treated wood was supplied by Ekokem Oy.

The SW and BW samples were used to investigate the role of calcium and potassium in char gasification. To do this, samples were created of the two woods which contained varied amounts of Ca and K. The spruce wood was ground and sieved to 125 – 250 μm particle size. The wood samples were leached of the naturally occurring ash forming elements and potassium or calcium were then added back in varying amounts, as described by Perander et al. [102]. The leaching process involved washing the spruce wood with HNO_3 and rinsing with ultrapure water. Adding potassium and calcium to the demineralized wood was done in two ways. The first method involved doping Ca or K to carboxylic or phenolic sites of the wood through an ion-exchange process using either $Ca(NO_3)_2$

Table 4.1: Proximate and ultimate analysis for dry wood samples used in this work. Pine sawdust analysis taken from Moilanen and Saviharju [90], spruce wood analysis from [12]. The * indicates that the mass fraction was not measured and was determined by the mass balance. The - indicates that the property was not measured for that sample.

Sample	Volatile matter, %	Fixed carbon, %	Ash, %	C, %	H, %	N, %	O, %	S, %
Pine sawdust (PS)	83.1	16.8	0.1	51.0	6.0	0.1	42.8*	n.d.
Spruce wood (SW)	85.4	14.6	0.23	50.3	6.2	0.1	43.2	<0.01
Birch wood (BW)	89.5	10.19	0.35	48.9	6.16	<0.05	44.90	<0.05
CCA wood	-	-	9.4	47.0	5.45	0.14	37.25*	0.08

or KNO_3 solutions. The second method of adding Ca or K to the demineralized wood involved impregnating the wood with either K_2CO_3, $CaCO_3$ or CaC_2O_4 [71]. The spruce wood samples were used in TGA measurements described in Section 4.2.

Birch wood samples were prepared in a similar way as the spruce samples. The birch wood was first ground to smaller than 2 mm particle size. Leaching was done using a process described by Kharzraie Shoulaifar et al. [59, 60] which involves first washing the wood with ethylenediaminetetraacetic acid (EDTA) and rinsing with ultrapure water. This was then followed by washing the wood in a HCl solution, and finally rinsing with ultrapure water again. The demineralized wood was then doped with Ca or K using the same method as the spruce wood, but to lower concentrations.

The concentration of inorganics, as measured by ICP-OES, for all the samples used in this work is shown in Table 4.2. The leaching processes used for the SW and BW achieved similar results and were successful in removing most of the inorganic elements from the wood. The doping levels of the SW were generally much higher than the concentrations found in the raw wood, but the concentrations are comparable to those found in some energy crops [93]. The concentrations found in the doped BW samples are much closer to what was found in the raw wood.

4.2 TGA measurements

Char reactivity was measured by isothermal TGA tests using a device depicted in the schematic diagram shown in Figure 4.1. The main advantages of this device over a traditional TGA is that the raw biomass is loaded into the sample holder, which is then lowered into a preheated reactor zone using a mechanical winch system, at which point the biomass undergoes rapid heating and devolatilization. The sample holder consisted of a platinum wire mesh cage, designed to allow good contact between the gas and sample. Additional details of the device, sample holder and previous measurements performed using it can be found in [130]. The lowering time of the sample holder is approximately 7 seconds and the heating rate is 50-100°C/s. The char forms at this time as well, and begins gasification immediately. A sample size of approximately 50 mg was used for each test and the particle size was 125 – 250 μm. Both gasifying agents (H_2O, CO_2) and inhibiting gases (H_2, CO) can be used in the TGA, as well as inert N_2. All tests were conducted at atmospheric pressure and used a gas flow of 3.0 l min^{-1}.

Isothermal TGA measurements were conducted using raw spruce wood at 750, 800, 850, 900 and 950°C to determine at which temperatures is the gasification occurring in the kinetic regime. It was concluded that at 850°C there were no diffusion effects observed and so additional isothermal gasification tests using the doped and impregnated samples were conducted at that temperature using the TGA.

4.3 Fluidized bed measurements

Two different sets of fluidized bed gasification tests were conducted using two different laboratory scale bubbling fluidized bed reactors. The first tests were performed in order to measure the effects of potassium and calcium doping on char reactivty. These batch tests were conducted at the University of Seville, Spain. The second set of tests were conducted by the Gas Technology Institute in Illinois, USA. These were continuous feed gasification tests designed to measure arsenic emissions using chromated copper arsenate (CCA) wood.

Table 4.2: Inorganic concentrations as measured by ICP-OES for raw woods, leached woods and doped wood samples. The dash entry, -, indicates that this element was not analyzed for the sample while n.d. indicates the elemental concentration was below the detection limit.

Sample	Concentration (mg/kg)											
	Ca	K	Mg	P	Mn	Zn	Ba	Fe	Si	As	Cr	Cu
PS	299	102	71	23	-	-	-	13	39	-	-	-
SW	724	215	95	4	98	-	-	3.6	59	-	-	-
BW	760	570	210	91	50	22	10	5.4	-	-	-	-
SW leached	7	n.d.	n.d.	n.d.	n.d.	n.d.	n.d.	n.d.	n.d.	-	-	-
SW Ca low	740	n.d.	n.d.	n.d.	n.d.	n.d.	n.d.	n.d.	n.d.	-	-	-
SW Ca med	2500	n.d.	n.d.	n.d.	n.d.	n.d.	n.d.	n.d.	n.d.	-	-	-
SW Ca high	4600	n.d.	n.d.	n.d.	n.d.	n.d.	n.d.	n.d.	n.d.	-	-	-
SW $CaCO_3$ low	580	n.d.	n.d.	n.d.	n.d.	n.d.	n.d.	n.d.	n.d.	-	-	-
SW $CaCO_3$ med	2500	n.d.	n.d.	n.d.	n.d.	n.d.	n.d.	n.d.	n.d.	-	-	-
SW $CaCO_3$ high	4000	n.d.	n.d.	n.d.	n.d.	n.d.	n.d.	n.d.	n.d.	-	-	-
SW CaC_2O_4 low	610	n.d.	n.d.	n.d.	n.d.	n.d.	n.d.	n.d.	n.d.	-	-	-
SW CaC_2O_4 med	1400	n.d.	n.d.	n.d.	n.d.	n.d.	n.d.	n.d.	n.d.	-	-	-
SW CaC_2O_4 high	3000	n.d.	n.d.	n.d.	n.d.	n.d.	n.d.	n.d.	n.d.	-	-	-
SW K low	12	1200	n.d.	n.d.	n.d.	n.d.	n.d.	n.d.	30	-	-	-
SW K med	12	6000	n.d.	n.d.	n.d.	n.d.	n.d.	n.d.	30	-	-	-
SW K high 1	12	12500	n.d.	n.d.	n.d.	n.d.	n.d.	n.d.	30	-	-	-
SW K high 2	10	12000	n.d.	n.d.	n.d.	n.d.	n.d.	n.d.	30	-	-	-
SW K_2CO_3 low	64	3300	n.d.	n.d.	n.d.	n.d.	n.d.	n.d.	36	-	-	-
SW K_2CO_3 med	47	9800	n.d.	n.d.	n.d.	n.d.	n.d.	n.d.	52	-	-	-
SW K_2CO_3 high	50	17000	n.d.	n.d.	n.d.	n.d.	n.d.	n.d.	78	-	-	-
BW leached	44	n.d.	n.d.	n.d	n.d.	n.d.	n.d.	26	-	-	-	-
BW Ca low	460	n.d.	n.d.	29	n.d.	n.d.	n.d.	26	-	-	-	-
BW Ca med	545	n.d.	n.d.	23	n.d.	12	n.d.	n.d.	-	-	-	-
BW Ca high	600	n.d.	n.d.	22	n.d.	11	n.d.	n.d.	-	-	-	-
BW K low	60	370	n.d.	21	n.d.	7	n.d.	n.d.	-	-	-	-
BW K med	84	491	n.d.	24	n.d.	6	n.d.	n.d.	-	-	-	-
BW K high	39	568	n.d.	21	n.d.	20	n.d.	n.d.	-	-	-	-
CCA wood	6608	968	1034	247	370	565	109	5694	-	6777	5405	6242

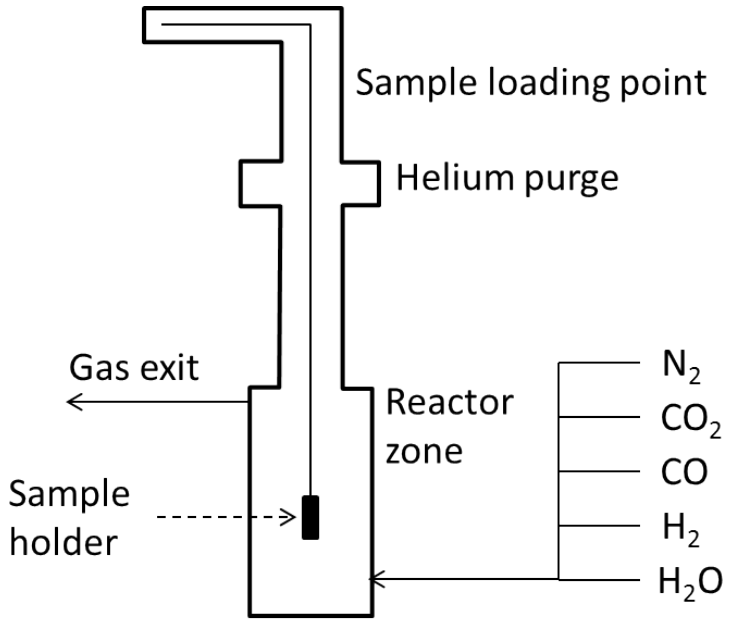

Figure 4.1: A schematic diagram of the pressurized TGA device used for measuring char conversion rates.

4.3.1 Batch tests for char reactivity

Fluidized bed gasification measurements were conducted on a laboratory bubbling fluidized bed reactor. The reactor is constructed of stainless steel with a bed section having an internal diameter of 51 mm and the freeboard section having an internal diameter of 81 mm. The reactor is externally heated by a 10 kW electric oven and gases are fed into the reactor through a distribution plate located at the bottom of the bed. Fuel is added batchwise into the reactor through a feeding valve located at the top of the freeboard section. The exit gas composition from the reactor is measured using a gas analyzer and the concentration of CO_2, CO, H_2 and CH_4 is recorded. A schematic diagram of the reactor setup can be seen in Figure 4.2. This reactor has been used in previous studies for gasification of a variety of fuels [97 – 99].

In nearly all tests olivine was used as the bed material, although bauxite was also used in a few tests. In all cases the bed mass was 500 g. In order to minimize elutriation of the wood from the reactor, the gas velocity into the reactor was maintained at a relatively low velocity of 0.2 m/s. This velocity was sufficient for fluidization as the minimum fluidization velocity of the bed was determined to be 0.18 m/s.

The experimental procedure for the fluidized bed tests began with pelletizing the wood samples. The particle size of the wood was <2 mm and pellets of one gram were made using a pellet press to prevent immediate elutriation of the small wood particles. The reactor was then heated to the desired test temperature and the gas flow switched to N_2. Two pellets were added to the reactor through the fuel feed value at the top of the freeboard. When the pellets entered the reactor the wood immediately began to pyrolyze and the pyrolysis gas composition was measured. When the exit gas composition was measured to be only N_2, pyrolysis was considered to be complete and the gas flow into

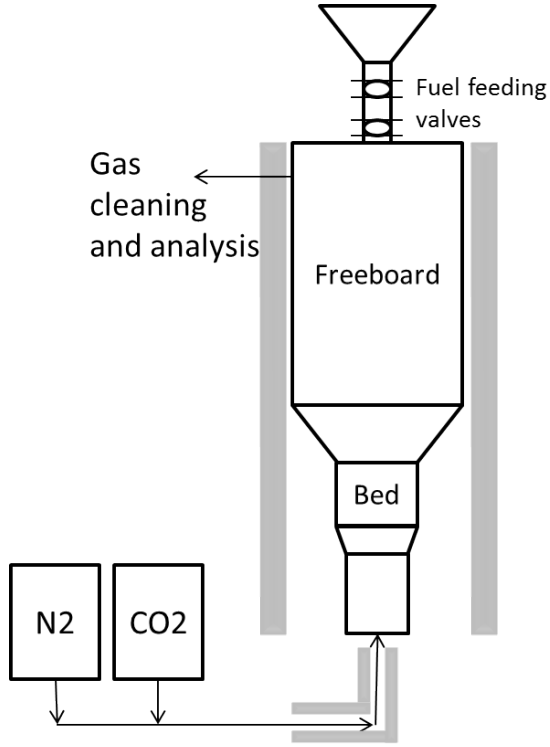

Figure 4.2: A schematic diagram of the bubbling fluidized bed reactor used for char gasification measurements.

the reactor was switched to 20% CO_2 and 80% N_2 to begin gasification of the char. When gasification was complete, typically determined by the CO concentration falling below the detectable limit, the gas flow into the reactor was switch to air in order to combust the remaining char. Char conversion, as defined by Equation 3.1, was calculated according to Reaction R1. The amount of char combusted was determined according to Equation R5 and the total char was the sum of the gasified and combusted char.

4.3.2 Continuous tests for arsenic removal

Continuous feed gasification tests were conducted to investigate the behavior of arsenic in CCA wood. The diameter of the reactor's bed section was 5.08 cm and was 61 cm in length. The freeboard section dimensions were 10.16 cm in diameter and 71.12 cm in length. The bed section was externally heated by an electric oven.

The gasifier included a gas cleaning system which was designed to remove As, Cr and Cu from the product gas and to allow for measurement of the amount of those elements which were removed. The gas cleaning system involved first cooling the product gas to 260°C by passing the gas through a heat exchanger. Once the gas was cooled a Hastelloy sintered metal particulate filter with pore size of 10 μm removed the fly ash. The temperature of the gas entering the particulate filter was controlled by directing part of the product gas through a bypass of the heat exchanger, as seen in Figure 4.3. In order to determine the amount of As, Cr and Cu left in the product gas after the particulate filter, the gas was

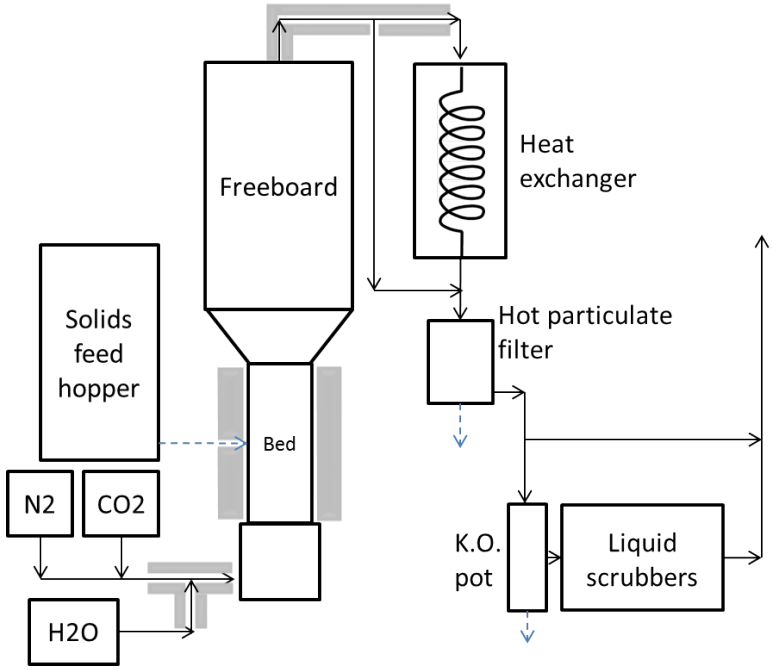

Figure 4.3: A schematic diagram of the bubbling fluidized bed reactor used for continuous feed CCA wood gasification measurements. The black lines indicate gas flows and the blue, dashed lines indicate solid flows. The gray boxes show external heaters.

cooled to approximately 21°C and passed through a series of liquid scrubbers. The liquid scrubbers contained a solution of nitric acid and hydrogen peroxide which was removed after each test and the As, Cr and Cu content was measured using ICP-AES. Bottom ash was not removed during the test runs, but samples of the spent solids (solids remaining in the bed after completion of a test) were taken.

The CCA wood was ground to below 2 mm particle size and was then pelletized. The pellets were approximately 5 mm x 10 mm in size. The gas flow was set to N_2 and the reactor was preheated by the electric oven. Once the desired temperature was reached fuel was fed into the bed using a screw feeder. After approximately one hour of fuel feeding the gas flow was switched to include air and steam while maintaining the same fluidization velocity of approximately 0.43 m/s. The tests consisted of 1-1.5 hours of steady state operation. The targeted operating conditions for the tests are given in Table 4.3.

4.4 Char analysis

Char samples were collected using two methods from the reactivity measurements performed in the fluidized bed described in 4.3.1. Raw birch wood chars and K doped chars were collected from the fluidized bed reactor cyclone. This was done by increasing the gas velocity into the reactor which pushed the less dense char particles out of the bed and into the cyclone. Samples collected in this way were a mix of approximately 20% bed material and 80% char by weight. Leached and Ca doped wood char could not be

Table 4.3: Target operation conditions for continuous feed gasification tests of CCA wood.

Temperature, °C	850
Pressure, bar	1.72
Solids feed rate, kg/h	0.45
Steam/feed ratio, kg/kg	0.35
Steam feed rate, m^3/h	0.22
Oxygen/feed ratio, kg/kg	0.13
Air flow rate, m^3/h	0.14

collected in this way because the char would not exit the reactor, even at very high gas velocities. This was due to bed particles becoming embedded in the char, making the char particles heavier. This is discussed in more detail in Section 5.1.4. Instead, the entire bed was collected which contained the char. Char particles were then separated by hand from the bed material.

Char samples were imaged using a scanning electron microscope and X-ray microanalysis (SEM-EDS) which gives some indication of char structure and the location and distribution of metals on the char surface. Specific surface area of the char and pore size distributions were measured by physiorption of N_2 using a Micormeritics ASAP 2020. Surface area was calculated using the BET model and pore size distribution according to the Barret-Joyner-Halenda model (BJH). ICP-OES was used to determine the metal concentrations of the char samples.

4.5 Isolating char gasification in TGA measurements with simultaneous devolatilization and char gasification

In many studies on char gasification the sample is pyrolyzed first in N_2 and the gas is then switched to H_2O or CO_2 for gasification. This allows for the complete separation of the two processes. The fluidized bed reactivity measurements in the present work use this experimental technique. However, this method can cause issues related to gas diffusion in which observed peaks in gasification rates are in reality due to gas dispersion in the reactor rather than behavior of the fuel sample [37]. In addition, this arrangement does not reflect the reality of a fluidized bed gasifier in which the raw fuel particle is injected into the reactor and thermochemical processes overlap in time.

The TGA measurements used in this work generally try to approximate these conditions by lowering the sample into a preheated reactor which has a gas flow containing the gasifying agent. As a result, pyrolysis and char formation begin immediately and as the char forms gasification also occurs. Because pyrolysis occurs much more quickly than gasification the period of overlap is relatively small when compared with typical gasification times. However, separating mass loss due to char gasification from mass loss due to devolatilization is important for accurate char reactivity measurements.

Two methods for separating devolatilization and char gasification have been used in this work and are described in Sections 4.5.1 and 4.5.2.

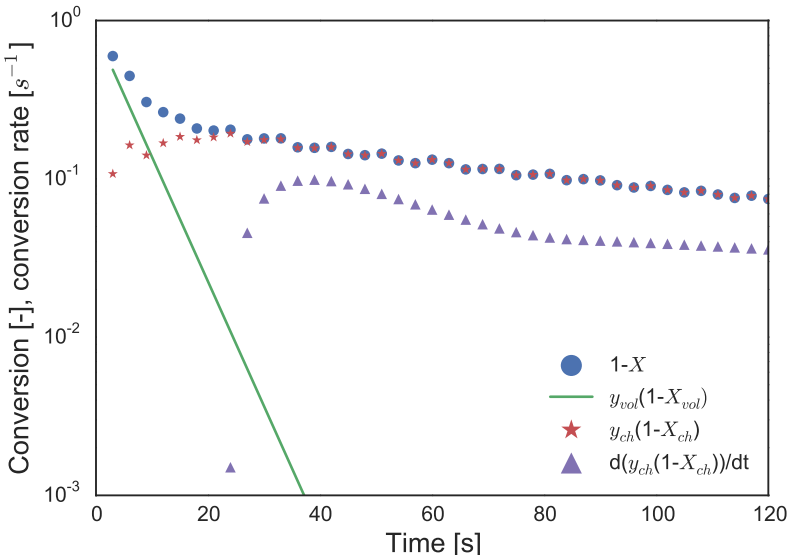

Figure 4.4: An example calculation of char gasification conversion from TGA data using the process described by Equations 4.1-4.4.

4.5.1 First order pyrolysis reaction model

The first method was originally developed by Umeki et al. [126]. This method assumes that devolatilization can be expressed as a single first order reaction, given by

$$r_{dev} = k_{dev}(1 - X_{vol}), \tag{4.1}$$

where r_{dev} is the rate of devolatilization, k_{dev} is the rate coefficient for devolatilization, and X_{dev} is the degree of conversion for the volatiles. Conversion of the sample results from either loss of volatiles or char gasification, and can be expressed as a sum of these two processes,

$$1 - X = y_{vol}(1 - X_{vol}) + y_{ch}(1 - X_{ch}) \tag{4.2}$$

Assuming char gasification does not occur during devolatilization, the conversion of the sample during devolatilization can be written as

$$1 - X = 1 - y_{vol}(1 - \exp(-k_{dev}t)), \tag{4.3}$$

where y_{vol} is the volatile fraction of the sample. Equation 4.3 can then be fit to the experimental conversion data to determine the parameters y_{vol} and k_{dev}. An additional constraint when determining the parameters of Equation 4.3 is obtained from the assumption that there is no char gasification during pyrolysis, which means that $y_{ch}(1 - X_{ch}) = y_{ch} = (1 - y_{vol})$ until the start of char gasification. Char conversion is then calculated from the overall sample conversion,

$$1 - X = 1 - y_{vol}(1 - \exp(-k_{dev}t)) + y_{ch}(1 - X_{ch}), \tag{4.4}$$

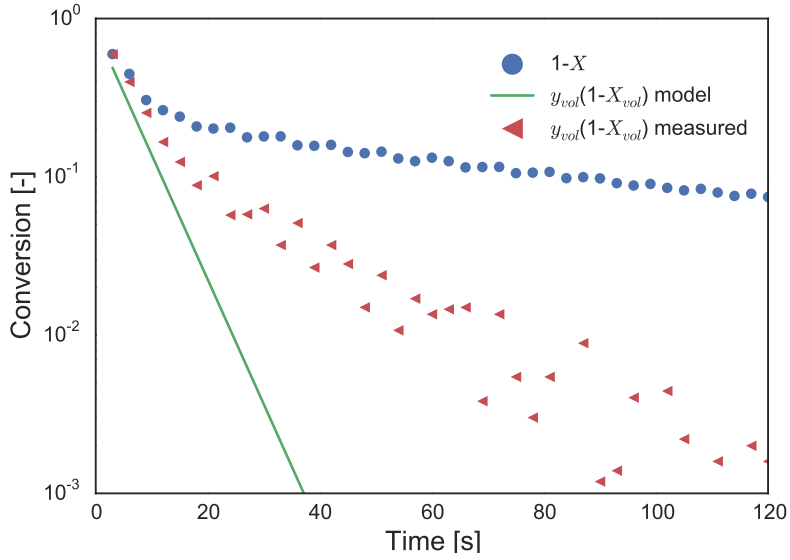

Figure 4.5: A comparison between the fitted pyrolysis model obtained using Equation 4.3 and the measured pyrolysis rate obtained by pyrolyzing spruce wood in N_2 at 850°C.

where y_{ch} is the char fraction, by solving for X_{ch}. The initial starting time of char gasification was taken as the time at which the derivative of $y_{ch}(1 - X_{ch})$ (i.e. the char conversion rate) was the maximum. This method for determining the starting time of char gasification will only be appropriate if the conversion rate peaks early in the char conversion, which is not the case in some studies using raw and catalyst loaded biomasses [117, 139].

The calculation process described above is shown in Figure 4.4 for spruce wood conversion in 100% CO_2 at 850°C. It can be seen that the maximum point of the char conversion rate curve, $d(y_{ch}(1 - X_{ch}))/dt$, occurs at approximately 40 seconds, at which point char gasification is assumed to begin.

The reliability of this procedure to separate the pyrolysis and gasification conversions is based on the accuracy of Equation 4.1 to describe the pyrolysis behavior of the sample. In order to investigate this pyrolysis tests were conducted in N_2 at 850°C using the TGA described in Section 4.2. A comparison of the measured pyrolysis conversion and the predicted prolysis conversion obtained from Equation 4.1 is shown in Figure 4.5. It can be seen in Figure 4.5 that in the initial stage of pyrolysis, from approximately 0-30 seconds, the pyrolysis model fits the measured conversion well as the solid green line showing the model results matches closely with the measured data points. However, the measured conversion shows that there is a second stage of pyrolysis which is much slower and continues for more than 100 seconds for the depicted spruce wood sample. Because this slower stage of pyrolysis is not modeled by Equation 4.1, using the method described above may result in mass loss which is due devolatilization being attributed to char gasification. In many cases the difference is not significant as the pyrolysis measurements show that the observable overlap between pyrolysis and gasification lasts around 120 seconds while char gasification can continue for many times longer than this.

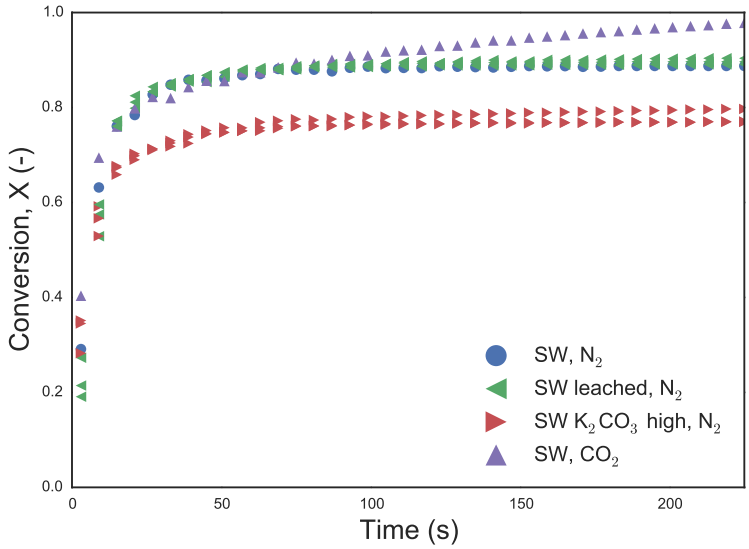

Figure 4.6: Conversion vs time for raw spruce, leached spruce and K_2CO_3 high spruce at 850°C in N_2. The conversion curve of raw spruce in CO_2 is also included to show the difference between sample conversion of only pyrolysis and sample conversion of pyrolysis and char gasification.

4.5.2 Removing devolatilization effects by measuring pyrolysis conversion rate in N_2

In order to better separate mass loss due to devolatilization from mass loss due to char gasification in the TGA measurements a new method was developed which did not rely on fitting a kinetic model for pyrolysis. Instead, repeated pyrolysis measurements were conducted in N_2 and the results averaged together to create a pyrolysis conversion profile. This pyrolysis conversion profile was then subtracted from the conversion measurements taken in gasifying atmospheres. The conversion data in gasifying conditions contains overlapping mass loss due to devolatilization and char gasification, while the difference between the conversion profile in gasifying conditions and the pyrolysis conversion profile gives only the effects of char gasification.

Potassium has been shown to have a larger influence on pyrolysis behavior compared with calcium [4, 28, 102], and as a result the samples which were selected for the pyrolysis measurements were the raw spruce wood, leached spruce wood and spruce wood impregnated with K_2CO_3. As can be seen in Figure 4.6 the K_2CO_3 high samples reach approximately 80% conversion during pryolysis, indicating about 20% char yield. The char yield for the raw spruce is slightly higher than the leached spruce, but both are significantly lower than the K_2CO_3 high sample.

Despite the large differences in char yield the conversion rate during pyrolysis of all the samples is approximately the same during the measurement period, as can be seen in Figure 4.7. This is because the TGA microbalance starts recording measurements only once the sample holder has lowered into place and stabilized, which can take between 7 and 20 seconds from when the sample first begins to lower into the reactor. As a result

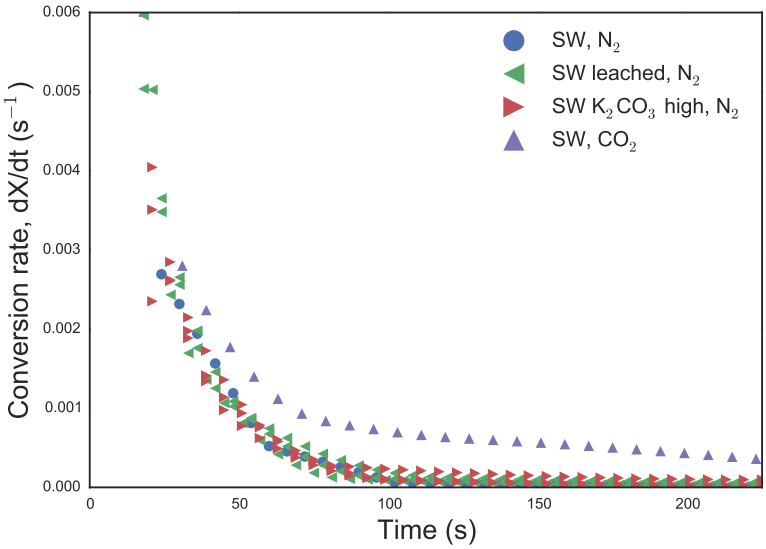

Figure 4.7: Conversion rate vs time for raw spruce, leached spruce and K_2CO_3 high spruce at 850°C in N_2. The conversion rate curve of raw spruce in 100% CO_2 at 850°C is also included to show the difference between sample conversion of only pyrolysis and sample conversion of pyrolysis and char gasification.

some behavior of the samples during the initial pyrolysis is not recorded. At the time of the initial mass measurement of the TGA the K_2CO_3 impregnated samples already show a clearly higher mass than the leached and raw spruce wood samples. From this it can be concluded that the difference in pyrolysis behavior of the K_2CO_3 samples compared with the raw and leached wood occurs early in pyrolysis, during the first 25 seconds. After this point the samples behave nearly identically, as can be seen in Figure 4.7.

An example of the complete process for separating char gasification from pyrolysis is shown in Figure 4.8. The pyrolysis tests conducted in N_2 were averaged together to create the conversion rate profile for pyrolysis. This is then subtracted from the conversion rate curve of the sample taken in CO_2 which contains mass loss due to pyrolysis and mass loss due to char gasification. The resulting difference is the conversion rate of the char gasification.

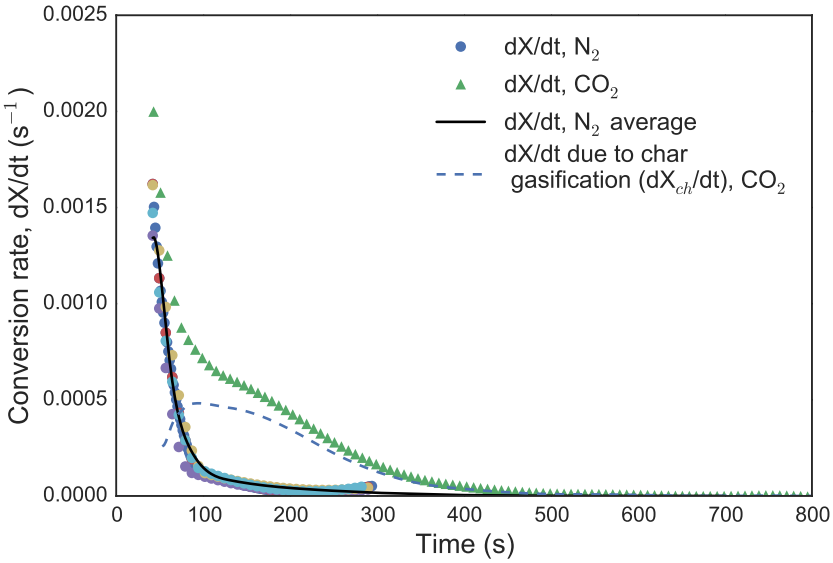

Figure 4.8: An example of the process used to separate mass loss due to char gasification from pyrolysis. The averaged pyrolysis conversion rate measured in N_2 is shown by the black line. The pyrolysis effects are subtracted from the conversion as measured in CO_2, shown by the green triangles, resulting in only the char gasification, shown by the blue dashed line. The measurements here are the same as shown in Figure 4.7.

5 Results and discussion

Experimental and modeling results are presented in this chapter. Section 5.1 presents the experimental and modeling results from TGA and fluidized bed measurements of wood gasification, focusing on the effects of calcium and potassium on char behavior. Section 5.2 presents the experimental results from fluidized bed tests of CCA wood gasification, in addition to the equilibrium modeling results of the arsenic behavior.

5.1 Char reactivity measurements

Wood was gasified using the TGA described in Section 4.2 and the fluidized bed described in Section 4.3.1. The results from these measurements are used to determine the effects of potassium and calcium on the char behavior and reactivity. Char conversion rate models were fit to the experimental data in order to predict char conversion as a function of inorganic content in the original wood.

5.1.1 Activation energies

Char gasification reactivity in 100% CO_2 for pine sawdust and spruce wood, measured in the same experimental setup described in Section 4.2 is shown in Figure 5.1 for various temperatures. The PS is less reactive than the SW, likely due to the lower ash content of the sawdust. A linear regression for each of the samples is also shown in Figure 5.1 and was used to calculate an apparent activation energy given in Table 5.1, according to Equation 3.5. For the SW sample, the reactivity at 950°C is lower than predicted by the linear regression while the reactivities for 750-900°C fit well. This indicates that at 950°C the gasification reaction is no longer in the kinetic regime and the observed reaction rate is controlled by a combination of mass diffusion in the char pores and surface kinetics.

Figure 5.1 also shows the Arrhenius plot for raw, leached, Ca medium and Ca high birch wood using reactivity measurements obtained from the fluidized bed gasification tests

Table 5.1: Activation energies calculated from the linear regression shown in Figure 5.1 for CO_2 gasification of pine sawdust and spruce wood, according to Equation 3.5.

Sample	A (s^{-1})	E_a (kJ/mol)
PS	$3.08 \cdot 10^{11}$	285
SW	$1.38 \cdot 10^{10}$	265
BW	$3.34 \cdot 10^{6}$	200
BW leached	$2.43 \cdot 10^{4}$	160
BW Ca med	$5.19 \cdot 10^{4}$	160
BW Ca high	$2.51 \cdot 10^{5}$	170

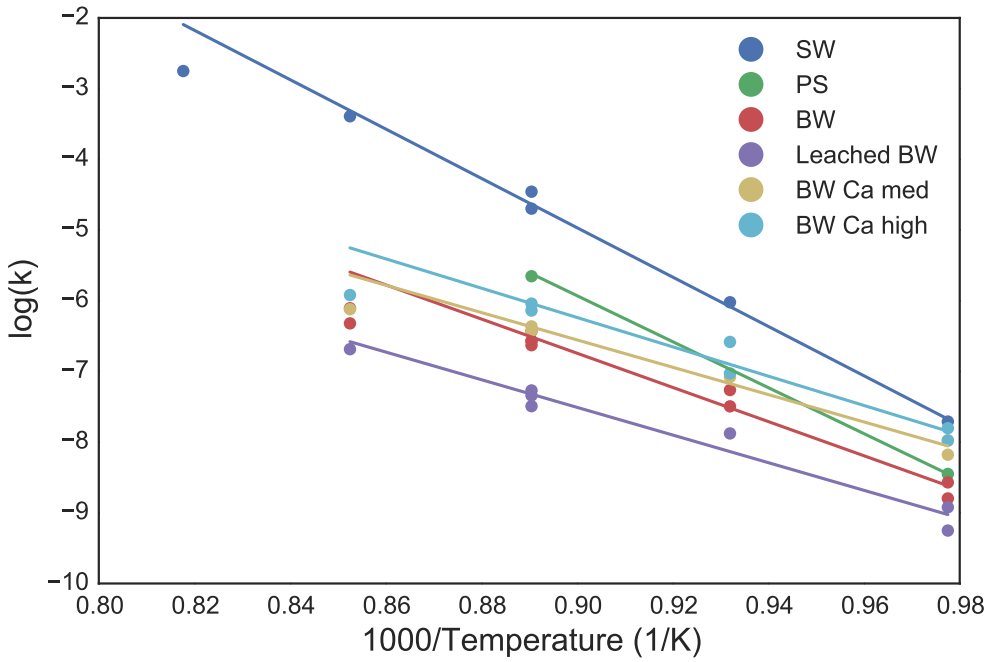

Figure 5.1: Arrhenius plot for spruce wood and pine sawdust for char gasification in 100% CO_2. The kinetic term, k, is taken as the average value from 30% to 80% char conversion.

described in Section 4.3.1. The reactivity for most samples in the fluidized bed at 900°C are lower than predicted by linear regression line in Figure 5.1, indicating that at 900°C gasification is no longer kinetically controlled. The temperature at which the gasification transitions from regime I (kinetically controlled) to regime II (pore diffusion controlled) is lower in the fluidized bed, despite the better solid-gas mixing, due to the larger sample particle size. The reactivities in the fluidized bed are generally lower than those obtained from the TGA because the TGA measurements were conducted in 100% CO_2 while the fluidized bed used 20% CO_2 and 80% N_2. Ensuring that char reactivity measurements are conducted in the kinetic regime also allows for ignoring inter-particle mass transfer effects inside the fluidized bed.

If assuming a more complex reaction mechanism than the single step given by Equation 3.5, it is common to use a Langmuir–Hinshelwood mechanism which can be expressed, in general, by Equation 2.1. This mechanism typically involves a reversible adsorption step followed by an irreversible desorption step, such as given by Reactions R6 and R7. This type of kinetic expression has been shown to fit well to gasification reactivity measurements for birch wood in previous studies [8].

The following equations [8], slightly modified versions of Equations 2.1 and 2.1 and 2.2, were used to account for the inhibition effects of CO and H_2O on the gasification rates,

$$r_{CO_2} = \frac{k_1 p_{CO_2}}{1 + \frac{k_1}{k_3} p_{CO_2} + \frac{k_2}{k_3} p_{CO}}, \tag{5.1}$$

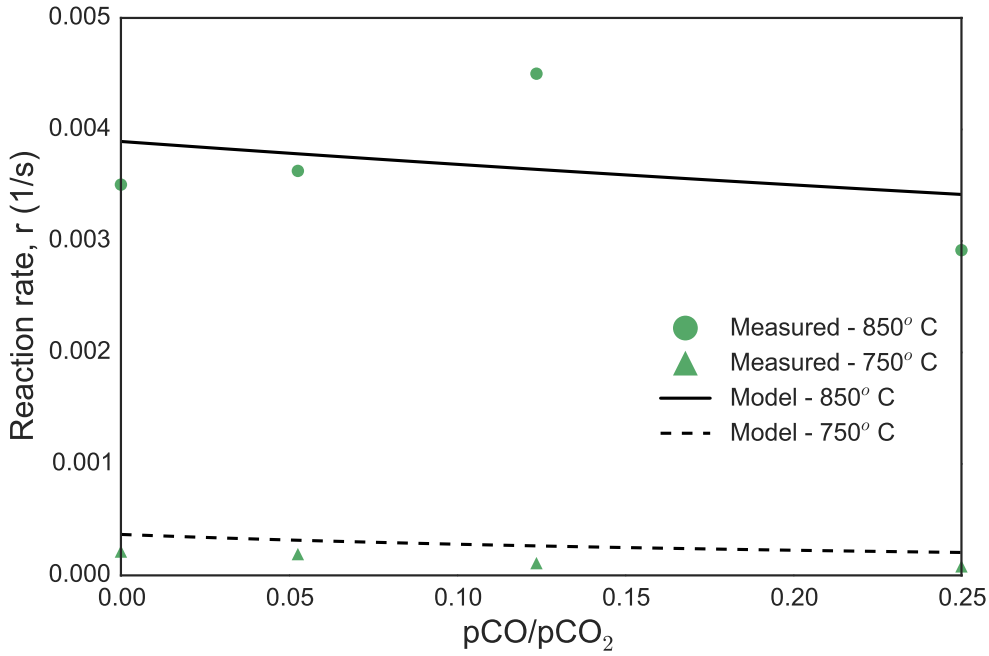

Figure 5.2: Reactivity values for PS samples from TGA measurements conducted at 850°C and 750°C in atmospheres containing both CO_2 and CO as well as the predicted reactivity from fitting Equation 2.1 to the experimental data. All measurements were conducted at 1 bar pressure.

Table 5.2: Frequency factors and activation energies obtained by fitting Equation 2.1 to the experimental data for pine sawdust gasification in CO_2/CO and H_2O/H_2 containing atmospheres.

Reaction	k_1		k_2		k_3	
	A	E_a (kJ/mol)	A	E_a (kJ/mol)	A	E_a (kJ/mol)
CO2/CO	$5.94{\cdot}10^7$	179	0.536	12	$1.28{\cdot}10^8$	226
H2O/H2	$6.39{\cdot}10^5$	153	$7.86{\cdot}10^4$	107	$4.90{\cdot}10^7$	212

$$r_{H_2O} = \frac{k_1 p_{H_2O}}{1 + \frac{k_1}{k_3} p_{H_2O} + \frac{k_2}{k_3} p_{H_2}}. \tag{5.2}$$

The kinetic terms were determined by fitting Equation 5.1 and 5.2 to the measured reaction rate data from tests conditions shown in Table 5.3 using a least squares fitting routine. Equations 5.1 and 5.2 account well for the inhibition effects of CO and H_2, though the inhibition from CO is significantly less than that of H_2, as can be seen from the model fit shown in Figures 5.2 and 5.3. The frequency factors and activation energies for each reaction step for pine sawdust are shown in Table 5.2. The activation energies obtained for the pine sawdust are consistent with the values for birch wood [8], although as the author of that study noted there is significant variation in these activation energy values when considering the values reported for chars originating from non-woody biomasses.

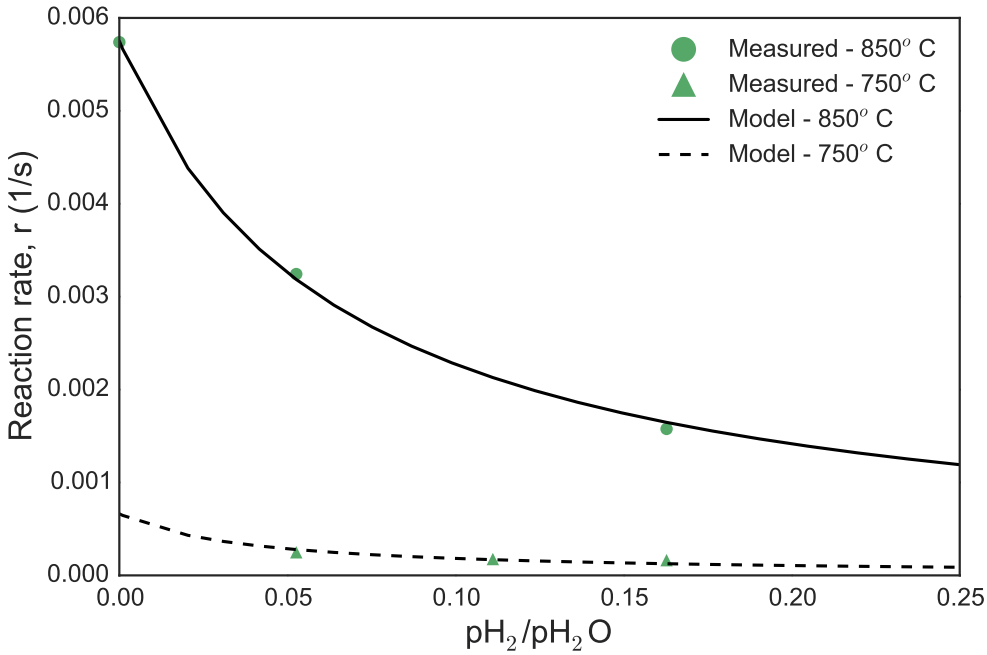

Figure 5.3: Reactivity values for PS samples from TGA measurements conducted at 850°C and 750°C in atmospheres containing both H_2O and H_2 as well as the predicted reactivity from fitting Equation 2.1 to the experimental data. All measurements were conducted at 1 bar pressure.

5.1.2 Modeling pine sawdust gasification in a TGA

The test conditions used for gasification of pine sawdust in the TGA are given in Table 5.3. The method presented by Umeki et al. [126], and summarized in Section 4.5.1, for separating the effects of devolatilization and char gasification was used to isolate the mass loss due to char conversion. The resulting conversion rate curves have similar features to biomass gasification results on similar TGA devices [89, 125] and some examples can be seen in Figure 5.4.

A variety of char conversion models were evaluated for their ability to accurately model the measured conversion rate data. The models used were: the three parallel reaction model, Equation 3.9; the RPM, Equation 3.8; the MRPM, Equation 3.7; the HRPM, Equation 3.14; the HMRPM, Equation 3.15; and finally the uniform conversion model (UCM) given by,

$$\frac{dX_{ch}}{dt} = k(1 - X_{ch}). \tag{5.3}$$

The parallel reaction model was found to fit the measured data well (Figure 5.4). However, the model's kinetic terms $k_{ccg,1}$, k_{ncg}, and $k_{ccg,2}$ have complex pressure and temperature dependence which is currently not well understood. In addition, the structural term ξ is also dependent on the gasification temperature, indicating that the model does not separate the kinetic and structural equations in the way shown by Equation 3.4. As a result of these issues the parallel reaction model is primarily useful in modeling char conversion rates for a single temperature and pressure test condition. This limitation

Table 5.3: TGA conditions for pine sawdust char gasification tests.

Temperature (°C)	CO_2 (bar)	CO (bar)	H_2O (bar)	H_2 (bar)
750	1	0	0	0
750	0.95	0.05	0	0
750	0.89	0.11	0	0
750	0.8	0.2	0	0
850	1	0	0	0
850	0.95	0.05	0	0
850	0.89	0.11	0	0
850	0.8	0.2	0	0
750	0	0	1	0
750	0	0	0.95	0.05
750	0	0	0.9	0.1
750	0	0	0.86	0.14
850	0	0	1	0
850	0	0	0.95	0.05
850	0	0	0.86	0.14

makes the model difficult to use in situations in which char conversion rates need to be predicted at a variety of temperatures and gas pressures, such as in a reactor model.

The uniform conversion model and models derived from the RPM adhere to the form of Equation 3.4 and separate the temperature and pressure dependence from the conversion dependence in the conversion rate equation. This makes them better suited for predicting char conversion rates at a range of temperatures and gas pressures and therefore they are more suitable for use in reactor modeling. The results of fitting the UCM, RPM, MRPM and HRPM to char conversion rate data of pine sawdust gasified at 850°C in 95% H_2O/5% H_2 are shown in Figure 5.5. The UCM reflects the overall decreasing trend of the conversion rate curve, but over predicts the conversion rate at low char conversion and underpredicts the conversion rate at high char conversion. The RPM and MRPM models both model the behavior of the char conversion rate well at high char conversion, but at low char conversion the models deviate significantly from the measured conversion rate. Only the HRPM manages to accurately model the conversion rate behavior at both low and high char conversion levels.

The model results showing the predicted conversion times for each model as well as the experimentally measured conversion times are given in Figures 5.6 and 5.7 for steam and CO_2 gasification, respectively. The RPM, MRPM and HRPM perform similarly and predict conversion times well for all conditions. The UCM shows larger deviation from the measured conversion times for some test conditions.

In order to determine clearly which conversion rate model best fit the measured data for pine sawdust gasification the mean percentage error for predicted conversion times was calculated for each model. The mean percentage error was calculated as,

$$e = \frac{1}{N_j}\sum_{j=1}^{N_j}\frac{1}{N_i}\sum_{i=1}^{N_i}|(t_{i,j,exp} - t_{i,j,model})/t_{i,j,exp}|, \tag{5.4}$$

where N_j is the number of TGA data sets, $N_{j,i}$ is the number of data points in data set j, $t_{j,i,exp}$ is the experimental conversion time for data point i in set j, and $t_{j,i,model}$

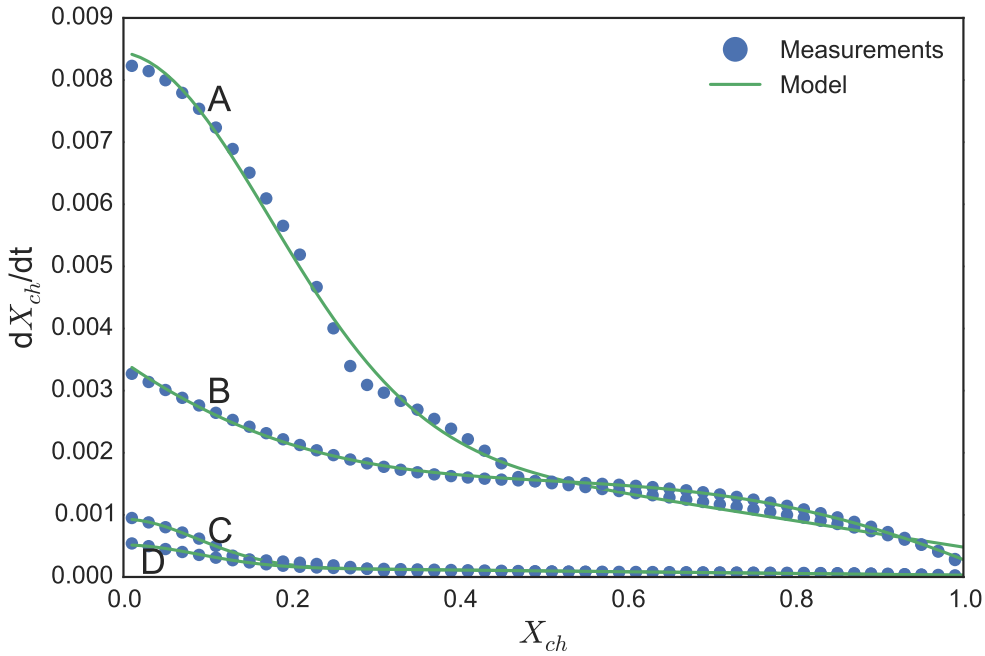

Figure 5.4: Char conversion rate measurements for pine sawdust and the results of fitting the parallel reaction model to the measured data. The test conditions are: A) 850°C, 1 bar CO_2 B) 850°C, 0.8 bar CO_2, 0.2 bar CO C) 750°C, 1 bar CO_2 D) 750°C, 0.95 bar CO_2, 0.05 bar CO.

Table 5.4: Mean absolute percentage errors for the best fit of the UCM, RPM, MRPM, HRPM and HMRPM to experimental data of pine sawdust gasification in CO_2 and H_2O.

	CO_2 (%)	H_2O (%)
UCM	82	110
RPM	33	28
MRPM	28	26
HRPM	22	19
MHRPM	22	18

is the model result corresponding to $t_{j,i,exp}$. The calculated error values are given in Table 5.4. The UCM has the largest error of the tested models and the models based on the RPM decrease the mean percentage error to below 33%. The MRPM offers some improvement over the standard RPM but the improvement is minor considering the increased complexity of the model and two additional fitting parameters. This is likely due to the low ash content of the sawdust which minimizes the benefits of the MRPM, which was intended to account for behavior of inorganics during char gasification.

5.1.3 Effects of K and Ca on char gasification in TGA

Doped and impregnated spruce wood (see Section 4.1 for sample details) was gasified in a TGA at 850°C in 100% CO_2. The conversion rate curves for K doped and K_2CO_3

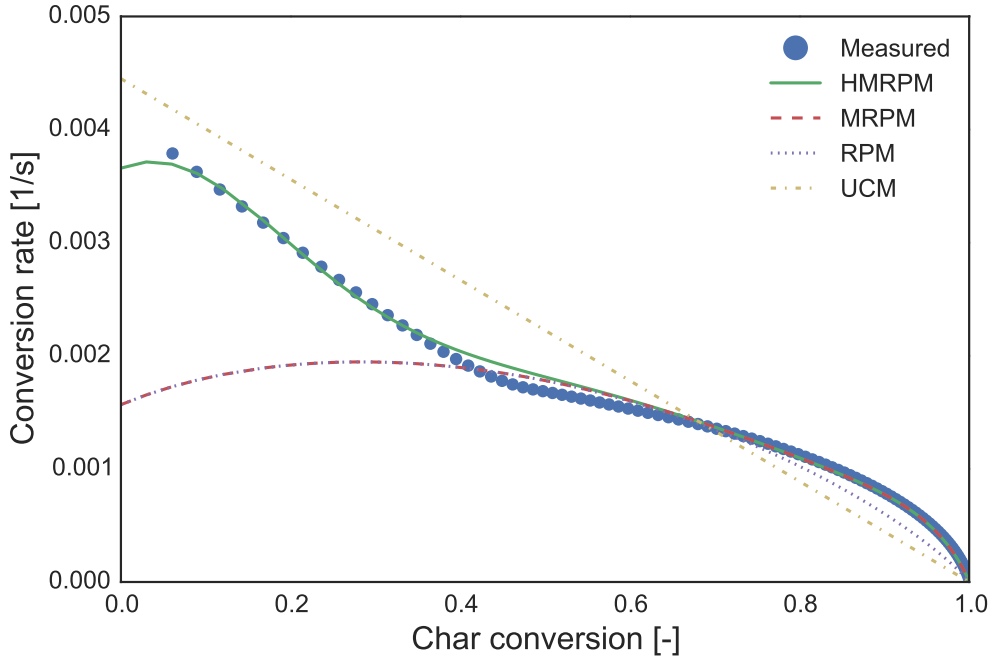

Figure 5.5: Measured conversion rate for pine sawdust at 850°C in 95% H_2O/5% H_2 compared to the best fit result for the RPM, MRPM, HRPM and UCM.

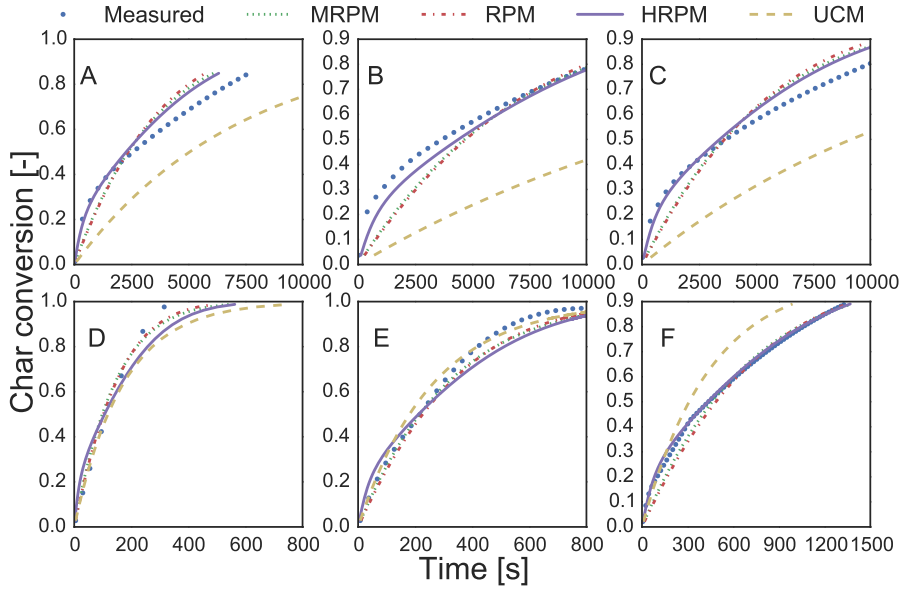

Figure 5.6: Measured conversion times for pine sawdust for six test conditions in H_2O/H_2 atmospheres compared to the best fit result for the RPM, MRPM, HRPM and UCM. (A) 750°C, 0.95 bar H2O, 0.05 bar H2; (B) 750°C, 0.9 bar H2O, 0.1 bar H2; (C) 750°C, 0.86 bar H2O, 0.14 bar H2; (D) 850°C, 1 bar H2O; (E) 850°C, 0.95 bar H2O, 0.05 bar H2; (F) 850°C, 0.86 bar H2O, 0.14 bar H2.

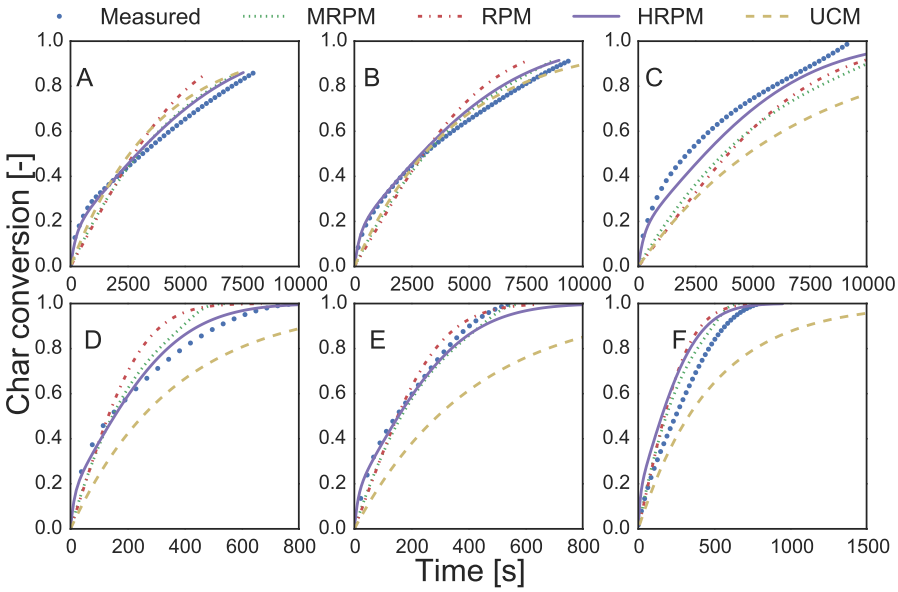

Figure 5.7: Measured conversion times for pine sawdust for six test conditions in CO_2/CO atmospheres compared to the best fit result for the RPM, MRPM, HRPM and UCM. (A) 750°C, 1 bar CO2; (B) 750°C, 0.95 bar CO2, 0.05 bar CO; (C) 750°C, 0.8 bar CO2, 0.2 bar CO; (D) 850°C, 1 bar CO2; (E) 850°C, 0.89 bar CO2, 0.11 bar CO; (F) 850°C, 0.8 bar CO2, 0.2 bar CO.

impregnated samples are shown in Figure 5.8. The conversion rate increases as a function of K concentration regardless of whether the potassium is added by doping to the organic sites or if it is added by impregnating with K_2CO_3. This indicates that the reaction mechanism for potassium catalyzed gasification in CO_2 is the same regardless of how the potassium is added. This could imply that potassium reacts with CO_2 to form potassium carbonate on the char surface, and then K_2CO_3 is the active species during the catalytic gasification. However, as it has been observed that K_2CO_3 decomposes when impregnated on char and heated [94], it is more likely that the impregnated potassium carbonate and doped elemental potassium react to form the same active surface complex such as through the mechanism proposed by Kopyscinski et al. [67] and shown in Reactions R27-R30. The conversion rate curves for the potassium catalyzed samples share significant similarities with the behavior of KNO_3 impregnated chars as reported by Struis et al. [118]. In that work the peak conversion rate was observed around $X_{ch} = 0.5$, compared with $X_{ch} = 0.46$ from the current work. The nearly linear relationship between the maximum char conversion rate and the potassium concentration is shown in Figure 5.9

As with potassium, addition of calcium to the spruce wood increased the char reactivity compared with the acid washed wood sample. However, the calcium doped and impregnated samples behaved differently depending on the form in which the calcium was added to the wood, as can be seen in the conversion rate curves shown in Figures 5.10 and 5.11. When calcium was doped to the organic sites the char behaved similarly as with the potassium doped samples, although the peak in conversion rate occurred slightly earlier in the conversion process with Ca doped samples. The catalytic effect of calcium has been observed to occur earlier in the char conversion than potassium in many earlier studies [118, 120, 139], however typically the conversion rate peak for calcium catalyzed char

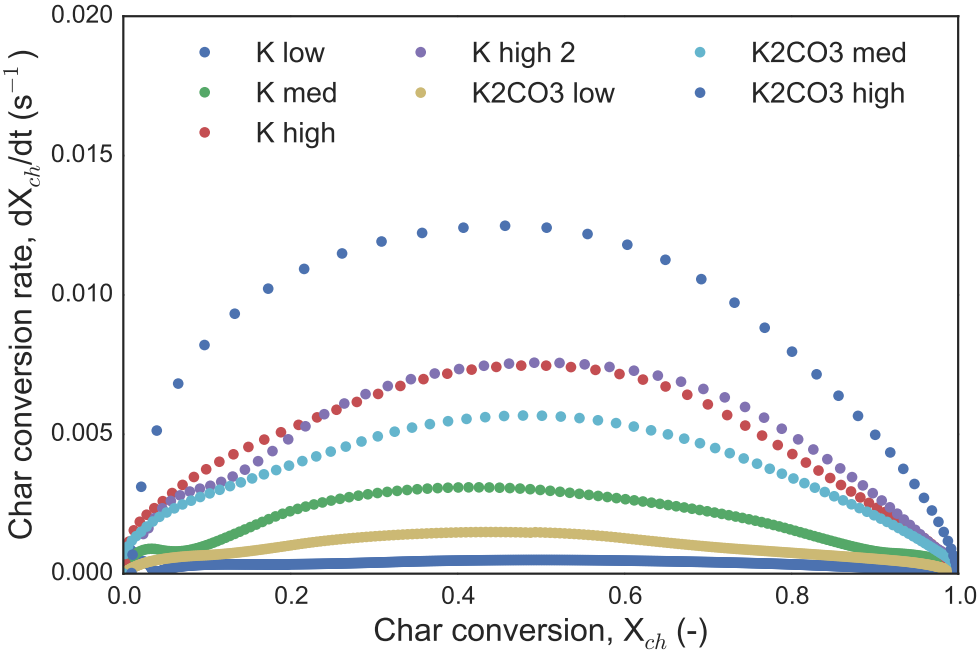

Figure 5.8: Conversion rate measurements for K doped and K_2CO_3 impregnated spruce wood in 100% CO_2 and 850°C.

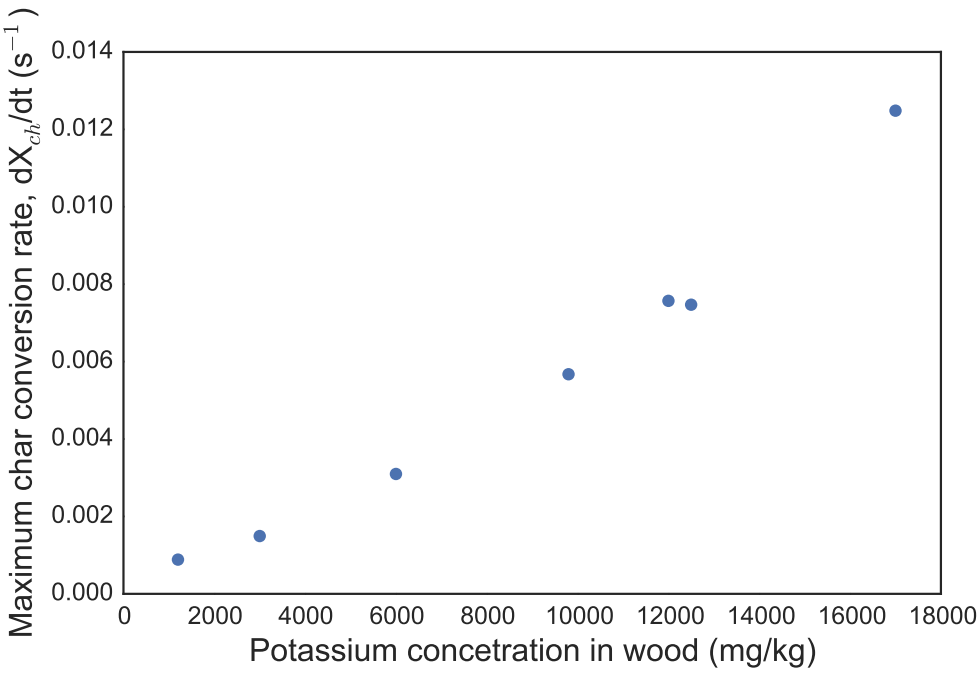

Figure 5.9: The maximum conversion rate for K doped and K_2CO_3 impregnated spruce wood in 100% CO_2 and 850°C as a function of the potassium concentration in the wood.

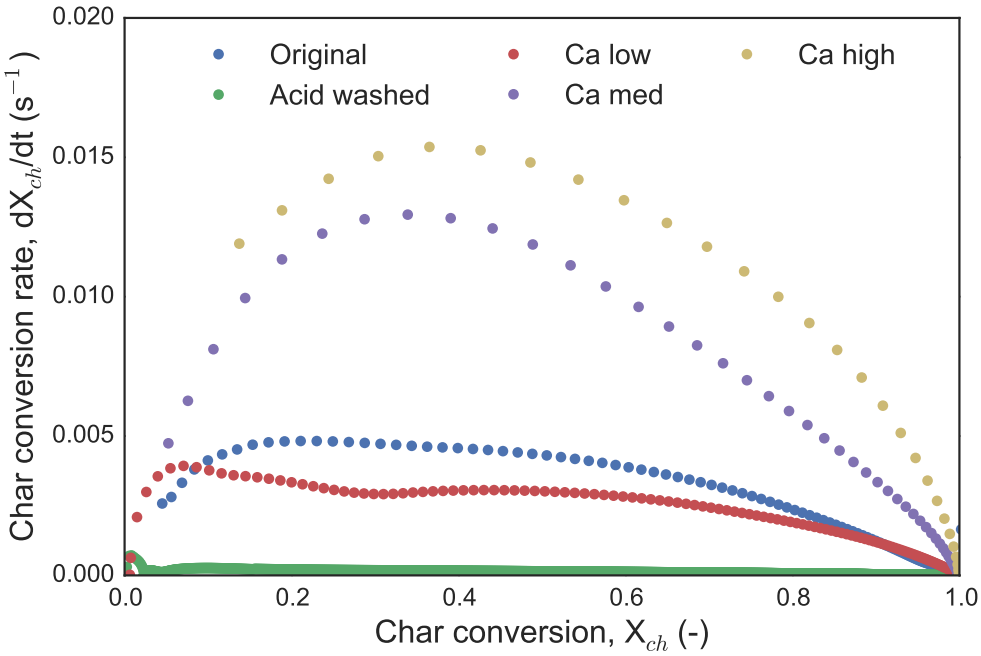

Figure 5.10: Conversion rate measurements for Ca doped spruce wood in 100% CO_2 and 850°C.

gasification occurs at lower char conversion than what has been observed in the current experiments. A possible explanation for this comes from the fact that the heating rate in the isothermal TGA used in this work is higher than the slow heating used in most gasification studies with a TGA. At higher heating rates the char precursor phase has been observed to undergo melting [15] which may result in the catalysts being covered which can cause the catalytic effect of the calcium to only be observed until after the catalyst is exposed [133].

The conversion behavior of the $CaCO_3$ and CaC_2O_4 impregnated spruce wood differed from the Ca doped wood and also from each other (Figure 5.11). In these samples the conversion rate peaked very early, usually between $X_{ch} = 0.1$ and $X_{ch} = 0.3$. After the peak the conversion rate decreased rapidly. This is similar in behavior to what was reported by Struis et al. [118] when using $Ca(NO_3)_2$ impregnated chars. In that work the conversion rate decreased rapidly from the start of gasification until approximately $X_{ch} = 0.2$ and this behavior was explained as resulting from sintering of the ash. The CaC_2O_4 impregnated samples were relatively unreactive, likely due to poor dispersion of the calcium on the char surface.

It has been reported in an earlier study that $CaCO_3$ is the active species in calcium catalyzed char gasification [13] and so it is possible that all three types of calcium sample (Ca doped, $CaCO_3$ impregnated, and CaC_2O_4 impregnated) have similar reaction pathway. However, the initial form of the calcium was different in each sample, as was dispersion of the calcium on the char which was noted by Perander et al. [102]. These differences cause the varied behavior between the calcium catalyzed samples.

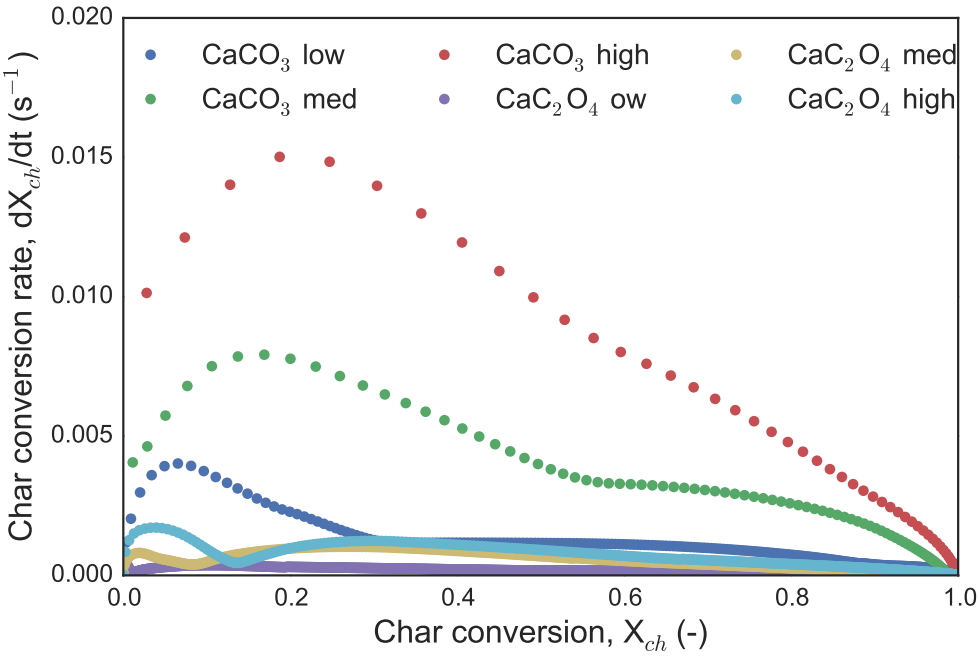

Figure 5.11: Conversion rate measurements for $CaCO_3$ and CaC_2O_4 impregnated spruce wood in 100% CO_2 and 850°C.

It was reported by Perander et al. [102] that the instantaneous reaction rate taken at three different stages of conversion was approximately linearly proportional to the catalyst concentration for for the K, Ca, K_2CO_3 and CaC_2O_4 loaded samples. While the same data was used in that work, the instantaneous reaction rates were obtained using the char gasification isolation method discussed in Section 4.5.1 which was shown to create errors at low conversions. However, the linear dependence of instantaneous reaction rate on catalyst concentration is indication that increased catalyst loading creates increased numbers of active sites which leads to a proportionally higher reaction rate.

Char conversion models were fitted to the conversion rate data obtained from the TGA measurements using a least squares fitting routine. The MRPM proposed by Zhang et al. [139], shown in Equation 3.7, and a similar model based on the RPM developed by Struis et al. [118], shown in Equation 3.10, were used. In addition, Equation 3.11 was used to model the $CaCO_3$ and CaC_2O_3 impregnated samples, as those samples showed the same type of initial catalytic deactivation stage which Equation 3.11 was developed from. The results of fitting Equation 3.7 and 3.10 to the conversion rate data of the K and K_2CO_3 loaded wood is shown in Figure 5.12 and for Ca doped wood in Figure 5.13. Both models are able to fit the measured conversion rate curves well. The results for fitting Equation 3.11 to the $CaCO_3$ and CaC_2O_4 impregnated wood measurements is shown in Figure 5.14. The model fits the measured conversion rate curve well, with the exception being at low conversion levels. At low conversion the measured conversion rate is much lower than predicted by the model, likely due to the influence of devolatilization gases which are still present at the beginning of char gasification and can inhibit the gasification reactions. Devolatilization gases will influence the beginning of char conversion in all cases, but

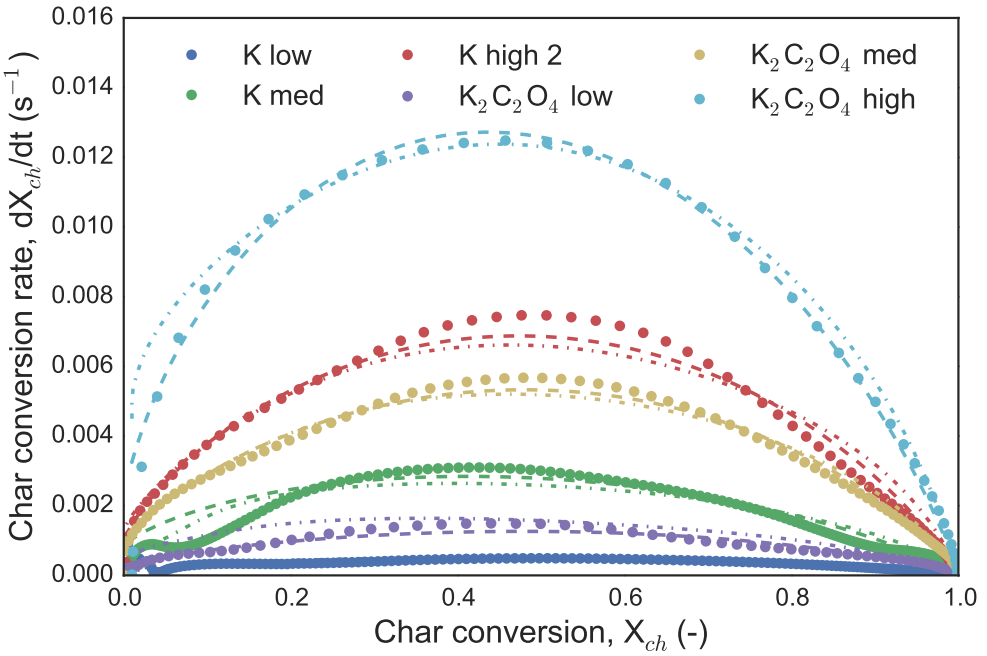

Figure 5.12: Conversion rate measurements for K doped and K_2CO_3 impregnated spruce wood in 100% CO_2 and 850°C. The dashed lines show the best fit for Equation 3.7 and the dot-dash lines shows the best for for Equation 3.10 to the experimental data.

because calcium tends to have a catalytic effect earlier in the char conversion process the effect of the volatile gases will likely be greater in these samples.

The mean percentage error was calculated for each of the models using Equation 5.4 and the results are given in Table 5.5. Equations 3.7 and 3.10 were both good in fitting the measured conversion rates for Ca and K doped and K_2CO_3 impregnated wood. However, Equation 3.10 gave slightly lower mean percentage error values and so was a better fit to the data. The best fit parameters for each of the equations is given in Table 5.6.

Table 5.5: The mean absolute percentage errors for Eqs. 3.7, 3.10 and 3.11 in calculating the experimental conversion times for each type of sample. Because the K and K_2CO_3 behaved similarly they are grouped together.

	Error (%)		
Samples	Eq 3.7	Eq 3.10	Eq 3.11
Ca	19	8	-
$CaCO_3$	-	-	64
CaC_2O_4	-	-	34
K & K_2CO_3	46	22	-

The dependence of the best fit parameters shown in Table 5.6 on the K or Ca concentration in the wood was investigated and is shown in Figures 5.15-5.19 along with linear regression lines. Figure 5.15 shows the best fit parameters for Equation 3.7 when fit to the conversion

Table 5.6: Best fit parameters for Ca, $CaCO_3$, CaC_2CO_4, K and K_2CO_3 samples using Eqs. 3.7, 3.10 and 3.11. These are the parameters plotted in Figures 5.15-5.19.

	Eq. 3.7				Eq. 3.10				Eq. 3.11					
Sample	k	ψ	c	a	k	ψ	g	b	k	ψ	b	g	A	ξ
Ca low	$1.3{\cdot}10^{-3}$	7.7	0	$7.5{\cdot}10^{-3}$	$1.5{\cdot}10^{-4}$	3.4	0.27	160	-	-	-	-	-	-
Ca med	$2.7{\cdot}10^{-3}$	27	0	$7.5{\cdot}10^{-2}$	$1.5{\cdot}10^{-4}$	7.9	0.36	300	-	-	-	-	-	-
Ca high	$5.9{\cdot}10^{-3}$	35	0	0.77	$1.5{\cdot}10^{-4}$	9.4	0.40	290	-	-	-	-	-	-
$CaCO_3$ low	-	-	-	-	-	-	-	-	$5.8{\cdot}10^{-5}$	5.8	0.32	8.3	$9.8{\cdot}10^{-3}$	$1.81{\cdot}10^{-2}$
$CaCO_3$ med	-	-	-	-	-	-	-	-	$1.1{\cdot}10^{-4}$	5.1	0.81	0.17	$5.0{\cdot}10^{-2}$	$2.67{\cdot}10^{-2}$
$CaCO_3$ high	-	-	-	-	-	-	-	-	$2.2{\cdot}10^{-5}$	5.0	0.72	8.8	$1.1{\cdot}10^{-1}$	$3.52{\cdot}10^{-2}$
CaC_2O_4 low	-	-	-	-	-	-	-	-	$6.8{\cdot}10^{-5}$	0.23	0.13	7.2	$4.4{\cdot}10^{-4}$	$2.41{\cdot}10^{-3}$
CaC_2O_4 med	-	-	-	-	-	-	-	-	$1.2{\cdot}10^{-4}$	0.11	0.19	9.1	$1.1{\cdot}10^{-3}$	$2.32{\cdot}10^{-3}$
CaC_2O_4 high	-	-	-	-	-	-	-	-	$2.0{\cdot}10^{-4}$	0.005	0.20	12	$2.2{\cdot}10^{-4}$	$1.30{\cdot}10^{-3}$
K low	$1.5{\cdot}10^{-4}$	18	1.1	0.36	$1.4{\cdot}10^{-4}$	$6.7{\cdot}10^{-5}$	1.7	$1.0{\cdot}10^{-3}$	-	-	-	-	-	-
K med	$6.0{\cdot}10^{-4}$	28	2.9	0.16	$1.4{\cdot}10^{-4}$	$1.3{\cdot}10^{-5}$	1.8	$1.0{\cdot}10^{-2}$	-	-	-	-	-	-
K high 1	$8.1{\cdot}10^{-4}$	57	5.9	0.57	$1.4{\cdot}10^{-4}$	$1.7{\cdot}10^{-5}$	2.2	$3.0{\cdot}10^{-2}$	-	-	-	-	-	-
K high 2	$8.8{\cdot}10^{-4}$	58	5.1	0.37	$1.4{\cdot}10^{-4}$	$1.1{\cdot}10^{-5}$	2.3	$2.5{\cdot}10^{-2}$	-	-	-	-	-	-
K_2CO_3 low	$2.6{\cdot}10^{-4}$	25	3.7	0.46	$1.4{\cdot}10^{-4}$	$5.5{\cdot}10^{-5}$	1.7	$4.0{\cdot}10^{-3}$	-	-	-	-	-	-
K_2CO_3 med	$8.1{\cdot}10^{-4}$	42	4.5	0.42	$1.4{\cdot}10^{-4}$	$1.1{\cdot}10^{-5}$	2.2	$2.0{\cdot}10^{-2}$	-	-	-	-	-	-
K_2CO_3 high	$1.7{\cdot}10^{-3}$	75	7.2	0.22	$1.4{\cdot}10^{-4}$	$8.7{\cdot}10^{-5}$	2.4	$4.9{\cdot}10^{-2}$	-	-	-	-	-	-

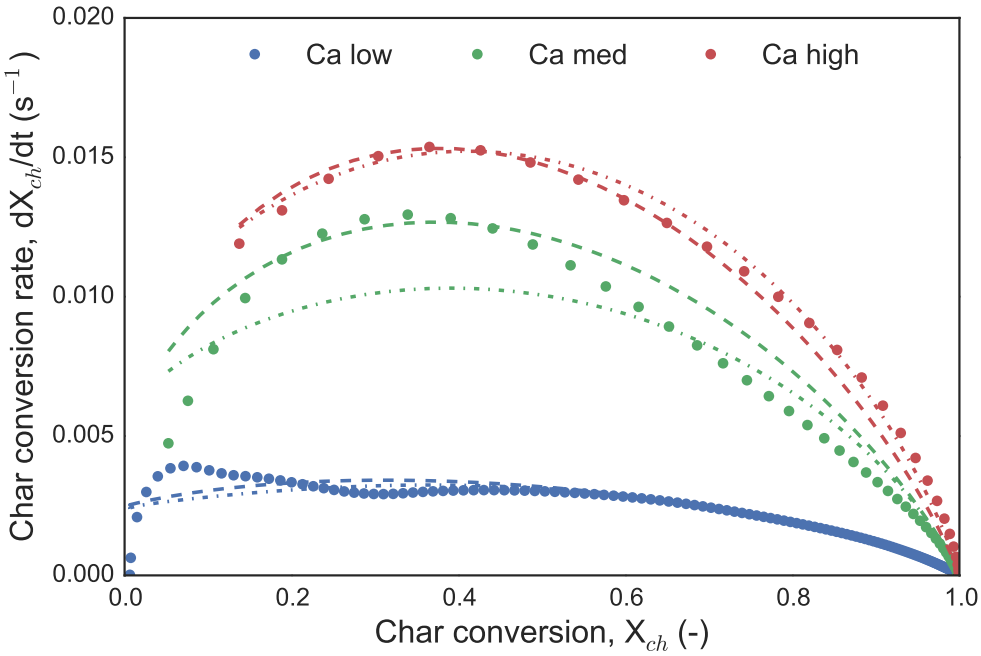

Figure 5.13: Conversion rate measurements for Ca doped spruce wood in 100% CO_2 and 850°C. The dashed lines show the best fit for Equation 3.7 and the dot-dash lines shows the best for for Equation 3.10 to the experimental data.

rate data for K doped and K_2CO_3 impregnated spruce wood. The parameters k, ψ, and c all show a clear linear dependence on the potassium concentration in the wood. The parameter a showed no dependence on potassium concentration. This is in contrast to the results reported by Zhang et al. [139] where the best fit parameters for Equation 3.7 showed that both c and a were dependent on potassium concentration. The values for c obtained here are slightly higher than those reported by Zhang et al. but the range is approximately the same. The best fit parameters for Equation 3.10 as a function of potassium concentration are shown in Figure 5.16. The parameters g and b both show a linear dependence on the potassium concentration but ψ shows no correlation. All the ψ values are very small, below 0.0001, which agrees with the results from Struis et al. [117]. It was observed that when using Equation 3.10 the kinetic term, k, could be fixed at the value obtained for the acid washed sample with no negative impact on the goodness of the fit and so k is not shown in Figure 5.16. Doing this isolates the effects of the catalysts to the remaining three parameters (ψ, g and b).

The best fit parameters for Equation 3.7 for the Ca doped wood as a function of the calcium concentration is shown in Figure 5.17. The parameters k, ψ and a all show some dependence on the calcium concentration whereas c is approximately zero for all cases. The results for Equation 3.10 for the Ca doped wood is shown in Figure 5.18. In this case all the parameters show some dependence on the calcium concentration, but the correlation for parameter b is not as strong as the others. As with the potassium loaded samples the kinetic term, k, was fixed at the value obtained for the acid washed sample and so is not shown in Figure 5.18. The best fit parameters for Equation 3.11 for the

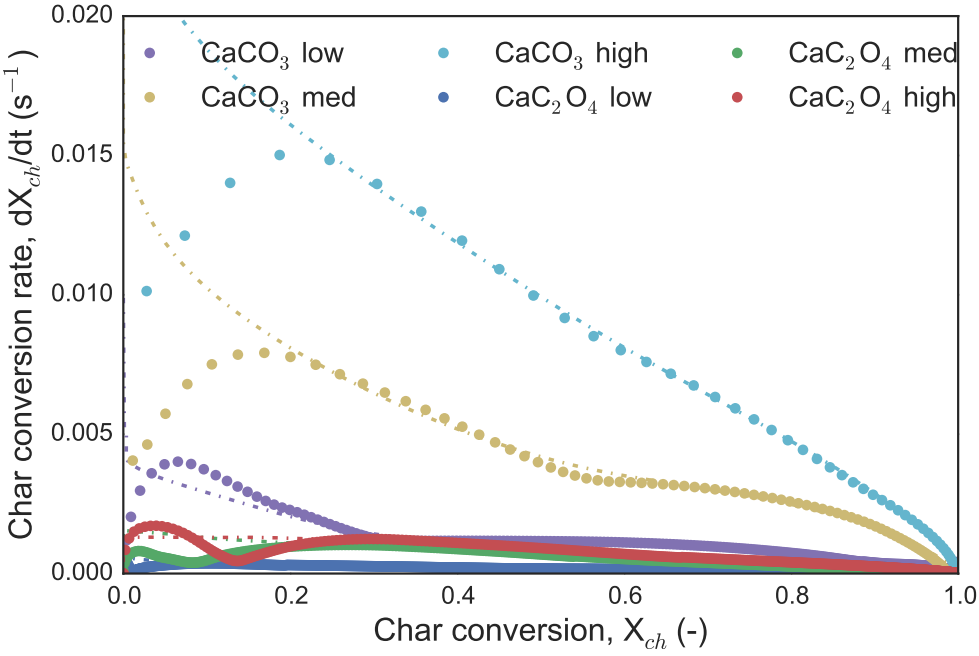

Figure 5.14: Conversion rate measurements for $CaCO_3$ and CaC_2O_4 impregnated spruce wood in 100% CO_2 and 850°C. The dot-dash lines show the best fit for Equation 3.11 to the experimental data.

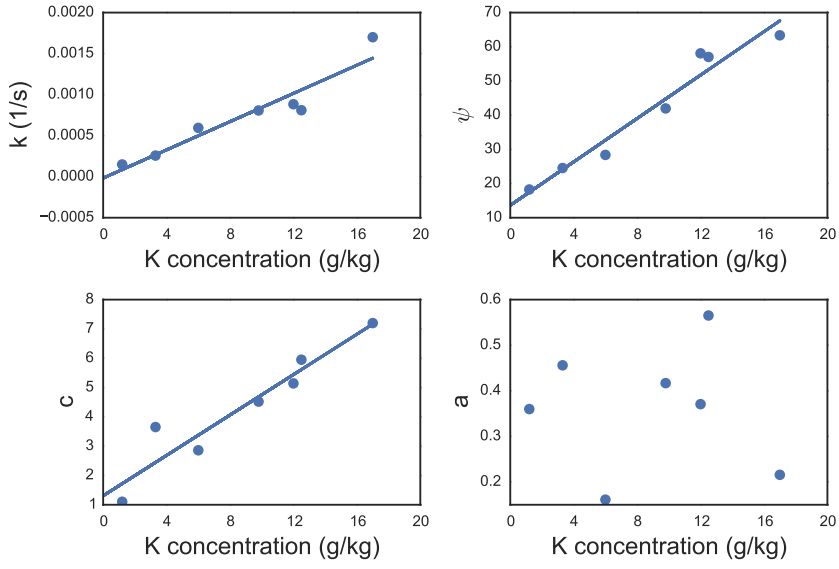

Figure 5.15: Best fit parameters for Equation 3.7 vs the potassium concentration in the K doped and K_2CO_3 impregnated wood.

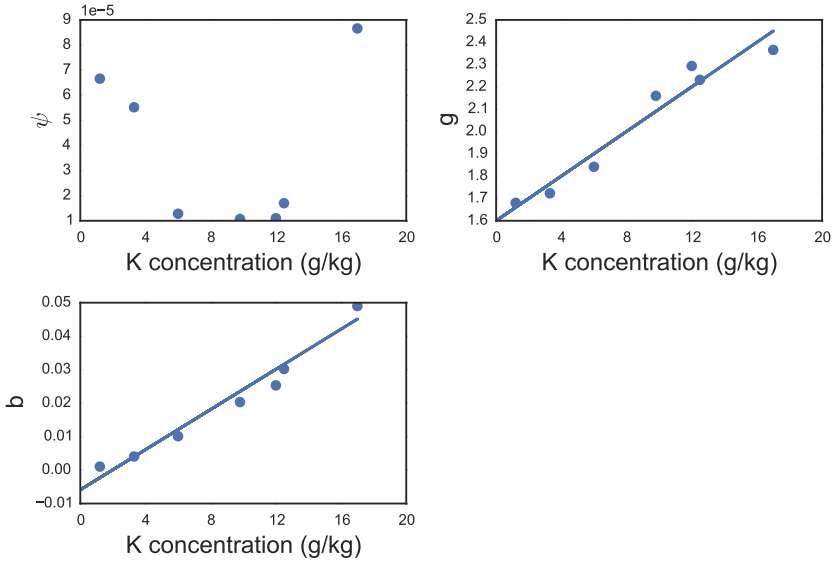

Figure 5.16: Best fit parameters for Equation 3.10 vs the potassium concentration in the K doped and K_2CO_3 impregnated wood.

conversion rate data of the $CaCO_3$ and CaC_2O_4 impregnated samples as a function of calcium concentration in the wood are shown in Figure 5.19.

As discussed in Section 2.2.2, in the original RPM the structural parameter ψ described the evolution of the pore structure during conversion and could be calculated from physical properties of the char. The parameter can also be obtained from conversion rate measurements, such as by fitting the RPM to the experimental data. Even when obtaining ψ by fitting to experimental data, it can be assumed that the larger the value of ψ, the greater the influence of the changing pore structure on the conversion rate. While this physical interpretation of ψ may hold for non-catalytic gasification of char, the meaning is less clear when catalysts on the char surface cause changes in the conversion rate independent of the pore structure. If fitting the RPM to conversion rate data of catalytic char gasification the physical interpretation of ψ becomes more difficult to determine, as the term will describe a combination of both structural and catalytic effects. The modified versions of the RPM given in Equations 3.7, 3.10 and 3.11, contain separate terms to describe the catalytic effects. However, when obtaining the all the parameters simultaneously by fitting the model to conversion rate data, as was done in this work, there is no way to isolate the effects of the catalysts to the catalytic terms and the effects of the pore structure to ψ. As such, while the models fit the experimental conversion rate data well, any attempt to gain insight from the best fit parameters into the physical processes occurring on the char during conversion are tenuous.

A simple empirical model was developed to predict char conversion rates based on inorganic concentrations in the parent wood, using the best fit parameters for the conversion models discussed above. A set of correlations for the best fit parameters was obtained using the linear regression lines shown in Figures 5.15-5.19. The empirical model assumes that the total conversion rate of the char is a sum of the conversion rate due to the catalytic

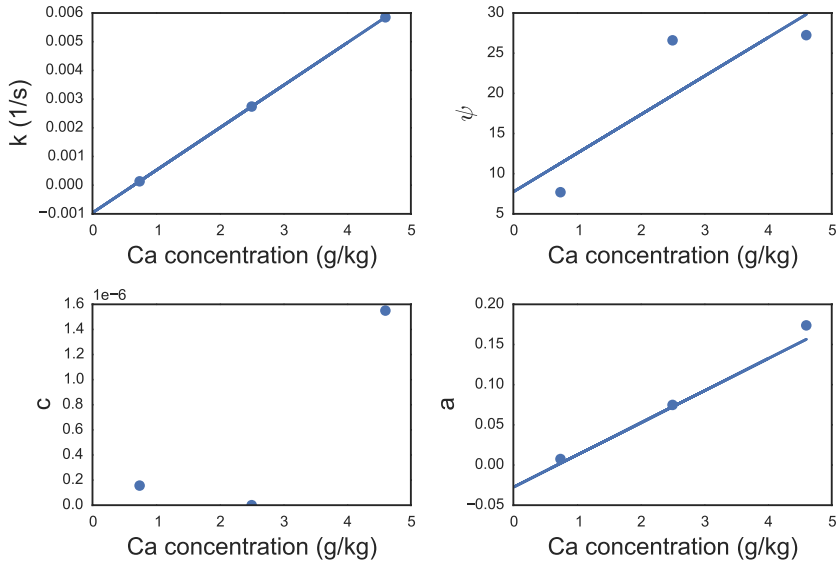

Figure 5.17: Best fit parameters for Equation 3.7 vs the calcium concentration in the Ca doped wood.

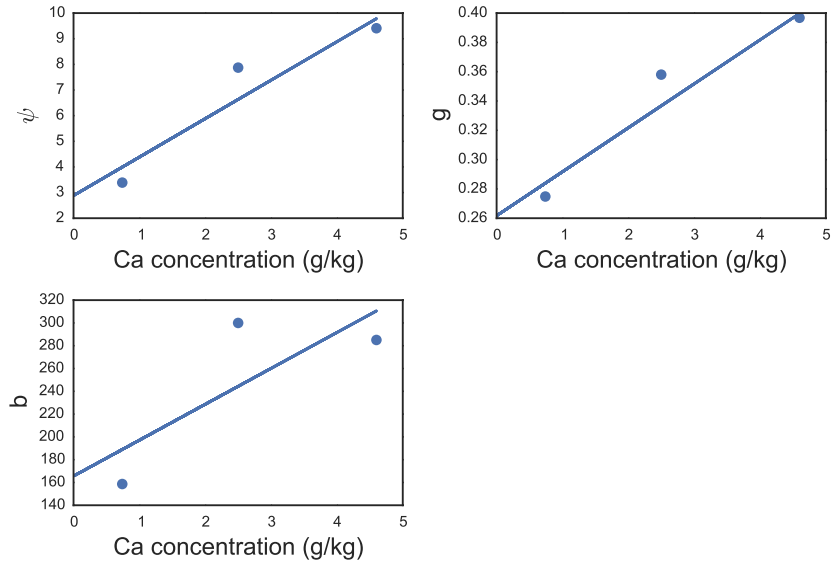

Figure 5.18: Best fit parameters for Equation 3.10 vs the calcium concentration in the Ca doped wood.

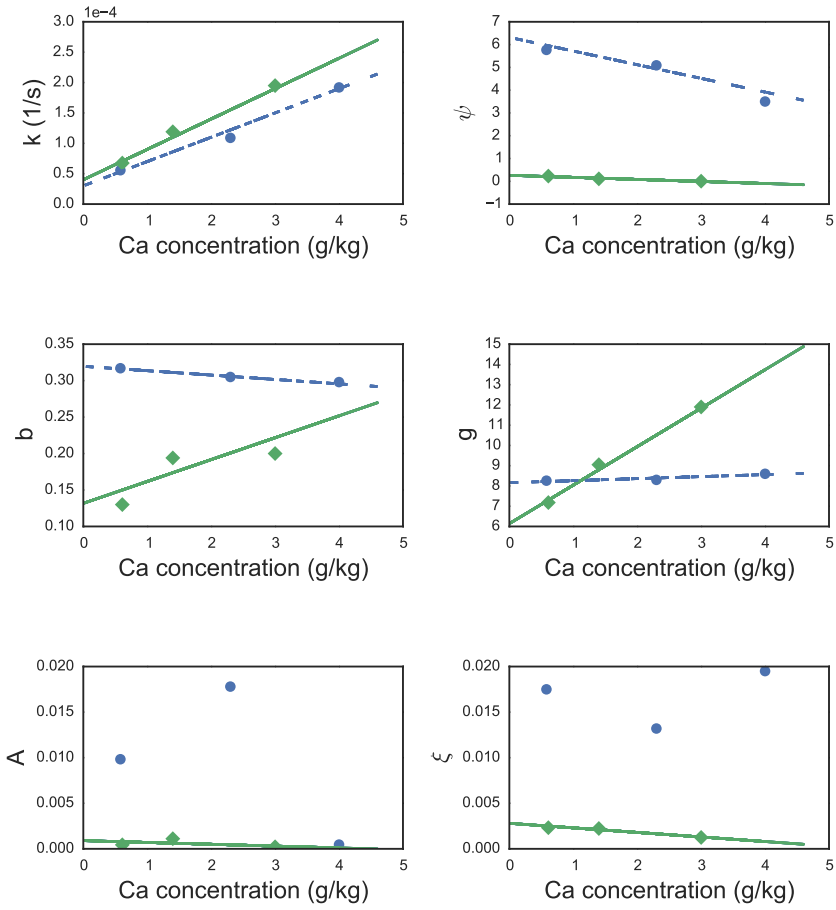

Figure 5.19: Best fit parameters for Equation 3.11 vs the calcium concentration in the $CaCO_3$ and CaC_2O_3 impregnated wood. The blue circles and blue dashed line show the parameters and regression line for the $CaCO_3$ loaded wood and the green diamonds and green solid line show the parameters and regression line for the CaC_2O_4 loaded wood.

effects of calcium and potassium, as given by

$$\frac{dX_{ch}}{dt} = (\frac{dX_{ch}}{dt})_{Ca} + (\frac{dX_{ch}}{dt})_{K}. \tag{5.5}$$

The conversion rate due to calcium and potassium, dX_{ch}/dt_{Ca} and dX_{ch}/dt_{K} respectively, is given by Equation 3.10. The parameters for Equation 3.10 can be calculated from the linear regressions shown in Figures 5.16 and 5.18, and are given by:

$$k_{Ca} = 1.43 \cdot 10^{-4}, \tag{5.6}$$

$$\psi_{Ca} = 0.0015 * w_{Ca} + 2.88, \tag{5.7}$$

$$g_{Ca} = 0.000031 * w_{Ca} + 0.2628, \tag{5.8}$$

$$b_{Ca} = 0.0317 * w_{Ca} + 165, \tag{5.9}$$

$$k_{K} = 1.43 \cdot 10^{-4}, \tag{5.10}$$

$$\psi_{K} = 0, \tag{5.11}$$

$$g_{K} = 0.000050 * w_{K} + 1.6, \tag{5.12}$$

$$b_{K} = 0.0000029 * w_{K} - 0.0059, \tag{5.13}$$

where w_{Ca} and w_k are the concentrations of calcium and potassium in the original biomass (g/kg).

The empirical model given by Equations 5.5-5.13 was used to predict the conversion time for the same samples shown in Table 5.5. For the Ca doped samples, using the empirical model gave a mean percentage error of 13% while for the potassium loaded samples the mean percentage error was 29%. These values are slightly higher than for the best fit values shown in Table 5.5 but the increase in error is not large.

The empirical model was also used to predict the conversion rate for raw spruce wood gasified in 100% CO_2. The result of the empirical model is shown with the measured conversion rate in Figure 5.20. The empirical model under predicts the conversion rate, particularly at low char conversion. This is likely due to the presence of other inorganics in the wood which are not accounted for in the model, such as Mn and Fe. Manganese in particular has been shown to be catalytically active in similar wood chars [4].

5.1.4 Effects of K and Ca on char gasification in fluidized bed

The effects of potassium and calcium on birch wood gasification was investigated using a fluidized bed reactor, as described in Section 4.3.1. Pyrolysis gas yields as a function of pyrolysis temperature are shown in Figure 5.21 and 5.22 for raw birch wood. The pyrolysis gas composition changes little as the temperature increases from 750°C to 900°C, though CO_2 shows an increasing trend. The undetected fraction of the pyrolysis products, consisting primarily of condensible tars and water vapor and calculated by mass balance, decreased as temperature increased indicating reduced tar yield at higher temperatures.

The pyrolysis yield results differ from many other published results in a number of ways. The largest difference comes from the high yield of CO_2 obtained in the present work, around 0.5 g/g fuel. This was much higher than what is commonly reported [38, 96]. Similarly the CO yield was correspondingly lower compared to other studies. The undetected faction (tars and water vapor) is also lower than was expected. These

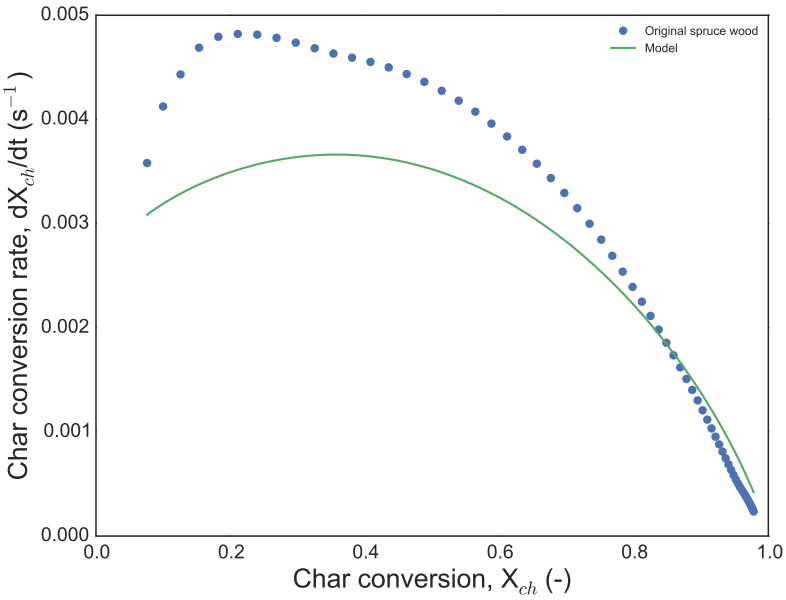

Figure 5.20: The conversion rate curve for raw spruce wood in 100% CO_2 at 850°C compared with the results from the empirical model given by Equations 5.5-5.13.

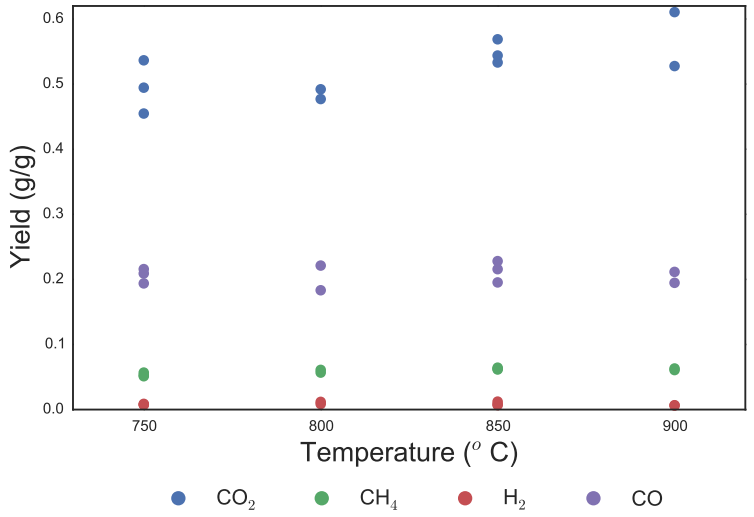

Figure 5.21: Pyroylsis yields for CO_2, CH_4, H_2 and CO from raw birch wood as a function of pyrolysis temperature. The multiple points for each gas at a given temperature show repeated measurements.

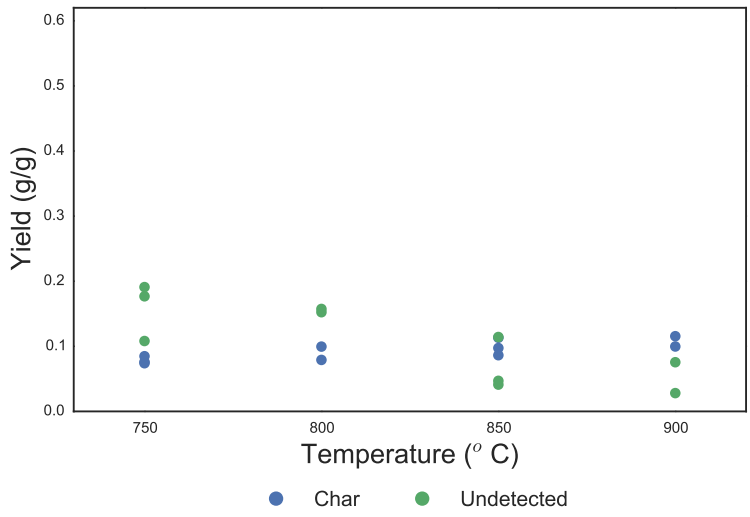

Figure 5.22: Pyroylsis yields of char and undetected fraction for raw birch wood as a function of pyrolysis temperature. The undetected fraction was calculated by mass balance and contained all the condensible products including tars and water vapor. The multiple points for product at a given temperature show repeated measurements.

issues are likely caused by the low gas velocity used in the measurements which created long gas residence times in the reactor of approximately 2.5-3.5 seconds. This long residence time, combined with the use of olivine as a bed material which has been shown to promote the water-gas shift reaction [107] as well as reduce tar yields [112], can lead to a change in the distribution of pyrolysis products.

The effect of potassium and calcium concentration of pyrolysis yields at 850°C is presented in Figure 5.23. There are few noticeable trends in the pyrolysis yields. The leached samples have the highest undetected fraction and slightly lower char and gas yields. This is consistent with earlier work which showed leached wood had decreased char and gas yields compared to unleached wood when pyrolyzed in a fluidized bed at 400°C [4]. Char yield increased linearly with potassium doping but calcium had little effect.

The leached birch wood char had a much lower conversion rate than the raw birch wood char (Figure 5.24). Potassium doping had little effect on char reactivity compared with the leached wood chars. The potassium doped woods had initially a slightly higher conversion rate than the leached wood, but after approximately 20% conversion there was no difference in the behavior of the K doped and leached wood. This applied for both the K med and K high samples, though the K concentration was different in each.

Calcium doped wood chars showed significantly increased conversion rate compared with the leached wood. The conversion rates for the calcium doped wood were proportional to the calcium concentration in the wood and were approximately in the same range as conversion rate for the raw birch wood. The calcium doped chars tended to show a higher initial conversion rate peak after which the conversion rate continuously decreased. After approximately 50% char conversion the raw birch wood tended to have a higher conversion rate than the calcium doped woods.

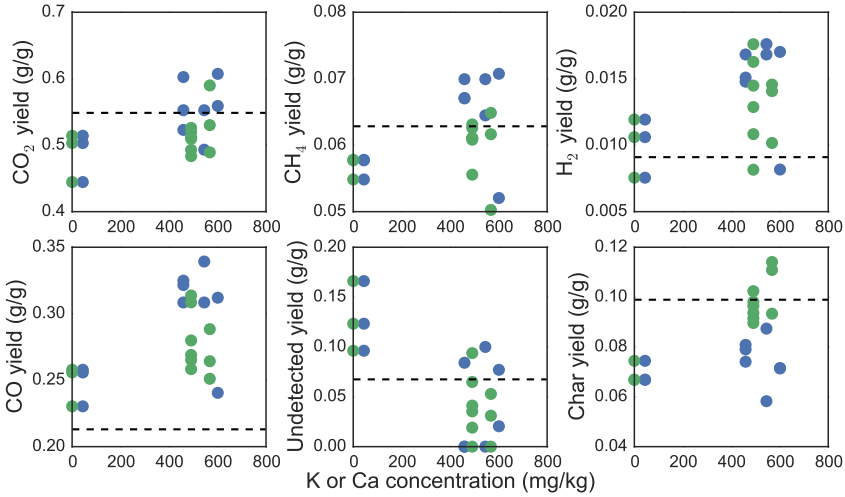

Figure 5.23: Pyrolysis yields for doped birch wood as a function of K or Ca concentration at 850°C. The blue points indicate the calcium concentration and green points the potassium concentration. The black dashed line shows the average yield for raw birch wood at at 850°C. Each point represents a single measurement.

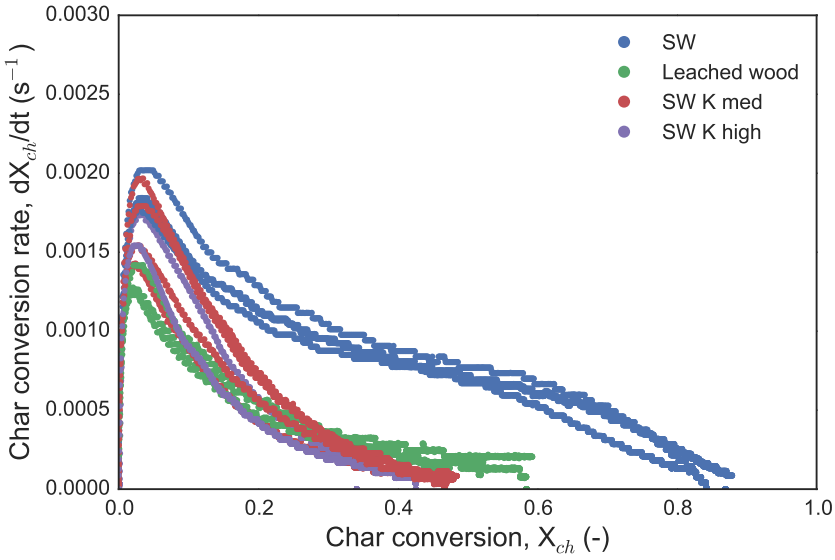

Figure 5.24: Conversion rate curves for raw, leached and K doped birch wood chars in 20% CO_2/80% N_2 at 850°C. Multiple measurements are shown for each sample to show the repeatability of the conversion rate curves.

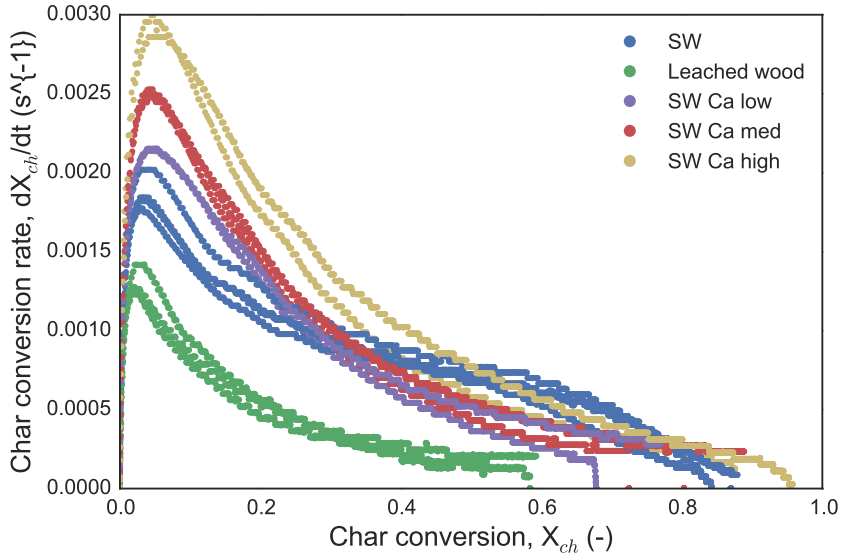

Figure 5.25: Conversion rate curves for raw, leached and Ca doped birch wood chars in 20% CO_2/80% N_2 at 850°C. Multiple measurements are shown for each sample to show the repeatability of the conversion rate curves.

Most earlier studies of the effects of calcium and potassium on char conversion have been done in TGA devices with slower heating rates. Because the pyrolysis conditions will effect the resulting char reactivity [14] it is difficult to make direct comparisons with earlier work. In addition to the different heating rates, most studies add the inorganic catalysts directly to the chars rather than to the parent biomass which will cause further differences. When chars were prepared using the same doping method but gasified in a TGA with lower heating rates (approximate 50°C/s) and with 100% CO_2 during devolatilization and gasification, both Ca and K doped samples showed increased reactivity compared to the leached wood [71, 102]. In those studies the inorganic catalyst concentrations were generally much higher than what was used in the current work, however.

Other studies, using a variety of char preparation and gasification methods, have reported a measurable increase in char reactivity after potassium loading [48, 55, 67, 86]. Potassium has been shown to react with silicon in the fuel [51, 56] and so the possibility that the potassium was being deactivated as a catalyst by reacting with the silicon in the olivine bed was also considered in the present work. In order to test this the bed material was replaced with a bauxite, a non-silicon containing material, for some tests. However, the reactivity of raw wood and K doped wood using the bauxite bed showed no differences compared to the olivine bed.

Char samples were collected from the fluidized bed using the methods described in Section 4.4. SEM images were taken of four chars: raw birch wood, leach wood, K doped medium and Ca doped medium and an image of each char is shown in Figure 5.26. The raw birch wood (subfigure A) and the K doped wood (subfigure B) retain the fibrous structure and shape of the parent wood particles. The leached wood (subfigure C) and Ca doped wood (subfigure D) show nearly complete loss of the wood structure. The leached and Ca doped wood show signs of plastic deformation which indicates the biomass goes through melting

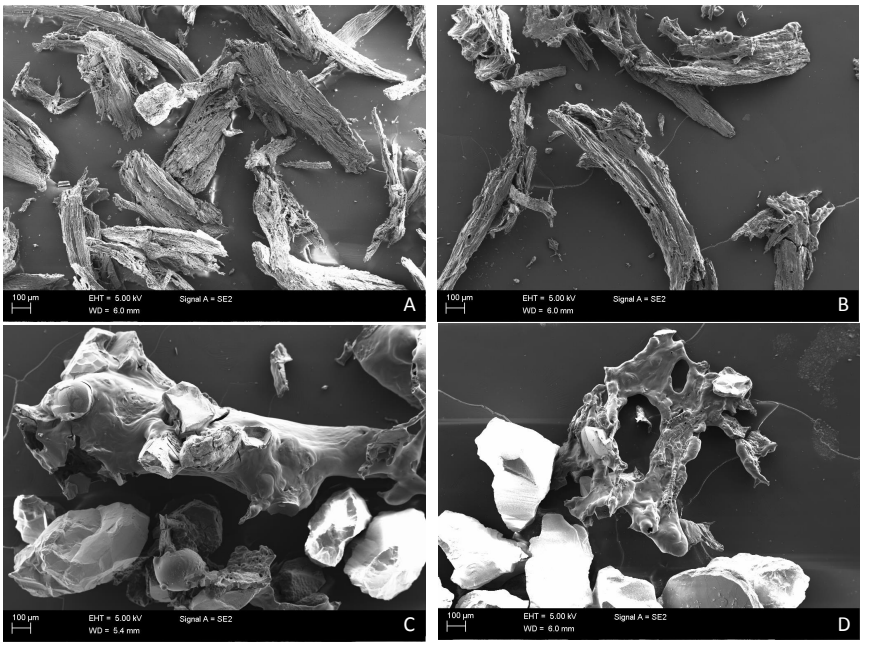

Figure 5.26: SEM images of chars collected from the fluidized bed after pyrolysis for the following samples: A) raw birch wood, B) K doped medium, C) Leached, D) Ca doped medium .

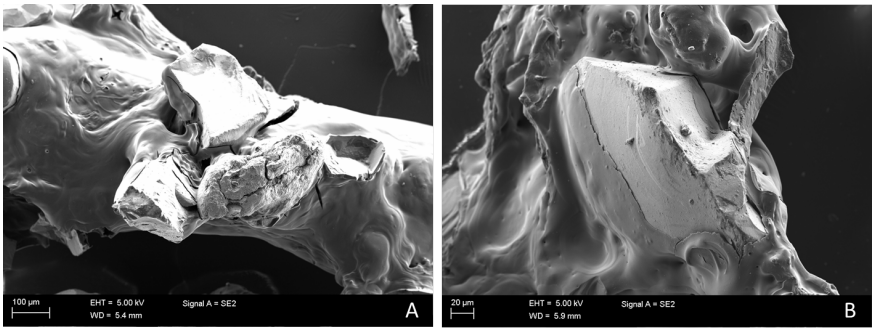

Figure 5.27: SEM images of chars collected from the fluidized bed after pyrolysis for the following samples: A) Leached, B) Ca doped medium. The bed particles can be seen embedded into the chars.

before the char is formed. Additionally, both the leached and Ca doped wood chars have become attached to bed particles, which is likely why it was not possible to push the char into the cyclone of the fluidized bed reactor by increasing the gas velocity. This is shown more clearly in Figure 5.27, which shows a close up image of the leached and Ca med chars.

It has been well documented that at high heating rates chars will show signs of plastic deformation, a result of the char precursor phase undergoing melting [14, 21, 124]. In the case of high heating rate chars which show loss of the structure of the parent material, SEM images often resemble the leached and Ca doped chars shown in Figure 5.26. This

Table 5.7: BET surface area measurements using N_2 for raw birch wood and K doped wood chars taken from the fluidized bed reactor.

Sample	Gasification time (s)	Approximate conversion	BET surface (m^2/g)
Raw birch	0	0	104
Raw birch	120	10	370
Raw birch	200	20	553
K med	0	0	0.08
K med	120	10	7.8
K med	400	20	1.3
K high	0	0	0.2

type of melting is not always observed when chars are generated in fluidized beds though. Guerrero et al. [41] compared a slow heating TGA and a fast heating fluidized bed for generating chars from eucalyptus wood. The chars generated in the fluidized bed did differ from the chars generated in the TGA, as the fluidized bed chars showed larger pores and increased surface area as a result of volatiles leaving the char more quickly. However, the fluidized bed chars did not show significant plastic deformation and so resembled the raw or K doped chars in the present work.

The influence of inorganics in the char formation process has been studied but is not thoroughly understood. Perander et al. [102] observed plastic deformation on CaC_2O_4 impregnated char, but not K, K_2CO_3 or Ca loaded chars. Jones et al. [53] showed that potassium in particular appears to influence the char formation process, as melting was observed during devolatilization of leached wood but not potassium impregnated wood.

EDS analysis was also done when preforming the SEM imaging to determine what elements are present on the char surface. The surface of the raw wood indicated large amounts of K and Ca while the leached wood showed basically no inorganics. The K doped wood char did show some presence of potassium on the char surface but it was much less than what was present on the surface of the raw wood despite the doping concentration to be approximately the same as in the raw wood. This can indicate that the potassium has been lost during devolatilization or that it has been covered by secondary char formation and is not exposed on the char surface.

In order to better understand the structural properties of the chars BET surface area measurements were conducted on the raw and K doped chars collected from the fluidized bed cyclone. It was not possible to separate enough of the leached and Ca doped wood chars from the bed material to perform the analysis. The measured BET surface area are given in Table 5.7. The specific surface area for raw birch wood after pyrolysis (i.e. 0% char conversion) is approximately 100 m^2/g, which is largely consistent with published values for biomass chars [34, 41, 42, 73, 82, 110, 116, 120]. The specific surface area increases as char conversion progresses which also agrees with most published results. However, while the specific surface area increases during conversion the instantaneous reaction rate remains nearly constant until around 80% char conversion. Because the instantaneous reaction rate should be proportional to the reactive surface area, this indicates that the BET surface area measurement is not a good measurement of reactive surface in this case.

The specific surface area of the K doped char is much lower than the surface area of the

Table 5.8: Calcium and potassium concentrations in the chars taken from the fluidized bed as measured by ICP-OES. The concentration on a wood basis was calculated assuming 9% fixed carbon for all samples.

Sample	Ca (mg/kg char C)	Ca (mg/kg wood)	K (mg/kg char C)	K (mg/kg wood)
Raw birch	8840	790	6130	550
K med	3220	290	5480	460
K high	2150	190	6160	550

raw birch wood char. Chars with similarly low surface areas have been reported in other works [2, 135], however in most cases such low surface areas are a result of incomplete pyrolysis, which is not the case in the current work. It has been observed that inorganics will block some of the meso- and micropores and result in decreased surface area and this is why leached chars tend to have higher surface areas than unleached chars [39]. There have also been studies which report that surface particles can hinder gas diffusion to carbon atoms resulting in decreased char reactivity [48, 102], but this has been observed for Ca catalyzed chars and only at high temperatures or high Ca concentrations.

If catalysts are ineffective at increasing the char reactivity, it is often a result of poor surface contact between the catalyst and the char, or due to uneven distribution of the catalyst on the char surface. This is particularly likely when using an impregnation method to load the catalysts onto the sample. The doping process used in the current work loads the metals to organic functional groups in the wood in the same way that most metals are naturally found in the wood [119]. As a result, it is unlikely that poor surface contact or poor dispersion of the potassium is the reason why the potassium doped char was unreactive.

To determine if potassium was volatilized and lost from the char during pyrolysis, the char samples were analyzed by ICP-OES. The measured potassium and calcium concentrations in the chars are shown in Table 5.8 on a char carbon basis and original biomass basis. It can be seen that the measured concentrations of potassium and calcium in the chars correspond well to the concentration in the original woods shown in Table 4.2. This indicates that most of the calcium and potassium stayed on the char rather than volatilizing during pyrolysis. It can be concluded from this that the low reactivity of the potassium doped wood is not due to loss of potassium.

The likely cause for the behavior of the potassium doped samples is coke formation on the char surface which blocks the char micropores and covers the potassium particles. The coke layer has little inorganics which is why the EDS analysis shows reduced potassium concentration on the char surface of the K doped samples compared to the raw wood and as a result the coke is relatively unreactive. The coke layer also prevents gas diffusion into the char structure where the active carbon sites are located. The presence of inorganics has been shown to influence interactions between coal volatiles and coal char which in turn affected char reactivity [79]. Coke formation on chars has also been shown to block pores in multiple studies [2, 111]. In addition, it has been shown that potassium catalyzes secondary reactions with volatiles to form seconday char in addition to increasing primary char [136]. Longer gas residence times, as in the current work, will increase the volatile-char reactions and result in increased coke formation on the potassium doped wood char.

Calcium appears to be the primary active catalyst in the gasification of spruce wood char,

though potassium and other elements may play a large role at high char conversion (i.e. char conversion greater than 60%). The presence of potassium in the wood increased char yields by catalyzing both primary and secondary char formation. The secondary char formed on the surface of the char, blocking pores and caused a decrease in char surface area. This secondary char layer was unreactive due to a low concentration of inorganics and caused the potassium doped wood char to have a lower gasification reactivity compared to leached wood. The raw birch wood char, which contained a similar potassium concentration as the K doped wood chars, did not show signs of significant secondary char formation. This may suggest there are interactions between the inorganic elements in the wood and that calcium may offset the effect of potassium in catalyzing secondary char formation.

5.2 Arsenic removal from gasification product gas

The behavior of arsenic in chromated copper arsenate (CCA) wood was modeled using equilibrium calculations and experimentally verified using a continuous feed bench scale fluidized bed gasifier. The goal of the work was to show, using equilibrium modeling, that the condensation temperature of arsenic in the product gas could be predicted, and the arsenic could be removed during lab scale gasification tests by cooling the product gas to the predicted condensation temperature. The proximate and ultimate analysis for the CCA wood is given in Table 4.1 and the ash composition in Table 4.2. A more detailed analysis of the ash components is given in Table 5.9. From these it can be seen that the arsenic concentration in the CCA wood is comparable to the concentration of the most prominent naturally occurring metals, such as calcium.

The details of the modeling approach and description of the conditions considered in the six cases (A1, A2, A3, B1, B2, B3) are given in Section 3.4. The portion of each trace element which will be found in the product gas as a function of temperature as predicted by the equilibrium model for cases B1, B2 and B3 are shown in Figures 5.28-5.30. The results for cases B1 and B2 are nearly identical and it was predicted that As begins to condense at approximately 250°C. For case B3 only 10% of the arsenic condenses around 250°C. The remaining arsenic stays in the gas phases until approximately 100°C.

The difference in behavior between cases B1 and B2 compared with B3 can be understood by examining the arsenic containing compounds which are predicted to exist as a function of temperature, as shown in Figures 5.31-5.33. In cases B1 and B2 arsenic is found as in the gas phase as As_4 until 250-300°C at which point solid or liquid As_2S_2 begins to be the thermodynamically favorable compound. In cases B3, which includes the bed material, CaS is predicted to form which captures the sulfur in the bed. As such, there is very little sulfur in the product gas and so As_2S_2 cannot form when the gas is cooled in the heat exchanger. In this case the arsenic will stay in the gas phase as As_4 until around 100°C, at which point As_2O_3 becomes the favorable compound.

While there have been no other studies which have modeled arsenic behavior in the same conditions and with arsenic concentrations as high as in the current work, some comparisons can be made to similar works. In gasification conditions for fuels with lower arsenic concentrations there have been a wide range of reported arsenic gas-solid transition temperatures. Using a similar equilibrium modeling approach for solid recovered fuels, Konttinen et al. [65] found the temperature range at which arsenic with thermodynamically favor solid or liquid phase to be 500-650°C. Diaz el al. [25] found the transition temperature to be 200-500°C for coal gasification. Jiang et al. [52] used

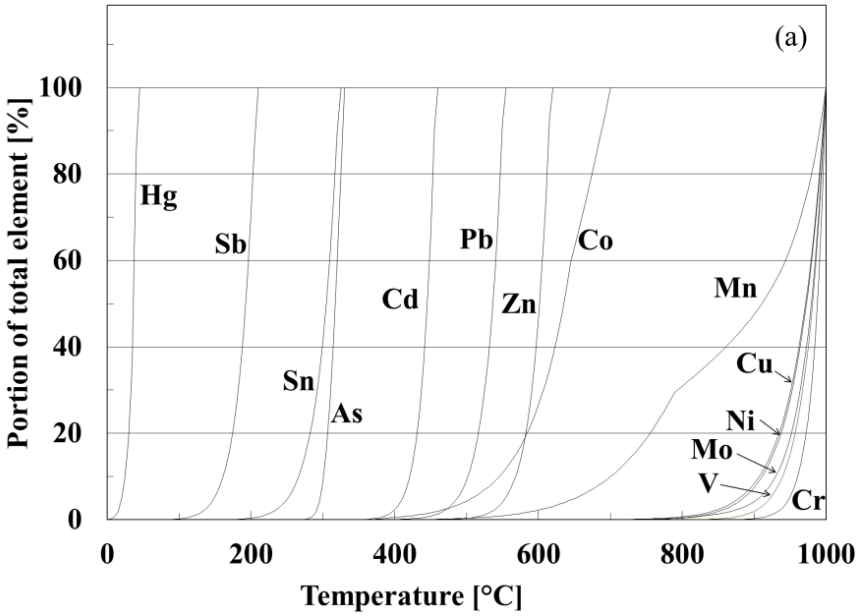

Figure 5.28: The distribution of elements in the product gas for case B1 (only main fuel ash elements included in equilibrium calculation and conditions are taken after the product gas cooling). Reprinted with permission from [72].

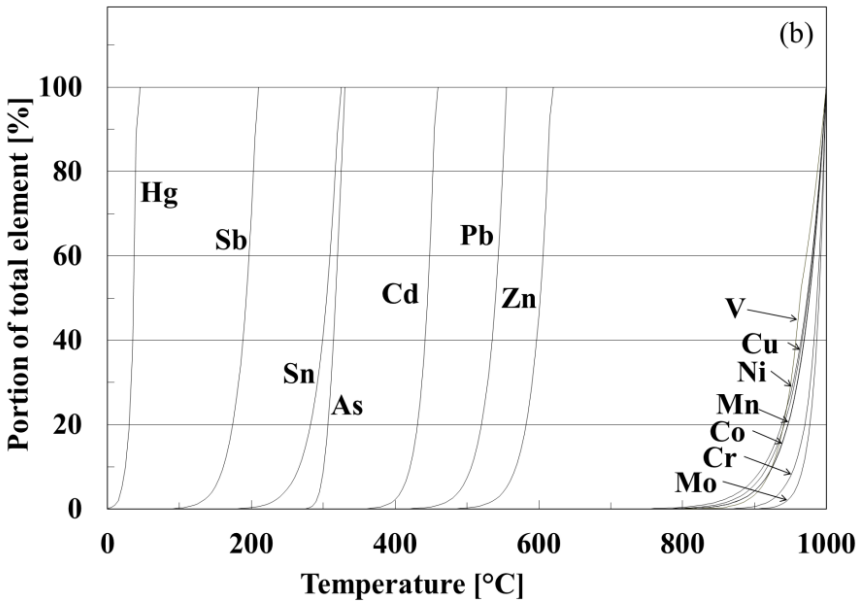

Figure 5.29: The distribution of elements in the product gas for case B2 (most fuel ash elements included in equilibrium calculation and conditions are taken after the product gas cooling). Reprinted with permission from [72].

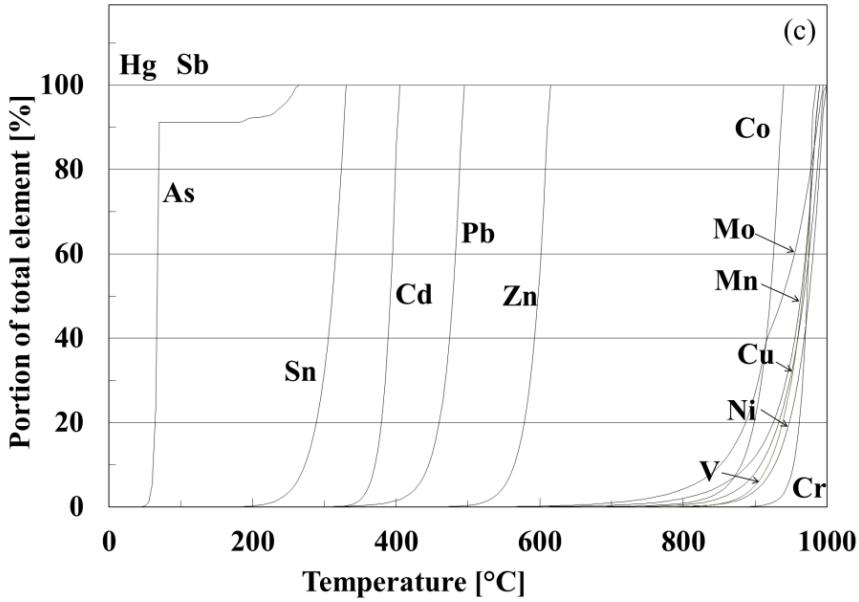

Figure 5.30: The distribution of As containing compounds in the product gas for case B3 (all fuel ash elements and bed material included in equilibrium calculation and conditions are taken after the product gas cooling). Reprinted with permission from [72].

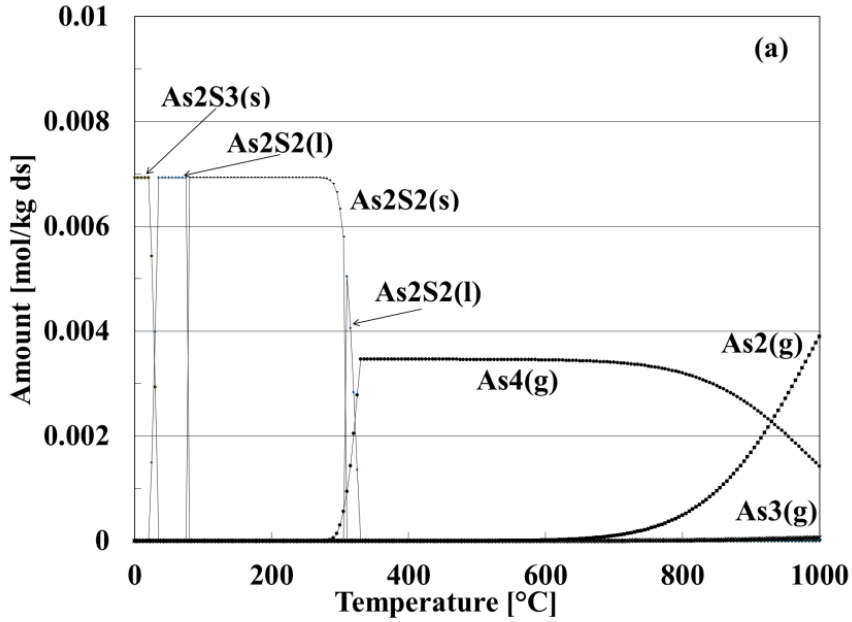

Figure 5.31: The distribution of elements in the product gas for case B1 (only main fuel ash elements included in equilibrium calculation and conditions are taken after the product gas cooling). Reprinted with permission from [72].

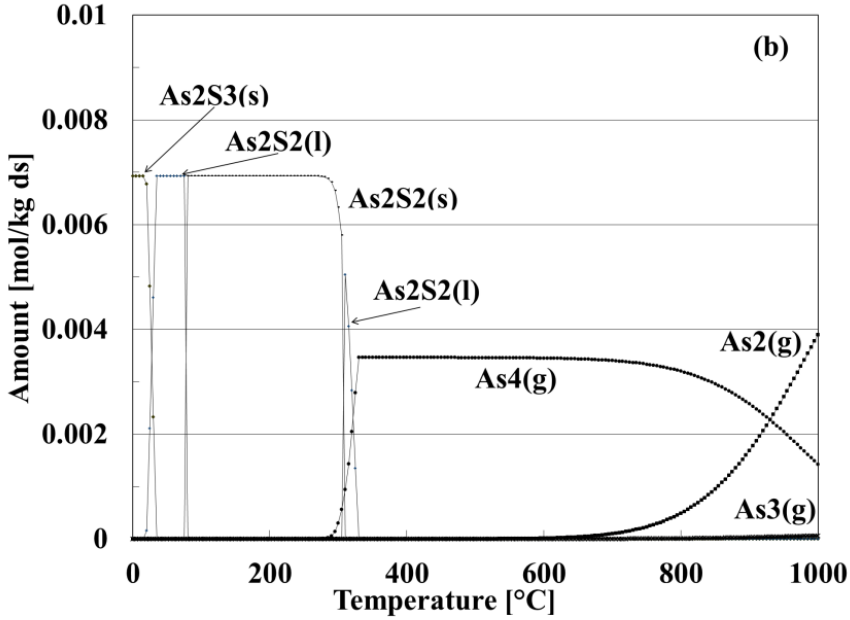

Figure 5.32: The distribution of elements in the product gas for case B2 (most fuel ash elements included in equilibrium calculation and conditions are taken after the product gas cooling). Reprinted with permission from [72].

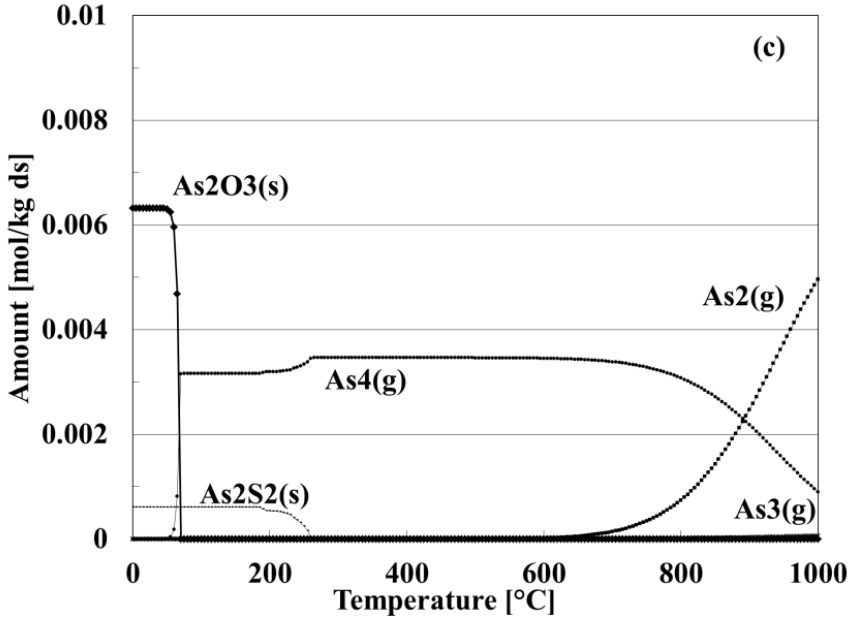

Figure 5.33: The distribution of elements in the product gas for case B3 (all fuel ash elements and bed material included in equilibrium calculation and conditions are taken after the product gas cooling). Reprinted with permission from [72].

Table 5.9: Detailed ash composition for CCA used in the fluidized bed gasification tests and equilibrium modeling.

Ash component	mg/kg ash
Al	8070
As	72,100
B	470
Ba	1160
Be	0.25
Ca	70,300
Cd	920
Co	33
Cr	57,500
Cu	66,400
Fe	60,600
K	10,300
Mg	11,000
Mn	3832
Mo	18
Na	5780
Ni	150
P	2630
Pb	1030
S	8260
Sb	270
Se	55
Sn	25
Ti	330
V	23
Zn	6010

equilibrium modeling for biomass coming from contaminated soils, however the arsenic concentrations in that biomass were still much lower than what was in the CCA wood used in the current work. Jiang et al. found the temperature at which arsenic is removed from the gas phase, according to the equilibrium calculation, to be 600-1000°C which is much higher than the temperature found by Diaz el al. or Konttinen et al.

Diaz-Somoano [24] reported equilibrium modeling results for coal gasification. That study indicated that condensed arsenic compounds will be thermodynamically favorable at temperatures below 700°C. Below 200°C no gaseous arsenic species were predicted to exist. Detailed species partitioning for arsenic compounds were only given for 2.5 MPa and the effect of HCl and H_2S in the gas atmosphere was examined. If H_2S was present in the gas atmosphere the equilibrium calculations predicted that at temperatures below 400°C arsenic will be primarily in the condensed phase. If there is no H_2S in the gas atmosphere then arsenic favors the condensed phase at temperatures below 800°C, first as FeAs and $FeAs_2$ and finally as As.

While arsenic and other more common trace elements may behave differently under combustion conditions compared to gasification conditions [33, 100], it can still be useful to compare the results of equilibrium modeling for combustion. Contreras et al. reported

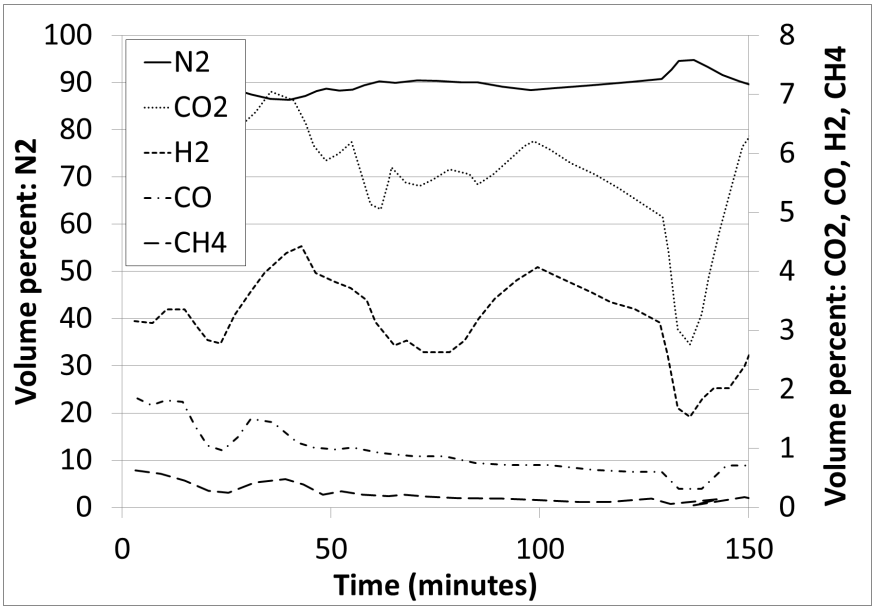

Figure 5.34: Exit gas composition from fluidized bed continuous gasification test using CCA wood for test #1. Reprinted with permission from [72].

Table 5.10: Arsenic balance for three continuous feed fluidized bed gasification tests using CCA wood.

	Test 1	Test 2	Test 3
As input, mol/s	$5.41{\cdot}10^{-7}$	$3.60{\cdot}10^{-6}$	$1.80{\cdot}10^{-6}$
As in product gas before filtering, mol/s	$4.60{\cdot}10^{-8}$	$9.74{\cdot}10^{-8}$	$4.75{\cdot}10^{-8}$
As in product gas after filtering, mol/s	$8.42{\cdot}10^{-10}$	$3.95{\cdot}10^{-9}$	$7.58{\cdot}10^{-9}$
Percent of As retained in bed, %	91.5	97.3	97.4
Percent of remaining As captured in filter, %	98.2	96.0	83.8
Total As removed from product gas, %	99.8	99.9	99.6

equilibrium results for arsenic species and the interactions with trace species during combustion [20]. If no interactions with trace species are considered then Contreras et al. reported the arsenic condensation temperature would be approximately 250°C, at which point As_2O_5 becomes thermodynamically favorable. If interactions with trace elements are considered in the equilibrium calculations then arsenic begins to be removed from the gas phase at temperatures as high as 1100°C. Shen et al. [111] also studied coal combustion using equilibrium modeling and reported that arsenic may form condensed compounds at temperatures around 1000°C.

The measured product gas composition as a function of gasification time is shown in Figure 5.34 and 5.35 for two continuous feed tests. The calculated arsenic material balance for all three gasification tests is shown in Table 5.10. The exit gas composition shows that good gasification was achieved as the H_2 content of the gas is relatively high. Most of the arsenic was captured in the bed and did not leave in the product. Of the arsenic that did leave in the product gas an average of 93% was captured by the hot filter, giving a total arsenic captured by the system (either in the bed or hot filter) of 99.8%.

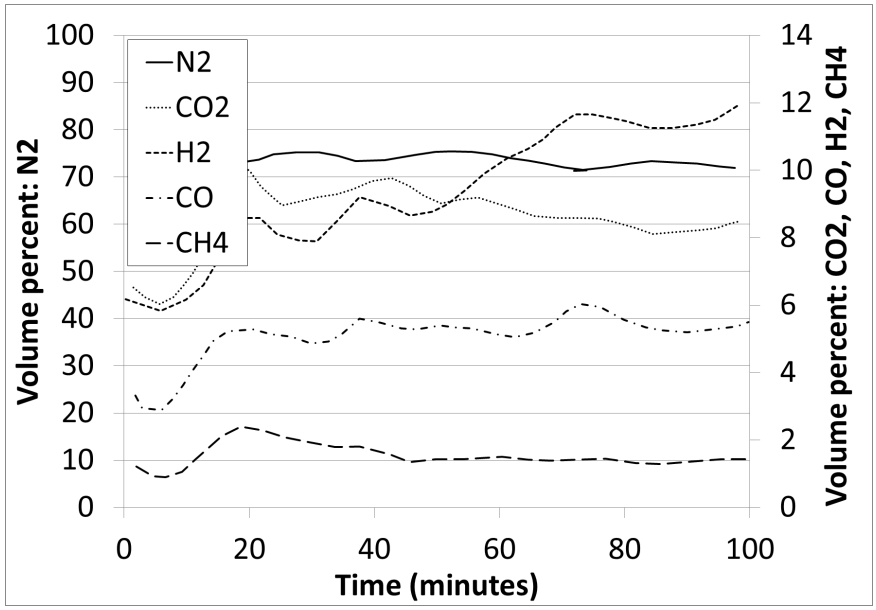

Figure 5.35: Exit gas composition from fluidized bed continuous gasification test using CCA wood for test #2. Reprinted with permission from [72].

Table 5.11: Arsenic balance for three continuous feed fluidized bed gasification tests using CCA wood.

	B1	B2	B3	Averaged measured
As in gas after cleaning at 260°C, %	0.4	0.4	99.5	0.2

The experimental results showed that most of the arsenic in the product gas can be captured at 260°C by the hot filter, which agrees with modeling cases B1 and B2. Modeling case B3 predicted that most of the arsenic would remain in the gas phase after being cooled to 260°C and so does not agree with the experimental results. A comparison of the equilibrium modeling results and experimental results for the total arsenic remaining in the gas phase after filtering at 260°C is shown in Table 5.11.

6 Conclusion

The role of inorganics in biomass gasification has been studied in this work, with a focus on the catalytic effects of potassium and calcium during char gasification as well as the behavior of arsenic in the product gas. The catalytic effects of potassium and calcium were investigated using both thermogravimetric analysis and in a fluidized bed. The experimental data was used in modeling the char conversion rate curves as a function of inorganic concentrations. Arsenic behavior in biomass gasification was investigated using continuous feed fluidized bed gasification tests and modeled using equilibrium calculations.

As discussed in Chapter 2 the underlying mechanism of catalytic char gasification is still not thoroughly understood and as a result there is no consensus in the approach to modeling. Despite evidence that the random pore model may not describe the reality of the char gasification process, it remains commonly used and has been shown to accurately model the conversion rate curves of many fuels. A modified version of the random pore model was used in this work to model the catalytic gasification of spruce wood char in a TGA and the fitting parameters of the model were correlated to the potassium and calcium concentration in the wood samples. From this, an empirical model was developed to allow for the prediction of the conversion rate of the wood based on the initial ash composition.

While the effect of catalysts on the char gasification behavior is complex, as seen in the complexity of the models used to describe the behavior, the changes in the conversion rate curve of the char were generally proportional to the concentration of catalyst in the wood. This was true even at very high catalyst loading, for example the spruce wood K high samples containing approximately 60 times the potassium as the original spruce wood. This may indicate that the presence of the inorganic catalysts is the primary determinant of the conversion rate behavior of the char under the conditions tested in the TGA.

Birch wood was loaded with Ca or K and gasified in a fluidized bed reactor and showed both similarities and differences to the behavior of the spruce wood in the TGA. In the fluidized bed, as in the TGA, the calcium doped samples showed increased reactivity as a function of Ca concentration. However the potassium doped wood did not show any catalytic effects when gasified in the fluidized bed, unlike the TGA. It was determined that the likely cause of this was due to secondary char formation on the char surface which was catalyzed by the potassium. The secondary char covered the micropores of the char and had little inorganics in it which made it comparatively unreactive. As both the Ca and K doped wood exhibited behaviors not seen in the raw wood, it is likely that there are interactions between the inorganics in the char which effect the physical structure and reactivity of the char.

The behavior of arsenic in gasification of CCA wood was also investigated using equilibrium modeling and validated using fluidized bed tests. The equilibrium modeling predicted

that the arsenic would condense from the product gas at approximately 250°C if the bed material is not included in the equilibrium calculations, while if the bed material was included the arsenic would not condense until below 100°C. Experiments indicated that by cooling the product gas to 260°C before filtering the gas approximately 99.8% of the arsenic could be removed. Both the modeling and experimental results can be applied to large scale gasification systems for using biomass fuels with high arsenic content.

Inorganics in biomass, whether naturally occurring or added, have a varied of effects on the operation of a gasifier. Positive effects, such as increased char reactivity, may seem small compared to the negative effects, such as corrosion, bed agglomeration and toxic emissions. However, as the reactivity of char has been shown to be largely determined by the presence and concentration of inorganics it is important to understand this aspect. While there are methods for modeling the effects of inorganics in catalyzing char gasification, further research into interconnected issues of surface area, pore sizes, pyrolysis conditions and inorganic concentrations is needed. Similarly, while equilibrium modeling has been shown to predict the behavior of arsenic during gasification in some cases there are many gaps in understanding which arsenic compounds are most relevant.

Bibliography

[1] "Gasification & Syngas Technologies Council," 2016. [Online]. Available: http://www.gasification-syngas.org/

[2] Abu El-Rub, Z., Bramer, E. A., and Brem, G., "Experimental comparison of biomass chars with other catalysts for tar reduction," *Fuel*, vol. 87, no. 10-11, pp. 2243–2252, 2008.

[3] Agency, I. E., "Medium-term renewable energy market report 2015," 2015. [Online]. Available: https://www.iea.org/bookshop/708-Medium-Term_Renewable_Energy_Market_Report_2015

[4] Aho, A., DeMartini, N., Pranovich, A., Krogell, J., Kumar, N., Eränen, K., Holmbom, B., Salmi, T., Hupa, M., and Murzin, D. Y., "Pyrolysis of pine and gasification of pine chars–influence of organically bound metals." *Bioresource technology*, vol. 128, pp. 22–9, jan 2013. [Online]. Available: http://www.ncbi.nlm.nih.gov/pubmed/23196217

[5] Ahrenfeldt, J., Thomsen, T. P., Henriksen, U., and Clausen, L. R., "Biomass gasification cogeneration - A review of state of the art technology and near future perspectives," *Applied Thermal Engineering*, vol. 50, no. 2, pp. 1407–1417, 2013. [Online]. Available: http://dx.doi.org/10.1016/j.applthermaleng.2011.12.040

[6] Ballal, G. and Zygourakis, K., "Evolution of pore surface area during noncatalytic gas-solid reactions. 1. Model development," *Industrial & Engineering Chemistry Research*, vol. 26, no. 5, pp. 911–921, may 1987. [Online]. Available: http://pubs.acs.org/doi/abs/10.1021/ie00065a011

[7] Barrio, M. and Hustad, J., "CO2 Gasification of Birch Char and the Effect of CO Inhibition on the Calculation of Chemical Kinetics," in *Progress in Thermochemical Biomass Conversion*. Oxford, UK: Blackwell Science Ltd, pp. 47–60. [Online]. Available: http://doi.wiley.com/10.1002/9780470694954.ch3

[8] Barrio, M., "Experimental investigation of small-scale gasification of woody biomass," Ph.D. dissertation, Norwegian University of Science and Technology, 2002. [Online]. Available: http://ntnu.diva-portal.org/smash/record.jsf?pid=diva2:126378

[9] Baskar, C., Baskar, S., and Dhillon, R. S., Eds., *Biomass Conversion*. Springer, 2012. [Online]. Available: http://www.springer.com/engineering/energy+technology/book/978-3-642-28417-5

[10] Bhatia, S. K. and Perlmutter, D. D., "A random pore model for fluid-solid reactions: I. Isothermal, kinetic control," *AIChE Journal*, vol. 26, no. 3, pp. 379–386, may 1980. [Online]. Available: http://doi.wiley.com/10.1002/aic.690260308

[11] Bourguignon, D., "Biomass for electricity and heating," European Parliamentary Research Service, Tech. Rep., 2015. [Online]. Available: http://www.europarl.europa.eu/RegData/etudes/BRIE/2015/568329/EPRS{_}BRI(2015)568329{_}EN.pdf

[12] Branca, C., Di Blasi, C., Galgano, A., and Broström, M., "Effects of the Torrefaction Conditions on the Fixed-Bed Pyrolysis of Norway Spruce," *Energy & Fuels*, vol. 28, pp. 5882–5891, 2014. [Online]. Available: http://dx.doi.org/10.1021/ef501395b

[13] Cazorla-Amoros, D., Linares-Solano, a., Salinas-Martinez de Lecea, C., and Joly, J. P., "A temperature-programmed reaction study of calcium-catalyzed carbon gasification," *Energy & Fuels*, vol. 6, no. 3, pp. 287–293, 1992. [Online]. Available: http://pubs.acs.org/doi/abs/10.1021/ef00033a008

[14] Cetin, E., Moghtaderi, B., Gupta, R., and Wall, T., "Influence of pyrolysis conditions on the structure and gasification reactivity of biomass chars," *Fuel*, vol. 83, no. 16, pp. 2139–2150, nov 2004. [Online]. Available: http://linkinghub.elsevier.com/retrieve/pii/S0016236104001437

[15] Cetin, E., Gupta, R., and Moghtaderi, B., "Effect of pyrolysis pressure and heating rate on radiata pine char structure and apparent gasification reactivity," *Fuel*, vol. 84, no. 10, pp. 1328–1334, jul 2005. [Online]. Available: http://www.sciencedirect.com/science/article/pii/S0016236104003291

[16] Chen, S. G. and Yang, R. T., "Unified Mechanism of Alkali and Alkaline Earth Catalyzed Gasification Reactions of Carbon by CO 2 and H 2 O," *Energy & Fuels*, vol. 11, no. 2, pp. 421–427, 1997. [Online]. Available: http://dx.doi.org/10.1021/ef960099o

[17] Chum, H., A., Faaij, J., Moreira, G., Berndes, P., Dhamija, H., Dong, B., Gabrielle, Goss Eng, A., Lucht, W., Mapako, M., Masera Cerutti, O., McIntyre, T., Minowa, T., and Pingoud, K., "Bioenergy. In IPCC Special Report on Renewable Energy Sources and Climate Change Mitigation," Intergovernmental Panel on Climate Change, Tech. Rep., 2011. [Online]. Available: https://www.ipcc.ch/pdf/special-reports/srren/Chapter2Bioenergy.pdf

[18] Collins, S. M., "S.Amdt.3140 to S.Amdt.2953," 2016. [Online]. Available: https://www.congress.gov/amendment/114th-congress/senate-amendment/3140/text

[19] Commission, E., "Energy roadmap 2050," 2011. [Online]. Available: https://ec.europa.eu/energy/en/topics/energy-strategy/2050-energy-strategy

[20] Contreras, M. L., Arostegui, J. M., and Armesto, L., "Arsenic interactions during co-combustion processes based on thermodynamic equilibrium calculations," *Fuel*, vol. 88, no. 3, pp. 539–546, 2009.

[21] Dall'Ora, M., Jensen, P. A., and Jensen, A. D., "Suspension combustion of wood: Influence of pyrolysis conditions on char yield, morphology, and reactivity," *Energy and Fuels*, vol. 22, no. 5, pp. 2955–2962, 2008.

[22] de Lasa, H., Salaices, E., Mazumder, J., and Lucky, R., "Catalytic Steam Gasification of Biomass: Catalysts, Thermodynamics and Kinetics," *Chemical Reviews*, vol. 111, no. 9, pp. 5404–5433, sep 2011. [Online]. Available: http://pubs.acs.org/doi/abs/10.1021/cr200024w

[23] Di Blasi, C., "Combustion and gasification rates of lignocellulosic chars," *Progress in Energy and Combustion Science*, vol. 35, no. 2, pp. 121–140, apr 2009. [Online]. Available: http://linkinghub.elsevier.com/retrieve/pii/S0360128508000440

[24] Diaz-Somoano, M. and Martinez-Tarazona, M. R., "Retention of trace elements using fly ash in a coal gasification flue gas," *Journal of Chemical Technology and Biotechnology*, vol. 77, no. 3, pp. 396–402, 2002. [Online]. Available: {\T1\textless}GotoISI{\T1\textgreater}://000174216200030$\delimiter"026E30F$nhttp://onlinelibrary.wiley.com/store/10.1002/jctb.599/asset/599{_}ftp.pdf?v=1{&}t=h0x7hkhl{&}s=5f68db939c5beacb7935775c36fd834a5494864a

[25] ———, "Retention of arsenic and selenium compounds using limestone in a coal gasification flue gas." *Environmental science & technology*, vol. 38, no. 3, pp. 899–903, 2004. [Online]. Available: http://www.ncbi.nlm.nih.gov/pubmed/14968880

[26] Duman, G., Uddin, M. A., and Yanik, J., "The effect of char properties on gasification reactivity," *Fuel Processing Technology*, vol. 118, pp. 75–81, feb 2014. [Online]. Available: http://linkinghub.elsevier.com/retrieve/pii/S0378382013002671

[27] Dupont, C., Nocquet, T., Da Costa, J. A., and Verne-Tournon, C., "Kinetic modelling of steam gasification of various woody biomass chars: influence of inorganic elements." *Bioresource technology*, vol. 102, no. 20, pp. 9743–8, oct 2011. [Online]. Available: http://www.ncbi.nlm.nih.gov/pubmed/21862327

[28] Eom, I. Y., Kim, J. Y., Kim, T. S., Lee, S. M., Choi, D., Choi, I. G., and Choi, J. W., "Effect of essential inorganic metals on primary thermal degradation of lignocellulosic biomass," *Bioresource Technology*, vol. 104, pp. 687–694, 2012. [Online]. Available: http://dx.doi.org/10.1016/j.biortech.2011.10.035

[29] Ergun, S., "Kinetics of the Reaction of Carbon with Carbon Dioxide," *The Journal of Physical Chemistry*, vol. 60, no. 4, pp. 480–485, apr 1956. [Online]. Available: http://pubs.acs.org/doi/abs/10.1021/j150538a022

[30] Fatehi, H. and Bai, X.-S., "Structural evolution of biomass char and its effect on the gasification rate," *Applied Energy*, jan 2016. [Online]. Available: http://www.sciencedirect.com/science/article/pii/S0306261915016669

[31] Feng, B. and Bhatia, S. K., "Variation of the pore structure of coal chars during gasification," *Carbon*, vol. 41, no. 3, pp. 507–523, jan 2003. [Online]. Available: http://www.sciencedirect.com/science/article/pii/S0008622302003573http://linkinghub.elsevier.com/retrieve/pii/S0008622302003573

[32] Floess, J. K., Longwell, J. P., and Sarofim, a. F., "Intrinsic reaction kinetics of microporous carbons. 2. Catalyzed chars," *Energy & Fuels*, vol. 2, no. 6, pp. 756–764, 1988. [Online]. Available: http://pubs.acs.org/doi/abs/10.1021/ef00012a007

[33] Frandsen, F., Dam-Johansen, K., and Rasmussen, P., "Trace elements from combustion and gasification of coal—An equilibrium approach," *Progress in Energy and Combustion Science*, vol. 20, no. 2, pp. 115–138, jan 1994. [Online]. Available: http://www.sciencedirect.com/science/article/pii/0360128594900078

[34] Fu, P., Hu, S., Xiang, J., Yi, W., Bai, X., Sun, L., and Su, S., "Evolution of char structure during steam gasification of the chars produced from rapid pyrolysis of rice husk," *Bioresource Technology*, vol. 114, pp. 691–697, 2012. [Online]. Available: http://dx.doi.org/10.1016/j.biortech.2012.03.072

[35] Gadsby, J., Long, F. J., Sleightholm, P., and Sykes, K. W., "The Mechanism of the Carbon Dioxide-Carbon Reaction," *Proceedings of the Royal Society A: Mathematical, Physical and Engineering Sciences*, vol. 193, no. 1034, pp. 357–376, jul 1948. [Online]. Available: http://rspa.royalsocietypublishing.org/cgi/doi/10.1098/rspa.1948.0051

[36] Gomez, A. and Mahinpey, N., "A new model to estimate CO2 coal gasification kinetics based only on parent coal characterization properties," *Applied Energy*, vol. 137, pp. 126–133, jan 2015. [Online]. Available: http://linkinghub.elsevier.com/retrieve/pii/S0306261914010514

[37] Gomez, A., Silbermann, R., and Mahinpey, N., "A comprehensive experimental procedure for CO2 coal gasification: Is there really a maximum reaction rate?" *Applied Energy*, vol. 124, pp. 73–81, jul 2014. [Online]. Available: http://linkinghub.elsevier.com/retrieve/pii/S0306261914002220

[38] Gómez-Barea, A. and Leckner, B., "Modeling of biomass gasification in fluidized bed," *Progress in Energy and Combustion Science*, vol. 36, no. 4, pp. 444–509, aug 2010. [Online]. Available: http://linkinghub.elsevier.com/retrieve/pii/S0360128509000707

[39] Gopalakrishnan, R., Fullwood, M. J., and Bartholomew, C. H., "Catalysis of Char Oxidation by Calcium Minerals: Effects of Calcium Compound Chemistry on Intrinsic Reactivity of Doped Spherocarb and Zap Chars," *Energy & Fuels*, vol. 8, no. 4, pp. 984–989, 1994. [Online]. Available: http://pubs.acs.org/doi/abs/10.1021/ef00046a025

[40] Goring, G. E., Curran, G. P., Zielke, C. W., and Gorin, E., "Kinetics of Carbon Gasification by Steam. Mechanism of Interaction of Low Temperature Char and Steam-Hydrogen Mixtures at 1600 °F." *Industrial & Engineering Chemistry*, vol. 45, no. 11, pp. 2586–2591, nov 1953. [Online]. Available: http://pubs.acs.org/doi/abs/10.1021/ie50527a060

[41] Guerrero, M., Ruiz, M. P., Alzueta, M. U., Bilbao, R., and Millera, A., "Pyrolysis of eucalyptus at different heating rates: Studies of char characterization and oxidative reactivity," *Journal of Analytical and Applied Pyrolysis*, vol. 74, no. 1-2, pp. 307–314, 2005.

[42] Guizani, C., Jeguirim, M., Gadiou, R., Escudero Sanz, F. J., and Salvador, S., "Biomass char gasification by H2O, CO2 and their mixture: Evolution of chemical, textural and structural properties of the chars," *Energy*, vol. 112, pp. 133–145, 2016. [Online]. Available: http://linkinghub.elsevier.com/retrieve/pii/S0360544216308398

[43] HANAOKA, T. and OKUMURA, Y., "Effect of metal content on CO2 gasification behavior of K- and Fe-loaded bio-chars," *Journal of Thermal Science and Technology*, vol. 9, no. 2, pp. JTST0006–JTST0006, 2014. [Online]. Available: http://jlc.jst.go.jp/DN/JST.JSTAGE/jtst/2014jtst0006?lang=en{&}from=CrossRef{&}type=abstract

[44] Helsen, L. and Van den Bulck, E., "Review of disposal technologies for chromated copper arsenate (CCA) treated wood waste, with detailed analyses of thermochemical conversion processes." *Environmental pollution (Barking, Essex : 1987)*, vol. 134, no. 2, pp. 301–14, mar 2005. [Online]. Available: http://www.sciencedirect.com/science/article/pii/S0269749104003380

[45] Henrich, E., Bürkle, S., Meza-Renken, Z. I., and Rumpel, S., "Combustion and gasification kinetics of pyrolysis chars from waste and biomass," *Journal of Analytical and Applied Pyrolysis*, vol. 49, no. 1, pp. 221–241, 1999.

[46] Higman, C. and Burgt, M. v. d., *Gasification*, second edition ed. Burlington: Gulf Professional Publishing, 2008.

[47] Hill, A. H., Anderson, G. L., Ghate, M. R., and Liou, W., "Coal Gasification With Internal Recirculation Catalysts." *ACS Division of Fuel Chemistry, Preprints*, vol. 31, no. 3, pp. 176–185, 1986.

[48] Huang, Y., Yin, X., Wu, C., Wang, C., Xie, J., Zhou, Z., Ma, L., and Li, H., "Effects of metal catalysts on CO2 gasification reactivity of biomass char." *Biotechnology advances*, vol. 27, no. 5, pp. 568–72, 2009. [Online]. Available: http://www.ncbi.nlm.nih.gov/pubmed/19393736

[49] Huo, W., Zhou, Z., Chen, X., Dai, Z., and Yu, G., "Study on CO2 gasification reactivity and physical characteristics of biomass, petroleum coke and coal chars." *Bioresource technology*, vol. 159, pp. 143–9, may 2014. [Online]. Available: http://www.ncbi.nlm.nih.gov/pubmed/24642484

[50] Hupa, M., "Ash-related issues in fluidized-bed combustion of biomasses: Recent research highlights," *Energy and Fuels*, vol. 26, no. 1, pp. 4–14, 2012.

[51] Hüttinger, K. J. and Minges, R., "The influence of the catalyst precursor anion in catalysis of water vapour gasification of carbon by potassium," *Fuel*, vol. 65, no. 8, pp. 1122–1128, aug 1986. [Online]. Available: http://linkinghub.elsevier.com/retrieve/pii/0016236186901808

[52] Jiang, Y., Ameh, A., Lei, M., Duan, L., and Longhurst, P., "Solid-gaseous phase transformation of elemental contaminants during the gasification of biomass," *Science of the Total Environment*, 2015. [Online]. Available: http://dx.doi.org/10.1016/j.scitotenv.2015.11.017

[53] Jones, J. M., Darvell, L. I., Bridgeman, T. G., Pourkashanian, M., and Williams, a., "An investigation of the thermal and catalytic behaviour of potassium in biomass combustion," *Proceedings of the Combustion Institute*, vol. 31 II, pp. 1955–1963, 2007.

[54] Juntgen, H. and Heek, K. V., "Kinetics and mechanism of catalytic gasification of coal," *Prepr. Pap., Am. Chem. Soc., Div. Fuel Chem.;(. . .)*, 1984.

[55] Kajita, M., Kimura, T., Norinaga, K., Li, C.-Z., and Hayashi, J.-i., "Catalytic and Noncatalytic Mechanisms in Steam Gasification of Char from the Pyrolysis of Biomass," *Energy & Fuels*, vol. 24, no. 1, pp. 108–116, jan 2010. [Online]. Available: http://pubs.acs.org/doi/abs/10.1021/ef900513a

[56] Kannan, M. and Richards, G., "Gasification of biomass chars in carbon dioxide: dependence of gasification rate on the indigenous metal content," *Fuel*, vol. 69, no. 6, pp. 747–753, jun 1990. [Online]. Available: http://www.sciencedirect.com/science/article/pii/001623619090041N

[57] Kapteijn, F., Abbel, G., and Moulijn, J. A., "CO2 gasification of carbon catalysed by alkali metals," *Fuel*, vol. 63, no. 8, pp. 1036–1042, aug 1984. [Online]. Available: http://www.sciencedirect.com/science/article/pii/0016236184901844

[58] Karlström, O., Brink, A., and Hupa, M., "Desorption kinetics of CO in char oxidation and gasification in O2, CO2 and H2O," *Combustion and Flame*, sep 2014. [Online]. Available: http://www.sciencedirect.com/science/article/pii/S0010218014002466

[59] Khazraie Shoulaifar, T., DeMartini, N., Ivaska, A., Fardim, P., and Hupa, M., "Measuring the concentration of carboxylic acid groups in torrefied spruce wood," *Bioresource Technology*, vol. 123, pp. 338–343, 2012. [Online]. Available: http://dx.doi.org/10.1016/j.biortech.2012.07.069

[60] Khazraie Shoulaifar, T., Demartini, N., Karlström, O., and Hupa, M., "Impact of organically bonded potassium on torrefaction: Part 1. Experimental," *Fuel*, vol. 165, pp. 544–552, 2016. [Online]. Available: http://dx.doi.org/10.1016/j.fuel.2015.06.024

[61] Kirkels, A. F. and Verbong, G. P. J., "Biomass gasification: Still promising? A 30-year global overview," *Renewable and Sustainable Energy Reviews*, vol. 15, no. 1, pp. 471–481, 2011. [Online]. Available: http://dx.doi.org/10.1016/j.rser.2010.09.046

[62] Klose, W. and Wolki, M., "On the intrinsic reaction rate of biomass char gasification with carbon dioxide and steam," *Fuel*, vol. 84, no. 7-8, pp. 885–892, may 2005. [Online]. Available: http://linkinghub.elsevier.com/retrieve/pii/S0016236104003606

[63] Koening, P., Squires, R., and Laurendeau, N., "Effect of potassium carbonate on char gasification by carbon dioxide," *Journal of Catalysis*, vol. 100, no. 1, pp. 228–239, jul 1986. [Online]. Available: http://www.sciencedirect.com/science/article/pii/0021951786900886

[64] Konttinen, J., Backman, R., Hupa, M., Moilanen, A., and Kurkela, E., "Trace element behavior in the fluidized bed gasification of solid recovered fuels - A thermodynamic study," Åbo Akademi University, Process Chemistry Centre, Combustion and Materials Chemistry, Tech. Rep., 2005.

[65] ———, "Trace element behavior in the fluidized bed gasification of solid recovered fuels - A thermodynamic study," *Fuel*, vol. 106, no. 0, pp. 621–631, 2013. [Online]. Available: http://www.sciencedirect.com/science/article/pii/S001623611200806X

[66] Kopyscinski, J., Habibi, R., Mims, C. a., and Hill, J. M., "K 2 CO 3 -Catalyzed CO 2 Gasification of Ash-Free Coal: Kinetic Study," *Energy & Fuels*, vol. 27, no. 8, pp. 4875–4883, aug 2013. [Online]. Available: http://pubs.acs.org/doi/abs/10.1021/ef400552q

[67] Kopyscinski, J., Rahman, M., Gupta, R., Mims, C. a., and Hill, J. M., "K2CO3 catalyzed CO2 gasification of ash-free coal. Interactions of the catalyst with carbon in N2 and CO2 atmosphere," *Fuel*, vol. 117, no. PARTB, pp. 1181–1189, 2014. [Online]. Available: http://dx.doi.org/10.1016/j.fuel.2013.07.030

[68] Koukkari, P., Pajarre, R., and Hack, K., "Setting kinetic controls for complex equilibrium calculations," *Zeitschrift für Metallkunde*, vol. 92, no. 10, pp. 1151–1157, 2001.

[69] Kouvo, P. and Backman, R., "Estimation of trace element release and accumulation in the sand bed during bubbling fluidised bed co-combustion of biomass, peat, and refuse-derived fuels," *Fuel*, vol. 82, no. 7, pp. 741–753, 2003.

[70] Kramb, J., Konttinen, J., Gómez-Barea, A., Moilanen, A., and Umeki, K., "Modeling biomass char gasification kinetics for improving prediction of carbon conversion in a fluidized bed gasifier," *Fuel*, vol. 132, pp. 107–115, sep 2014. [Online]. Available: http://www.sciencedirect.com/science/article/pii/S0016236114003354

[71] Kramb, J., DeMartini, N., Perander, M., Moilanen, A., and Konttinen, J., "Modeling of the catalytic effects of potassium and calcium on spruce wood gasification in CO2," *Fuel Processing Technology*, vol. 148, pp. 50–59, jul 2016. [Online]. Available: http://linkinghub.elsevier.com/retrieve/pii/S0378382016300303

[72] Kramb, J., Konttinen, J., Backman, R., Salo, K., and Roberts, M., "Elimination of arsenic-containing emissions from gasification of chromated copper arsenate wood," *Fuel*, vol. 181, pp. 319–324, 2016. [Online]. Available: http://linkinghub.elsevier.com/retrieve/pii/S0016236116302745

[73] Kudo, S., Hachiyama, Y., Kim, H.-S., Norinaga, K., and Hayashi, J.-i., "Examination of Kinetics of Non-catalytic Steam Gasification of Biomass/Lignite Chars and Its Relationship with the Variation of the Pore Structure," *Energy & Fuels*, vol. 28, no. 9, pp. 5902–5908, sep 2014. [Online]. Available: http://pubs.acs.org/doi/abs/10.1021/ef501517n

[74] Kwon, T.-W., Kim, S. D., and Fung, D. P., "Reaction kinetics of char—CO2 gasification," *Fuel*, vol. 67, no. 4, pp. 530–535, 1988. [Online]. Available: http://www.sciencedirect.com/science/article/pii/001623618890350X

[75] Lahaye, J. and Ehrburger, P., Eds., *Fundamental Issues in Control of Carbon Gasification Reactivity*. Dordrecht: Springer Netherlands, 1991. [Online]. Available: http://link.springer.com/10.1007/978-94-011-3310-4

[76] Lahijani, P., Zainal, Z. A., Mohamed, A. R., and Mohammadi, M., "CO2 gasification reactivity of biomass char: catalytic influence of alkali, alkaline earth and transition metal salts." *Bioresource technology*, vol. 144, pp. 288–95, sep 2013. [Online]. Available: http://www.ncbi.nlm.nih.gov/pubmed/23880130

[77] Lahijani, P., Zainal, Z. A., Mohammadi, M., and Mohamed, A. R., "Conversion of the greenhouse gas CO2 to the fuel gas CO via the Boudouard reaction: A review," *Renewable and Sustainable Energy Reviews*, vol. 41, pp. 615–632, jan 2015. [Online]. Available: http://linkinghub.elsevier.com/retrieve/pii/S1364032114007102

[78] Laine, N. R., Vastola, F. J., and Walker, P. L., "THE IMPORTANCE OF ACTIVE SURFACE AREA IN THE CARBON-OXYGEN REACTION 1,2," *The Journal of Physical Chemistry*, vol. 67, no. 10, pp. 2030–2034, oct 1963. [Online]. Available: http://pubs.acs.org/doi/abs/10.1021/j100804a016

[79] Li, X., Wu, H., Hayashi, J.-i., and Li, C.-Z., "Volatilisation and catalytic effects of alkali and alkaline earth metallic species during the pyrolysis and gasification of Victorian brown coal. Part VI. Further investigation into the effects of volatile-char interactions," *Fuel*, vol. 83, no. 10, pp. 1273–1279, jul 2004. [Online]. Available: http://www.sciencedirect.com/science/article/pii/S0016236103004186

[80] Lindberg, D., Backman, R., Chartrand, P., and Hupa, M., "Towards a comprehensive thermodynamic database for ash-forming elements in biomass and waste combustion - Current situation and future developments," *Fuel*

Processing Technology, vol. 105, pp. 129–141, 2013. [Online]. Available: http://dx.doi.org/10.1016/j.fuproc.2011.08.008

[81] Lizzio, A. a., Jiang, H., and Radovic, L. R., "On the kinetics of carbon (Char) gasification: Reconciling models with experiments," *Carbon*, vol. 28, no. 1, pp. 7–19, jan 1990. [Online]. Available: http://www.sciencedirect.com/science/article/pii/000862239090087Fhttp://linkinghub.elsevier.com/retrieve/pii/000862239090087F

[82] Manocha, S., Chauhan, V. B., and Manocha, L. M., "Porosity Development on Activation of Char from Dry and Wet Babbool Wood," *Carbon Letters*, vol. 3, no. 3, pp. 133–141, 2002.

[83] Marquez-Montesinos, F., Cordero, T., Rodriguez-Mirasol, J., and Rodriguez, J. J., "CO2 and steam gasification of a grapefruit skin char," *Fuel*, vol. 81, no. 4, pp. 423–429, 2002.

[84] Mayers, M., "The rate of reduction of carbon dioxide by graphite," *Journal of the American Chemical Society*, vol. 56, no. 1, pp. 70–76, 1934. [Online]. Available: http://pubs.acs.org/doi/abs/10.1021/ja01316a021

[85] Mckee, D. W., Spiro, C. L., J, K. E., and Lamby, P. G., "Catalytic Effects of Alkali Metal Salts in the Gasification of Coal Char," *Symposium on coal gasification*, pp. 74–86, 1982.

[86] McKee, D. W., Spiro, C. L., Kosky, P. G., and Lamby, E. J., "Catalysis of coal char gasification by alkali metal salts," *Fuel*, vol. 62, pp. 217–220, 1983.

[87] Ministry of Employment and the Economy, "Finnish bioeconomy strategy."

[88] Miura, K. and Silveston, P. L., "Analysis of gas-solid reactions by use of a temperature-programmed reaction technique," *Energy & Fuels*, vol. 3, no. 2, pp. 243–249, mar 1989. [Online]. Available: http://pubs.acs.org/doi/abs/10.1021/ef00014a020

[89] Moilanen, A., "Thermogravimetric characterisations of biomass and waste for gasification processes," Academic Dissertation, Åbo Akademi, 2006. [Online]. Available: http://www.vtt.fi/inf/pdf/publications/2006/P607.pdf

[90] Moilanen, A. and Saviharju, K., "Gasification reactivities of biomass fuels in pressurised conditions and product gas mixtures," in *Developments in Thermochemical Biomass Conversion*, Bridgwater, A. V. and Boocock, D. G. B., Eds. London: Blackie Academic and Professional, 1997, pp. 828–837.

[91] Molina, A. and Mondragón, F., "Reactivity of coal gasification with steam and CO2," *Fuel*, vol. 77, no. 15, pp. 1831–1839, dec 1998. [Online]. Available: http://linkinghub.elsevier.com/retrieve/pii/S0016236198001239

[92] Molina, A., Montoya, A., and Mondragón, F., "CO2 strong chemisorption as an estimate of coal char gasification reactivity," *Fuel*, vol. 78, no. 8, pp. 971–977, jun 1999. [Online]. Available: http://www.sciencedirect.com/science/article/pii/S0016236198002208http://linkinghub.elsevier.com/retrieve/pii/S0016236198002208

[93] Monti, A., Di Virgilio, N., and Venturi, G., "Mineral composition and ash content of six major energy crops," *Biomass and Bioenergy*, vol. 32, no. 3, pp. 216–223, mar 2008. [Online]. Available: http://linkinghub.elsevier.com/retrieve/pii/S0961953407001675

[94] Moulijn, J. A., Cerfontain, M., and Kapteijn, F., "Mechanism of the potassium catalysed gasification of carbon in CO2," *Fuel*, vol. 63, no. 8, pp. 1043–1047, aug 1984. [Online]. Available: http://www.sciencedirect.com/science/article/pii/0016236184901856

[95] Nanou, P., Gutiérrez Murillo, H. E., Van Swaaij, W. P. M., Van Rossum, G., and Kersten, S. R. a., "Intrinsic reactivity of biomass-derived char under steam gasification conditions-potential of wood ash as catalyst," *Chemical Engineering Journal*, vol. 217, pp. 289–299, 2013. [Online]. Available: http://dx.doi.org/10.1016/j.cej.2012.12.012

[96] Neves, D., Thunman, H., Matos, A., Tarelho, L., and Gómez-Barea, A., "Characterization and prediction of biomass pyrolysis products," *Progress in Energy and Combustion Science*, vol. 37, no. 5, pp. 611–630, sep 2011. [Online]. Available: http://linkinghub.elsevier.com/retrieve/pii/S0360128511000025

[97] Nilsson, S., Gómez-Barea, A., and Cano, D. F., "Gasification reactivity of char from dried sewage sludge in a fluidized bed," *Fuel*, vol. 92, no. 1, pp. 346–353, feb 2012. [Online]. Available: http://www.sciencedirect.com/science/article/pii/S0016236111004285http://linkinghub.elsevier.com/retrieve/pii/S0016236111004285

[98] Nilsson, S., Gómez-Barea, A., and Ollero, P., "Gasification of char from dried sewage sludge in fluidized bed: Reaction rate in mixtures of CO2 and H2O," *Fuel*, vol. 105, pp. 764–768, mar 2013. [Online]. Available: http://www.sciencedirect.com/science/article/pii/S0016236112007211

[99] Nilsson, S., Gómez-Barea, A., Fuentes-Cano, D., and Campoy, M., "Gasification kinetics of char from olive tree pruning in fluidized bed," *Fuel*, vol. 125, pp. 192–199, jun 2014. [Online]. Available: http://www.sciencedirect.com/science/article/pii/S0016236114001331

[100] Nzihou, A. and Stanmore, B., "The fate of heavy metals during combustion and gasification of contaminated biomass-A brief review," *Journal of Hazardous Materials*, vol. 256-257, pp. 56–66, jul 2013. [Online]. Available: http://www.sciencedirect.com/science/article/pii/S0304389413001660

[101] Nzihou, A., Stanmore, B., and Sharrock, P., "A review of catalysts for the gasification of biomass char, with some reference to coal," *Energy*, vol. 58, pp. 305–317, sep 2013. [Online]. Available: http://linkinghub.elsevier.com/retrieve/pii/S0360544213004787

[102] Perander, M., DeMartini, N., Brink, A., Kramb, J., Karlström, O., Hemming, J., Moilanen, A., Konttinen, J., and Hupa, M., "Catalytic effect of Ca and K on CO2 gasification of spruce wood char," *Fuel*, 2015. [Online]. Available: http://www.sciencedirect.com/science/article/pii/S0016236115002100

[103] Petersen, S. and Hack, K., "The thermochemistry library ChemApp and its applications," *International Journal of Materials Research*, vol. 98, no. 10, pp.

935 – 945, oct 2007. [Online]. Available: http://www.hanser-elibrary.com/doi/abs/10.3139/146.101551

[104] Peterson, D. and Haase, S., "Market assessment of biomass gasification and combustion technology for small- and medium-scale applications," 2009.

[105] Prins, M. J., Ptasinski, K. J., and Janssen, F. J. J. G., "Thermodynamics of gas-char reactions: first and second law analysis," *Chemical Engineering Science*, vol. 58, no. 3-6, pp. 1003 – 1011, feb 2003. [Online]. Available: http://linkinghub.elsevier.com/retrieve/pii/S0009250902006413

[106] Puig-Arnavat, M., Bruno, J. C., and Coronas, A., "Review and analysis of biomass gasification models," *Renewable and Sustainable Energy Reviews*, vol. 14, no. 9, pp. 2841 – 2851, dec 2010. [Online]. Available: http://linkinghub.elsevier.com/retrieve/pii/S1364032110002108

[107] Rapagnà, S., "Steam-gasification of biomass in a fluidised-bed of olivine particles," *Biomass and Bioenergy*, vol. 19, no. 3, pp. 187 – 197, sep 2000. [Online]. Available: http://linkinghub.elsevier.com/retrieve/pii/S0961953400000313

[108] Sandelin, K. and Backman, R., "Trace Elements in Two Pulverized Coal-Fired Power Stations," *Environmental Science & Technology*, vol. 35, no. 5, pp. 826 – 834, 2001. [Online]. Available: http://pubs.acs.org/doi/abs/10.1021/es000035z

[109] Scott, S., Davidson, J., Dennis, J., Fennell, P., and Hayhurst, A., "The rate of gasification by CO2 of chars from waste," *Proceedings of the Combustion Institute*, vol. 30, no. 2, pp. 2151 – 2159, jan 2005. [Online]. Available: http://www.sciencedirect.com/science/article/pii/S0082078404001146

[110] Seo, D. K., Lee, S. K., Kang, M. W., Hwang, J., and Yu, T.-U., "Gasification reactivity of biomass chars with CO2," *Biomass and Bioenergy*, vol. 34, no. 12, pp. 1946 – 1953, dec 2010. [Online]. Available: http://linkinghub.elsevier.com/retrieve/pii/S0961953410002655

[111] Shen, F., Liu, J., Zhang, Z., and Dai, J., "On-Line Analysis and Kinetic Behavior of Arsenic Release during Coal Combustion and Pyrolysis," *Environmental Science & Technology*, vol. 49, no. 22, pp. 13 716 – 13 723, 2015. [Online]. Available: http://pubs.acs.org/doi/10.1021/acs.est.5b03626

[112] Shen, Y. and Yoshikawa, K., "Recent progresses in catalytic tar elimination during biomass gasification or pyrolysis - A review," *Renewable and Sustainable Energy Reviews*, vol. 21, pp. 371 – 392, 2013. [Online]. Available: http://dx.doi.org/10.1016/j.rser.2012.12.062

[113] sheng Xu, R., liang Zhang, J., wei Wang, G., bin Zuo, H., cheng Zhang, P., and gang Shao, J., "Gasification behaviors and kinetic study on biomass chars in CO2 condition," *Chemical Engineering Research and Design*, pp. 1 – 9, 2015. [Online]. Available: http://dx.doi.org/10.1016/j.cherd.2015.10.014

[114] Sing, K., "The use of nitrogen adsorption for the characterisation of porous materials," *Colloids and Surfaces A: Physicochemical and Engineering Aspects*, vol. 187-188, pp. 3 – 9, aug 2001. [Online]. Available: http://www.sciencedirect.com/science/article/pii/S0927775701006124

[115] Singer, S. L. and Ghoniem, A. F., "Comprehensive gasification modeling of char particles with multi-modal pore structures," *Combustion and Flame*, vol. 160, no. 1, pp. 120–137, jan 2013. [Online]. Available: http://linkinghub.elsevier.com/retrieve/pii/S0010218012002581

[116] Sircar, I., Sane, A., Wang, W., and Gore, J. P., "Experimental and modeling study of pinewood char gasification with CO2," *Fuel*, vol. 119, pp. 38–46, mar 2014. [Online]. Available: http://linkinghub.elsevier.com/retrieve/pii/S0016236113010727

[117] Struis, R. P. W. J., von Scala, C., Stucki, S., and Prins, R., "Gasification reactivity of charcoal with CO2. Part II: Metal catalysis as a function of conversion," *Chemical Engineering Science*, vol. 57, no. 17, pp. 3593–3602, sep 2002. [Online]. Available: http://linkinghub.elsevier.com/retrieve/pii/S0009250902002555

[118] Struis, R., von Scala, C., Stucki, S., and Prins, R., "Gasification reactivity of charcoal with CO2. Part I: Conversion and structural phenomena," *Chemical Engineering Science*, vol. 57, no. 17, pp. 3581–3592, sep 2002. [Online]. Available: http://www.sciencedirect.com/science/article/pii/S0009250902002543h ttp://linkinghub.elsevier.com/retrieve/pii/S0009250902002543

[119] Su, P., Granholm, K., Pranovich, A., Harju, L., Holmbom, B., and Ivaska, A., "Sorption of metal ions to untreated, alkali-treated and peroxide-bleached TMP," *Cellulose*, vol. 17, no. 5, pp. 1033–1044, oct 2010. [Online]. Available: http://link.springer.com/10.1007/s10570-010-9439-1

[120] Suzuki, T., Nakajima, H., Ikenaga, N.-o., Oda, H., and Miyake, T., "Effect of mineral matters in biomass on the gasification rate of their chars," *Biomass Conversion and Biorefinery*, vol. 1, no. 1, pp. 17–28, feb 2011. [Online]. Available: http://www.springerlink.com/index/10.1007/s13399-011-0006-2

[121] Tilghman, M. B. and Mitchell, R. E., "Coal and biomass char reactivities in gasification and combustion environments," *Combustion and Flame*, vol. 2, 2015. [Online]. Available: http://linkinghub.elsevier.com/retrieve/pii/S0010218015001479

[122] Tola, V. and Pettinau, A., "Power generation plants with carbon capture and storage: A techno-economic comparison between coal combustion and gasification technologies," *Applied Energy*, vol. 113, pp. 1461 – 1474, 2014.

[123] Tremel, A. and Spliethoff, H., "Gasification kinetics during entrained flow gasification - Part III: Modelling and optimisation of entrained flow gasifiers," *Fuel*, vol. 107, pp. 170–182, 2013. [Online]. Available: http://dx.doi.org/10.1016/j.fuel.2013.01.062

[124] Trubetskaya, A., Jensen, P. A., Jensen, A. D., Steibel, M., Spliethoff, H., and Glarborg, P., "Influence of fast pyrolysis conditions on yield and structural transformation of biomass chars," *Fuel Processing Technology*, vol. 140, pp. 205–214, 2015. [Online]. Available: http://dx.doi.org/10.1016/j.fuproc.2015.08.034

[125] Umeki, K., Yamamoto, K., Namioka, T., and Yoshikawa, K., "High temperature steam-only gasification of woody biomass," *Applied Energy*, vol. 87, no. 3, pp. 791–798, mar 2010. [Online]. Available: http://linkinghub.elsevier.com/retrieve/pii/S0306261909004279

[126] Umeki, K., Moilanen, A., Gómez-Barea, A., and Konttinen, J., "A model of biomass char gasification describing the change in catalytic activity of ash," *Chemical Engineering Journal*, vol. 207-208, pp. 616–624, oct 2012. [Online]. Available: http://linkinghub.elsevier.com/retrieve/pii/S1385894712009163

[127] Vassilev, S. V., Baxter, D., Andersen, L. K., and Vassileva, C. G., "An overview of the chemical composition of biomass," *Fuel*, vol. 89, no. 5, pp. 913–933, 2010. [Online]. Available: http://dx.doi.org/10.1016/j.fuel.2009.10.022

[128] Veraa, M. J. and Bell, A. T., "Effect of alkali metal catalysts on gasif ication of coal char," vol. 57, pp. 194–200, 1978.

[129] Walker, P. L., Rusinko, F., and Austin, L. G., "Gas Reactions of Carbon," pp. 133–221, 1959.

[130] Whitty, K., Backman, R., and Hupa, M., "Influence of char formation conditions on pressurized black liquor gasification rates," *Carbon*, vol. 36, no. 11, pp. 1683–1692, 1998.

[131] Xu, K., Hu, S., Su, S., Xu, C., Sun, L., Shuai, C., Jiang, L., and Xiang, J., "Study on Char Surface Active Sites and Their Relationship to Gasification Reactivity," *Energy & Fuels*, vol. 27, no. 1, pp. 118–125, jan 2013. [Online]. Available: http://pubs.acs.org/doi/abs/10.1021/ef301455x

[132] Yergey, A. L. and Lampe, F. W., "Carbon gasification in the Boudouard reaction," *Fuel*, vol. 53, no. 4, pp. 280–281, oct 1974. [Online]. Available: http://linkinghub.elsevier.com/retrieve/pii/0016236174900490

[133] Yuan, S., Chen, X.-l., Li, J., and Wang, F.-c., "CO 2 Gasification Kinetics of Biomass Char Derived from High-Temperature Rapid Pyrolysis," *Energy & Fuels*, vol. 25, no. 5, pp. 2314–2321, may 2011. [Online]. Available: http://pubs.acs.org/doi/abs/10.1021/ef200051z

[134] Zanchi, G., Pena, N., and Bird, N., "Is woody bioenergy carbon neutral? A comparative assessment of emissions from consumption of woody bioenergy and fossil fuel," *GCB Bioenergy*, vol. 4, no. 6, pp. 761–772, 2012.

[135] Zanzi, R., Sjöström, K., and Björnbom, E., "Rapid pyrolysis of agricultural residues at high temperature," *Biomass and Bioenergy*, vol. 23, no. 5, pp. 357–366, nov 2002. [Online]. Available: http://linkinghub.elsevier.com/retrieve/pii/S0961953402000612

[136] Zaror, C. A., Hutchings, I. S., Pyle, D. L., Stiles, H. N., and Kandiyoti, R., "Secondary char formation in the catalytic pyrolysis of biomass," *Fuel*, vol. 64, no. 7, pp. 990–994, 1985.

[137] Zhang, J., Zhang, R., and Bi, J., "Effect of catalyst on coal char structure and its role in catalytic coal gasification," *Catalysis Communications*, vol. 79, pp. 1–5, apr 2016. [Online]. Available: http://www.sciencedirect.com/science/article/pii/S1566736716300358

[138] Zhang, W., "Automotive fuels from biomass via gasification," *Fuel Processing Technology*, vol. 91, no. 8, pp. 866–876, 2010.

[139] Zhang, Y., Ashizawa, M., Kajitani, S., and Miura, K., "Proposal of a semi-empirical kinetic model to reconcile with gasification reactivity profiles of biomass chars," *Fuel*, vol. 87, no. 4-5, pp. 475–481, apr 2008. [Online]. Available: http://linkinghub.elsevier.com/retrieve/pii/S0016236107002098

[140] Zhang, Y., Hara, S., Kajitani, S., and Ashizawa, M., "Modeling of catalytic gasification kinetics of coal char and carbon," *Fuel*, vol. 89, no. 1, pp. 152–157, jan 2010. [Online]. Available: http://linkinghub.elsevier.com/retrieve/pii/S0016236109002658

Publications

Publication I

Jason Kramb, Jukka Konttinen, Alberto Gómez-Barea, Antero Moilanen, Kentaro Umeki "Modeling biomass char gasification kinetics for improving prediction of carbon conversion in a fluidized bed gasifier", *Fuel*, vol. 132, 2014, pp. 107-115

Fuel 132 (2014) 107–115

Contents lists available at ScienceDirect

Fuel

journal homepage: www.elsevier.com/locate/fuel

Modeling biomass char gasification kinetics for improving prediction of carbon conversion in a fluidized bed gasifier

Jason Kramb [a,*], Jukka Konttinen [a], Alberto Gómez-Barea [b], Antero Moilanen [c], Kentaro Umeki [d]

[a] Department of Chemistry, Renewable Natural Resources and Chemistry of Living Environment, University of Jyväskylä, PO Box 35, FI-40014 University of Jyväskylä, Finland
[b] Bioenergy Group, Chemical and Environmental Engineering Department, Escuela Técnica Superior de Ingeniería, University of Seville, Camino de los Descubrimientos s/n, 41092 Seville, Spain
[c] VTT Technical Research Centre of Finland, PO Box 1000, 02044 VTT, Finland
[d] Division of Energy Science, Department of Engineering Sciences and Mathematics, Luleå University of Technology, 971 87 Luleå, Sweden

HIGHLIGHTS

- A novel conversion rate equation for biomass char gasification based on TGA data.
- TGA experiments conducted to simulate conditions in a fluidized bed gasifier.
- A fluidized bed gasifier model using the newly developed conversion rate expression.
- Comparison of reactor modeling results against pilot plant measurements.

ARTICLE INFO

Article history:
Received 28 January 2014
Received in revised form 1 April 2014
Accepted 6 April 2014
Available online 24 April 2014

Keywords:
Biomass
Gasification
Reaction kinetics
Modeling
Fluidized bed

ABSTRACT

Gasification of biomass in a fluidized bed (FB) was modeled based on kinetic data obtained from previously conducted thermogravimetric analysis. The thermogravimetric analysis experiments were designed to closely resemble conditions in a real FB gasifier by using high sample heating rates, in situ devolatilization and gas atmospheres of H_2O/H_2 and CO_2/CO mixtures. Several char kinetic models were evaluated based on their ability to predict char conversion based on the thermogravimetric data. A modified version of the random pore model was shown to provide good fitting of the char reactivity and suitability for use in a reactor model. An updated FB reactor model which incorporates the newly developed char kinetic expression and a submodel for the estimation of char residence time is presented and results from simulations were compared against pilot scale gasification data of pine sawdust. The reactor model showed good ability for predicting char conversion and product gas composition.

1. Introduction

Gasification of biomass has become a topic of increasing interest as a potentially renewable method of electricity, heat and liquid fuel production. The gasification process can be divided into a number of steps, of which char gasification is often the slowest. As a result, char gasification tends to represent a rate controlling step of the overall thermo-chemical conversion process. Char can contain 25% of the energy content of the biomass fuel [1] and the total char conversion can significantly influence the composition of the product gas as well as the overall efficiency of the gasification process. As a result, accurate prediction of char conversion is a key factor to optimize a biomass gasifier.

Mathematical models for fluidized bed gasification (FBG) can be used in all stages of the gasifier design and operation. The models can vary significantly in terms of complexity and scope, where the two extremes are often considered to be thermodynamic equilibrium models for simplicity and computation fluid dynamical models for complexity [2]. For all modeling approaches obtaining experimental data for model validation is a widely acknowledged challenge.

This work presents a method for predicting the reactivity of biomass char as a function of conversion, temperature and pressure based on experimental data obtained from dedicated thermogravimetric analysis, where operating conditions are applied to closely resemble conditions in a FBG. Various char reactivity models were examined for their ability to predict the experimental conversion rate and suitability for use in a FBG model. One of these char reactivity models was implemented into a FBG model and the modeling results were compared against

* Corresponding author. Tel.: +358 400299614.
E-mail address: jason.kramb@jyu.fi (J. Kramb).

http://dx.doi.org/10.1016/j.fuel.2014.04.014
0016-2361/

Nomenclature

Abbreviations

DAF	dry ash-free fuel
FB	fluidized bed
FBG	fluidized bed gasifier
HRPM	hybrid random pore model
MRPM	modified random pore model
PPW	proposed in present work
RPM	random pore model
TGA	thermogravimetric analysis
UCM	uniform conversion model

Symbols

α	kinetic parameter for hybrid models (–)
ψ	random pore model surface parameter (–)
τ	char residence time (s)
τ_2	time constant for bottom ash removal (s)
τ_3	time constant for fly ash removal (s)
τ_R	char conversion time (s)
ξ	catalytic deactivation coefficient (–)
c	modified random pore model parameter (–)
E	activation energy (J/mol)
k_0	frequency factor for Arrhenius terms (1/s)
k_3	Arrhenius term of K_r (1/s)
K_r	kinetic coefficient (1/s)
k_{1b}	Arrhenius term of K_r (1/s)
k_{1f}	Arrhenius term of K_r (1/s)
$k_{ccg,1}$	three parallel reaction model rate coefficient (1/s)
$k_{ccg,2}$	three parallel reaction model rate coefficient (1/s)
k_{ncg}	three parallel reaction model rate coefficient (1/s)
m_0	initial char mass (g)
N	number of reactor sections in FBG model (–)
$n_{c,fix}$	char carbon flow from devolatilization stage (mols/s)
$N_{C,tot}$	total carbon inventory in the reactor bed (mol)
$n_{CO_2,eq,(i)}$	equilibrium adjusted CO_2 flow leaving reactor section i (mol/s)
$n_{H_2O,eq,(i)}$	equilibrium adjusted steam flow leaving reactor section i (mol/s)
p	modified random pore model parameter (–)
p_i	partial pressure of gas i (bar)
r	conversion rate (1/s)
r''	instantaneous reaction rate (1/s)
$r^*_{(i)}$	apparent instantaneous reactivity in ith section of gasifier model (1/s)
T	temperature (°C)
$W_{b,tot}$	total bed inventory (kg)
$w_{c,ch,b}$	weight percentage of carbon in char in the bed (–)
$w_{c,ch,d}$	weight percentage of carbon in char from devolatilization (–)
X_{ch}	char conversion (–)
X_c	overall fuel carbon conversion (–)
$X_{g,(i)}$	fractional molar conversion of reactant gas in section i of FBG reactor model (–)

measured char conversion and product gas composition from a pilot scale gasifier. The focus of the model is to examine the effects of char reactivity on the performance of FBGs. The model is intentionally simple in that the required inputs are easily obtained experimental characterization of the fuel and basic reactor operating conditions.

2. Theory and methods

This section presents the approach followed in this work to model a FBG from thermogravimetric analysis (TGA) measurements. Four different aspects are discussed: (i) definitions of char reactivity and reaction rates; (ii) how to calculate these quantities from TGA measurements in which the whole conversion of the sample occurs, including devolatilization and char gasification; (iii) selection of a model to represent the effects of temperature, gas composition and carbon conversion in the form of a kinetics equation; (iv) development of a FBG model where the char reactivity model is implemented together with devolatilization and reactor considerations (e.g. input flow rate of biomass fuel, ash bed inventory, reactor size).

2.1. Definitions

Char conversion of a fuel sample being converted at uniform and constant temperature and gas composition is defined as,

$$X_{ch} = \frac{m_0 - m_t}{m_0} \tag{1}$$

where m_0 and m_t are, respectively, the ash-free mass of the sample at the start of gasification and time t.

The conversion rate is defined as,

$$r = \frac{dX_{ch}}{dt}, \tag{2}$$

and the instantaneous reactivity is calculated by normalizing the conversion rate by the mass of the sample at time t,

$$r'' = -\frac{1}{m_t}\frac{dm_t}{dt} = \frac{1}{1 - X_{ch}}\frac{dX_{ch}}{dt}. \tag{3}$$

2.2. Measuring char reactivity for FBG from thermogravimetric measurements

As the purpose of this work is to model gasification of biomass in FBGs, the TGA experiments were designed to mimic the conditions of those gasifiers as closely as possible. The experimental setup and data used in the present work has been described in detail elsewhere [3]. In the experiments the sample is lowered into the preheated reactor chamber causing devolatilization and gasification reactions to begin immediately. This way of operation closely simulates the char generation in a FBG in a number of key ways: high heating rates during devolatilization, devolatilization occurs in the presence of the gasification agent, and, most importantly, the sample is not cooled between devolatilization and char gasification.

The tests were carried out in isothermal conditions on pine sawdust samples at 750 °C and 850 °C using atmospheres containing mixtures of either H_2O/H_2 or CO_2/CO. Proximate and ultimate analysis of the fuel samples have been published previously by Moilanen and Saviharju [4]. The volume fraction of each gas component in the atmosphere during each TGA test was varied to observe the inhibiting effects of H_2 and CO on the char reactivity. Table 1 summarizes the operating conditions for the TGA tests [4].

While this setup more accurately resembles a fuel particle being injected into a hot fluidized bed, it adds the complication of separating the devolatilization and gasification stages in order to correctly model only the char gasification. The approach used in this work to define the initial char conversion is based on the

Table 1
TGA testing conditions of pine sawdust used for char reactivity modeling showing reactor temperature and gas partial pressures [4].

CO_2 gasification			H_2O gasification		
Temperature (°C)	p_{CO_2} (bars)	p_{CO} (bars)	Temperature (°C)	p_{H_2O} (bars)	p_{H_2} (bars)
750	1	0	750	1	0
750	0.95	0.05	750	0.95	0.05
750	0.89	0.11	750	0.9	0.1
750	0.8	0.2	750	0.86	0.14
850	1	0	850	1	0
850	0.95	0.05	850	0.95	0.05
850	0.89	0.11	850	0.86	0.14
850	0.8	0.2			

method proposed by Umeki et al. [5] who established clearly how to obtain char conversion versus time data from similar TGA data where the overall fuel conversion takes place. For all TGA experiments the starting point of gasification was between 60 and 120 s from when the sample was lowered into the reactor chamber.

2.3. Modeling of char reactivity

A variety of approaches have been proposed to describe the gasification reactivity of biomass char in the past [2,6]. The variation of conversion rate with temperature, gas composition and carbon conversion can be written in the general form as

$$dX_{ch}/dt = f(T, p_i, X_{ch}), \tag{4}$$

where T is the temperature at which the conversion occurs and p_i is the partial pressure of gas species i. Most often in char gasification reactivity studies, it is assumed that the effects of operating conditions and char conversion can be separated in a convenient form to fit the measurements, giving the following expression to represent the conversion rate

$$dX_{ch}/dt = K_r(T, p_i)F(X_{ch}), \tag{5}$$

where $K_r(T, p_i)$ is the kinetic coefficient and the second term, $F(X_{ch})$, is the term which expresses the reactivity dependence on conversion and can take a number of different forms. Both terms, $K_r(T, p_i)$ and $F(X_{ch})$, may contain parameters to be fit by measurements [6].

Experimental representation of the function f in Eq. (4) is difficult and there is not yet a general model where f is explicitly obtained. Despite this, there are some models that have tried to find such an expression for certain operating conditions. A model of this type, the three parallel reaction model [5], is briefly analyzed below. In contrast, a variety of expressions have been presented in literature to fit both $K_r(T, p_i)$ and $F(X_{ch})$ to measurements. Some of these models are based on fundamental description of the processes taken at the char surface and others by empirical expressions. Table 2 shows the conversion rate equations that were considered in this work for modeling char gasification reactivity of pine sawdust.

The Langmuir–Hinshelwood kinetic model has been widely used to model the kinetic coefficient, $K_r(T, p_i)$, in gasification processes. Although there remains some criticism to this kinetic model [7], the Langmuir–Hinshelwood model has been widely used with success to model measurements in char reactivity [8], and so has been chosen to represent $K_r(T, p_i)$ in this study. In previous work [9] Eqs. (6) and (7), as described by Barrio [10], have been used for the kinetic coefficient for CO_2 and steam gasification:

$$K_{r-CO_2} = \frac{k_{1f}p_{CO_2}}{1 + \frac{k_{1f}}{k_3}p_{CO_2} + \frac{k_{1b}}{k_3}p_{CO}} \tag{6}$$

and

$$K_{r-H_2O} = \frac{k_{1f}p_{H_2O}}{1 + \frac{k_{1f}}{k_3}p_{H_2O} + \frac{k_{1b}}{k_3}p_{H_2}}. \tag{7}$$

These equations account for the inhibiting effects of CO and H_2 on the gasification reaction rate and show a good ability to predict the measured reactivities. The kinetic parameters (k_{1f}, k_{1b}, k_3) have the form of the Arrhenius equation,

$$k = k_0 exp(-E/RT), \tag{8}$$

where k_0 is the frequency factor and E the activation energy. Fig. 1 shows the predicted reactivities from Eqs. (6) and (7) with the measured averaged reactivity (averaged from approximately 30–80% char conversion) at 750 °C and 850 °C for both steam and CO_2 gasification [9]. Throughout this work it can be assumed that all kinetic coefficients, K_r, follow Eqs. (6) and (7) for CO_2 and H_2O gasification respectively.

Regarding the variation of reactivity with conversion, represented by $F(X_{ch})$, five reactivity models (see Table 2) are examined in this work using the TGA experimental data for sawdust: the uniform conversion model (UCM), random pore model (RPM), modified random pore model (MRPM), and a 'hybrid' version of the RPM (HRPM) and MRPM (HMRPM) which attempts to better model the higher conversion rate which is observed at low conversion levels.

Table 2
Char conversion equations considered for modeling TGA data. All equations were used for both CO_2 and steam gasification. As mentioned, the kinetic coefficient terms, K_r, follow Eqs. (6) and (7) for CO_2 and steam gasification respectively. Acronyms: UCM – Uniform conversion model, RPM – Random pore model, MRPM – Modified random pore model, HRPM – Hybrid random pore model, HMPRM – Hybrid modified random pore model, PPW – Proposed in the present work.

Model	$f(T, p_i, X_{ch}) = K_r(T, p_i)\,F(X_{ch})$	Eq.	Model parameters	Reference
UCM	$K_r(1 - X_{ch})$	(10)	K_r	[14]
RPM	$K_r(1 - X_{ch})\sqrt{1 - \psi log(1 - X_{ch})}$	(11)	K_r, ψ	[11]
MRPM	$K_r(1 - X_{ch})\sqrt{1 - \psi log(1 - X_{ch})}(1 + (cX_{ch})^p)$	(12)	K_r, ψ, c, p	[13]
HRPM	$K_r\left(\alpha \exp(-\xi X_{ch}^2) + (1 - X_{ch})\sqrt{1 - \psi log(1 - X_{ch})}\right)$	(13)	K_r, α, ξ, ψ	PPW
HMRPM	$K_r\left(\alpha \exp(-\xi X_{ch}^2) + (1 - X_{ch})\sqrt{1 - \psi log(1 - X_{ch})}(1 + (cX_{ch})^p)\right)$	(14)	$K_r, \alpha, \xi, \psi, c, p$	PPW

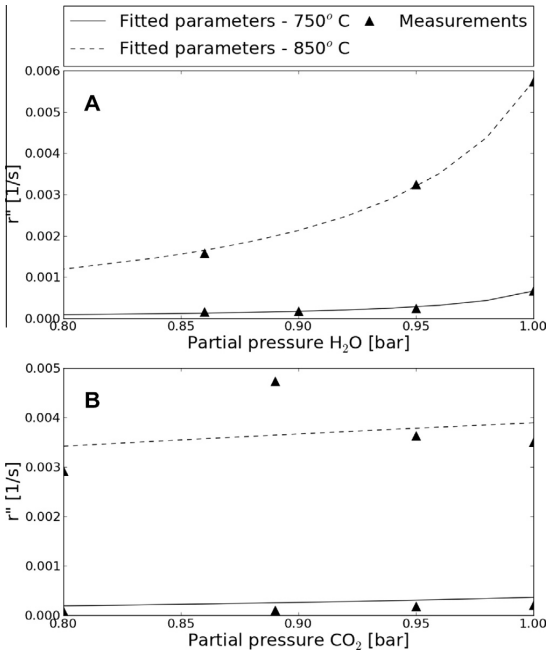

Fig. 1. Average reactivity values for steam (A) and CO_2 (B) gasification from TGA data and the reactivities calculated from fitted kinetic parameters using Eq. (7) and Eq. (6) [9].

The three parallel reaction model was developed by Umeki et al. [5] to describe the catalytic activity of ash in biomass gasification and is an example of a conversion model in the form of Eq. (4). The model can be expressed as

$$r = k_{ccg,1} exp(-\xi X_{ch}^2) + k_{ncg}(1 - X_{ch}) + k_{ccg,2}, \quad (9)$$

where ξ is a structural parameter for the fuel type and $k_{ccg,1}$, k_{ncg} and $k_{ccg,2}$ are kinetic coefficients. The model divides the char gasification into three stages: a regime of high reactivity where catalyst deactivation occurs, a slower first-order kinetic regime in which non-catalytic gasification takes place, and a zeroth order kinetic regime where the catalyst is again influential. Fig. 2 shows the model prediction for the conversion rate of four sets of TGA reactivity data from sawdust. While this parallel reaction model can accurately predict the reactivity and conversion time of biomass char for CO_2 gasification, the kinetic coefficients $k_{ccg,1}$, k_{ncg}, and $k_{ccg,2}$ have complex pressure and temperature dependence. The correlation factor ξ has also been shown to have dependence on temperature. As a result, the three parallel reaction model is currently limited to predicting conversion rates only at the temperature and pressure conditions of the experimental data. This limitation makes this model currently unsuitable for use in the carbon conversion predictor presented below.

The random pore model developed by Bhatia [11,12] attempts to describe the changes in the pore structure during the conversion of the fuel. It has been widely used for oxidation and gasification of numerous fuels. Zhang et al. [13] created a modified random pore model (MRPM) in order to fit conversion data of biomass chars which showed a maximum in the conversion rate at high char conversion. This was done by adding a new conversion term to the original RPM, as shown in Eq. (12). The two dimensionless parameters introduced in the MRPM were shown to be correlated with the amount of active potassium in the fuel sample.

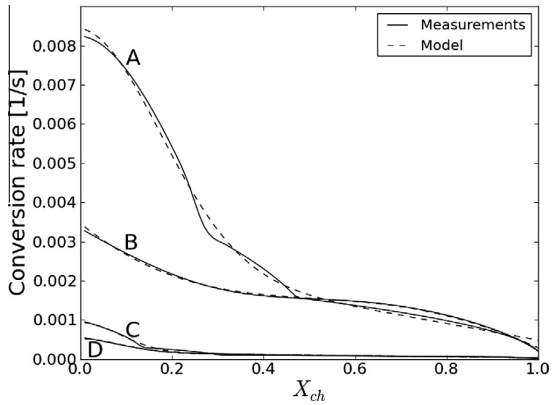

Fig. 2. Four sets of TGA conversion rate data with corresponding predictions from the three parallel reaction model developed by Umeki et al. [5] shown in Eq. (9). (A) 850 °C, 1 bar CO_2; (B) 850 °C, 0.8 bar CO_2, 0.2 bar CO; (C) 780 °C, 1 bar CO_2; (D) 780 °C, 0.95 bar CO_2, 0.05 bar CO.

Both the RPM and MRPM showed good ability to fit the measured conversion rate curves of pine sawdust for high conversion ($X_{ch} > 0.4$) as seen in Figs. 3 and 4 which show measured conversion rates for two TGA test conditions and the predicted conversion rates for various models. The TGA measurements typically show slightly higher conversion rates at the end of char conversion ($X_{ch} > 0.8$) than predicted by the RPM, but this is not as pronounced as what was observed by Zhang et al. [13] and as a result the improvements offered by the MRPM in modeling the dX_{ch}/dt curve is less significant. The deviation of the models from the measured data at low char conversion is attributed to the char generation conditions. In previous works where the random pore model or modified random pore model have been used, the char samples were prepared before gasification, usually by heating at a controlled rate in a nitrogen atmosphere [13,15]. This differs significantly from the in situ char formation process described in Section 2.2 and used in this work. The higher than expected char reactivity at low conversion may be explained by small amounts of remaining volatiles being released through ongoing devolatilization, as well as the dependence of char properties and reactivity on

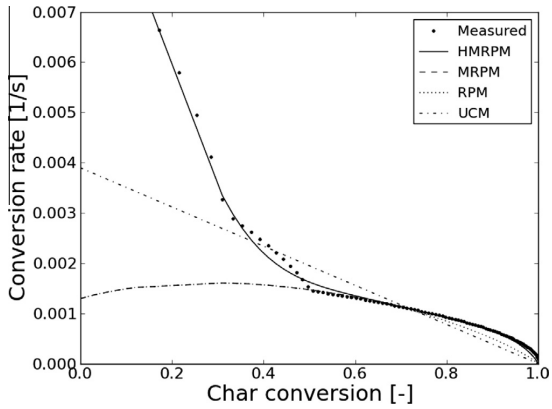

Fig. 3. Measured char conversion rate from CO_2 gasification at 850 °C, 1 bar CO_2 and the predicted conversion rates from the UCM, RPM, MRPM, and HMRPM. The RPM and MRPM are identical for $0 < X_{ch} < 0.6$, after which the RPM model begins to show lower conversion rate than the MRPM.

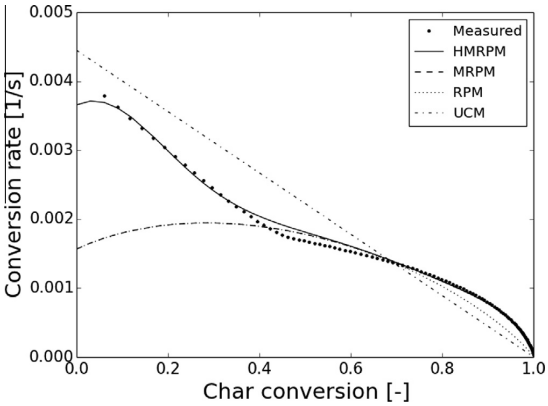

Fig. 4. Measured char conversion rate from steam gasification at 850 °C, 0.95 bar H_2O, 0.05 bar H_2 and the predicted conversion rates from the UCM, RPM, MRPM, and HMRPM. The RPM and MRPM are identical for $0 < X_{ch} < 0.7$, after which the RPM model begins to show lower conversion rate than the MRPM.

devolatilization conditions. It has been shown for several types of biomass that higher pyrolysis heating rates will generally lead to higher reactivities [16]. This section of the conversion curve also corresponds with the regime describing catalytic gasification with deactivation of the catalyst in the three parallel reaction model and this fact was used to develop the present version of a char kinetic model as discussed below.

In order to improve the ability of the modified random pore model to predict the conversion rate of the char as measured in the TGA, a hybrid kinetic model was developed which considers two different periods during char gasification: an initial period following the catalytic gasification with deactivation of the catalyst regime from the three parallel reaction model shown in Eq. (9) and a second period following either the RPM or MRPM. In order to separate the kinetic and structural terms of the conversion rate equation according to Eq. (5), it was assumed that the kinetic coefficient $k_{ccg,1}$ was proportional to the kinetic coefficient of the RPM/RMPRM ($k_{ccg,1} = \alpha K_r$) and that the correlation factor ξ was not dependent on temperature. These hybrid models are shown by Eqs. (13) and (14) in Table 2.

2.4. Carbon conversion predictor model

An improved carbon conversion predictor has been developed to model biomass gasification in a fluidized bed. The original model has been described previously [9,17]. The goal of the model is to limit the required inputs to easily obtained data on the fuel properties and reactor parameters while providing an accurate estimate of the overall carbon conversion and product gas composition. A schematic outline of the model is shown in Fig. 5. The basic input to the model consists of proximate and ultimate analysis of the fuel as well as the char reactivity data from the TGA measurements. The reactor feed rates for air, steam and the fuel and the reactor operating conditions are also required. The model contains a simple devolatilization submodel which assumes this stage (releasing of volatiles from the fuel particle) to happen instantly when the fuel particle is injected into the reactor. The products of the devolatilization submodel, char and gas streams, are calculated based on thermochemical equilibrium which is explained in more detail elsewhere [9].

Fig. 6 shows the basic calculation procedure involved in the FBG model. The fluidized bed is divided into N vertical sections which are modeled as ideally stirred reactors. For each vertical section

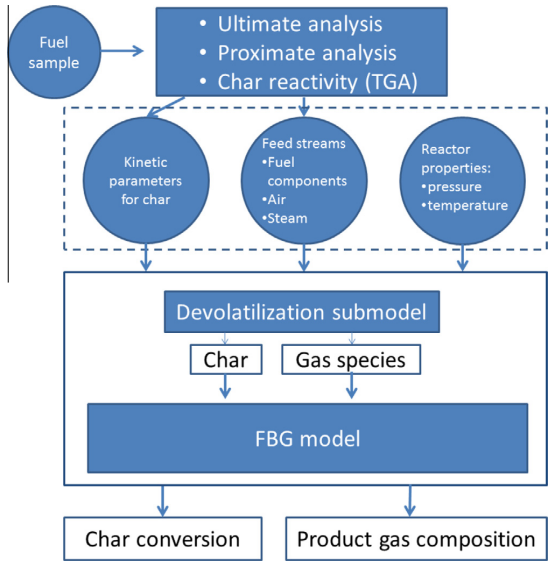

Fig. 5. A schematic diagram of the carbon conversion predictor, including model inputs and the outputs of the pyrolysis and FBG submodels.

the char conversion and product gas composition is calculated and the gas composition leaving section i is used for calculating the char reactions of section $i+1$. In order to be consistent with previous results from the carbon conversion predictor [9], $N = 8$ was used in this work. This value was chosen in the original model because when the number of vertical sections of the gasifier model is greater than eight the model results become sufficiently independent of this parameter.

In addition, the updated reactor model incorporates a new submodel to calculate the char residence time, τ, which was not calculated in the previous version of the model [9] but assumed

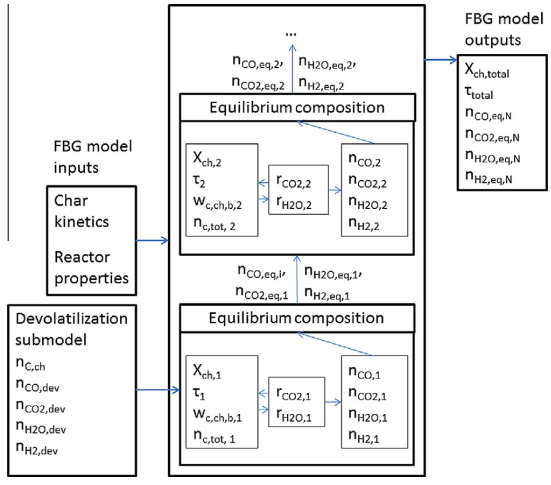

Fig. 6. A schematic diagram of the FBG submodel showing the basic calculation procedure for determining char conversion. The final outputs of the model are the overall char conversion, X_{ch}, char residence time, τ, and product gas composition ($n_{CO,eq,N}$, $n_{CO_2,eq,N}$, $n_{H_2O,eq,N}$, $n_{H_2,eq,N}$). These are taken as the values calculated in the final reactor section.

to equal the char conversion time, τ_R. The equations developed by Gómez-Barea and Leckner [18] were implemented in the new version of the FBG model, which relate τ with the mass fraction of carbon in the char of the reactor bed, $w_{c,ch,b}$, and the char conversion attained in the reactor, X_{ch}. These are shown in Eqs. (15)–(17) respectively:

$$\tau = \frac{1}{(1/\tau_2 + 1/\tau_3)}\left(1 - \frac{w_{c,ch,d}/\tau_R}{(1/\tau_2 + 1/\tau_3 + 1/\tau_R)}\right), \tag{15}$$

$$w_{c,ch,b} = \frac{(1/\tau_2 + 1/\tau_3)w_{c,ch,d}}{1/\tau_2 + 1/\tau_3 + (1 - w_{c,ch,d})/\tau_R}, \tag{16}$$

and

$$X_{ch} = 1 - \frac{w_{c,ch,b}}{w_{c,ch,d}}\left(\frac{\tau}{\tau_2} + \frac{\tau}{\tau_3}\right), \tag{17}$$

where τ_2 is the time constant for bottom ash removal, τ_3 is the time constant for fly ash removal, $w_{c,ch,d}$ is the mass fraction of carbon in char from the devolatilization submodel and τ_R is the char conversion time which is calculated as

$$\tau_R = \int_0^{X_{ch}} 1/\left(K_r\left(\alpha\exp(-\xi X_{ch}^2) + (1 - X_{ch})\sqrt{1 - \psi log(1 - X_{ch})}\right)\right) dX_{ch} \tag{18}$$

according to the proposed HRPM shown in Eq. (13). This method allows for the accounting of carbon lost through bottom and fly ash on carbon conversion and residence time, which was missing in the original model design. Due to the new conversion dependence of the reaction time an initial guess for X_{ch} must be made at the beginning of the calculation process. These calculations are then iterated until the values of τ and X_{ch} converge.

The balance equation for the carbon consumed in the steam and CO_2 gasification reactions in the ith section of the reactor are given as,

$$\frac{N_{C,tot}}{N} r^*_{H_2O,(i)} = n_{H_2O,eq(i-1)} X_{g,H_2O,(i)}, \tag{19}$$

and

$$\frac{N_{C,tot}}{N} r^*_{CO_2,(i)} = n_{CO_2,eq(i-1)} X_{g,CO_2,(i)}, \tag{20}$$

where $N_{C,tot}$ is the total carbon inventory in the reactor bed, $r^*_{H_2O,(i)}$ and $r^*_{CO_2,(i)}$ are the effective char reactivities in the ith section of the reactor, $n_{H_2O,eq,(i-1)}$ and $n_{CO_2,eq,(i-1)}$ are the flows of steam and CO_2 from the previous reactor section, and finally $X_{g,H_2O,(i)}$ and $X_{g,CO_2,(i)}$ are the fractional molar conversion of the reactant gases. The carbon inventory, $N_{c,tot}$, and $w_{c,ch,b}$ are related by the total bed inventory, $W_{b,tot}$, which must be supplied as a model input. The effective reactivities, $r^*_{H_2O,(i)}$ and $r^*_{CO_2,(i)}$, are assumed to be of the form $r^* = \beta r''_{avg}$ where r''_{avg} is the averaged reactivity from the beginning of char conversion to X_{ch} as calculated in Eq. (17). The coefficient β is found by the carbon balance relation,

$$X_{ch} n_{c,fix} = N_{c,tot}(r''_{H_2O,avg} + r''_{CO_2,avg})\beta, \tag{21}$$

where $n_{c,fix}$ is the carbon flow from the devolatilization stage. It can then be shown that

$$\beta = \frac{X_{ch}}{\tau(r''_{H_2O,avg} + r''_{CO_2,avg})}. \tag{22}$$

The requirement to maintain simplicity in the carbon conversion predictor has imposed some limitations in the current FBG model. First, the temperature of the reactor is a required input to the model, rather than calculated through an energy balance. Similarly, methane concentration in the product gas is determined from the methane yields determined experimentally during measurements in FBG and is therefore considered an input term. The yield of methane depends on the fuel type and process temperature. For a typical FBG biomass fuels the methane yield is in the range of 50–80 g/kg daf [19]. Finally, the estimation method for τ_3 as a function of operating conditions prevents the use of the model without additional measurements from which the fly ash flow can be estimated. The method used for estimating τ_3 for a pilot plant is discussed in Section 3.2.

3. Results

3.1. Reactivity modeling

The reactivity models from Table 2 were fitted to the measured TGA reactivity data and the ability of each model to accurately predict observed char conversion times was evaluated. For all models the kinetic coefficient $K_r(T, p_i)$ was taken as Eq. (6) for CO_2 gasification and Eq. (7) for steam gasification. For each reactivity model a single set of parameters was found using a least squares method which minimized the error between the model prediction and measured conversion times for all sets of TGA data.

The mean absolute percentage error in predicting experimental conversion times for each model was calculated as,

$$\epsilon = \frac{1}{N_j}\sum_{j=1}^{N_j}\frac{1}{N_{j,i}}\sum_{i=1}^{N_i}|(t_{i,j,exp} - t_{i,j,model})/t_{i,j,exp}| \tag{23}$$

where N_j is the number of TGA data sets, $N_{j,i}$ is the number of data points in data set j, $t_{i,j,exp}$ is the experimental conversion time for data point i in set j, and $t_{i,j,model}$ is the model value for point $t_{i,j,exp}$. The errors are shown in Table 3. The RPM offers significant improvement over the uniform conversion model in all the cases, especially at high conversion. The MRPM improves conversion time prediction slightly compared with the RPM. Using the HRPM and HMRPM decreases the error in predicting conversion time significantly compared with the original RPM and MRPM. The HMRPM gives either minimal or no improvement over the HRPM. The relatively small benefit in using the MRPM over the RPM and the HMRPM over the HRPM is likely this is due to the low ash content, and therefore low potassium content, of the sawdust which would reduce the potential benefits for using the additional terms proposed by Zhang et al. in the MRPM. It was concluded that the HRPM was the best option for modeling the measured char conversion rate as it combines good conversion time predictions with a reasonable amount of fitting parameters. The best fit kinetic and structural parameters in the HRPM for CO_2 and H_2O gasification are shown in Table 4.

The conversion times predicted by the RPM, MRPM, HRPM and UCM are shown with the measured values for twelve sets of TGA data for both CO_2 and H_2O gasification in Figs. 7 and 8 (see Table 1 for all test conditions). It is clear that the UCM often deviates significantly from the measured conversion times, in particular for the H_2O tests. This was expected as the UCM in steam gasification has the highest mean absolute percentage error as shown in Table 3. The RPM and MRPM tend to produce very similar conversion time results and while the HRPM improves upon the RPM and

Table 3
Mean absolute percentage error for estimating conversion times of pine sawdust for five char reactivity models when compared with TGA experiments.

	CO_2 (%)	H_2O (%)
UCM	82	110
RPM	33	28
MRPM	28	26
HRPM	22	19
HMRPM	22	18

Table 4
Arrhenius and structural parameters for CO_2 and H_2O gasification of pine sawdust using the HRPM. The units are s^{-1} for the frequency factors, k_0, and J/mol for the activation energies, E.

	CO_2			H_2O	
	k_0	E		k_0	E
k_{1f}	$1.2 \cdot 10^{11}$	$1.6 \cdot 10^5$	k_{1f}	$1.9 \cdot 10^7$	$2.0 \cdot 10^5$
k_{1b}	$5.9 \cdot 10^8$	$1.7 \cdot 10^5$	k_{1b}	$2.9 \cdot 10^{10}$	$2.4 \cdot 10^5$
k_3	$2.2 \cdot 10^{10}$	$2.8 \cdot 10^5$	k_3	$2.4 \cdot 10^9$	$2.5 \cdot 10^5$
ψ	α	ξ	ψ	α	ξ
5.30	5.6	48	3.9	3.8	24

MRPM in most test conditions there are examples where the HRPM underperforms. This is to be expected due to the range of test conditions which have been used for the kinetic parameter fitting and it is unlikely that a simple conversion rate expression, such as the HRPM, will be able to produce the most accurate char conversion times in every situation. For this reason the mean absolute percentage error (Table 3) was used in determining the best model for describing the char conversion, indicating the superiority of the HRPM as described above. For both CO_2 and H_2O tests the improvement for using the HRPM was greater at 750 °C than 850 °C, which shows that accurate modeling of the early stage of char conversion is particularly important at lower temperatures.

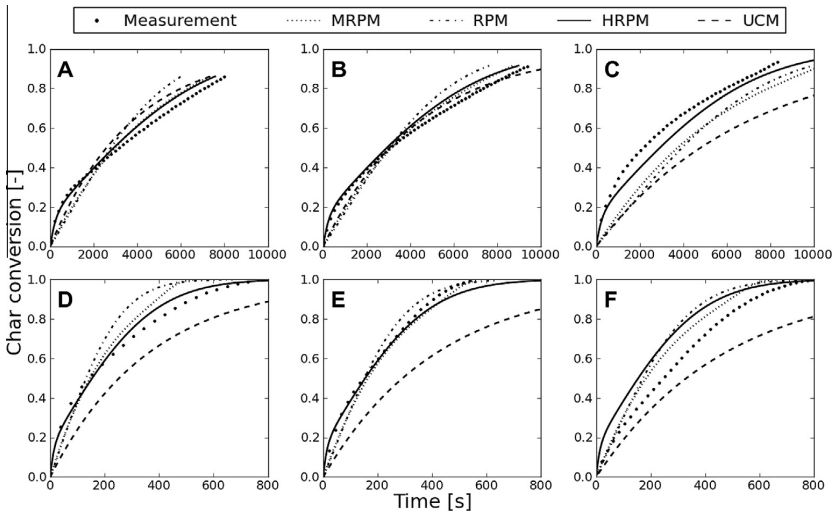

Fig. 7. Conversion times for CO_2 gasification as predicted by the UCM, the RPM, MRPM and the HRPM. The predicted conversion times are compared with the measured conversion time from the TGA data. (A) 750 °C, 1 bar CO_2; (B) 750 °C, 0.95 bar CO_2, 0.05 bar CO; (C) 750 °C, 0.8 bar CO_2, 0.2 bar CO; (D) 850 °C, 1 bar CO_2; (E) 850 °C, 0.89 bar CO_2, 0.11 bar CO; (F) 850 °C, 0.8 bar CO_2, 0.2 bar CO.

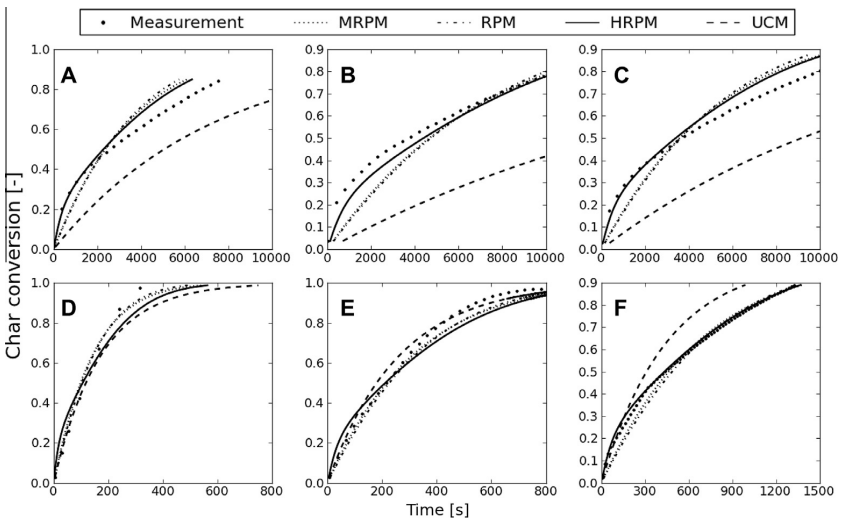

Fig. 8. Conversion times for H_2O gasification as predicted by the UCM, the RPM, MRPM and the HRPM. The predicted conversion times are compared with the measured conversion time from the TGA data. (A) 750 °C, 0.95 bar H_2O, 0.05 bar H_2; (B) 750 °C, 0.9 bar H_2O, 0.1 bar H_2; (C) 750 °C, 0.86 bar H_2O, 0.14 bar H_2; (D) 850 °C, 1 bar H_2O; (E) 850 °C, 0.95 bar H_2O, 0.05 bar H_2; (F) 850 °C, 0.86 bar H_2O, 0.14 bar H_2.

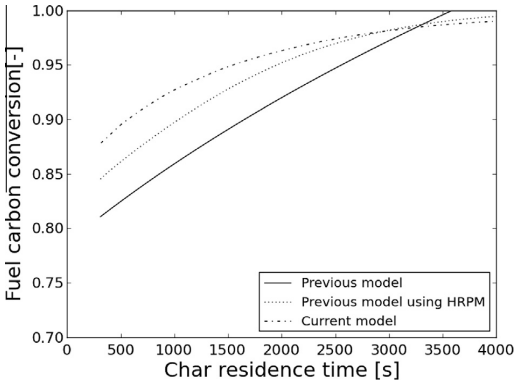

Fig. 9. Modeling results from the carbon conversion predictor showing carbon conversion as a function of char residence time in the reactor at 780 °C for three models: the model as reported by Konttinen et al. [9], the model as reported by Konttinen et al. but using the HRPM, and the current model described in Section 2.4.

Table 5
Operating conditions for pilot scale tests using pine sawdust (SD) [20], corresponding to modeling results.

	Test A	Test B
Fuel	Pine SD	Pine SD
Bed temperature, °C	780	840
Bed additive	Dolomite	Sand
Bed additive rate, g/s	0.44	0
Fuel feed rate, g/s	12.8	9.7
Steam feed, g/s	2.0	2.5
Bottom ash discharge, g/s	0	0
Estimated bed inventory, kg	12.7	12.7
Estimated fly ash discharge, g/s	0.8	0.2

3.2. Reactor modeling

The goal of the carbon conversion predictor is to estimate the carbon conversion of a FBG using relatively simple inputs. Results from the improved model were compared to previously published results, which used a more simple reactor model and the UCM to describe char reactivity [9]. The carbon conversion as a function of residence time at 780 °C is shown in Fig. 9 for three versions of the reactor model. Because the original model reported by Konttinen et al. [9] does not have any method for predicting carbon loss through fly ash and the simplicity of UCM kinetics, carbon reaches total conversion at around $\tau = 3500$ s, as shown by the sold line in Fig. 9. The FBG model structure was then left unchanged but the UCM was replaced with the HRPM kinetic model developed in this work. The results from this is shown by the dotted line in Fig. 9 and the conversion vs. residence time curve shows the significant slowdown in conversion rate that is expected as X_{ch} nears unity. Next the results from the current reactor model are shown by the alternating dot dash line in Fig. 9. The results from incorporating the new kinetics model into the old FBG model structure differ from the results obtained from the current FBG model, despite both using the HRPM for gasification kinetics, due to the assumption in the previous model that the char conversion time is equal to the char residence time ($\tau = \tau_R$). In the current model the char conversion time and the char residence time are related through Eq. (15).

Modeling of a pilot scale FBG was also conducted. The pilot scale tests were conducted using coal, peat and pine sawdust fuels at atmospheric and pressurized conditions [20]. For this modeling work only tests using pine sawdust were considered. The details of the pilot plant operation are shown in Table 5. In all tests bottom ash was not removed, and so $1/\tau_2 = 0$. While fly ash was removed during the tests the removal rate was not measured and so was estimated for modeling purposes. The rate of entrainment of fly ash, $1/\tau_3$, can be calculated by implementing an entrainment submodel as described by Gómez-Barea and Leckner [18], however in this work such a submodel has not been applied. Instead τ_3 was indirectly estimated from measurements by assuming all fuel ash, unconverted carbon and added bed material went to fly ash. The carbon conversion, fuel ash and added bed material were reported for the pilot plant tests which were simulated (see Table 5) so the flow rate of fly ash was estimated from measured parameters. From these data, the char residence time, τ, can be estimated which corresponds to a given value of τ_3.

The predicted carbon conversion and product gas composition from both the current reactor model and the previously published version of the model are compared to the measured values in Table 6. The results show reasonable agreement with the experimental data. Prediction of carbon conversion has improved significantly due to the improved char conversion model. The error in the char conversion prediction at 780 °C is noticeably larger than 840 °C which may be due to the addition of dolomite in the lower temperature test and to uncertainties in the experimental measurement leading to over reporting of the carbon conversion. While the differences in experimental setups can make comparison of results tenuous, fluidized bed gasification tests performed by others using pine sawdust generally report reaching lower carbon conversion at temperatures around 780 °C [21,22] than what is measured in the pilot tests used in this work.

The average error in the product gas composition also decreased in the current model. The error in the gas composition model results increases with temperature but the temperature dependent

Table 6
Measurements of carbon conversion and product gas composition of pine sawdust at 780 °C and 840 °C [20] compared with the results from the carbon conversion predictor model. The error values reported in the table are the absolute error.

	780 °C			840 °C		
	Measured	Current model	Previous model	Measured	Current model	Previous model
Carbon conversion	95.9	89.2	81.0	97.8	98.6	100
Dry gas composition (vol.%)						
N_2	53.0	50.3	53.2	58.0	54.4	52.3
H_2	10.9	15.2	13.6	8.4	13.0	14.2
CO_2	15.7	16.3	17.7	15.1	16.5	15.4
CO	14.2	13.7	10.8	14	12.3	14.3
CH_4[a]	5.7	4.4	4.7	4.1	3.8	3.7
H_2O (wet gas)	13.8	13.5	16.1	19.1	15.6	13.8
Average |error| in gas composition		12.9%	15.9%		17.8%	20.2%

[a] Methane production in the model is calculated using an empirical adjustment factor where 15% of volatile carbon is assumed to form CH_4, corresponding to 78 g/kg daf.

trends in the gas composition are correct with the exception of CO_2. Hydrogen content of the product gas is overestimated by the model at both temperatures and has the largest error of the product gas components. Overestimation of hydrogen formation in biomass gasification is common to equilibrium models and has been noted elsewhere [23–25]. As this model adjusts the product gas composition according to the equilibrium of the water–gas shift reaction this could contribute to the overestimation of H_2 and CO_2 in the final gas composition. Published work indicates that it is unlikely that water–gas shift reaction equilibrium is achieved at either 780 °C or 840 °C [2] and so this simplification of the model limits the accuracy of the product gas composition estimation.

4. Conclusion

A method for modeling char reactivity of pine sawdust measured in TGA experiments has been presented. Based on the TGA measurements for sawdust a catalytic gasification with deactivation of the catalyst stage was observed at low char conversion. By combining the three parallel reaction model with the random pore model, significant improvement in estimated char conversion times was achieved. This reactivity model showed good ability to predict the measured char conversion times and was used to model a pilot scale fluidized bed gasifier. An existing carbon conversion predictor model for fluidized bed gasification of biomass was updated to include the newly developed char gasification kinetic expression and submodel for estimation of char conversion and residence time. The results of the model show improved ability to estimate measured carbon conversion and product gas composition of pine sawdust in a pilot scale fluidized bed gasifier. The FBG model cannot currently be used to completely predict gasifier behavior because some measurements are required to estimate the entrainment of char from the gasifier. Developing an entrainment submodel is required to address this issue.

Acknowledgment

Financial support for this work from the Academy of Finland through the GASIFREAC project is gratefully acknowledged.

References

[1] Baskar C, Baskar S, Dhillon RS, editors. Biomass conversion. Springer; 2012.
[2] Gómez-Barea A, Leckner B. Modeling of biomass gasification in fluidized bed. Prog Energy Combust Sci 2010;36(4):444–509. http://dx.doi.org/10.1016/j.pecs.2009.12.002.
[3] Moilanen A. Thermogravimetric characterisations of biomass and waste for gasification processes. PhD thesis. Åbo Akademi; 2006.
[4] Moilanen A, Saviharju K. Gasification reactivities of biomass fuels in pressurised conditions and product gas mixtures. In: Bridgwater AV, Boocock DGB, editors. Developments in thermochemical biomass conversion. London: Blackie Academic and Professional; 1997. p. 828–37.
[5] Umeki K, Moilanen A, Gómez-Barea A, Konttinen J. A model of biomass char gasification describing the change in catalytic activity of ash. Chem Eng J 2012;207–208:616–24. http://dx.doi.org/10.1016/j.cej.2012.07.025.
[6] Di Blasi C. Combustion and gasification rates of lignocellulosic chars. Prog Energy Combust Sci 2009;35(2):121–40.
[7] Katta S, Keairns DL. Study of kinetics of carbon gasification reactions. Ind Eng Chem Fund 1981;20(1):6–13.
[8] Klose W, Wolki M. On the intrinsic reaction rate of biomass char gasification with carbon dioxide and steam. Fuel 2005;84(7–8):885–92. http://dx.doi.org/10.1016/j.fuel.2004.11.016.
[9] Konttinen JT, Moilanen A, DeMartini N, Hupa M. Carbon conversion predictor for fluidized bed gasification of biomass fuels—from TGA measurements to char gasification particle model. Biomass Convers Biorefin 2012;2(3):265–74.
[10] Barrio M. Experimental investigation of small-scale gasification of woody biomass. PhD thesis. Norwegian University of Science and Technology; 2002.
[11] Bhatia DDPSK. A random pore model for fluid–solid reactions: I. Isothermal, kinetic control. AIChE J 1980;26(3):379–86.
[12] Bhatia DDPSK. A random pore model for fluid–solid reactions: II. Diffusion and transport effects. AIChE J 1981;27(2):247–54.
[13] Zhang Y, Ashizawa M, Kajitani S, Miura K. Proposal of a semi-empirical kinetic model to reconcile with gasification reactivity profiles of biomass chars. Fuel 2008;87(4–5):475–81. http://dx.doi.org/10.1016/j.fuel.2007.04.026.
[14] Kunii D, Levenspiel O. Fluidization engineering. Butterworth-Heinermann; 1990.
[15] Okumura Y, Hanaoka T, Sakanishi K. Effect of pyrolysis conditions on gasification reactivity of woody biomass-derived char. Proc Combust Inst 2009;32(2):2013–20. http://dx.doi.org/10.1016/j.proci.2008.06.024.
[16] Cetin E, Moghtaderi B, Gupta R, Wall T. Influence of pyrolysis conditions on the structure and gasification reactivity of biomass chars. Fuel 2004;83(16):2139–50. http://dx.doi.org/10.1016/j.fuel.2004.05.008.
[17] Konttinen J, Moilanen A, Hupa M, Kurkela E. Carbon conversion predictor for fluidized bed gasification of biomass fuels—model concept. In: Science in thermal and chemical biomass conversion; 2006. p. 590–604.
[18] Gómez-Barea A, Leckner B. Estimation of gas composition and char conversion in a fluidized bed biomass gasifier. Fuel 2012;107:419–31. http://dx.doi.org/10.1016/j.fuel.2012.09.084.
[19] Jand N, Brandani V, Foscolo PU. Thermodynamic limits and actual product yields and compositions in biomass gasification processes. Ind Eng Chem Res 2006;45(2):834–43.
[20] Kurkela E, Ståhlberg P, Laatikainen-Luntama J. Pressurized fluidized-bed gasification experiments with wood, peat and coal at VTT in 1991–1994. Part 2. Experiences from peat and coal gasification and hot gas filtration. VTT Publications; 1994.
[21] Herguido J, Corella J, Gonzalez-Saiz J. Steam gasification of lignocellulosic residues in a fluidized bed at a small pilot scale. Effect of the type of feedstock. Ind Eng Chem Res 1992;31(5):1274–82. http://dx.doi.org/10.1021/ie00005a006.
[22] Lv PM, Xiong ZH, Chang J, Wu CZ, Chen Y, Zhu JX. An experimental study on biomass air–steam gasification in a fluidized bed.. Bioresource Technol 2004;95(1):95–101. http://dx.doi.org/10.1016/j.biortech.2004.02.003.
[23] Puig-Arnavat M, Bruno JC, Coronas A. Review and analysis of biomass gasification models. Renew Sust Energy Rev 2010;14(9):2841–51. http://dx.doi.org/10.1016/j.rser.2010.07.030.
[24] Li X, Grace J, Lim C, Watkinson aP, Chen H, Kim J. Biomass gasification in a circulating fluidized bed. Biomass Bioenergy 2004;26(2):171–93. http://dx.doi.org/10.1016/S0961-9534(03)00084-9.
[25] Ruggiero M, Manfrida G. An equilibrium model for biomass gasification processes. Renewable Energy. 1999;16(1–4):1106–9. http://dx.doi.org/10.1016/S0960-1481(98)00429-7.

Publication II

Jason Kramb, Nikolai DeMartini, Magnus Perander, Antero Moilanen, Jukka Konttinen "Modeling of the catalytic effects of potassium and calcium on spruce wood gasification in CO2", *Fuel Processing Technology*, vol. 148, 2016, pp. 50-59

Fuel Processing Technology 148 (2016) 50–59

Contents lists available at ScienceDirect

Fuel Processing Technology

journal homepage: www.elsevier.com/locate/fuproc

Research paper

Modeling of the catalytic effects of potassium and calcium on spruce wood gasification in CO_2

Jason Kramb [a,b,*], Nikolai DeMartini [c], Magnus Perander [c], Antero Moilanen [d,1], Jukka Konttinen [b]

[a] Department of Chemistry, Renewable Natural Resources and Chemistry of Living Environment, University of Jyväskylä, PO Box 35, FI-40014 Jyväskylä, Finland
[b] Department of Chemistry and Bioengineering, Tampere University of Technology, PO Box 541, FI-33101 Tampere, Finland
[c] Johan Gadolin Process Chemistry Centre, Åbo Akademi University, FI-20500 Turku, Finland
[d] VTT Technical Research Centre of Finland, PO Box 1000, 02044, VTT, Finland

ARTICLE INFO

Article history:
Received 21 August 2015
Received in revised form 12 January 2016
Accepted 25 January 2016
Available online 1 March 2016

Keywords:
Biomass
Gasification
Reaction kinetics
Modeling

ABSTRACT

Using previously reported thermogravimetric analysis measurements, the effects of calcium and potassium on the char gasification rate of spruce wood were modeled. Spruce wood was leached of inorganic ash elements and doped with measured amounts of potassium and calcium. The wood was gasified in an isothermal thermogravimetric analysis device in CO_2 where the devolatilization of the wood, char formation and char gasification all occurred inside the preheated reactor. A new method for separating the effects of devolatilization and char gasification is presented. Kinetic models were evaluated for their ability to describe the observed catalytic effects of potassium and calcium on the gasification rate. Two modified versions of the random pore model were able to accurately describe the measured conversion rates and the parameters of the kinetic models were found to be dependent on the calcium and potassium concentrations. Empirical correlations were developed to predict the char conversion rate from only the potassium and calcium concentration of the sample.

1. Introduction

A large range of gasification reactivities has been observed between different biomass and coal chars [1]. While there are many differences between coal and biomass chars, the factors that affect the reactivity are largely the same and are commonly thought to include surface area, pore structure, active site density and the presence of inorganics (ash materials) [1–5]. These factors can be interrelated, especially as the presence of inorganics can influence the other char properties.

Many metals have been shown to have a catalytic effect on coal, biomass char and carbon gasification [3,6–9]. Some of these metals occur naturally in biomass in significant amounts and in some cases their presence can be the cause of the majority of the difference in char gasification reactivity between difference biomass samples [1]. Calcium and potassium in particular have been observed to have a significant influence on biomass char gasification rates [10–12]. However, the effects are often limited to a particular time during the conversion process and the results are not always consistent between the various studies. Understanding the behavior of these metals and their impact on char gasification rates is essential in modeling the overall biomass char gasification process.

The work presented in this paper builds upon the work of Perander et al. [13] and investigates the effects of potassium and calcium on the conversion rate of spruce char in CO_2 as a function of char conversion. This was done by applying previously published kinetic models to a large set of isothermal thermogravimetric analysis (TGA) data. Empirical correlations were developed which allowed the parameters from the kinetic models to be estimated given the potassium and calcium concentrations, thus allowing the char conversion rate to be predicted from only the inorganic concentrations in the biomass. This work focuses on modeling the overall impacts of Ca and K on the apparent char conversion rates. It has been shown that the presence of catalysts will affect the measured surface area in addition to the active site density [11,14] and there has been some effort to understand the effects of catalysts on the development of the char surface area during the conversion process [15–17]. In this work these effects are not separated, however, and the apparent conversion rate is used for modeling purposes, which is consistent with other studies when fitting data to conversion rate models [10,12,18].

2. Theory and methods

2.1. Definitions

Total sample conversion, X, is given by $X = (m_0 - m_t)/m_0$, where m_0 is the initial mass of the sample and m_t is the sample mass at time t. Similarly, the ash free char conversion is given as $X_{ch} = (m_{ch,0} - m_{ch,t})$ where $m_{ch,0}$ and $m_{ch,t}$ are the initial ash free char mass and the ash

* Corresponding author at: Tampere University of Technology, Department of Chemistry and Bioengineering, P.O. Box 541, FI-33101 Tampere, Finland.
E-mail address: jason.kramb@tut.fi (J. Kramb).
[1] Present address: Department of Chemistry and Bioengineering, Tampere University of Technology, PO Box 541, FI-33101 Tampere, Finland.

http://dx.doi.org/10.1016/j.fuproc.2016.01.031
0378-3820/

free char mass at time t, respectively. The ash mass was taken as the mass at the end of char gasification. The instantaneous reaction rate is then calculated in the standard way,

$$r = -\frac{1}{m_{ch,t}}\frac{dm_{ch}}{dt} = \frac{1}{1-X_{ch}}\frac{dX_{ch}}{dt}. \quad (1)$$

2.2. Sample preparation

The biomass used in this study is wood from Norwegian spruce (*Picea abies*). A detailed description of the leaching and catalyst loading procedures can be found by Perander et al. [13] and a brief summary of the sample preparation procedure is given below. Particles of size 125–250 particles were obtained by milling the wood. The wood was leached of the ash forming elements by washing the milled wood with HNO_3 and rinsing with ion-exchange water.

The catalytic metals were added to the demineralized spruce wood in different ways. For the doped samples, either K or Ca was loaded onto carboxylic and phenolic sites in the demineralized wood. For the impregnated samples, the K or Ca was added as salts. The salts used in this work were K_2CO_3, $CaCO_3$ and CaC_2O_4.

For the Ca and K doped samples, calcium and potassium were loaded to the organic functional groups through ion-exchange by using a $Ca(NO_3)_2$ and KNO_3 solution respectively. The concentration of Ca or K that bonded to the organic sites was adjusted by adjusting the pH of the solution using either KOH or $Ca(OH)_2$. Potassium carbonate was impregnated into the demineralized wood by mixing the wood with a K_2CO_3 solution, followed by drying of the wet wood. The advantage of this approach compared to dry mixing is that the dispersion of K_2CO_3 in the spruce wood is better, however because of the solution is alkaline, some of the K will be added to organic sites and some of the salt will precipitate as $KHCO_3$ rather than K_2CO_3. Calcium oxalate was impregnated into the demineralized wood by mixing calcium oxalate monohydrate ($CaC_2O_4 * H_2O$) with wet wood which was then dried. Thus the calcium oxalate was not as well distributed in the wood as the K_2CO_3. Finally, for the $CaCO_3$ impregnated sample, $CaCO_3$ was dissolved in dilute nitric acid with a pH of 4 and the wood was mixed with this solution. This resulted in some Ca loaded by ion-exchanged to the organic sites as well as some calcium loaded as $CaHCO_3$ and $Ca(NO_3)_2$.

The complete list of samples and their elemental concentrations can be found in [13] and is also given in Table A.1 in Appendix A.

2.3. Experimental setup

The TGA device used in these measurements has been described in detail by Whitty et al. [19]. Tests were conducted in the isothermal TGA at 850 °C. The biomass samples were lowered into a preheated reactor where the sample undergoes devolatilization and char gasification. Perander et al. [13] showed that when using this test configuration the gasification reactions for the original spruce wood are in the kinetically controlled regime at temperatures up to and including 900 °C. The doped samples with increased catalyst concentrations are more reactive than the original spruce wood but the peak conversion rate in the samples with highest Ca and K concentration at 850 °C is still lower than the peak conversion rate of the original biomass at 900 °C. Because the original spruce wood is kinetically limited at 900 °C it can be concluded that doped samples are kinetically limited at 850 °C.

2.4. Isolating char conversion in isothermal TGA measurements with in-situ devolatilization

While the benefits of the test configuration used are clear (e.g. rapid heating during devolatilization, char is not cooled before gasification), it also presents the complication that there are two simultaneous processes occurring which cause sample mass loss: devolatilization and char gasification. Devolatilization occurs much more rapidly than char gasification but the two processes overlap to some extent during the first 50–300 s.

In previous work using similar experimental setups, methods have been used to determine a time at which the devolatilization rate will be low enough that afterwards all mass loss can be assumed to result from char gasification [20,21]. This time is then taken as the starting point of char gasification and has typically been between 60 and 120 s for biomass samples at temperatures of 750–850 °C.

In the current work, a new method for separating devolatilization and char gasification was developed. For this, repeated TGA measurements using acid washed and potassium doped samples were taken in a nitrogen atmosphere to obtain a devolatilization profile for the samples at 850 °C. These pyrolysis measurements were conducted on an identical TGA device in a different facility [22] and their results were confirmed to be comparable to the device which was used for the CO_2 tests. Acid washed and potassium doped samples were chosen because they represented the extreme cases of the devolatilization behavior, due to potassium having been previously shown to have a significant effect on devolatilization behavior while calcium has little impact [13,23,24].

In this work the conversion rate profiles for acid washed and potassium doped samples in N_2 were nearly identical; however, the final char yield for the potassium doped samples was approximately twice that of the acid washed samples. This can be explained by the fact that the first measurement from the TGA was recorded after 30 s from when the sample is lowered into the preheated reactor. At the time of this initial measurement the masses of the two sample types already show a clear separation with the potassium doped samples having twice the mass of the acid washed samples. From this it can be concluded that the difference in devolatilization behavior between the two samples types occurs in the first 30 s of the mass loss, which was not recorded in the TGA measurements. The increased char yield of the potassium doped samples is consistent with other studies [25,26]. One explanation for this occurrence is that the presence of alkali metals will inhibit the release of some volatiles [27] such as larger aromatic ring systems [28].

Because the doping process had no significant impact on the devolatilization rate during the measurement time, a single devolatilization profile was created for all of the samples by averaging the measured conversion rate in N_2 of the potassium doped and acid washed samples.

This mass loss effect was then removed from the TGA data taken in CO_2, leaving only the difference between the two tests, which is the mass loss due to char gasification. Fig. 1 illustrates the results of this

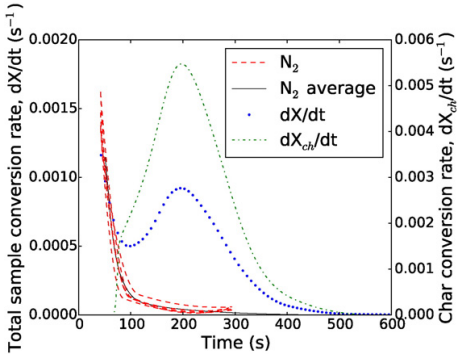

Fig. 1. An example of the process to calculate char conversion from the original TGA conversion rate curve. The dashed lines show conversion rates measured in N_2, which are averaged together giving the solid line. This average of the N_2 is subtracted from the conversion rate curve obtained in CO_2 (dotted line), isolating the effects of the char gasification. The resulting char conversion rate is shown by the dash-dot line. The first 30 s of data from the TGA is unusable due to unstable mass reading and so is omitted from the plot. The dashed lines, solid line and dotted line show sample conversion and go to the left axis. The dash-dot line goes to the right axis. All measurements were conducted at 850 °C.

process by showing an example of an original sample conversion rate curve which includes mass loss due to devolatilization and the resulting char conversion rate curve. The dotted line in Fig. 1 shows the original sample conversion rate curve in CO_2 which contains mass loss due to devolatilization as well as char gasification. The dashed lines show the conversion rate curves of samples in N_2, which contain only mass loss due to devolatilization. These are averaged together, giving the solid line, and then subtracted from the measurement in CO_2 and then converted from sample conversion rate (dX/dt) to char conversion rate (dX_{ch}/dt) resulting in the dash-dot line. For this particular sample, the char conversion curve begins at a low rate and increases to a maximum at $t \approx 200$ s. The low initial conversion rate is due to volatile gases which are leaving the sample and interfering with the char gasification.

2.5. Kinetic models

Numerous models have been proposed for describing biomass char gasification with varying levels of complexity. A review of the common reaction mechanisms and kinetic models has been performed by Di Blasi [1]. Typically conversion rate models will have a general form of

$$dX_{ch}/dt = k(T, p_i)F(X), \tag{2}$$

where k is the kinetic term with dependence on temperature, T, and the partial pressure, p_i, of the reacting gas (CO_2 or H_2O) and possibly inhibiting gases (CO or H_2). The $F(X)$ term contains the conversion dependence and may attempt to describe the structural changes that occur inside the char particles. Examples of the many forms the kinetic term can take can be found in the review by Di Blasi.

Many of the structural models have been originally developed to describe the behavior of coal, but continue to be used for biomass chars. A short review of some of the common structural models has been performed by Molina and Mondragón [4]. The random pore model (RPM) [29,30] is one of the most commonly used structural models and has successfully been used for numerous types of fuels. One appealing feature of the RPM is that the structural parameter, ψ, used in the RPM can be calculated based on measurements of the pore structure of the sample. However, in many cases ψ is determined based on the reaction rate measurements. A discussion of the difference between these two methods of calculating ψ was given by Bhatia and Vartak [31]. In the current work ψ is determined based on the conversion rate measurements from the TGA.

While it has been noted in numerous studies on biomass samples that alkali and alkali earth metals have significant impacts on char gasification rates, there has been limited progress in extending conversion rate models to include the effects of these catalysts. It has also been noted that in some cases the conversion dependent terms of the conversion rate models actually describe a combination of effects caused by structural changes in the char particle and catalytic effects caused by the presence of inorganics in the char [12].

The assumptions made in the formulations of the original random pore model become less valid when studying catalytic gasification, such as in the present work. This is because in highly catalyzed gasification the reaction rate is no longer primarily determined by the growth and coalescence of the internal pores of the char but instead by the presence of the catalysts, or some combination of these two effects. As a result of this, traditional surface area measurements may no longer show any correlation to the reactivity of the char and instead the concept of active sites may be more useful in explaining the measured conversion rate. This was shown clearly by Suzuki et al. [11] where alkali/alkaline earth metal impregnated biomass samples, similar to the samples used in this work, were gasified. It was shown there that surface area as measured by BET typically had no correlation to the char reactivity but O_2 uptake, indicating active carbon sites, did give a good indicator for the gasification rates. As a result, the physical interpretation of the RPM parameter ψ in these cases may not be clear due to the superposition of structural and catalytic effects. In many cases the original RPM will be unable to fit measured reaction rates for catalytic gasification at all.

One approach to account for the catalytic effects of inorganics during char gasification is to modify the random pore model in some way to better describe experimental data. One such model developed by Zhang et al. [10] adds two additional fitting parameters (c and p) to the random pore model and is given by,

$$dX_{ch}/dt = k(1-X)\sqrt{1-\psi\, log(1-X)}\left(1 + (cX)^p\right). \tag{3}$$

The random pore model can describe conversion rate curves which have a maximum conversion rate occurring below $X_{ch} = 0.393$, but Eq. (3) was shown to fit well to experimental data which showed maximum conversion rates occurring much later. The parameters c and p in Eq. (3) were shown to be correlated to the concentration of potassium in the biomass samples used in that study. It was concluded that the peak in the conversion rate curves that occurred late in the conversion process were largely attributable to the catalytic effects of potassium.

Another example of a kinetic model which extends the random pore model to include catalytic effects was presented by Struis et al. [12] and includes a time dependent term as shown in Eq. (4),

$$dX_{ch}/dt = k(1-X)\sqrt{1-\psi\, log(1-X)}\left(1 + (g+1)(bt)^g\right). \tag{4}$$

The terms g and b are, again, fitting parameters. This model was able to accurately describe the effects of impregnation of metals into wood samples on the char gasification rates. In this work, these two models (Eqs. (3) and (4)) were evaluated against the experimental char conversion rates.

3. Results and discussion

3.1. Conversion rate and instantaneous reaction rate curves

Calcium doping has a pronounced effect on the conversion rate of the samples, as can be seen in Fig. 2a. The samples show significantly higher conversion rates throughout the conversion process when compared with the acid washed samples, though the conversion rate peaks early ($X_{ch} = 0.1$–0.4). The result differs from some other measurements of catalytic effects of calcium on activated carbon which have shown the conversion rate curve to be highest in the range $0 < X_{ch} < 0.1$ and dropping significantly after about $X_{ch} \approx 0.5$ [10]. Suzuki et al. reported the instantaneous reaction rate of Ca doped biomass to peak at $X_{ch} \approx 0.2$ [11]. A possible reason for this difference is because the chars in this work were formed at high heating rates. At high heating the char precursor phase may undergo melting which can result in chars which lose the cellular structure of the original biomass and instead have smoother surfaces with larger pore structures [32]. This may cause the calcium to become covered by char and the catalytic benefits of the calcium are not observed until the catalyst is exposed [33].

The conversion behavior of the $CaCO_3$ and CaC_2O_4 samples differed significantly from the Ca doped samples. The conversion rate and instantaneous reactivity profiles for the $CaCO_3$ and CaC_2O_4 samples are shown in Fig. 2b. The conversion rate peaks very early in these samples, typically between $X_{ch} = 0.1$ and $X_{ch} = 0.3$, but then the conversion rate decreases rapidly. This shows some similarity to the conversion rate curves reported by Struis et al. [12] with $Ca(NO_3)_2$ impregnated chars, where the conversion rate decreased rapidly from $X_{ch} = 0$ to $X_{ch} = 0.2$, presumably as a result of sintering. In the current measurements the catalytic deactivation occurs more slowly and continues to $X_{ch} \approx 0.6$ in some cases, but this is again likely a result of the differing char formation methods.

It has been reported that the active species in calcium catalyzed gasification is $CaCO_3$ [34], hence the reaction pathway for the three types of calcium samples may be similar. In addition, $CaCO_3$ crystals can be seen forming on the Ca and CaC_2O_4 samples during gasification [13].

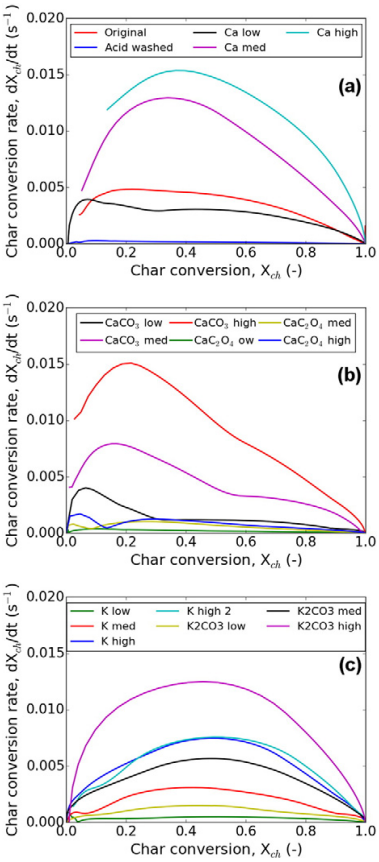

Fig. 2. Char conversion rate curves obtained from TGA data. The samples shown in the subplots are: a) original spruce wood, acid washed, and Ca doped samples; b) $CaCO_3$ and CaC_2O_4 impregnated samples; c) K and K_2CO_3 loaded samples. All measurements were done at 850 °C and in 100% CO_2 atmosphere.

However, the initial form of the calcium catalyst is different between the samples as described in Section 2.2. As a result the behavior of the calcium during devolatilization will vary and the resulting catalyst dispersion on the char surface will be significantly different between the samples, as noted by Perander et al. [13]. This variation in initial form of the calcium catalyst in the samples and the resulting difference in catalyst dispersion cause the observed difference in gasification rates of the Ca, $CaCO_3$ and CaC_2O_4 samples.

The char conversion rate curves for the potassium loaded samples are shown in Fig. 2c. It is clear that the general shape of the conversion rate curve remains the same regardless of the level of potassium. The conversion rate curves for the potassium doped samples also show similar behavior to the calcium doped samples, but the maximum conversion rate occurs later in the conversion process. This agrees with previous work showing that Ca catalytic effects occur earlier than potassium [10–12]. The maximum conversion rate is reached at an average of $X_{ch} = 0.46$. This closely resembles the shape of the conversion rate curve of KNO_3 impregnated chars as reported by Struis et al. [12] where a maximum was observed at $X_{ch} \approx 0.5$. In contrast to the $CaCO_3$ and CaC_2O_4 impregnated samples, which differed significantly from the Ca doped samples, the K_2CO_3 samples behaved very similarly to the K doped samples. The similarity in behavior of K and K_2CO_3 samples indicates that both have the same reaction pathway when catalyzing the char gasification. This is supported by the formation of K_2CO_3 crystals on the K doped samples [13], indicating that the potassium forms K_2CO_3, starting during devolatilization.

The instantaneous reaction rate increases throughout the conversion process but then begins to increase rapidly around $X_{ch} = 0.9$ and peaks slightly before the end of the conversion process. This behavior is similar to the potassium impregnated samples tested by Suzuki et al. [11], although in those tests the peak was slightly broader.

3.2. Modeling results

All parameters in the kinetic models, including the structural parameter ψ, were determined using a least-squares fitting routine. The results from fitting Eqs. (3) and (4) to the measured conversion rate data of the calcium doped samples are shown in plot a of Fig. 3. It is clear that both kinetic models can match the measured values reasonably well. The absolute mean percentage error for each model in predicting the conversion was calculated in the same method as in previous work [21] and given by

$$\epsilon = \frac{1}{N_j}\sum_{j=1}^{N_j}\frac{1}{N_i}\sum_{t=1}^{N_i}\left|\left(t_{i,j,exp} - t_{i,j,model}\right)/t_{i,j,exp}\right|, \tag{5}$$

where N_j is the total number of TGA measurements, N_i is the number of data points in the jth TGA measurement, $t_{i,j,exp}$ is the experimental conversion time for point i in TGA set j, and $t_{i,j,model}$ is the modeled conversion time for data point i in TGA set j. The errors are given in Table 1. Eqs. (3) and (4) also fit extremely well to the conversion rate curves obtained from the potassium loaded samples, as shown in Fig. 3c.

Because $CaCO_3$ and $_2O_4$ showed noticeably different behavior than the Ca or K doped samples, Eqs. (3) and (4) did not fit well to these measurements. In previous works where a decrease in reactivity was observed early in the conversion process an exponential decay term was added to the conversion rate equation to represent the catalytic deactivation [12,20,21]. The approach taken by Struis [12] was followed here, and the quickly decreasing catalytic effect due to sintering of the catalyst is given by the expression

$$dX_{ch}/dt = A_{cat}\, exp(-\xi t) + Eq.4, \tag{6}$$

where A_{cat} is the initial reaction rate contribution of the catalyst and ξ is an exponential rate constant which describes the deactivation of the catalyst. The results from fitting Eq. (6) to the measured conversion rate curves for the $CaCO_3$ and CaC_2O_4 samples are shown in plot b of Fig. 3. The model results match the experimental results well with the exception being at very low conversion ($X_{ch} < 0.1$) where the conversion rate is lower than expected due to inhibition from volatilized gases.

The parameters which gave the optimal fit for each kinetic model are given in Table 2 and also shown in Figs. 4 through Fig. 8. The results for fitting Eq. (3) to the Ca doped samples differ significantly from the results reported by Zhang et al. [10]. It is clear from Fig. 4 that there is a strong dependence of k, ψ and p on the calcium concentration of the sample. This is in contrast to Zhang et al., where a variety of biomass samples with different amounts of Ca and K were tested. In that work the Ca concentration in the biomass was not shown to have a significant correlation to the c and p parameters of Eq. (3).

Fig. 5 shows the best-fit parameters for Eq. (4) to the Ca doped samples. To reduce the number of fitting terms in the model, the kinetic coefficient k was taken as a constant and was equal to the kinetic coefficient found for the acid washed samples. This isolates all of the effects of the added calcium to the other three parameters (ψ, g and b). Doing this did not cause any negative impact on the ability of Eq. (4) to fit the measured data. The remaining parameters have clear dependence on the Ca concentration. The best fit parameters for $CaCO_3$ and CaC_2O_4 impregnated samples are shown in Fig. 6.

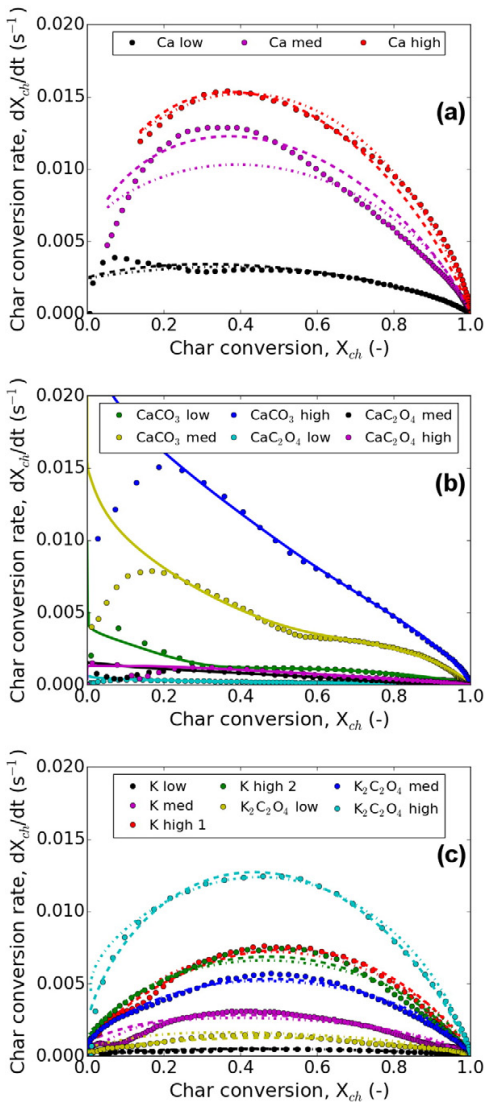

Fig. 3. Measured char conversion rate curves and model results. For subplots a and c the measured conversion rate is shown by the dots, results from Eq. (3) shown by the dashed line (- -), and results from Eq. (4) by the dot-dash line (-·-). For subplot b measured conversion is shown by the dotted line (··) and results from Eq. (6) by the solid line. The samples shown in the subplots are: a) original spruce wood, acid washed and Ca doped samples; b) $CaCO_3$ and CaC_2O_4 impregnated samples; c) K doped and K_2CO_3 samples. The colors shown in the legends apply for all line types. All measurements were done at 850 °C and in 100% CO_2 atmosphere.

Fig. 7 shows the dependence of the parameters in Eq. (3) on the potassium concentration in the biomass sample. The parameters k, ψ and c all have a strong linear dependence on the potassium concentration, while p varies within the range of 0.1 to 0.6. The linear dependence of c on potassium concentration matches well with the results reported by Zhang et al. but the values of c obtained here are slightly higher. Whether the potassium has been added in the form of K or K_2CO_3 has no impact on the trends of the parameters in this work.

The best fit parameters for Eq. (4) to the K doped and K_2CO_3 samples are shown in Fig. 8. The structural parameter, ψ, is very small for all of the samples which agrees with the results from Struis et al. [12]. The kinetic coefficient was again fixed at the value obtained from the acid washed samples.

3.3. Predictive empirical model for biomass reaction rates

A simple empirical model was developed in order to predict the gasification reaction rate of spruce wood char from only the potassium and calcium concentration. This was done by creating set of correlations for the parameters of the conversion rate models using only the results of the demineralized wood and Ca and K doped samples. Because Eq. (4) gave the best results for the Ca and K doped samples it was chosen to be used in the predictive model. The parameters for Eq. (4) were correlated to the potassium and calcium concentrations in the samples by using the linear best fit lines shown in Figs. 5 and 8. In the case of ψ_K, the RPM structural term for the potassium reaction, the best fit values of ψ_K were very small and uncorrelated to the potassium concentration

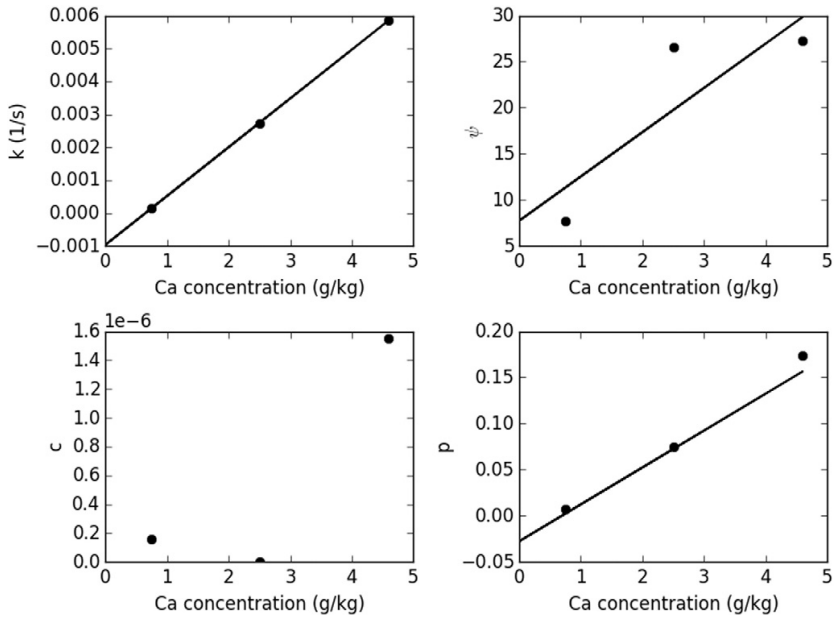

Fig. 4. Best fit parameters for Eq. (3) to the Ca doped samples.

and so this parameter was set to zero. The complete set of correlations obtained from the best fit lines are shown in Eqs. (8)–(15):

$$dX_{ch}/dt = dX_{ch}/dt_{Ca} + dX_{ch}/dt_K \tag{7}$$

$$k_{Ca} = 1.43e{-}4, \tag{8}$$

$$\psi_{Ca} = 0.0015 * [Ca] + 2.88, \tag{9}$$

$$g_{Ca} = 0.000031 * [Ca] + 0.2628, \tag{10}$$

$$b_{Ca} = 0.0317 * [Ca] + 165, \tag{11}$$

$$k_K = 1.43e{-}4, \tag{12}$$

$$\psi_K = 0, \tag{13}$$

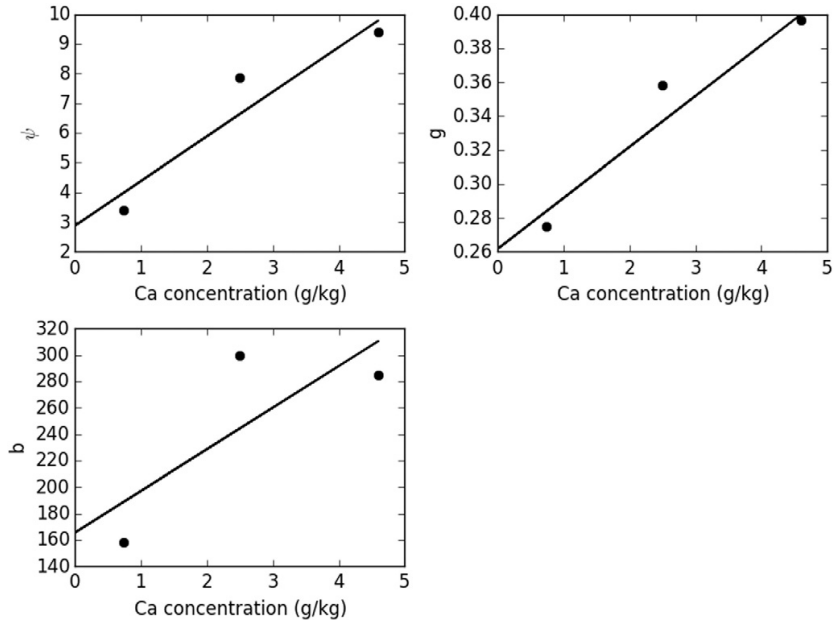

Fig 5. Best fit parameters for Eq. (4) to the Ca doped samples.

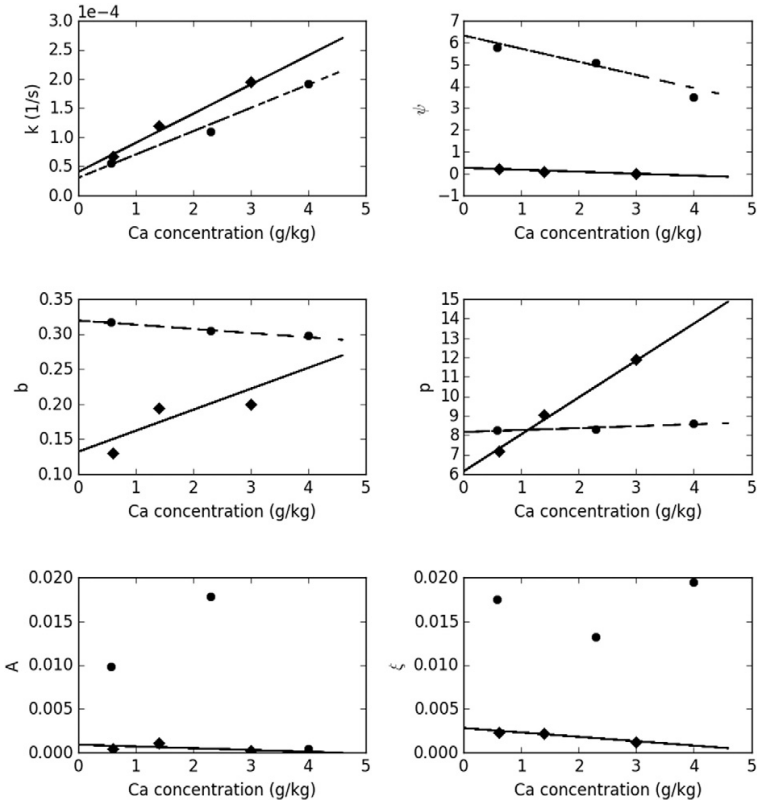

Fig 6. Best fit parameters for Eq. (6) to the $CaCO_3$ and CaC_2O_4 impregnated samples. The circles show the parameters for $CaCO_3$ and the dashed line shows a linear best fit. The diamonds show the parameters for the CaC_2O_4 samples and the solid line a linear best fit.

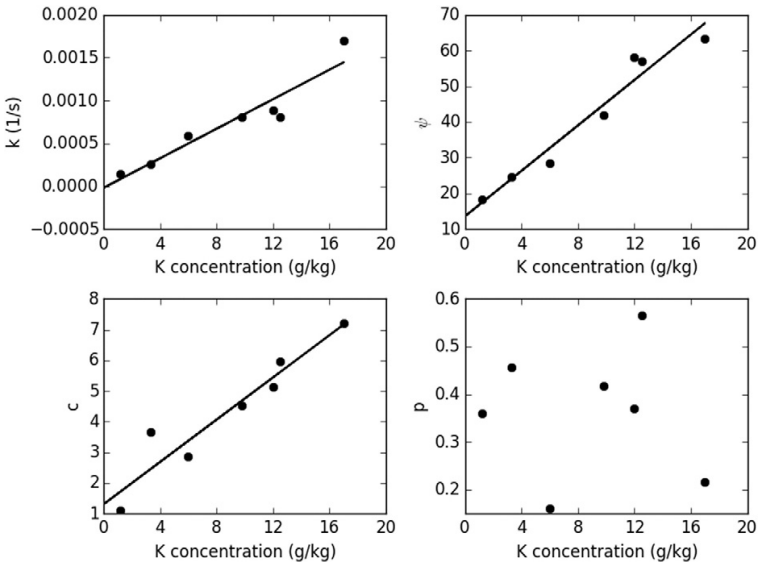

Fig. 7. Best fit parameters for Eq. (3) to the K doped and K_2CO_3 samples and linear trend lines. The parameter *p* has no apparent correlation to K concentration so no best fit line was included.

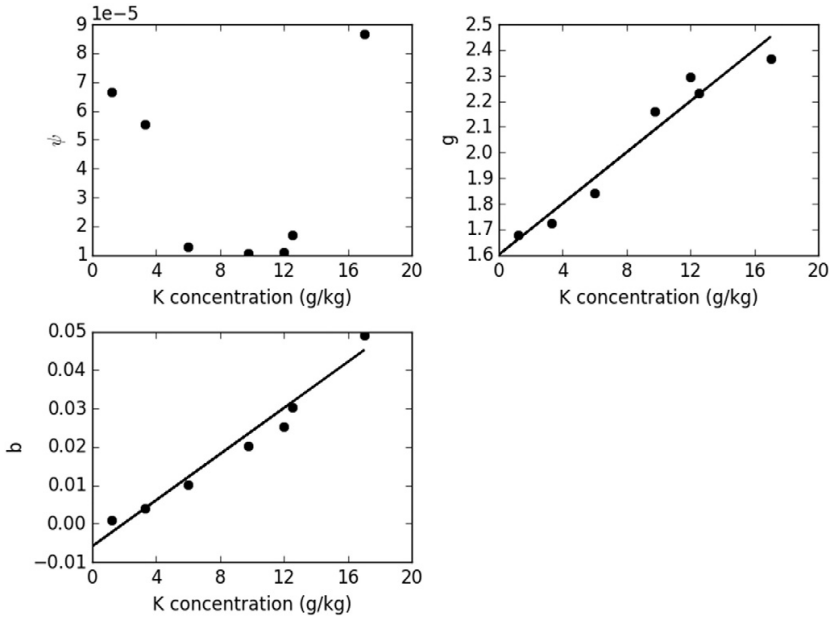

Fig. 8. Best fit parameters for Eq. (4) to the K doped and K_2CO_3 samples and linear trend liens. The structural term ψ was not correlated to K concentration so no trend line was included.

$$g_K = 0.000050 * [K] + 1.6, \tag{14}$$

$$b_K = 0.0000029 * [K] - 0.0059, \tag{15}$$

where dX_{ch}/dt_{Ca} is the portion of the conversion rate caused by the catalytic effects of Ca (given by Eq. (4)), dX_{ch}/dt_K is the portion of the conversion rate caused by the catalytic effects of K (given by Eq. (4)), and [Ca] and [K] are the concentrations of calcium and potassium respectively.

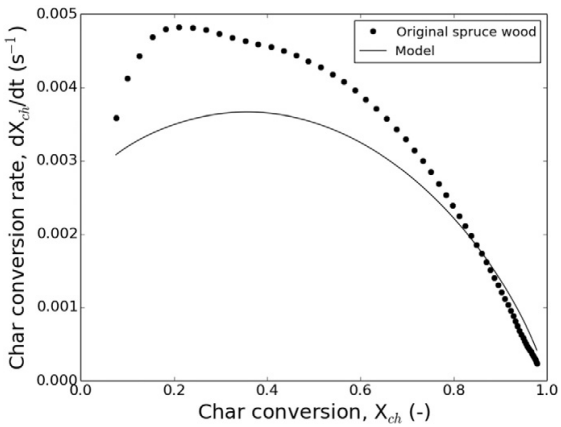

Fig. 9. The char conversion rate curve obtained from the empirical model give by Eqs. (7)–(15) and (4) compared to the conversion rate curve of the original spruce wood at 850 °C.

Eqs. (7)–(15) were used with Eq. (4) to predict the conversion times for the K and Ca doped samples in order to compare against the results shown in Table 1, where Eq. (4) was also used but with the best fit parameters instead. Using the new correlations the mean absolute percentage error for Ca doped samples was 13% and was 29% for K/K_2CO_3 samples. Because the errors in Table 1 were obtained using the best fit parameters they will be lower than when using the correlations shown in Eqs. (8)–(15), however the difference in error is not significant.

The empirical model was used to predict the conversion rate of the original spruce wood using the Ca and K concentration for the spruce wood sample given in Table A.1. The results are shown in Fig. 9 and show good ability to match the measured conversion rate. The model predicts lower than observed conversion rates, particularly at the beginning of conversion. The spruce wood contains other metals which have shown to be catalytically active, in particular manganese [24], which are not included in this kinetic model. There may also be interactions between the Ca and K which increase their catalytic effect.

Table 1
The mean absolute percentage errors for Eqs. (3), (4) and (6) in calculating the experimental conversion times for each type of sample. Because the K and K_2CO_3 behaved similarly they are grouped together.

	Error (%)		
Samples	Eq. (3)	Eq. (4)	Eq. (6)
Ca	19	8	–
$CaCO_3$	–	–	64
CaC_2O_4	–	–	34
K & K_2CO_3	46	22	–

Table 2
Best fit parameters for Ca, $CaCO_3$, CaC_2O_4, K and K_2CO_3 samples using Eqs. (3), (4) and (6). These are the parameters plotted in Figs. 4–8.

	Eq. (3)				Eq. (4)				Eq. (6)					
Sample	k	ψ	c	p	k	ψ	g	b	k	ψ	b	p	A	ξ
Ca low	1.3e-3	7.7	0	7.5e-3	1.5e-4	3.4	0.27	160	–	–	–	–	–	–
Ca med	2.7e-3	27	0	7.5e-2	1.5e-4	7.9	0.36	300	–	–	–	–	–	–
Ca high	5.9e-3	35	0	0.77	1.5e-4	9.4	0.40	290	–	–	–	–	–	–
$CaCO_3$ low	–	–	–	–	–	–	–	–	5.8e-5	5.8	0.32	8.3	9.8e-3	1.81e-02
$CaCO_3$ med	–	–	–	–	–	–	–	–	1.1e-4	5.1	0.81	0.17	5.0e-2	2.67e-02
$CaCO_3$ high	–	–	–	–	–	–	–	–	2.2e-5	5.0	0.72	8.8	1.1e-1	3.52e-02
CaC_2O_4 low	–	–	–	–	–	–	–	–	6.8e-5	0.23	0.13	7.2	4.4e-4	2.41e-03
CaC_2O_4 med	–	–	–	–	–	–	–	–	1.2e-4	0.11	0.19	9.1	1.1e-3	2.32e-03
CaC_2O_4 high	–	–	–	–	–	–	–	–	2.0e-4	0.005	0.20	12	2.2e-4	1.30e-03
K low	1.5e-4	18	1.1	0.36	1.4e-4	6.7e-5	1.7	1.0e-3	–	–	–	–	–	–
K med	6.0e-4	28	2.9	0.16	1.4e-4	1.3e-5	1.8	1.0e-2	–	–	–	–	–	–
K high 1	8.1e-4	57	5.9	0.57	1.4e-4	1.7e-5	2.2	3.0e-2	–	–	–	–	–	–
K high 2	8.8e-4	58	5.1	0.37	1.4e-4	1.1e-5	2.3	2.5e-2	–	–	–	–	–	–
K_2CO_3 low	2.6e-4	25	3.7	0.46	1.4e-4	5.5e-5	1.7	4.0e-3	–	–	–	–	–	–
K_2CO_3 med	8.1e-4	42	4.5	0.42	1.4e-4	1.1e-5	2.2	2.0e-2	–	–	–	–	–	–
K_2CO_3 high	1.7e-3	75	7.2	0.22	1.4e-4	8.7e-5	2.4	4.9e-2	–	–	–	–	–	–

4. Conclusion

A method to separate the effects of devolatilization and char gasification for TGA measurements with in situ char formation has been presented. This method was used to analyze TGA measurements conducted on spruce wood samples which were loaded with Ca, $CaCO_3$, CaC_2O_4, K and K_2CO_3. Previously published kinetic models were used to describe the kinetic effects of these metals on char gasification. A strong dependence of the parameters from the kinetic models on the metal concentration in the sample was observed. The potassium affected the char gasification in the same way regardless of whether it was added to the sample as K or K_2CO_3, while the behavior of the calcium as a catalyst was strongly dependent on the form in which it was added. The catalytic effects of potassium tend to occur primarily late in the conversion process. While the calcium is active earlier than potassium its effects here are seen later than in some other studies. This might be due to melting of the char precursor caused by the high heating rate of the sample.

While the overall behavior of the potassium and calcium catalytic effects are complex and difficult to model in all situations, the simple set of empirical equations developed here can be used to predict the reaction rate of spruce wood. Because the reaction rate behavior can be predicted relatively well using only the potassium and calcium concentrations of the original spruce wood it can be concluded that these are the most active catalytic metals in this biomass. The empirical model underpredicts the reaction rate at low char conversion, possibly due to small additional catalytic effects by Mn, Fe, Mg and Na which are present in the wood, or to interactions between the metals. In the future this empirical modeling approach will be validated by applying it to other biomass samples. Additional work will aim to separate the effects of surface area and mineral content on char reactivity by measuring char surface area and active site densities as a function of char conversion and catalyst loading.

Acknowledgments

Financial support for the GASIFREAC project provided by the Academy of Finland (253571), as well as support from the Doctoral Program in Energy Efficiency and Systems (EES), is gratefully acknowledged. The authors also wish to thank Peter Backman and Jere Lehtinen for conducting the TGA measurements. The work done by Nikolai DeMartini is part of the activities at the Johan Gadolin Process Chemistry Centre, a Centre of Excellence financed by Åbo Akademi University.

Appendix A. Complete sample list

The potassium and calcium concentrations for all the samples used in this work are given in Table A.1. More details on the sample preparation and characterization can be found in Perander et al. [13].

Table A.1
Complete sample list including potassium and calcium concentrations used in this work.

Sample name	Calcium (mg/kg)	Potassium (mg/kg)
Original spruce	724	215
Acid washed	7	0
Ca low	740	–
Ca med	2500	–
Ca high	4600	–
$CaCO_3$ low	580	–
$CaCO_3$ med	2500	–
$CaCO_3$ high	4000	–
CaC_2O_4 low	610	–
CaC_2O_4 med	1400	–
CaC_2O_4 high	3000	–
K low	12	1200
K med	12	6000
K high 1	12	12,500
K high 2	10	12,000
K_2CO_3 low	64	3000
K_2CO_3 med	47	9800
K_2CO_3 high	50	17,000

References

[1] C. Di Blasi, Combustion and gasification rates of lignocellulosic chars, Prog. Energy Combust. Sci. 35 (2) (2009) 121–140, http://dx.doi.org/10.1016/j.pecs.2008.08.001.
[2] P. Samaras, E. Diamadopoulos, G.P. Sakellaropoulos, The effect of mineral matter and pyrolysis conditions on the gasification of Greek lignite by carbon dioxide, Fuel 75 (9) (1996) 1108–1114, http://dx.doi.org/10.1016/0016-2361(96)00058-0.
[3] Y. Zhang, S. Hara, S. Kajitani, M. Ashizawa, Modeling of catalytic gasification kinetics of coal char and carbon, Fuel 89 (1) (2010) 152–157, http://dx.doi.org/10.1016/j.fuel.2009.06.004.
[4] A. Molina, F. Mondragón, Reactivity of coal gasification with steam and CO_2, Fuel 77 (15) (1998) 1831–1839, http://dx.doi.org/10.1016/S0016-2361(98)00123-9.
[5] P. Lahijani, Z.A. Zainal, M. Mohammadi, A.R. Mohamed, Conversion of the greenhouse gas CO_2 to the fuel gas CO via the Boudouard reaction: a review, Renew. Sust. Energ. Rev. 41 (2015) 615–632, http://dx.doi.org/10.1016/j.rser.2014.08.034.
[6] Y. Huang, X. Yin, C. Wu, C. Wang, J. Xie, Z. Zhou, L. Ma, H. Li, Effects of metal catalysts on CO_2 gasification reactivity of biomass char, Biotechnol. Adv. 27 (5) (2009) 568–572, http://dx.doi.org/10.1016/j.biotechadv.2009.04.013.

[7] M. Kajita, T. Kimura, K. Norinaga, C.-Z. Li, J.-I. Hayashi, Catalytic and noncatalytic mechanisms in steam gasification of char from the pyrolysis of biomass, Energy Fuel 24 (1) (2010) 108–116, http://dx.doi.org/10.1021/ef900513a.
[8] C. Dupont, T. Nocquet, J.A. Da Costa, C. Verne-Tournon, Kinetic modelling of steam gasification of various woody biomass chars: influence of inorganic elements, Bioresour. Technol. 102 (20) (2011) 9743–9748, http://dx.doi.org/10.1016/j.biortech.2011.07.016.
[9] T. Suzuki, H. Ohme, Y. Watanabe, Alkali metal catalyzed CO_2 gasification of carbon, Energy Fuel 6 (1992) 343–351.
[10] Y. Zhang, M. Ashizawa, S. Kajitani, K. Miura, Proposal of a semi-empirical kinetic model to reconcile with gasification reactivity profiles of biomass chars, Fuel 87 (4–5) (2008) 475–481, http://dx.doi.org/10.1016/j.fuel.2007.04.026.
[11] T. Suzuki, H. Nakajima, N.-O. Ikenaga, H. Oda, T. Miyake, Effect of mineral matters in biomass on the gasification rate of their chars, Biomass Conver. Biorefine. 1 (1) (2011) 17–28, http://dx.doi.org/10.1007/s13399–011-0006-2.
[12] R.P.W.J. Struis, C. von Scala, S. Stucki, R. Prins, Gasification reactivity of charcoal with CO_2. Part II: metal catalysis as a function of conversion, Chem. Eng. Sci. 57 (17) (2002) 3593–3602, http://dx.doi.org/10.1016/S0009-2509(02)00255–5.
[13] M. Perander, N. DeMartini, A. Brink, J. Kramb, O. Karlström, J. Hemming, A. Moilanen, J. Konttinen, M. Hupa, Catalytic effect of Ca and K on CO_2 gasification of spruce wood char, Fuel 150 (2015) 464–472, http://dx.doi.org/10.1016/j.fuel.2015.02.062.
[14] J.A. Moulijn, F. Kapteijn, Towards a unified theory of reactions of carbon with oxygen-containing molecules, Carbon 33 (8) (1995) 1155–1165, http://dx.doi.org/10.1016/0008–6223(95)00070-T.
[15] H. Wu, K. Yip, F. Tian, Z. Xie, C.-Z. Li, Evolution of char structure during the steam gasification of biochars produced from the pyrolysis of various mallee biomass components, Ind. Eng. Chem. Res. 48 (23) (2009) 10431–10438, http://dx.doi.org/10.1021/ie901025d.
[16] A. Karimi, N. Semagina, M.R. Gray, Kinetics of catalytic steam gasification of bitumen coke, Fuel 90 (3) (2011) 1285–1291, http://dx.doi.org/10.1016/j.fuel.2010.12.006.
[17] T. Wigmans, A. Hoogland, P. Tromp, J.A. Moulijn, The influence of potassium carbonate on surface area development and reactivity during gasification of activated carbon by carbon dioxide, Carbon 21 (1) (1983) 13–22, http://dx.doi.org/10.1016/0008–6223(83)90151–3.
[18] G. Duman, M.A. Uddin, J. Yanik, The effect of char properties on gasification reactivity, Fuel Process. Technol. 118 (2014) 75–81, http://dx.doi.org/10.1016/j.fuproc.2013.08.006.
[19] K. Whitty, R. Backman, M. Hupa, Influence of char formation conditions on pressurized black liquor gasification rates, Carbon 36 (11) (1998) 1683–1692, http://dx.doi.org/10.1016/S0008-6223(98)00167–5.
[20] K. Umeki, A. Moilanen, A. Gómez-Barea, J. Konttinen, A model of biomass char gasification describing the change in catalytic activity of ash, Chem. Eng. J. 207–208 (2012) 616–624, http://dx.doi.org/10.1016/j.cej.2012.07.025.
[21] J. Kramb, J. Konttinen, A. Gómez-Barea, A. Moilanen, K. Umeki, Modeling biomass char gasification kinetics for improving prediction of carbon conversion in a fluidized bed gasifier, Fuel 132 (2014) 107–115, http://dx.doi.org/10.1016/j.fuel.2014.04.014.
[22] A. Moilanen, Thermogravimetric Characterisations of Biomass and Waste for Gasification Processes, Academic Dissertation, Å bo Akademi, 2006.
[23] I.Y. Eom, J.Y. Kim, T.S. Kim, S.M. Lee, D. Choi, I.G. Choi, J.W. Choi, Effect of essential inorganic metals on primary thermal degradation of lignocellulosic biomass, Bioresour. Technol. 104 (2012) 687–694, http://dx.doi.org/10.1016/j.biortech.2011.10.035.
[24] A. Aho, N. DeMartini, A. Pranovich, J. Krogell, N. Kumar, K. Eränen, B. Holmbom, T. Salmi, M. Hupa, D.Y. Murzin, Pyrolysis of pine and gasification of pine chars—influence of organically bound metals, Bioresour. Technol. 128 (2013) 22–29, http://dx.doi.org/10.1016/j.biortech.2012.10.093.
[25] D.J. Nowakowski, J.M. Jones, R.M.D. Brydson, A.B. Ross, Potassium catalysis in the pyrolysis behaviour of short rotation willow coppice, Fuel 86 (15) (2007) 2389–2402, http://dx.doi.org/10.1016/j.fuel.2007.01.026.
[26] K. Raveendran, A. Ganesh, K.C. Khilar, Influence of mineral matter on biomass pyrolysis characteristics, Fuel 74 (12) (1995) 1812–1822, http://dx.doi.org/10.1016/0016–2361(95)80013–8.
[27] X. Shenqi, Z. Zhijie, X. Jie, Y. Guangsuo, W. Fuchen, Effects of alkaline metal on coal gasification at pyrolysis and gasification phases, Fuel 90 (5) (2011) 1723–1730, http://dx.doi.org/10.1016/j.fuel.2011.01.033.
[28] C.Z. Li, C. Sathe, J.R. Kershaw, Y. Pang, Fates and roles of alkali and alkaline earth metals during the pyrolysis of a Victorian brown coal, Fuel 79 (3–4) (2000) 427–438, http://dx.doi.org/10.1016/S0016-2361(99)00178–7.
[29] S.K. Bhatia, D.D. Perlmutter, A random pore model for fluid–solid reactions: I. Isothermal, kinetic control, AICHE J. 26 (3) (1980) 379–386, http://dx.doi.org/10.1002/aic.690260308.
[30] S.K. Bhatia, D.D. Perlmutter, A random pore model for fluid–solid reactions: II. Diffusion and transport effects, AICHE J. 27 (2) (1981) 247–254, http://dx.doi.org/10.1002/aic.690270211.
[31] S. Bhatia, B. Vartak, Reaction of microporous solids: the discrete random pore model, Carbon 34 (11) (1996) 1383–1391, http://dx.doi.org/10.1016/S0008-6223(96)00080–2.
[32] E. Cetin, R. Gupta, B. Moghtaderi, Effect of pyrolysis pressure and heating rate on radiata pine char structure and apparent gasification reactivity, Fuel 84 (10) (2005) 1328–1334, http://dx.doi.org/10.1016/j.fuel.2004.07.016.
[33] S. Yuan, X.-L. Chen, J. Li, F.-C. Wang, CO_2 gasification kinetics of biomass char derived from high-temperature rapid pyrolysis, Energy Fuel 25 (5) (2011) 2314–2321, http://dx.doi.org/10.1021/ef200051z.
[34] D. Cazorla-Amoros, A. Linares-Solano, C. de Salinas-Martinez Lecea, J.P. Joly, A temperature-programmed reaction study of calcium-catalyzed carbon gasification, Energy Fuel 6 (3) (1992) 287–293, http://dx.doi.org/10.1021/ef00033a008.

Publication III

Jason Kramb, Jukka Konttinen, Rainer Backman, Kari Salo, Michael Roberts "Elimintaion of arsenic-containinrapg emissions from gasification of chromated copper arsenate wood", *Fuel*, vol. 181, 2016, pp. 319-324

Fuel 181 (2016) 319–324

Contents lists available at ScienceDirect

Fuel

journal homepage: www.elsevier.com/locate/fuel

Elimination of arsenic-containing emissions from gasification of chromated copper arsenate wood

Jason Kramb [a,*], Jukka Konttinen [a], Rainer Backman [b], Kari Salo [c], Michael Roberts [d]

[a] Tampere University of Technology, Department of Chemistry and Bioengineering, POB 541, FI-33101 Tampere, Finland
[b] Umeå University, Energy Technology and Thermal Process Chemistry, SE-90187 Umeå, Sweden
[c] Gasification Technologies Inc., Helsinki, Finland
[d] Gas Technology Institute, 1700 S Mount Prospect Road, Des Plaines, IL 60018, USA

HIGHLIGHTS

- Bench-scale gasification tests of CCA wood.
- Product gas cleaning system for removing arsenic using a hot filter.
- Equilibrium modeling of arsenic behavior using combined thermodynamic database.

ARTICLE INFO

Article history:
Received 8 March 2016
Received in revised form 21 April 2016
Accepted 21 April 2016

Keywords:
Gasification
Arsenic
CCA wood
Equilibrium modeling

ABSTRACT

The behavior of arsenic in chromated copper arsenate containing wood during gasification was modeled using thermodynamic equilibrium calculations. The results of the model were validated using bench-scale gasification tests. It is shown that over 99.6% of arsenic can be removed from the product gas by a hot filter when the gas is cooled below the predicted condensation temperature.

1. Introduction

Gasification of biomass and recycled fuels is of particular interest for efficient production of power and heat, as well as allowing for the possibility of liquid biofuel and chemical production. Wood materials treated with special chemicals can be used in certain purposes, such as railway sleepers. The chemical treatments often contain toxic elements which can complicate the disposal of the wood. Generating energy by using a thermochemical process, such as combustion and gasification is one option. Elevated contents of some inorganic chemicals containing toxic species, such as arsenic, makes direct combustion of the material difficult due to possible toxic emissions in the flue gases.

Chromated copper arsenate (CCA) containing wood is one such chemically treated material. Helsen et al. [1] has thoroughly reviewed the possible disposal methods for CCA wood, focusing on thermochemical conversion methods. In the review the authors point out that gas cleaning for removal of arsenic is the key obstacle for gasification of CCA woods.

A review about gasification of fuels containing elevated levels of heavy metals was presented in Konttinen et al. [2]. Considering Arsenic-containing species in gasification product gas, Diaz et al. [3,4] indicated that they are volatile at temperatures of the gasification process and they are condensed at a temperature range of 200–500 °C. The results of gasification of waste-type solid fuels by Konttinen et al. [2] indicated that Arsenic-containing species are condensed at temperatures below 500 °C. The condensation temperature of the heavy metal species in gasification product gases is dependent on the fuel used and other process conditions, such as type of the gasification process and the operating pressure. The railway sleepers of this study contain such high amounts of arsenic that the results of heavy metal condensation in earlier studies may not be applicable.

Konttinen et al. [2] also presented a method and a process to remove inorganic species and elements from the gasification

* Corresponding author.
E-mail address: jason.kramb@tut.fi (J. Kramb).

http://dx.doi.org/10.1016/j.fuel.2016.04.109
0016-2361/

product gases by cooling the gases to a certain temperature, thus the harmful inorganic are condensed and removed by the fly ash in the particulate filter. The idea of removing inorganic species from fly ashes in connection with gasification of waste has also been commercially demonstrated in the 160 MWth WtE gasification plant in Lahti, Finland.

The objective of this work has been to investigate the use of CCA containing wood as feedstock to a gasification process for energy generation. It has been of particular interest to prove that the vaporized heavy metals species, such as those containing arsenic, can be removed by condensation from the gasification product gas, even in the case of high heavy metals contents of the fuel. The chemistry and phase changes of inorganic species in the product gas can be investigated using thermodynamic equilibrium modeling. The calculation system and its principles are the same as those presented earlier in Konttinen et al. [2]. The modeled results are also validated experimentally by using a bench-scale gasification setup.

2. Methods

2.1. Equilibrium modeling of As behavior

Thermodynamic equilibrium calculations were performed using the Excel-interface ChemSheet [5] which uses ChemApp [6] for Gibbs energy minimization of the chemical system to find the equilibrium solution. The thermodynamic database used for the calculations was developed by selecting thermodynamic data for 29 elements and their compounds from several different databases and combining the results together. A database was formed, including data from gas, solid and liquid phases (and liquid solutions), for the elements and their compounds that are relevant in reducing gasification conditions [7]. A total of 199 gas compounds were included as well as 505 solid and liquid phases. This method of combining several databases was used previously by Konttinen et al. for modeling the behavior of trace elements in biomass gasification [2]. A complete list of the arsenic containing compounds included in the equilibrium calculations is given in Table 1.

The equilibrium modeling was done for six conditions. Cases A1, A2 and A3 are modeling the conditions inside the gasifier, at temperature 850 °C. Cases B1, B2 and B3 model the conditions after the gas cleaning, where the product gas has been cooled from the gasification temperature to 260 °C. The inputs for B cases are taken as the output gas composition from the corresponding A case (e.g. the output from A1 is used as the input for B1). The elements included in the equilibrium calculations were increased stepwise. For cases A1 and B1 the main ash elements of the biomass were excluded. For cases A2 and B2 the main ash elements are included, but Ca, Al and Si are still excluded. For cases A3 and B3 all fuel ash components were included as well as the bed material feed. The bed material used was dolomite and had a measured chemical composition of 21.23% calcium, 12.01% magnesium and 12.74% carbon on a weight basis, which is generally consistent with the nominal dolomite composition. The inputs values for the equilibrium calculations were based on the measurements of the fuel properties and feed rates for the experimental measurements described below and are given in Tables 2–4.

Table 1
The arsenic containing compounds which included in the thermodynamic database used in the equilibrium calculations.

Gas	Liquid	Solid
As	As	As_2O_3 arsenolite
As_2	As_2O_3	As_2O_3 claudetite
As_2S_3	As_2S_2	As_2O_5
As_3	As_2S_3	As_2S_2 realgar
As_4		As_2S_3 orpiment
As_4O_{10}		As rhombohedral
As_4O_6		$Ca_3(AsO_4)_2$
As_4O_7		$Cd_3(AsO_4)_2$
As_4O_8		$Co_3(AsO_4)_2$
As_4O_9		$Cu_3(AsO_4)_2$
As_4S_4		$Ni_3(AsO_4)_2$
$AsCl_3$		$Zn_3(AsO_4)_2$
AsH		
AsH_2		
AsH_3		
AsO		
AsO_2		
AsS		

Table 2
Ultimate analysis of the treated (dried, crushed and pelletized) CCA-wood sample.

Property	wt% dry basis
Carbon	46.95
Hydrogen	5.46
Nitrogen	0.14
Sulfur	0.08
Oxygen (as balance)	37.25
Ash	9.4
Moisture (wt% wet)	8.4

Table 3
Ash composition of the CCA wood ash.

Ash component	mg/kg ash
Al	8070
As	72,100
B	470
Ba	1160
Be	0.25
Ca	70,300
Cd	920
Co	33
Cr	57,500
Cu	66,400
Fe	60,600
K	10,300
Mg	11,000
Mn	3832
Mo	18
Na	5780
Ni	150
P	2630
Pb	1030
S	8260
Sb	270
Se	55
Sn	25
Ti	330
V	23
Zn	6010

Table 4
Targeted operating conditions.

Temperature, °C	850
Pressure, bar	1.72
Solids feed rate, kg/h	0.45
Steam/feed ration, kg/kg	0.35
Steam feed rate, m^3/h	0.22
Oxygen/feed ration, kg/kg	0.13
Air flow rate, m^3/h	0.14

2.2. Experimental procedure

Samples of pelletized Arsenic-containing wood waste, designated as CCA-wood, were tested in a bench-scale gasification unit which is located at Gas Technology Institute (GTI) in Des Plaines, Illinois. Approximately 20 kg of CCA wood was sent to GTI for testing from Finland. The wood was dried and ground to particle size below 2 mm. It was then pelletized to a particle size of approximately 5 mm × 10 mm. The ultimate analysis of the sample is given in Table 2 and the complete ash analysis is given in Table 3.

A schematic diagram of the bench scale gasification unit is shown in Fig. 1. The bed section of the reactor consisted of a 5.08 cm diameter pipe which was 61 cm in length and was heated with an electrical furnace. The freeboard section had a diameter of 10.16 cm and a length of 71.12 cm. Fuel was fed to the bed using a screw feeder. Feed gases (air, N_2 and steam) were preheated before being fed to the bed.

Three experimental tests were run, each using the targeted operating conditions shown in Table 4. Dolomite was used as the bed material and the basic experimental test procedure began with pressurizing the reactor, then heating to the desired temperature using N_2. Once the desired temperature was reached the CCA wood was fed into the reactor through a screw feeder. After approximately one hour of wood feeding in N_2 the gas flow was switched to include steam and air while maintaining the same fluidization velocity. The tests lasted 1–1.5 h of steady state operation.

A gas cleaning system was designed to remove As, Cr and Cu compounds which may be in the product gas leaving the gasifier. This system involved first cooling the gas to 260 °C with a heat exchanger. After the heater exchanger a particulate filter collected the fly ash. The temperature into the particulate filter was controlled by a bypass of the heat exchanger. After the particulate filter the gas flows through a liquid scrubber system using solutions of nitric acid and hydrogen peroxide. The liquids from the scrubber system were removed after each test and the amounts of As, Cr and Cu collected was measured using inductively coupled plasma atomic emission spectroscopy. A schematic diagram of the gas cleaning system is shown in Fig. 1.

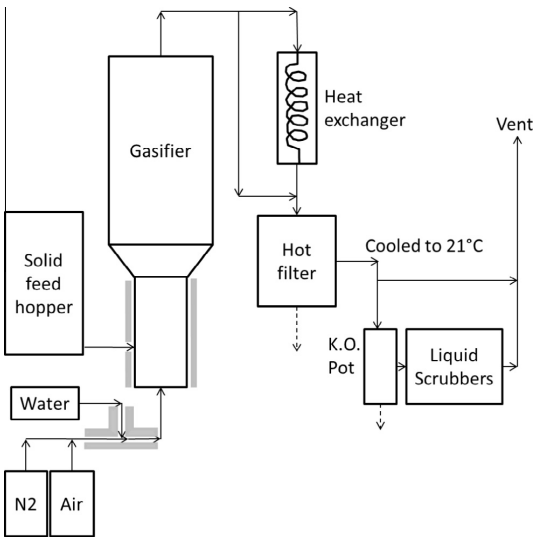

Fig. 1. Schematic diagram of bench scale gasifier setup including the gas cleaning system. Solid lines indicate gas flow and dashed lines indicate solid/liquid removal from system. The gray colored boxes indicated external heating elements.

3. Results

3.1. Equilibrium modeling results

The results from the equilibrium calculations for the percentage of trace elements which will be found in the exit gas at different temperatures for cases B1, B2 and B3 are shown in Fig. 2. For cases B1 and B2, Arsenic was predicted to condense at approximately 250 °C. For case B3 10% of the Arsenic was predicted to condense by 200 °C but the remaining 90% stays in the gas phase until cooled to below 100 °C.

The difference in behavior of As in case B3 compared with cases B1 and B2 is due to the change in sulfur concentration between these cases. When the bed additives ($MgCO_3$ and $CaCO_3$) are

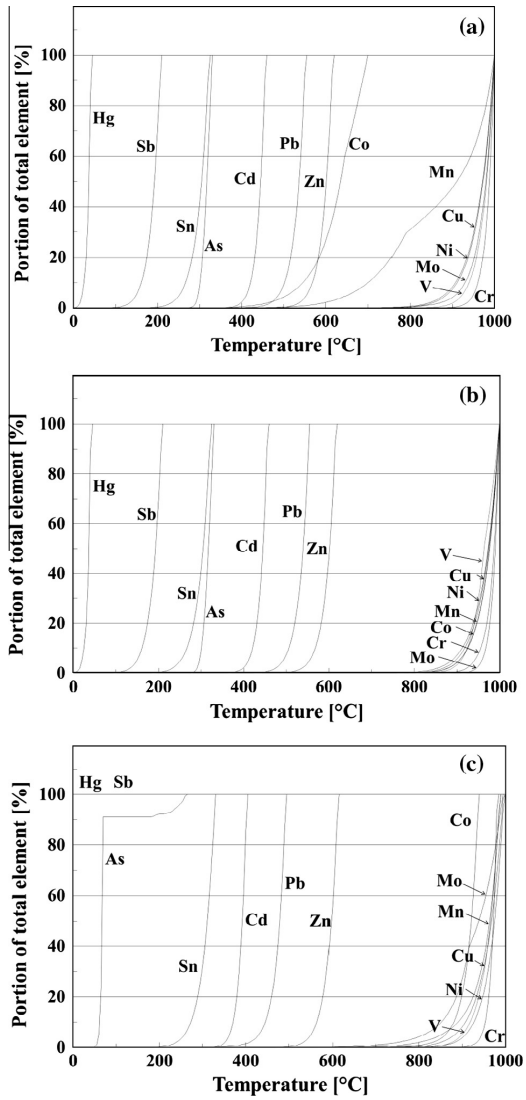

Fig. 2. Percentage of various trace elements which are predicted to be found in the exit gas as a function of temperature. Subplots (a), (b) and (c) show the results for modeling cases B1, B2 and B3 respectively.

included in the equilibrium calculation in case B3, CaS is predicted to form which captures the sulfur in the bed. As seen in Fig. 3, in cases B1 and B2 arsenic primarily forms As_2S_2 at temperatures below 300 °C. Because the sulfur has been captured in the bed for case B3, As_2S_2 cannot form and the arsenic stays in gaseous form until below 100 °C when it will form As_2O_3.

Comparison with previously published equilibrium modeling results is difficult due to the large number of conditions which will influence the formation of the various arsenic compounds and affect the equilibrium composition (e.g. temperature, pressure, fuel composition, gas feeds). Konttinen et al. [2] used the same methodology as the current work to model the behavior of trace elements

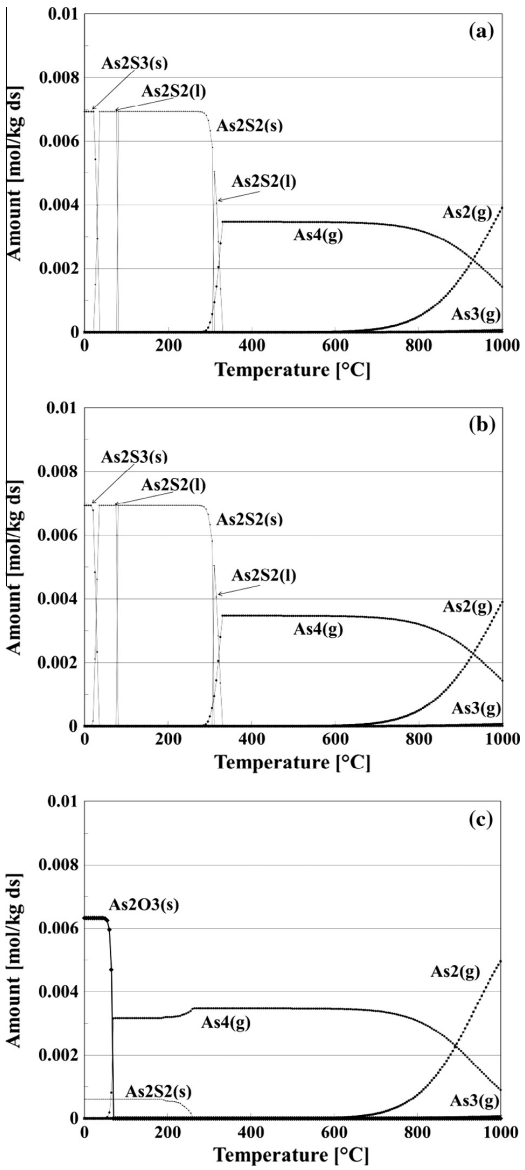

Fig. 3. Distribution of arsenic species as a function of temperature. Subplots (a), (b) and (c) show the results for modeling cases B1, B2 and B3 respectively.

in solid recovered fuel. However, the condensing temperature range for arsenic in that study was found to be 500–650 °C. In comparison, Diaz et al. [3] reported a condensation temperature of 200–500 °C for equilibrium modeling of coal gasification. Jiang et al. [8] also predicted the solid–gas transition temperature for arsenic during biomass gasification using equilibrium modeling. While the biomass used in that study came from contaminated soils and generally contained elevated levels of arsenic, the As concentration in the fuel was much lower than the CCA wood used in the present work. The transition temperature predicted by Jiang et al. was 600–1000 °C which is significantly higher than Diaz et al. [3] or Konttinen et al. [2].

Helble et al. [9] reported equilibrium partitioning of arsenic for coal gasification at ambient pressure while Bunt and Waanders [10] modeled a coal gasifier at elevated pressure (2.8 MPa) and Diaz-Somoano and Martinez-Tarazona [4] reported equilibrium results for the pressure range 0.1–4 MPa. Helble et al. showed at temperatures above 375 °C the arsenic existed in gas phase, primarily as AsO. Condensed phase arsenic forms below 375 °C as As_2S_2. The temperature at which As_2S_2 begins to become the dominant species agrees with the results for case B1 and B2 presented in Fig. 3.

According to the equilibrium composition reported by Diaz-Somoano [4] condensed species form between 200 and 700 °C and below 200 °C no gaseous arsenic species exist. Detailed partitioning results are given only for 2.5 MPa, where two cases are considered: the gas atmosphere contains some HCl or the gas atmosphere contains some H_2S. If H_2S is present in the gas then small amounts of condensed phase arsenic species form between 500 and 800 °C but it is not until 400 °C that the condensed phase dominates. If there is no H_2S present then FeAs is the dominant species from 800 °C to 400 °C. From 400 °C to 350 °C $FeAs_2$ is the most stable and below 350 °C As is dominant.

Contreras et al. [11] performed a detailed equilibrium study on arsenic species formed through interactions with trace elements during combustion. If the interactions with the trace elements are not considered then Contreras reported the condensation temperature for As to be approximately 250 °C, at which point As_2O_5 forms according to the equilibrium calculations. When interactions with trace elements are included, condensed phase arsenic compounds form at temperatures as high as 1100 °C. The primary arsenic compounds formed with the ash elements were $FeAsO_4$, $AlAsO_4$, $NaAs_3O_8$, K_3AsO_4, $Mg_3(AsO_4)_2$ and $Ca(AsO_2)_2$. These compounds are not included in the present study, but the proportion of many of the trace ash elements to arsenic is low and therefore the compounds are unlikely to have a significant impact on the overall distribution of arsenic. Shen et al. [12] also used equilibrium modeling to predict arsenic compounds in coal combustion and the results were reasonably consistent with Contreras et al. [11] and predicted that solid arsenic compounds would begin to form around 1000 °C. It has been noted previously that trace elements may behave significantly differently under combustion and gasification conditions [13,14] and so compounds found to be most relevant by Contreras et al. or Shen et al. may not exist in the conditions studied in the current work.

3.2. Experimental results

The product gas composition from test number 1 and 3 of the bench scale BFB is shown in Figs. 4 and 5 respectively. Additionally, the arsenic material balance for tests 1–3 are shown in Table 5. From the arsenic balance it is clear that a large portion of the arsenic is retained in the bed of the gasifier and is removed with the bottom ash. Of the arsenic which leaves the gasifier in the product gas, most is captured by the hot filter at 260 °C. All three tests achieved over 99.6% capture efficiency of the fuel arsenic.

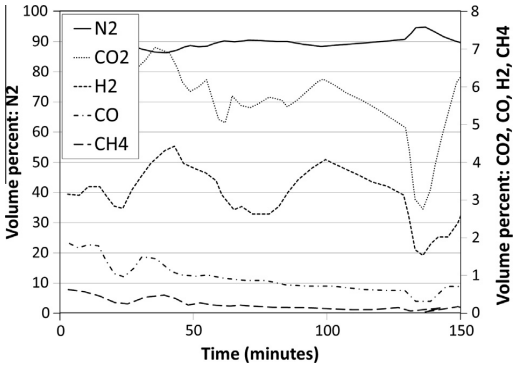

Fig. 4. Gas composition from steady state operation of bench scale gasifier during test #1.

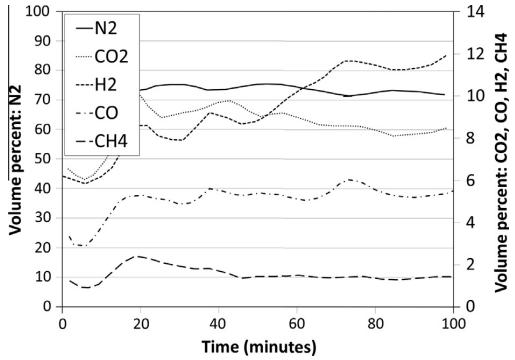

Fig. 5. Gas composition from steady state operation of bench scale gasifier during test #3.

Table 5
Arsenic balance for three bench scale gasification tests.

	Test 1	Test 2	Test 3
Arsenic input, mol/s	5.41e−7	3.60e−6	1.80e−6
As in product gas before filtering, mol/s	4.60e−8	9.74e−8	4.75e−8
As in product gas after filtering, mol/s	8.42e−10	3.95e−9	7.68e−9
Percent of As retained in bed, %	91.5	97.3	97.4
Percent of remaining As captured in filter, %	98.2	96.0	83.8
Total As removed, %	99.8	99.9	99.6

The experimental results are in contrast to the results of the equilibrium calculations, which did not predict condensed arsenic compounds to be formed in the gasifier at 850 °C. Arsenic has previously been shown to be captured by calcium at high temperatures [15] and so it is likely the fuel arsenic is reacting with the dolomite additive and being retained in the bed. Calcium arsenate ($Ca_2(AsO_4)_2$) was shown to be the Ca–As species present in the earlier work and this species is included in the thermodynamic database used for the equilibrium calculation but was not predicted to form.

Modeling cases B1 and B2 predict well the removal of arsenic by cooling to 260 °C as seen in Table 6. Case B3 however greatly underestimates the arsenic removal. As discussed in Section 3.1, in case B3 the sulfur is removed by the calcium in the bed which prevents As_2S_2 from forming in the hot filter. As a result the arsenic is not predicted to condense until a much lower temperature.

Table 6
Amount of arsenic remaining in the product gas after filtering at 260 °C for equilibrium calculations and the averaged measured value from three experimental runs.

	B1	B2	B3	Average measured
Arsenic in gas after cleaning, %	0.4	0.4	99.5	0.2

It was observed by Konttinen et al. [2] that the conditions modeled in case A3 and B3, where all elements from all feeds are included in the equilibrium calculation, will produce compounds which are not kinetically realistic, and will therefore be unlikely to produce results which match experimental measurements. In that earlier work it was concluded that the conditions modeled in case B2 most closely resembled the experimental conditions and this is supported by the current results.

4. Conclusion

Multicomponent, multiphase equilibrium calculations can be used to predict reactions of arsenic in gasification of fuels with unusually high As concentrations. By cooling the product gas to 260 °C, over 99.6% of arsenic can be captured when gasifying CCA wood. This was shown in a bench scale gasifier and supported with equilibrium calculations. Predicting the behavior of arsenic during gasification using equilibrium models remains difficult due to lack of thermodynamic data on various arsenic compounds which may form during interactions with ash and bed materials, as well as kinetic limitations on some of the arsenic reactions.

Acknowledgements

Financial support from the Academy of Finland through the Doctoral Program in Energy Efficiency and Systems (EES) is gratefully acknowledged.

References

[1] Helsen L, Van den Bulck E. Review of disposal technologies for chromated copper arsenate (CCA) treated wood waste, with detailed analyses of thermochemical conversion processes. Environ Pollut 2005;134(2):301–14.
[2] Konttinen J, Backman R, Hupa M, Moilanen A, Kurkela E. Trace element behavior in the fluidized bed gasification of solid recovered fuels – a thermodynamic study. Fuel 2013;106:621–31.
[3] Diaz-Somoano M, Martinez-Tarazona MR. Retention of arsenic and selenium compounds using limestone in a coal gasification flue gas. Environ Sci Technol 2004;38(3):899–903.
[4] Díaz-Somoano M, Martínez-Tarazona MR. Trace element evaporation during coal gasification based on a thermodynamic equilibrium calculation approach. Fuel 2003;82(2):137–45.
[5] Koukkari P, Pajarre R, Hack K. Setting kinetic controls for complex equilibrium calculations. Zeitschrift für Met. 2001;92(10):1151–7.
[6] Petersen S, Hack K. The thermochemistry library ChemApp and its applications. Int J Mater Res 2007;98(10):935–45.
[7] Konttinen J, Backman R, Hupa M, Moilanen A, Kurkela E. Trace element behavior in the fluidized bed gasification of solid recovered fuels – a thermodynamic study. Åbo Akademi University, Process Chemistry Centre, Combustion and Materials Chemistry. Report 05-02, Åbo Akademi University; 2005. ISBN 952-12-1510-0. Available from: https://www.abo.fi/personal/media/19399/05_02.pdf.
[8] Jiang Y, Ameh A, Lei M, Duan L, Longhurst P. Solid-gaseous phase transformation of elemental contaminants during the gasification of biomass. Sci Total Environ 2015.
[9] Helble J. Trace element partitioning during coal gasification. Fuel Jun. 1996;75(8):931–9.
[10] Bunt JR, Waanders FB. Trace element behaviour in the Sasol–Lurgi MK IV FBDB gasifier. Part 1 – The volatile elements: Hg, As, Se, Cd and Pb. Fuel 2008;87(12):2374–87.
[11] Contreras ML, Arostegui JM, Armesto L. Arsenic interactions during co-combustion processes based on thermodynamic equilibrium calculations. Fuel 2009;88(3):539–46.

[12] Shen F, Liu J, Zhang Z, Dai J. On-line analysis and kinetic behavior of arsenic release during coal combustion and pyrolysis. Environ Sci Technol 2015;49 (22):13716–23.
[13] Frandsen F, Dam-Johansen K, Rasmussen P. Trace elements from combustion and gasification of coal—an equilibrium approach. Prog Energy Combust Sci 1994;20(2):115–38.
[14] Nzihou A, Stanmore B. The fate of heavy metals during combustion and gasification of contaminated biomass – a brief review. J Hazard Mater 2013;256–257:56–66.
[15] Mahuli S, Agnihotri R, Chauk S, Ghosh-Dastidar A, Fan LS. Mechanism of arsenic sorption by hydrated lime. Environ Sci Technol 1998;31(11):3226–31.

Publication IV

Jason Kramb, Alberto Gómez-Barea, Nikolai DeMartini, Henrik Romar, Tharaka Doddapaneni, Jukka Konttinen "The effects of calcium and potassium on CO2 gasification of birch wood in a fluidized bed", *To be submitted to Fuel in August 2016*

The effects of calcium and potassium on CO_2 gasification of birch wood in a fluidized bed

Jason Kramb[a], Alberto Gómez-Barea[b], Nikolai DeMartini[c], Henrik Romar[d], Tharaka Rama K C Doddapaneni[a], Jukka Konttinen[a]

[a]*Department of Chemistry and Bioengineering, Tampere University of Technology, PO Box 541, FI-33720 Tampere, Finland*
[b]*Chemical and Environmental Engineering Department, Escuela Técnica Superior de Ingeniería, University of Seville, Camino de los Descubrimientos s/n. 41092 Seville, Spain*
[c]*Johan Gadolin Process Chemistry Centre, Åbo Akademi University, FI-20500 Turku, Finland*
[d]*University of Oulu, Research Unit of Sustainable Chemistry, P.O.Box 3000, FI-90014 University of Oulu, Finland*

Abstract

Birch wood was leached of its naturally occurring ash forming elements and doped with three concentrations of calcium or potassium before being gasified in a laboratory bubbling fluidized bed reactor. The wood samples were pelletized and inserted into a fluidized bed reactor where they were first pyrolyzed with N_2 and then gasified with CO_2. In addition to tracking the gas concentration of the exit gas, char samples were taken from the fluidized bed and analyzed to study the char properties. The presence of potassium in the biomass was found to have a significant influence on the structure of the resulting char, however potassium did not have an observable catalytic effect on the gasification reaction with CO_2. In contrast, calcium did increase the char conversion rate and is likely the primary active catalyst in gasification of birch wood with CO_2.

Keywords: biomass, gasification, fluidized bed, catalysts, char

1. Introduction

Biomass naturally contains between 0.1-35% ash forming elements by weight, depending on the type of biomass and the environment in which it grew, and waste derived fuels can reach nearly 50% ash [1]. While the composition of these inorganics can vary greatly, for woody it is common that potassium and calcium are two elements which are found in significant quantities [2–4].

The presence of ash forming elements has been shown to influence the thermochemical conversion of biomass in numerous ways. For example, it has been shown that K, Na and Mn increase mass loss during torrefaction of wood [5]. The mineral content of biomass has been shown to have a number of effects on the pyrolysis behavior of the fuel [6], and potassium in particular has been identified as having effects on char and gas yields during pyrolysis [7–9]. The presence of some inorganics in chars has been shown to increase the reactivity of the char during gasification [10–18].

Much of the work done to investigate the role of inorganics in gasification reactions has been done on small scales, using only a few milligrams of sample in a thermogravimetic analysis (TGA) device [12–17] or fixed bed reactor [18]. In many cases the chars are created first and then have metals added [13, 15, 18], rather than adding the metals to the parent material [16, 17]. The method of char preparation is important as Suzuki et al. reported that adding K and Ca to leached wood produces higher char reactivity than adding K or Ca to leached char when gasifying in CO_2 [19]. While adding the metals to pre-made chars removes the complicating factor of the effect of the metals on char formation and guarantees that the initial char structure is uniform for all samples, it does not reflect the reality of fuel behavior in actual gasification processes.

In the present work birch wood was leached of its naturally occurring ash forming elements and then doped with different concentrations of potassium or calcium. The wood samples were pelletized and inserted into a fluidized bed reactor where they were first pyrolyzed with N_2 and then gasified with CO_2. Char samples were collected for further analysis to better understand the causes for the observed changes in char reactivity. The char analysis techniques include: SEM-EDS, BET surface area measurements, and ICP-OES analysis.

2. Experimental methods

2.1. Sample preparation

Wood chips made from Finnish birch wood (Betula pendula) were milled to particle sizes of less than 2 mm. The ultimate and proximate analysis of the birch wood powder is given in Table 1. The wood powder was then leached of ash forming elements by following the method used by Kharzraie Shoulaifar et el. [5, 20]. This procedure involves first adding the wood to a sodium EDTA solution for two hours. After this, the wood was rinsed with ultra pure water, added to a 0.01 M HCl solution for two hours, and finally rinsed again with ultra pure water.

The leached wood was then doped with two concentrations of potassium or three concentrations of calcium following the process described by Perander et al. [17]. The doping was done by adding the leached wood powder to either a KNO_3 or $Ca(NO_3)_2$ solution. This method dopes the metal to organic functional groups through ion-exchange. The concentration of

Email address: jason.kramb@tut.fi (Jason Kramb)

	Weight % (dry basis)
Moisture (wet)	1.99
Ash	0.35
Volatiles	89.46
Fixed carbon	10.19
Carbon	48.94
Hydrogen	6.16
Nitrogen	<0.05
Sulphur	<0.05
Oxygen	44.90

Table 1: Ultimate and proximate analysis for raw birch wood used in the fluidized bed tests.

Sample	Concentration (mg/kg)							
	Ca	K	Mg	P	Mn	Zn	Ba	Fe
Raw birch	760	570	210	91	50	22	10	5.4
Leached	44							
Ca low	460			29				26
Ca med	545			23		12		
Ca high	600			22		11		
K med	84	491		24		6		
K high	39	568		20				

Table 2: Elemental composition for the raw birch wood, leached wood, Ca doped and K doped samples as determined by ICP-OES. If no value is present then the concentration was below the detection limit.

K and Ca in the final wood was adjusted by changing the concentration of the K and Ca nitrates in the solution.

The success of the leaching and doping process was determined by measuring the elemental composition of the wood samples. This was done using inductively coupled plasma optical emission spectrometry (ICP-OES) and the results are shown in Table 2.

2.2. Fluidized bed reactor

Char reactivity was measured using a laboratory bubbling fluidized bed (FB) reactor. This reactor has been used in previous studies [21–23] and is constructed from stainless steel. The FB section of the reactor has an internal diameter of 51 mm and height of 200 mm. The freeboard has an internal diameter of 81 mm and height of 250 mm. The reactor is externally heated by a 10 kW electrical oven. Gases are preheated and fed into the reactor through the distribution plate at the bottom of the FB. Fuel is added batchwise through the top of the reactor. Gases exit the reactor and pass through a system to remove tar and condensable species before being analyzed for CO, CO_2, H_2, and CH_4 concentration with an accuracy of 0.01%.

2.3. Fluidized bed experimental procedure

To prevent immediate entrainment out of the fluidized bed, the wood powder was pressed into pellets of approximately one gram using a pellet press. The FB reactor was preheated to the desired temperature and the gas flow was switched to N_2. Two pellets were added to the reactor through the fuel feel valve at the top of the freeboard. Pyrolysis was considered to be complete once the gas analyzer indicated that no CO, CO_2, H_2 or CH_4 were present in the exit gas from the reactor, at which point the gas flow was changed to 20% CO_2 and 80% N_2. Typically the time to complete pyrolysis was 10 minutes. The bed material used in most of the tests was olivine, although some tests were also carried out using bauxite as the bed material. In all cases the bed mass was 500 g. In order to minimize elutriation of the wood particles the gas velocity into the reactor was kept relatively low at 0.2 m/s, which was still over the minimum fluidization velocity for the olivine bed of 0.18 m/s.

Char conversion, is defined as

$$X_{ch} = \frac{m_0 - m}{m_0}, \tag{1}$$

where m_0 and m are the initial mass of char and char mass at time t, was calculated from the CO concentration measured in the product gas assuming CO is generated through the Boudouard reaction given by Equation R1,

$$C + CO_2 \longrightarrow 2\,CO. \tag{R1}$$

Once the CO concentration became too low to measure reliably (i.e. below 0.01%) the gas flow into the reactor was switched to air and the remaining char was combusted. The amount of char combusted was calculated from the CO_2 concentration in the exit gas during the combustion stage. Char conversion rate and instantaneous reaction rate are defined by Equations 2 and 3 respectively,

$$r = \frac{dX_{ch}}{dt}, \tag{2}$$

$$k = -\frac{1}{m}\frac{dm}{dt} = \frac{1}{1 - X_{ch}}\frac{dX_{ch}}{dt}. \tag{3}$$

The term reactivity is used in a general way in this work, and refers to the tendency of the char to react with CO_2.

In order to study char gasification kinetics, the gasification must occur in the kinetically controlled regime (i.e. Regime I). Char reactivity measurements were first conducted at 750°C, 800°C, 850°C and 900°C in order to calculate the activation energy of the gasification reaction and ensure the operating conditions to be in the kinetic regime. Based on these measurements 850°C was selected as the temperature for the majority of the char gasification tests.

Char samples were collected from the fluidized bed by increasing the gas velocity into the reactor which pushed the low density char particles into the cyclone where they were collected. For the leached wood and Ca doped wood it was not possible to collect chars using this method as the chars would not entrain from the bed, even at very high gas velocities. To collect the char in these tests, the entire bed, containing the char and olivine, was removed from the reactor and the char was recovered by screening.

A complete list of fluidized bed tests conducted is included given in Table A.6 in Appendix A.

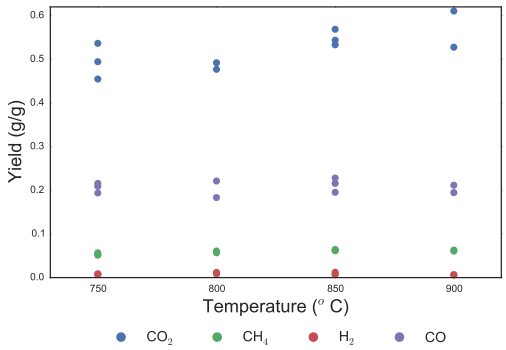

Figure 1: Pyrolysis gas yields as a function of pyrolysis temperature for raw birch wood. The yields were calculated on a dry biomass basis.

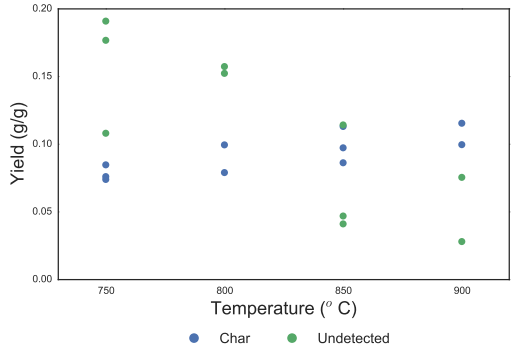

Figure 2: Char and undetected (condensable) fraction as a function of pyrolysis temperature for raw birch wood. The yields were calculated on a dry biomass basis.

2.4. Char characterization

Chars collected from the fluidized bed were analyzed in a number of ways to better understand the relationship between the calcium and potassium content of the biomass and the char reactivity.

First, the char samples were analyzed by scanning electron microscopy with X-ray microanalysis (SEM-EDS) which gives some indication of the char structure and distribution of the metals on the char surface. Surface areas and pore distributions were measured on a Micromeritics ASAP 2020 by physisorption of nitrogen (N_2). For the adsorption tests 100 mg of each sample was weight into a quartz tube. Prior to measurement the samples were evacuated at 10 μm Hg at an elevated temperature (160°C) in order to remove any contaminating gases from the samples. Surface areas were measured under isothermal conditions obtained by immersing the sample container into liquid nitrogen by the addition of small portions of N_2. The surface areas were calculated using the BET (Brunauer-Emmerson-Teller) model [24]. Pore size distributions were calculated from the adsorption isotherms according to the BJH (Barret-Joyner-Halenda) model [25]. Finally the char samples were analyzed with ICP-OES to determine the total metal content which remains on the char.

3. Results and discussion

3.1. Pyrolysis gas and char yields

Pyrolysis yields were measured for each fluidized bed test. The pyroylsis gas composition for raw birch wood varied little at temperatures between 750°C and 900°C, as seen in Figure 1. The char (carbon only) and undetected fraction yields are shown in Figure 2. Carbon dioxide was the primary pyrolysis gas component, typically over 50%. Because only CO_2, CO, CH_4 and H_2 could be measured by the gas analyzer, some of the sample will leave the reactor without being detected, typically as tars or light hydrocarbons which are removed from the exit gas before reaching the analyzer. The amount of these undetected products was calculated by subtracting the mass of the measured gas flow from the sample input mass. This undetected fraction decreased as the pyrolysis temperature increased, which likely signifies a decrease in tar production at higher temperatures. The char yield was largely unaffected by increasing pyrolysis temperature, remaining around 9% by mass for all temperatures. This is in contrast to the widely reported observation of a decrease in char yield with increasing pyrolysis temperature [26–28].

The measured yield of CO_2 at approximately 0.5 g/g fuel was much higher than what is commonly reported for this temperature range while the CO yield was low [26, 29]. In addition, the undetected fraction of pyrolysis products, consisting primarily of condensable tars and water vapor, is slightly below the level which is generally reported. The distribution of pyrolysis products is likely due to a combination of two factors: the low gas velocity into the reactor which resulted in longer than normal gas residence times of approximately 2.5-3.5 seconds; and the use of olivine as a bed material, which has been shown to promote the water-gas shift reaction [30] in addition to reducing tar yields through promoting tar decomposition (see, e.g., [31]).

Pyrolysis gas composition for the doped samples at 850°C showed few significant trends, as can be seen in Figure 3. Both calcium and potassium doping slightly increased the measured gas yields while reducing the undetected fraction. Potassium doping also clearly increased the char yield.

Leached wood has been reported to have decreased char and gas (CO and CO_2) yield compared with unleached wood when pyrolyzed in a fluidized bed at 400°C [9]. Addition of potassium to the leached wood increased char and gas yields while calcium had little effect in that study. Eom et al. [8] also reported that potassium doping increased char yields and affect pyrolysis product formation while calcium had little effect. The behavior of the potassium doped samples in the present work is largely consistent with the reported effects of potassium on

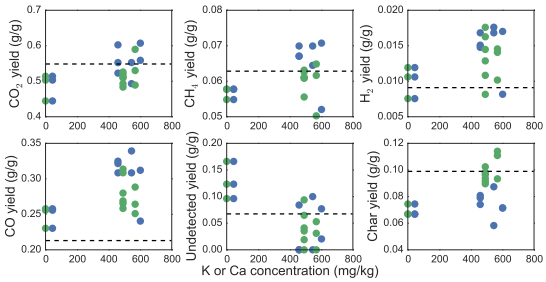

Figure 3: Pyrolysis gas yields and char yields as a function of K and Ca doping concentration. Green points indicate K concentration and blue points indicate Ca concentration. The black dashed line indicates the averaged yield of the raw birch wood. The yields were calculated on a dry biomass basis.

biomass pyrolysis. The observed influence of calcium on pyrolysis gas composition is in contrast to previous studies which did not report such an effect, but the large differences in pyrolysis conditions (peak temperature, applied heating rate and fuel particle size) make comparisons difficult.

3.2. Char reactivity

Char conversion rate measurements showed high repeatability between multiple tests at a given operating condition. To show this, the conversion rate curves from multiple runs of raw birch wood and leached wood are given in Figure 4. The averaged conversion rate curve for all the samples are given in Figures 5 and 6 which show conversion rate measurements for all the wood samples at 850°C. The leached wood char was clearly less reactive than the raw birch wood char throughout the measured conversion range. The calcium doped wood chars show higher conversion rate peaks with increased Ca doping concentration, as can be seen in Figure 5. All the Ca doped wood chars have a higher conversion rate peak than the raw birch wood char despite having lower Ca concentrations. All the wood chars show decreasing conversion rates throughout the conversion process, and between approximately 50-80% char conversion the raw birch wood is faster than the Ca doped woods.

Potassium doped wood chars exhibited very low reactivity, similar to the leached wood chars, as shown in Figure 6. The initial conversion rate of potassium doped wood char was generally higher than the leached wood, nearly at the same level as the raw birch wood char. However the conversion rate quickly dropped off to the level of the leached wood. The reactivity of the potassium doped wood chars was also not dependent on the potassium concentration in the wood, as all samples were equally unreactive (see Figure 6).

Comparison of conversion rate curves for char gasification between studies is difficult because pyrolysis conditions have a large effect on the resulting char reactivity [32]. As most studies with K or Ca doped chars have been performed in TGA devices with much different heating rates and gasification conditions than the fluidized bed reactor used in the present work, and doping is often done to chars directly rather than the parent

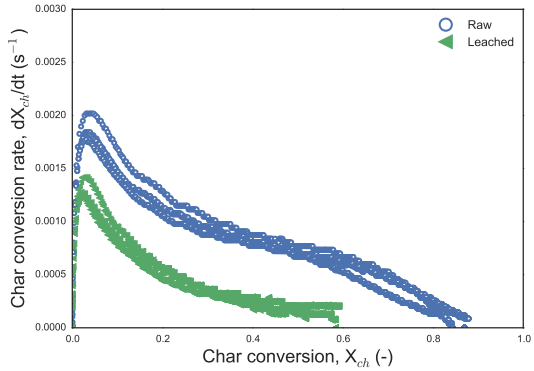

Figure 4: Conversion rate measurements of chars from raw birch wood and leached birch wood at 850°C in 20% CO_2 and 80% N_2. Multiple measurements for each sample are shown to demonstrate the repeatability of the measurement.

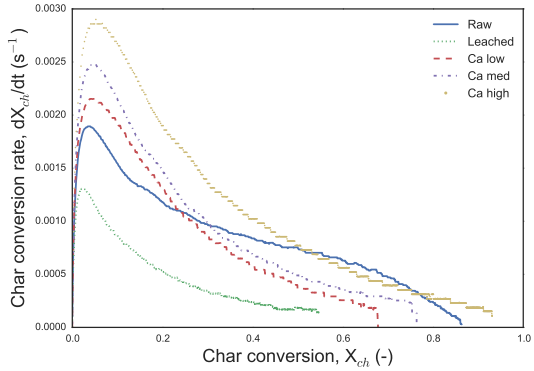

Figure 5: Conversion rate measurements of chars from raw birch wood, leached birch wood and Ca doped birch wood at 850°C in 20% CO_2 and 80% N_2. The lines are an average result from multiple measurements using each sample.

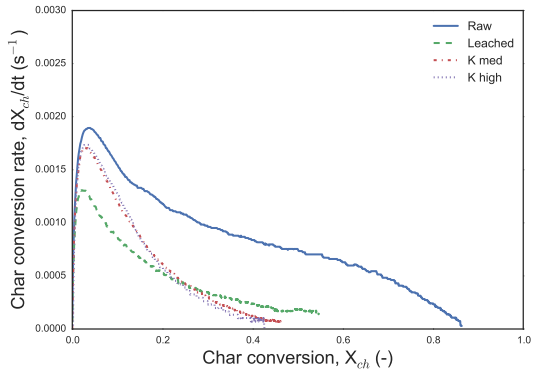

Figure 6: Conversion rate measurements of chars from raw birch wood, leached birch wood and K doped birch wood at 850°C in 20% CO_2 and 80% N_2. The lines are an average result from multiple measurements using each sample.

biomass, the resulting conversion rate curves will be different even for similar doping concentrations. In work using a similar wood and a similar leaching/doping method but at much higher K and Ca concentrations the wood was gasified in a TGA [17, 33]. In that work the wood was lowered in a sample holder into a preheated reactor with 100% CO_2 flow. The resulting heating rates were lower than the current work (approximately 50°C/s) and the devolatilization occurred in a CO_2 atmosphere. Both calcium and potassium doped samples showed increased reactivity compared to the leached wood, but the lowest doping level for the K doped wood was four times greater than the maximum doping in the present work. The catalytic effects of potassium were observed slightly later in the char conversion process than with calcium.

Suzuki et al. [19] loaded Ca and K to leached cedar wood, which was then gasified in a TGA. While the metal loading process used in that study was different than in the present work, it has been shown that potassium loaded wood will behave similarly whether the potassium is added as K_2CO_3 or doped through ion-exchange [17]. Suzuki et al. reported that at potassium loading levels approximately twice what was used in the present work there was an increase in reactivity compared with leached wood char. However, the influence of potassium was greatest at the end of the conversion process, and at low loading levels it was most significant at char conversion greater than 90%.

Numerous other studies report an increase in char reactivity with potassium doping [16, 18, 34, 35], though the char preparation and gasification methods tend to differ significantly from the present work. As potassium has been shown to deactivate as a catalyst by reacting with silicon in chars [36, 37], to rule out the possibility the potassium was reacting with the silicon in the bed material the olivine bed was replaced with bauxite. However, reactivity tests with raw birch wood and K doped wood using bauxite gave the same result as with the olivine bed.

In order to determine the effect of calcium on the activation energy of the char gasification reaction, char conversion rate measurements were conducted at 750°C, 800°C, 850°C, and 900°C for the raw birch wood, leached wood, Ca med and Ca high wood samples. The instantaneous reactivity at 20% was taken as the reference char conversion in order to calculate the apparent activation energy for the gasification reaction, according to Equation 4,

$$k = A \exp\left(\frac{-E_a}{RT}\right). \quad (4)$$

The instantaneous reaction rates are shown in the Arrhenius plot given in Figure 7. The calculated activation energies are given in Table 3. The activation energy for the raw birch wood is largely consistent with published activation energies for CO_2 gasification [38], which is typically in the range of 200-250 kJ/mol. The leached and Ca doped woods were found to have lower activation energies than the raw birch wood char, however there was no clear dependence of the activation energy on the calcium concentration in the wood. This is consistent with previous studies which report no significant dependence of activation on inorganic content [39, 40]. There is some disagreement on this issue, as other studies have reported both increases [41] and decreases [14, 42] in activation energy with catalyst loading and it is not understood what causes the conflicting results.

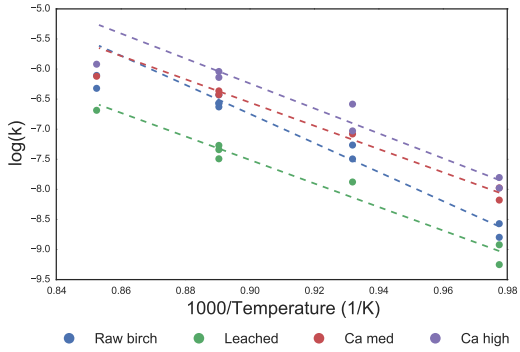

Figure 7: Arrhenius plot of log(k) vs 1000/T for raw birch, leached, Ca med and Ca high chars. The instantaneous reactivity was taken at 20% char conversion. The dashed lines indicated the linear regression line for the 750-850°C temperatures. It can be seen that for the raw wood, Ca med and Ca high samples the reactivity at 900°C falls well under the regression line.

Sample	Ea (kJ/mol)	R^2
Raw birch	197	0.9797
Leached	159	0.9563
Ca med	157	0.9883
Ca high	169	0.9571

Table 3: Activation energies for raw birch, leached, Ca med and Ca high chars and the R^2 for the linear regression.

3.3. Char characterization

Three types of characterization were performed on the char samples collected from the fluidized bed. First, SEM images were taken including SEM-EDS analysis. The SEM gave a qualitative understanding of the char structure and and the EDS analysis showed the composition of the char surface. Next, BET surface area was measured to understand the effect of the doping on the total surface area of the char. Finally, ICP-OES analysis was done to measure the inorganic contents of the chars.

SEM images were taken of chars from the raw birch wood, leached wood, K doped wood and Ca doped wood and are shown in Figure 8. The chars which were imaged were collected from the reactor immediately after pyrolysis was finished. The raw birch wood char (Figure 8A) and K doped wood char (Figure 8B) were taken from the fluidized bed cyclone. The wood structure in these chars has been preserved and is clearly visible in the images. Significant amounts of K and Ca were detected on the surface of the raw birch wood char using EDS, however for the K doped wood char only a small amount of K was present, possibly indicating that potassium is no longer present on the char due to vaporization or that the

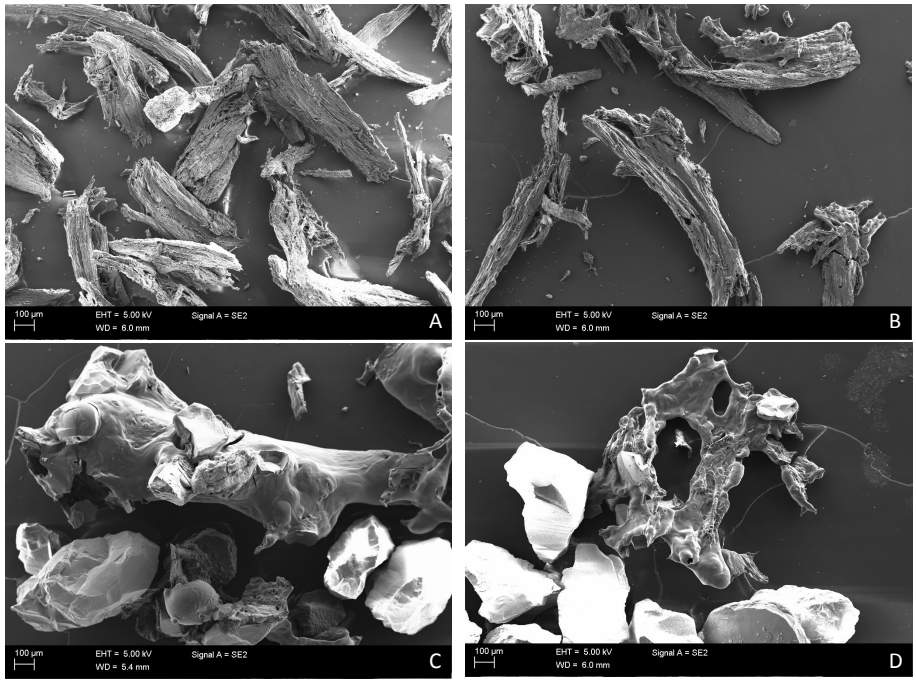

Figure 8: SEM images of char samples taken immediately after pyrolysis. The chars are: A) Raw birch, B) K med, C) Leached wood, D) Ca med.

potassium has been covered and was no longer exposed to the char surface.

The leached wood char (Figure 8C) and Ca doped wood char (Figure 8D) were obtained by manually separating the char from the bed. These chars show similar features, in that the wood structure has largely been lost and the surface of the char shows significant plastic deformation. In both images it can be seen that bed particles have become attached to the char, and this is likely the reason that the char could not be removed to the cyclone even at high gas velocities. This is shown more clearly in Figure 9 which shows a close up image of a bed particle embedded in a Ca med wood char particle.

It has been observed in many previous studies that wood chars will tend to retain the fibrous structure of the parent material at low heating rates, appearing similar to the raw and K doped wood chars in this work, but lose those structures and show signs of plastic deformation at high heating rates, resembling the leached and Ca doped wood chars [32, 43, 44]. Guerrero et al. [45] compared eucalyptus chars formed in a slow heating TGA and fast heating fluidized bed. While the chars formed in the fluidized bed did show larger pores and increased surface area due to the rapid release of volatiles, the chars did not exhibit significant plastic deformation or loss of structure and so resembled the raw and K doped wood chars in the current work. There has been some evidence that the presence of inorganics will cause changes in char structure despite equal heating rates, but the mechanism of this is not well understood. Perander et al. observed plastic deformation in chars from wood which was leached of ash forming elements and impregnated with CaC_2O_4, but not in chars impregnated with K_2CO_3 or doped with Ca or K [17]. Jones et al. also observed melting during devolatilization of leached wood but not potassium impregnated wood [46].

BET surface area measurements were conducted on the raw birch wood char and K doped wood char which were collected from the cyclone of the fluidized bed reactor. Acid washed wood and Ca doped wood chars could not be separated from the bed in large enough quantities to perform the BET surface area measurement. The results of the measurement is shown in Table 4. The specific surface area for the raw birch wood char is consistent with surface area values for biomass chars reported in literature [19, 45, 47–53] and the observed increase with conversion also agrees with commonly observed char behavior. While the specific surface area of the raw birch wood char increases with char conversion, the instantaneous reaction rate, as given by Equation 3, remains largely constant until approximately 80% char conversion. As such, the BET surface area measurement does not correspond to the reactive surface area of the char in this case. The inability of the BET surface area measurements to explain the char reactivity is consistent with other studies [19, 54], although there is no consensus on this as some work has shown a correlation may exist [47, 50].

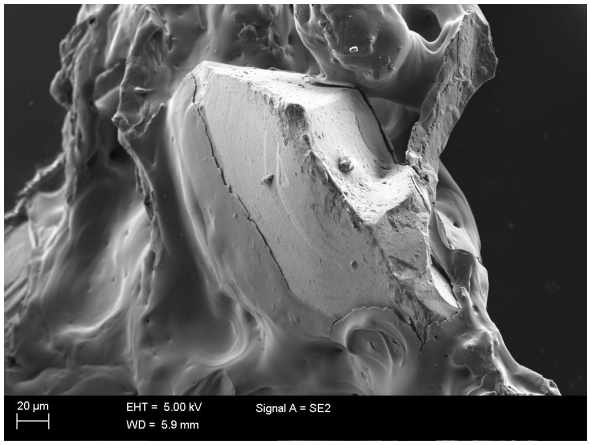

Figure 9: Close up image of bed particle embedded in Ca doped wood char.

Sample	Gasification time (s)	Approximate char conv. (%)	BET surface (m^2/g)
Raw birch	0	0	104
Raw birch	120	10	370
Raw birch	200	20	553
K med	0	0	0.08
K med	120	10	7.8
K med	400	20	1.3
K high	0	0	0.20

Table 4: BET surface area measurements using N_2 for raw birch wood and K doped wood chars taken from the fluidized bed reactor.

Sample	Ca (mg/kg char C)	K (mg/kg char C)
Raw birch	8840	6130
K med	3220	5480
K high	2150	6160

Table 5: ICP-OES results for raw birch wood and K med chars showing the concentration of calcium and potassium in the char.

Despite the similarities in appearance between the K doped and raw birch wood chars, the potassium doped chars have a much smaller specific surface area when compared to the raw birch wood char. Low surface area measurements for chars have been reported previously [28, 55], however typically such low surface area is a sign of incomplete pyrolysis which is not the case in the present work. The specific surface area of the K doped wood chars does not change during the conversion process to the same extent as the raw birch wood char, but the low surface area of the K doped wood char corresponds to the comparatively low reactivity of the chars. It is generally thought that inorganics on the char surface will block some meso- and micropores causing a decrease in the surface area of the char and is the reason why chars produced from leached materials will have higher surface areas [56]. In some it has also been reported that doped chars will have decreased reactivity due to surface particles hindering gas diffusion to the carbon atoms [16, 17], but this is typically seen for Ca gasification at high temperatures or high Ca concentration.

Poor surface contact between the catalyst and the char or uneven dispersion on the char surface can also lead to ineffective catalysts during gasification. This has been seen, for example, with CaC_2O_4 impregnated wood when gasified in CO_2 [17]. This is unlikely to be the case for the doping process used in the present work, as the potassium and calcium are loaded to organic functional groups in the same way that most metals are naturally found in the wood [57]. It is likely that cause of the low reactivity and low surface area of the chars from K doped wood is due to coke formation on the char surface which blocks the char pores and prevents diffusion of the gasifying gas into the char. Interactions between coal volatiles and coal char have been shown to effect char reactivity and is dependent on the presence of inorganics in the char [58], while coke formation on char has been shown to block pores on char surfaces [59, 60]. It has been shown that potassium not only increases primary char formation but also catalyzes secondary reactions with volatiles to form char [61], and longer gas residence times allow these secondary reactions to happen. While the raw birch wood has approximately the same potassium concentration as the K high doped wood the raw birch wood char did not show signs of significant coke formation on the char surface. Because the only difference between the wood samples was the concentration of ash elements, it is possible the presence of calcium or other inorganics in the raw wood inhibited the formation of the coke layer on the char surface which resulted in lower char yield, higher surface area, and increased reactivity compared to the K doped wood char.

To determine to what extent the calcium and potassium remain on the char after pyrolysis, the char samples were analyzed using ICP-OES and the results are shown in Table 5. If a fixed carbon amount of 9% is assumed for all samples these concentrations in the char correspond to 790 mg Ca/kg biomass and 550 mg K/kg biomass for the raw sample. For the K med sample, assuming again 9% fixed carbon, the values are 290 mg Ca/kg biomass and 490 mg K/kg biomass. And finally for K high, 190 mg Ca/kg biomass and 550 mg K/kg biomass. These values correspond well to the initial biomass concentrations shown in Table 2 and indicate that a significant amount of the calcium and potassium remain in the char. While the concentration of calcium in the K med sample is slightly higher than expected, it still shows a significant decrease from the amount in the raw birch wood as a result of the leaching. The potassium concentration in the K med and K high chars are close to the potassium concentration in the raw birch wood, indicating that the low reactivity of the K doped wood chars is not a result of volatilization of the potassium. This supports the conclusion that the K doped chars were covered with a unreactive coke layer which prevented the potassium from catalyzing the char gasification.

4. Conclusion

Four types of birch wood samples (raw, leached, Ca doped, and K doped birch wood) were gasified in a laboratory scale fluidized bed reactor. Each sample exhibited different behavior in the fluidized bed as a result of the varying amounts of inorganics in the wood. The leached wood, containing very little inorganics, showed significantly lower char conversion rate than the raw birch wood. When the leached wood was doped with calcium, the conversion rate of the resulting char increased as the calcium concentration increased. The leached wood and Ca doped wood chars both showed signs of large amounts of plastic deformation on the char surface and had bed particles embedded into the char. The embedded bed particles made the char particles heavier and prevented elutriation out of the bed.

Doping the leached wood with potassium, even up to approximately the same level as in the raw birch wood, did not result in a significant increase in char conversion rates compared with the leached wood char. The low conversion rates measured for the K doped wood chars were due to the formation of an unreactive coke layer on the char surface which blocked the char pores. The formation of the coke layer is indicated by the increased char yield and low BET surface area of the K doped wood chars.

These results suggest that calcium is the primary active element in birch wood gasification. However, neither the presence of potassium or calcium alone explained the behavior of the raw birch wood. It is therefore likely that there is some interaction between the inorganics during pyrolysis and char gasification.

Acknowledgments

Funding for this work from the following organizations is gratefully acknowledged: the Academy of Finland through the Doctoral Program in Energy Efficiency and Systems (EES) and IMUSTBC project; Junta de Andalucía in the project P12-TEP-1633 MO (FLETGAS2); the EU's Interreg program through the RENEPRO project. This work is part of the activities at the Johan Gadolin Process Chemistry Centre, a Centre of Excellence financed by Åbo Akademi University. Assistance in the experimental work from Israel Pardo, Estefania Ruiz and Mari Honkanen was appreciated.

Appendix A. Complete test list

The complete list of fluidized bed tests is shown in Table A.6. The test conditions and whether char was collected and through what method is given.

References

[1] S. V. Vassilev, D. Baxter, L. K. Andersen, C. G. Vassileva, An overview of the chemical composition of biomass, Fuel 89 (5) (2010) 913–933, ISSN 00162361, doi:10.1016/j.fuel.2009.10.022.

[2] M. K. Misra, K. W. Ragland, A. J. Baker, Wood ash composition as a function of furnace temperature, Biomass and Bioenergy 4 (2) (1993) 103–116, ISSN 09619534, doi:10.1016/0961-9534(93)90032-Y.

[3] M. Hupa, Ash-related issues in fluidized-bed combustion of biomasses: Recent research highlights, Energy and Fuels 26 (1) (2012) 4–14, ISSN 08870624, doi:10.1021/ef201169k.

[4] S. V. Vassilev, D. Baxter, L. K. Andersen, C. G. Vassileva, An overview of the composition and application of biomass ash. Part 1. Phase-mineral and chemical composition and classification, Fuel 105 (2013) 40–76, ISSN 00162361, doi:10.1016/j.fuel.2012.09.041.

[5] T. Khazraie Shoulaifar, N. Demartini, O. Karlström, M. Hupa, Impact of organically bonded potassium on torrefaction: Part 1. Experimental, Fuel 165 (2016) 544–552, ISSN 00162361, doi:10.1016/j.fuel.2015.06.024.

[6] K. Raveendran, A. Ganesh, K. C. Khilar, Influence of mineral matter on biomass pyrolysis characteristics, Fuel 74 (12) (1995) 1812–1822, ISSN 00162361, doi:10.1016/0016-2361(95)80013-8.

[7] D. J. Nowakowski, J. M. Jones, R. M. D. Brydson, A. B. Ross, Potassium catalysis in the pyrolysis behaviour of short rotation willow coppice, Fuel 86 (15) (2007) 2389–2402, ISSN 00162361, doi:10.1016/j.fuel.2007.01.026.

[8] I. Y. Eom, J. Y. Kim, T. S. Kim, S. M. Lee, D. Choi, I. G. Choi, J. W. Choi, Effect of essential inorganic metals on primary thermal degradation of lignocellulosic biomass, Bioresource Technology 104 (2012) 687–694, ISSN 09608524, doi:10.1016/j.biortech.2011.10.035.

[9] A. Aho, N. DeMartini, A. Pranovich, J. Krogell, N. Kumar, K. Eränen, B. Holmbom, T. Salmi, M. Hupa, D. Y. Murzin, Pyrolysis of pine and gasification of pine chars–influence of organically bound metals., Bioresource technology 128 (2013) 22–9, ISSN 1873-2976, doi:10.1016/j.biortech.2012.10.093.

[10] C. A. Mims, Alkali catalyzed carbon gasification I. Nature of the catalytic sites, ACS Division of Petroleum Chemistry, Preprints 180.

[11] D. W. McKee, Mechanisms of the alkali metal catalysed gasification of carbon, Fuel 62 (2) (1983) 170–175, ISSN 00162361, doi:10.1016/0016-2361(83)90192-8.

[12] Y. Zhang, S. Hara, S. Kajitani, M. Ashizawa, Modeling of catalytic gasification kinetics of coal char and carbon, Fuel 89 (1) (2010) 152–157, ISSN 00162361, doi:10.1016/j.fuel.2009.06.004.

[13] C. Dupont, T. Nocquet, J. A. Da Costa, C. Verne-Tournon, Kinetic modelling of steam gasification of various woody biomass chars: influence of inorganic elements., Bioresource technology 102 (20) (2011) 9743–8, ISSN 1873-2976, doi:10.1016/j.biortech.2011.07.016.

[14] J. K. Floess, J. P. Longwell, a. F. Sarofim, Intrinsic reaction kinetics of microporous carbons. 2. Catalyzed chars, Energy & Fuels 2 (6) (1988) 756–764, ISSN 0887-0624, doi:10.1021/ef00012a007.

[15] T. HANAOKA, Y. OKUMURA, Effect of metal content on CO2 gasification behavior of K- and Fe-loaded bio-chars, Journal of Thermal Science and Technology 9 (2) (2014) JTST0006–JTST0006, ISSN 1880-5566, doi:10.1299/jtst.2014jtst0006.

[16] Y. Huang, X. Yin, C. Wu, C. Wang, J. Xie, Z. Zhou, L. Ma, H. Li, Effects of metal catalysts on CO2 gasification reactivity of biomass char., Biotechnology advances 27 (5) (2009) 568–72, ISSN 1873-1899, doi:10.1016/j.biotechadv.2009.04.013.

[17] M. Perander, N. DeMartini, A. Brink, J. Kramb, O. Karlström, J. Hemming, A. Moilanen, J. Konttinen, M. Hupa, Catalytic effect of Ca and K on CO2 gasification of spruce wood char, Fuel ISSN 00162361, doi:10.1016/j.fuel.2015.02.062.

[18] M. Kajita, T. Kimura, K. Norinaga, C.-Z. Li, J.-i. Hayashi, Catalytic and Noncatalytic Mechanisms in Steam Gasification of Char from the Pyrolysis of Biomass, Energy & Fuels 24 (1) (2010) 108–116, ISSN 0887-0624, doi:10.1021/ef900513a.

[19] T. Suzuki, H. Nakajima, N.-o. Ikenaga, H. Oda, T. Miyake, Effect of mineral matters in biomass on the gasification rate of their chars, Biomass Conversion and Biorefinery 1 (1) (2011) 17–28, ISSN 2190-6815, doi:10.1007/s13399-011-0006-2.

[20] T. Khazraie Shoulaifar, N. DeMartini, A. Ivaska, P. Fardim, M. Hupa, Measuring the concentration of carboxylic acid groups in torrefied spruce wood, Bioresource Technology 123 (2012) 338–343, ISSN 09608524, doi:10.1016/j.biortech.2012.07.069.

[21] S. Nilsson, A. Gómez-Barea, D. Fuentes-Cano, M. Campoy, Gasification kinetics of char from olive tree pruning in fluidized bed, Fuel 125 (2014) 192–199, ISSN 00162361, doi:10.1016/j.fuel.2014.02.006.

[22] S. Nilsson, A. Gómez-Barea, P. Ollero, Gasification of char from dried sewage sludge in fluidized bed: Reaction rate in mixtures of CO2 and H2O, Fuel 105 (2013) 764–768, ISSN 00162361, doi:10.1016/j.fuel.2012.09.008.

[23] S. Nilsson, A. Gómez-Barea, D. F. Cano, Gasification reactivity of char from dried sewage sludge in a fluidized bed, Fuel 92 (1) (2012) 346–353,

Sample	Temperature °C	Gasification	No. of tests	Char collected
Raw birch	750	Complete	3	-
Raw birch	800	Complete	2	-
Raw birch	850	Complete	4	-
Raw birch	900	Complete	2	-
Raw birch	850	0 s	2	Cyclone
Raw birch	850	65 s	2	Cyclone
Raw birch	850	210 s	2	Cyclone
Leached	750	Complete	2	-
Leached	800	Complete	1	-
Leached	850	Complete	4	-
Leached	900	Complete	1	-
Leached	850	0 s	2	Bed removal
Ca low	850	Complete	3	-
Ca med	750	Complete	2	-
Ca med	800	Complete	1	-
Ca med	850	Complete	3	-
Ca med	900	Complete	1	-
Ca high	750	Complete	2	-
Ca high	800	Complete	2	-
Ca high	850	Complete	2	-
Ca high	900	Complete	2	-
Ca high	850	0 s	2	Bed removal
K med	850	Complete	4	-
K high	850	Complete	2	-
K med	850	0 s	2	Cyclone
K med	850	120 s	2	Cyclone
K med	850	400 s	2	Cyclone
K high	850	0 s	2	Cyclone

Table A.6: Complete list of fluidized bed measurements, test conditions and method of char collection. All gasification was done using 80% N_2/20% CO_2.

ISSN 00162361, doi:10.1016/j.fuel.2011.07.031.
[24] S. Brunauer, P. H. Emmett, E. Teller, Adsorption of Gases in Multimolecular Layers, Journal of the American Chemical Society 60 (2) (1938) 309–319, ISSN 0002-7863, doi:10.1021/ja01269a023.
[25] E. P. Barrett, L. G. Joyner, P. P. Halenda, The Determination of Pore Volume and Area Distributions in Porous Substances. I. Computations from Nitrogen Isotherms, Journal of the American Chemical Society 73 (1) (1951) 373–380, ISSN 0002-7863, doi:10.1021/ja01145a126.
[26] A. Gomez-Barea, S. Nilsson, F. V. Barrero, M. Campoy, Devolatilization of wood and wastes in fluidized bed, Fuel Processing Technology 91 (11) (2010) 1624–1633, ISSN 03783820, doi:10.1016/j.fuproc.2010.06.011.
[27] D. S. Scott, J. Piskorz, M. a. Bergougnou, R. P. Overend, R. Graham, The role of temperature in the fast pyrolysis of cellulose and wood, Industrial & Engineering Chemistry Research 27 (1) (1988) 8–15, ISSN 0888-5885, doi:10.1021/ie00073a003.
[28] R. Zanzi, K. Sjöström, E. Björnbom, Rapid pyrolysis of agricultural residues at high temperature, Biomass and Bioenergy 23 (5) (2002) 357–366, ISSN 09619534, doi:10.1016/S0961-9534(02)00061-2.
[29] D. Neves, H. Thunman, A. Matos, L. Tarelho, A. Gómez-Barea, Characterization and prediction of biomass pyrolysis products, Progress in Energy and Combustion Science 37 (5) (2011) 611–630, ISSN 03601285, doi:10.1016/j.pecs.2011.01.001.
[30] S. Rapagnà, Steam-gasification of biomass in a fluidised-bed of olivine particles, Biomass and Bioenergy 19 (3) (2000) 187–197, ISSN 09619534, doi:10.1016/S0961-9534(00)00031-3.
[31] Y. Shen, K. Yoshikawa, Recent progresses in catalytic tar elimination during biomass gasification or pyrolysis - A review, Renewable and Sustainable Energy Reviews 21 (2013) 371–392, ISSN 13640321, doi:10.1016/j.rser.2012.12.062.
[32] E. Cetin, B. Moghtaderi, R. Gupta, T. Wall, Influence of pyrolysis conditions on the structure and gasification reactivity of biomass chars, Fuel 83 (16) (2004) 2139–2150, ISSN 00162361, doi:10.1016/j.fuel.2004.05.008.
[33] J. Kramb, N. DeMartini, M. Perander, A. Moilanen, J. Konttinen, Modeling of the catalytic effects of potassium and calcium on spruce wood gasification in CO2, Fuel Processing Technology 148 (2016) 50–59, ISSN 03783820, doi:10.1016/j.fuproc.2016.01.031.
[34] J. Kopyscinski, M. Rahman, R. Gupta, C. a. Mims, J. M. Hill, K2CO3 catalyzed CO2 gasification of ash-free coal. Interactions of the catalyst with carbon in N2 and CO2 atmosphere, Fuel 117 (PARTB) (2014) 1181–1189, ISSN 00162361, doi:10.1016/j.fuel.2013.07.030.
[35] D. W. McKee, C. L. Spiro, P. G. Kosky, E. J. Lamby, Catalysis of coal char gasification by alkali metal salts, Fuel 62 (1983) 217–220, ISSN 00162361, doi:10.1016/0016-2361(83)90202-8.
[36] M. Kannan, G. Richards, Gasification of biomass chars in carbon dioxide: dependence of gasification rate on the indigenous metal content, Fuel 69 (6) (1990) 747–753, ISSN 00162361, doi:10.1016/0016-2361(90)90041-N.
[37] K. J. Hüttinger, R. Minges, The influence of the catalyst precursor anion in catalysis of water vapour gasification of carbon by potassium, Fuel 65 (8) (1986) 1122–1128, ISSN 00162361, doi:10.1016/0016-2361(86)90180-8.
[38] C. Di Blasi, Combustion and gasification rates of lignocellulosic chars, Progress in Energy and Combustion Science 35 (2) (2009) 121–140, ISSN 03601285, doi:10.1016/j.pecs.2008.08.001.
[39] H. Juntgen, K. V. Heek, Kinetics and mechanism of catalytic gasification of coal, Prepr. Pap., Am. Chem. Soc., Div. Fuel Chem.;(....
[40] D. W. Mckee, C. L. Spiro, K. E. J, P. G. Lamby, Catalytic Effects of Alkali Metal Salts in the Gasification of Coal Char, Symposium on coal gasification.
[41] J. Kopyscinski, R. Habibi, C. a. Mims, J. M. Hill, K 2 CO 3 -Catalyzed CO 2 Gasification of Ash-Free Coal: Kinetic Study, Energy & Fuels 27 (8) (2013) 4875–4883, ISSN 0887-0624, doi:10.1021/ef400552q.
[42] P. Lahijani, Z. A. Zainal, A. R. Mohamed, M. Mohammadi, CO2 gasification reactivity of biomass char: catalytic influence of alkali, alkaline earth and transition metal salts., Bioresource technology 144 (2013) 288–95, ISSN 1873-2976, doi:10.1016/j.biortech.2013.06.059.
[43] A. Trubetskaya, P. A. Jensen, A. D. Jensen, M. Steibel, H. Spliethoff, P. Glarborg, Influence of fast pyrolysis conditions on yield and structural transformation of biomass chars, Fuel Processing Technology 140 (2015) 205–214, ISSN 03783820, doi:10.1016/j.fuproc.2015.08.034.
[44] M. Dall'Ora, P. A. Jensen, A. D. Jensen, Suspension combustion of wood: Influence of pyrolysis conditions on char yield, morphology, and reactivity, Energy and Fuels 22 (5) (2008) 2955–2962, ISSN 08870624, doi:10.1021/ef800136b.
[45] M. Guerrero, M. P. Ruiz, M. U. Alzueta, R. Bilbao, A. Millera, Pyrolysis of eucalyptus at different heating rates: Studies of char characterization and oxidative reactivity, Journal of Analytical and Applied Pyrolysis 74 (1-2) (2005) 307–314, ISSN 01652370, doi:10.1016/j.jaap.2004.12.008.
[46] J. M. Jones, L. I. Darvell, T. G. Bridgeman, M. Pourkashanian, a. Williams, An investigation of the thermal and catalytic behaviour of potassium in biomass combustion, Proceedings of the Combustion Institute 31 II (2007) 1955–1963, ISSN 15407489, doi:10.1016/j.proci.2006.07.093.
[47] D. K. Seo, S. K. Lee, M. W. Kang, J. Hwang, T.-U. Yu, Gasification reactivity of biomass chars with CO2, Biomass and Bioenergy 34 (12) (2010) 1946–1953, ISSN 09619534, doi:10.1016/j.biombioe.2010.08.008.
[48] P. Fu, S. Hu, J. Xiang, W. Yi, X. Bai, L. Sun, S. Su, Evolution of char structure during steam gasification of the chars produced from rapid pyrolysis of rice husk, Bioresource Technology 114 (2012) 691–697, ISSN 09608524, doi:10.1016/j.biortech.2012.03.072.
[49] M. B. Tilghman, R. E. Mitchell, Coal and biomass char reactivities in gasification and combustion environments, Combustion and Flame 2, ISSN 00102180, doi:10.1016/j.combustflame.2015.05.009.
[50] I. Sircar, A. Sane, W. Wang, J. P. Gore, Experimental and modeling study of pinewood char gasification with CO2, Fuel 119 (2014) 38–46, ISSN 00162361, doi:10.1016/j.fuel.2013.11.026.
[51] S. Manocha, V. B. Chauhan, L. M. Manocha, Porosity Development on Activation of Char from Dry and Wet Babbool Wood, Carbon Letters 3 (3).
[52] S. Kudo, Y. Hachiyama, H.-S. Kim, K. Norinaga, J.-i. Hayashi, Examination of Kinetics of Non-catalytic Steam Gasification of Biomass/Lignite Chars and Its Relationship with the Variation of the Pore Structure, Energy & Fuels 28 (9) (2014) 5902–5908, ISSN 0887-0624, doi:10.1021/ef501517n.
[53] C. Guizani, M. Jeguirim, R. Gadiou, F. J. Escudero Sanz, S. Salvador, Biomass char gasification by H2O, CO2 and their mixture: Evolution of chemical, textural and structural properties of the chars, Energy 112 (2016) 133–145, ISSN 03605442, doi:10.1016/j.energy.2016.06.065.
[54] K. Xu, S. Hu, S. Su, C. Xu, L. Sun, C. Shuai, L. Jiang, J. Xiang, Study on Char Surface Active Sites and Their Relationship to Gasification Reactivity, Energy & Fuels 27 (1) (2013) 118–125, ISSN 0887-0624, doi:10.1021/ef301455x.
[55] E. Biagini, P. Narducci, L. Tognotti, Size and structural characterization of lignin-cellulosic fuels after the rapid devolatilization, Fuel 87 (2) (2008) 177–186, ISSN 00162361, doi:10.1016/j.fuel.2007.04.010.
[56] R. Gopalakrishnan, M. J. Fullwood, C. H. Bartholomew, Catalysis of Char Oxidation by Calcium Minerals: Effects of Calcium Compound Chemistry on Intrinsic Reactivity of Doped Spherocarb and Zap Chars, Energy & Fuels 8 (4) (1994) 984–989, ISSN 0887-0624, doi:10.1021/ef00046a025.
[57] P. Su, K. Granholm, A. Pranovich, L. Harju, B. Holmbom, A. Ivaska, Sorption of metal ions to untreated, alkali-treated and peroxide-bleached TMP, Cellulose 17 (5) (2010) 1033–1044, ISSN 0969-0239, doi:10.1007/s10570-010-9439-1.
[58] X. Li, H. Wu, J.-i. Hayashi, C.-Z. Li, Volatilisation and catalytic effects of alkali and alkaline earth metallic species during the pyrolysis and gasification of Victorian brown coal. Part VI. Further investigation into the effects of volatile-char interactions, Fuel 83 (10) (2004) 1273–1279, ISSN 00162361, doi:10.1016/j.fuel.2003.12.009.
[59] Z. Abu El-Rub, E. A. Bramer, G. Brem, Experimental comparison of biomass chars with other catalysts for tar reduction, Fuel 87 (10-11) (2008) 2243–2252, ISSN 00162361, doi:10.1016/j.fuel.2008.01.004.
[60] Y. Shen, Chars as carbonaceous adsorbents/catalysts for tar elimination during biomass pyrolysis or gasification, Renewable and Sustainable Energy Reviews 43 (2015) 281–295, ISSN 13640321, doi:10.1016/j.rser.2014.11.061.
[61] C. A. Zaror, I. S. Hutchings, D. L. Pyle, H. N. Stiles, R. Kandiyoti, Secondary char formation in the catalytic pyrolysis of biomass, Fuel 64 (7) (1985) 990–994, ISSN 00162361, doi:10.1016/0016-2361(85)90156-5.

Tampereen teknillinen yliopisto
PL 527
33101 Tampere

Tampere University of Technology
P.O.B. 527
FI-33101 Tampere, Finland

ISBN 978-952-15-3883-4
ISSN 1459-2045